COO-1248-30

THE DISTRIBUTION OF ELECTRIC CHARGE AMONG THE PARTICLES OF AN ARTIFICIALLY CHARGED AEROSOL

A THESIS
SUBMITTED TO THE FACULTY OF THE GRADUATE SCHOOL
OF THE UNIVERSITY OF MINNESOTA

By

EARL OWEN KNUTSON

IN PARTIAL FULFILLMENT OF THE REQUIREMENTS
FOR THE DEGREE OF
DOCTOR OF PHILOSOPHY

December, 1971

DISCLAIMER

I dedicate this thesis to
my father and first teacher,

OLAF MAURICE KNUTSON

1903-1971

Acknowledgements

Although I, Earl O. Knutson, assume full responsibility for the dissertation which appears within these covers, I acknowledge that I have been generously aided in its preparation by several individuals and organizations. I wish to express my gratitude to some of these here.

My prime assistant in this thesis work has been my wife, Donna. Her sacrifice has made it possible for me to devote the necessary several months of long hours to this project. During this time, she did more than her share of work in caring for our two infant daughters. She displayed great patience with me through some trying periods and offered encouragement at times when it was sorely needed. To cap it all, she volunteered to type the final draft of this thesis, with its many difficult mathematical formulae. Her expertise in typing and proof reading will be apparent to anyone who reads this dissertation. I am grateful to her for her hard work in furtherance of this thesis.

The faculty advisor for my doctoral work has been Professor Kenneth Whitby. He has contributed to this thesis project in several ways. It was through discussions with him that I became aware of the questions to which this dissertation is addressed. At several times in the course of the work when the project appeared to be stalled, his suggestions provided the key to further progress. Furthermore, his critical review of the first two drafts of this thesis resulted in several suggestions which have improved this dissertation's readability. I profoundly thank Professor Whitby for his guidance.

This dissertation has benefitted also from several discussions with Professor B.Y.H. Liu. His interest in this project, particularly in the subject of electric mobility analysis, is much appreciated.

Several of my fellow graduate students have assisted in various ways in this thesis effort. The charging device referred to in this thesis as the triode corona charger was made available to me, at my convenience, by David Pui. Also, his interest in the later stages of the experimental work, and his pointed questions, helped the work progress. This is appreciated.

David Pui and Charles Lo volunteered to render the drawings for this dissertation in ink. This involved several hours of concentration on their part. Their artistry will be apparent to all readers of this thesis. It is certainly appreciated by the author.

I owe a great debt also to Dr. Fadejimi Bademosi, whose thesis work also concerned electric charging of aerosols and preceeded mine by about six months. It was he who constructed the mobility analyzer which, with some modification, was used in my experimental work.

Dr. Milos Tomaides assisted and advised me in obtaining optimum performance from the aerosol generators. His willingness to help at a moment's notice is appreciated.

The matter of financial support is vital in any thesis effort. The bulk of the work in this thesis was done with the generous financial support of the U. S. Atomic Energy Commission, through their contract AT(11-1)-1248 with the Particle Technology Laboratory at the University of Minnesota. I am grateful for their in-

terest in and support of my thesis work. In the same vein, the University Computer Center at the University of Minnesota made available, at no cost to me, the computer time necessary for the computational parts of this work. My thanks to them also.

In closing, I would like to record that it has been a privilege and a pleasure to have been affiliated for four years with the Particle Technology Laboratory at the University of Minnesota. During this time, I had access to a wide range of techniques and apparatus developed and collected for the study of aerosols at this laboratory. This environment contributed much to the thesis. I will remember the experience fondly.

ABSTRACT

One application of unipolar charging of aerosols is in the electrical method of particle size analysis. In this application, it is important that the charge imparted to the particles be uniquely related to their size. The question addressed by this thesis is the extent to which this objective can be met, in theory and in practice.

The uniformity of unipolar charging may be conveniently specified by stating the standard deviation of the charge imparted to monodisperse aerosols. Experimentally, this requires an accurate measurement of both the first and the second moment of the charge distribution. A secondary objective of this thesis was to further develop the electric mobility method as a tool for the study of the particle charge distribution in monodisperse aerosols.

It has been recognized by previous workers that there exists a theoretical limit to the charge uniformity attainable in unipolar charging. This limit is a direct consequence of the discrete nature of electric charge. It is shown in this thesis that the corresponding standard deviation for the case of diffusion charging is approximately $2.3 d_p^{\frac{1}{2}}$ charge units, where d_p is the particle diameter in microns. This value is nearly independent of the time of particle exposure to ions, so long as all particles are equally exposed.

In real charging devices, the particle exposure to ions

cannot be controlled precisely. It is determined in part by chance. This degrades the uniformity of particle charging. It is proposed in the thesis that the case where the particle exposure conforms to the negative exponential distribution, serves as a theoretical upper limit on the spread of the charge distribution. The corresponding standard deviation, again assuming diffusion charging, is of the order $12d_p$ charge units, with d_p expressed in microns.

In the experimental part of this thesis, two basically different charging devices were used to charge essentially monodisperse aerosols. The sonic jet charge employs turbulent mixing. In the triode charger, an attempt is made to maintain laminar flow. Three versions of the sonic jet charger were tested. Two charger flow rates were tried.

The aerosol used in the experiments was either dioctyl phthalate generated by condensation or polystyrene formed by atomizing a latex. The particle size was 0.4 to 1.0 microns. The initial charge was either zero or Boltzmann equilibrium. The concentration in the charger was varied up to about 300 particles per cc.

The central element in the apparatus for the experimental part of this thesis was an electric mobility analyzer. This was of the coaxial cylinder type with continuous through flow. Both the inlet and outlet flows were divided into two streams. A theory of operation for this analyzer was developed, based on the observation that the particle motion within the analyzer is

governed by an exact differential equation. This theory makes possible the precise determination of moments of the mobility distribution for the aerosol under test. The theory was verified by tests with singly charged monodisperse polystyrene particles.

It was found in the experiments that the aerosol composition, concentration and initial charge had no effect on the charge distribution after unipolar charging. For the sonic jet charger, the standard deviation of charge was about $8d_p$ charge units, increasing slightly with charger flow rate. For the triode charger, the standard deviation was about $5d_p$ units, independent of flow rate. Thus neither charger achieved optimum uniformity in unipolar charging. The result for the triode charger can be explained by assuming a fully developed plane-parallel flow through the charging region, with the attendent exposure time distribution. This suggests that the charging uniformity may be improved by modifying the flow field.

CONTENTS

List of Figures

List of Figures
(continued)

List of Tables

List of Symbols

Symbol	Meaning	First appeared Section	Page
a	particle radius	1.1	3
b	particle "electrical size" coefficient in Cunningham correction	2.4 5.1	22 78
$\bar{c}$	mean thermal speed of ions	3.2.1	34
d_p	particle diameter	1.1	3
$f(Z_p)$	mobility distribution	5.4	103
$\hat{f}(\log Z_p)$	distribution of $\log Z_p$	6.4.1	142
g_k	steady state ion flux to a particle carrying k charges for unit ion concentration	3.1	27
$h(t)$	exposure time distribution	4.0	59
k_b	Boltzmann's constant	2.4	22
k	particle charge in elementary units	3.0	26
k_s	particle saturation charge	3.2.3	42
$\bar{k}$	mean particle charge	3.3	42
n_p	particle charge in elementary units	1.1	3
n	ion concentration	3.1	27
$p(k;a,t)$	the minimum variance charge distribution	3.2	29
$p(k;a)$	charge distribution for non-uniform exposure time	4.1	60
q_c	analyzer clean air flow	5.3	91
q_a	analyzer aerosol flow	5.3	91
q_s	analyzer sampling flow	5.3	91
q_o	analyzer main outlet flow	5.3	91
q_a'	$= q_a/q_o$	5.4	106
q_s'	$= q_s/q_o$	5.4	106
r_1, r_2	inner and outer radii of the analyzing region	5.3	87

List of Symbols
(continued)

Symbol	Meaning	First appeared Section	Page
r	radial coordinate in analyzer	5.3	87
s	Laplace transform variable	3.2	32
t	time	3.1	27
t^*	minimum exposure time	4.3	68
var	denotes "variance of"	3.1	28
v_r, v_z	velocity components in analyzer	5.3	87
x	reduced particle mean charge	3.3.1	48
y	reduced variance of particle charge	3.3.1	48
z	axial coordinate in analyzer	5.3	87
A_{kj}	coefficient in partial fraction expansion	3.2	32
A	coefficient in Cunningham correction	5.1	78
C	Cunningham slip correction	5.1	77
D	diffusion coefficient of ions	3.2.2	38
E	denotes "expectation of"	3.1	28
E_o	applied electric field	3.2.2	42
E_r, E_z	electric field components in analyzer	5.3	87
I_o, I_1, I_2, ...	integrals-over-Ω	5.4	106
I_o^*, I_1^*, I_2^*, ...	integrals-over-N^*	5.4	106
K	particle dielectric constant	3.2.3	42
L	length of the analyzing region	5.3	87
N	the number of particles entering the mobility analyzer in one sampling cycle	5.4	103
N^*	the number of particles counted at the analyzer outlet in one sampling cycle	5.4	103

List of Symbols
(continued)

Symbol	Meaning	First appeared Section	Page
$P(k;a,s)$	Laplace transform of $p(k;a,t)$	3.2	32
Q	flow rate through charger	4.2	61
	coefficient in Cunningham correction	5.1	78
T_a	absolute temperature	2.4	22
T_k	time to accumilate k charges	3.1	27
T_e	exposure time (random variable)	4.0	59
V	volume of charging vessel	4.2	60
	voltage on center rod	5.3	91
Z_p	particle electric mobility	1.1	4
Z_i	ion electric mobility	3.2.2	38
Z_1	mobility of singly charged particle	5.1	77
Z_p^*	mid-point of mobility interval	5.3	96
$\overline{Z_p}, \overline{Z_p^2}, \ldots$	moments of the mobility distribution	5.4	106
α	parameter in regression analysis	2.0	9
	Taylor's series coefficient	3.3	46
β	parameters in regression analysis	2.0	9
	Taylor's seroes coefficient	3.3	46
γ	Taylor's series coefficient	3.3	46
ε	unit electric charge	1.1	3
λ	mean free path of air molecules	5.1	78
μ	air velocity	5.1	78
σ^2	variance of particle charge	3.3	46
ψ	stream function	5.3	89
$\psi_1, \psi_1', \psi_2', \psi_2$	key streamlines	5.3	89
ψ_{in}, ψ_{out}	particle inlet and outlet streamlines	5.3	95
ΔT_k	lifetime of k charged particle	3.1	27

List of Symbols
(continued)

Symbol	Meaning	First appeared Section	Page
$\Delta\phi$	number of electric field lines crossed between inlet and outlet	5.3	92
ΔZ_p	width of mobility interval	5.3	96
Ω	the passage function	5.4.	99
$f_s(d_p)$	size distribution function	7.2	165
Z_p	variance of electric mobility	6.4.1	140
ϕ	electric flux function	5.3	89

1.0 INTRODUCTION

This thesis concerns aerosols, atmospheric ions and certain of the interactions between them.

An aerosol is that particular type of colloid in which the discontinuous phase is a solid or liquid and the continuous phase is a gas, usually air. The term aerosol applies only to those dispersions which possess a degree of stability, or persistance. Thus it is required that the individual particles of the dispersion neither change size rapidly nor separate rapidly from the gas, at least under normal conditions. Rain, for example, is not an aerosol, but fog is.

An atmospheric ion is a molecule or cluster of molecules which has an excess or deficiency in its number of electrons. It therefore carries net electric charge. Ions are produced naturally in the atmosphere by the action of cosmic rays and other agencies. This thesis, however, is concerned with ions which are generated artificially and on demand by means of an electric corona discharge or by means of suitable radioactive materials. These methods can raise the ion concentration in local regions to millions of times the concentration of natural ions. Furthermore, they can be set up to produce ions of one sign only in the region of interest. In natural ions, both signs of charge are equally abundant.

Since ions are always present in the atmosphere, every aerosol particle has the opportunity to capture ions and become electrically charged. An aerosol which has been exposed sufficiently to natural ions acquires a state of charge which

may be called the natural charge for the aerosol. Conversely, an aerosol which has acquired charge by exposure to a high concentration of artificially generated ions, all of one sign, may be called an artificially charged aerosol. The natural charge of aerosols is discussed by Junge(1963) and by Bricard and Pradel(1966). Artificially charged aerosols are discussed by White(1963).

In the artificial charging of aerosols, a distinction is drawn between diffusion charging and field charging. In the former, little or no electric field is impressed on the charging region. The motion of ions is then due to their thermal agitation, modified only by the electric field due to other ions or to charged particles. In field charging, a strong electric field is impressed on the charging region. This impressed field strongly affects the motion of the ions and, therefore, the charging process.

In artificial aerosol charging, the amount of charge acquired by an individual aerosol particle may be controlled to some extent by controlling the conditions of charging. One application of controlled particle charging is the electrical method of particle size analysis (see Rohmann, 1923; Yoshikawa, Swartz, MacWaters and Fite, 1956; Drozin and LaMer, 1959; Whitby and Clark, 1966). Here the objective is to charge particles in such a way that the charge acquired is uniquely related to particle size, and vise versa. If this is achieved, then a measurement of particle charge suffices to determine its size as well. The degree to which particle charging can be con-

trolled is therefore a central question in this method of particle size analysis.

The purpose of this thesis is to make a clear statement regarding the extent to which the charge acquired by an aerosol particle in artificial charging can be controlled.

1.1 Definitions and conventions

If the aerosol particle in question is spherical, its size is conveniently specified by stating its diameter d_p. Sometimes the radius, denoted by a, is more convenient. If the particle is nonspherical it is customary to agree upon an equivalent diameter. An aerosol all of whose particles have the same size is called monodisperse. Such aerosols are rare in nature but can be approximated under laboratory conditions. Aerosols which are not monodisperse are polydisperse.

The basic amount of electric charge is ε, the elementary unit of charge. The value of ε is 4.803×10^{-10} statcoulomb = 1.601×10^{-19} coulomb. The charge carried by an aerosol particle is most conveniently specified by stating the number n_p of elementary charge units on the particle. Thus the variable n_p is restricted to the integer values 0, ±1, ±2, ±3,.... If all the particles of the aerosol have the same sign of charge (unipolar aerosol), the sign of n_p may be ignored to simplify the mathematical expressions. However if the aerosol has both negative and positive particles (bipolar aerosol), the sign of n_p must be retained.

The particle size and charge are two of its most funda-

mental and important attributes. However, other particle characteristics are sometimes more easily measured. When a charged particle suspended in a stagnant gas is subjected to a uniform electric field, it eventually acquires a steady drift velocity. In many cases, this drift velocity will be proportional to the applied electric field. The constant of proportionality, denoted here by Z_p, is called the electric mobility of the particle. The electric mobility depends on the particle size, the particle charge and properties of the suspending gas.

Consider an aerosol which has been charged by exposure to unipolar gaseous ions. If particles are picked at random from this aerosol and the size and charge of each is measured, the results may be presented by means of an n_p-d_p plane. Such a plot is given in figure 1, which was prepared from the data of Schweitzer(1930, table 1). Each point on the graph represents one particle measured. The most striking feature of figure 1 is the amount of scatter in the data points. To be sure, this scatter is in part due to random errors in the measurement of size and charge. It seems likely, however, that the scatter is largely real - a consequence of the particular charging device used by Schweitzer. Thus it is seen that the relationship between size and charge is not a unique, deterministic one. Instead, this relationship must be described in terms of statistical concepts.

One method of describing the relationship between the particle charge and the particle size is the correlation coefficient. This is a measure of the extent to which a pair of variables is

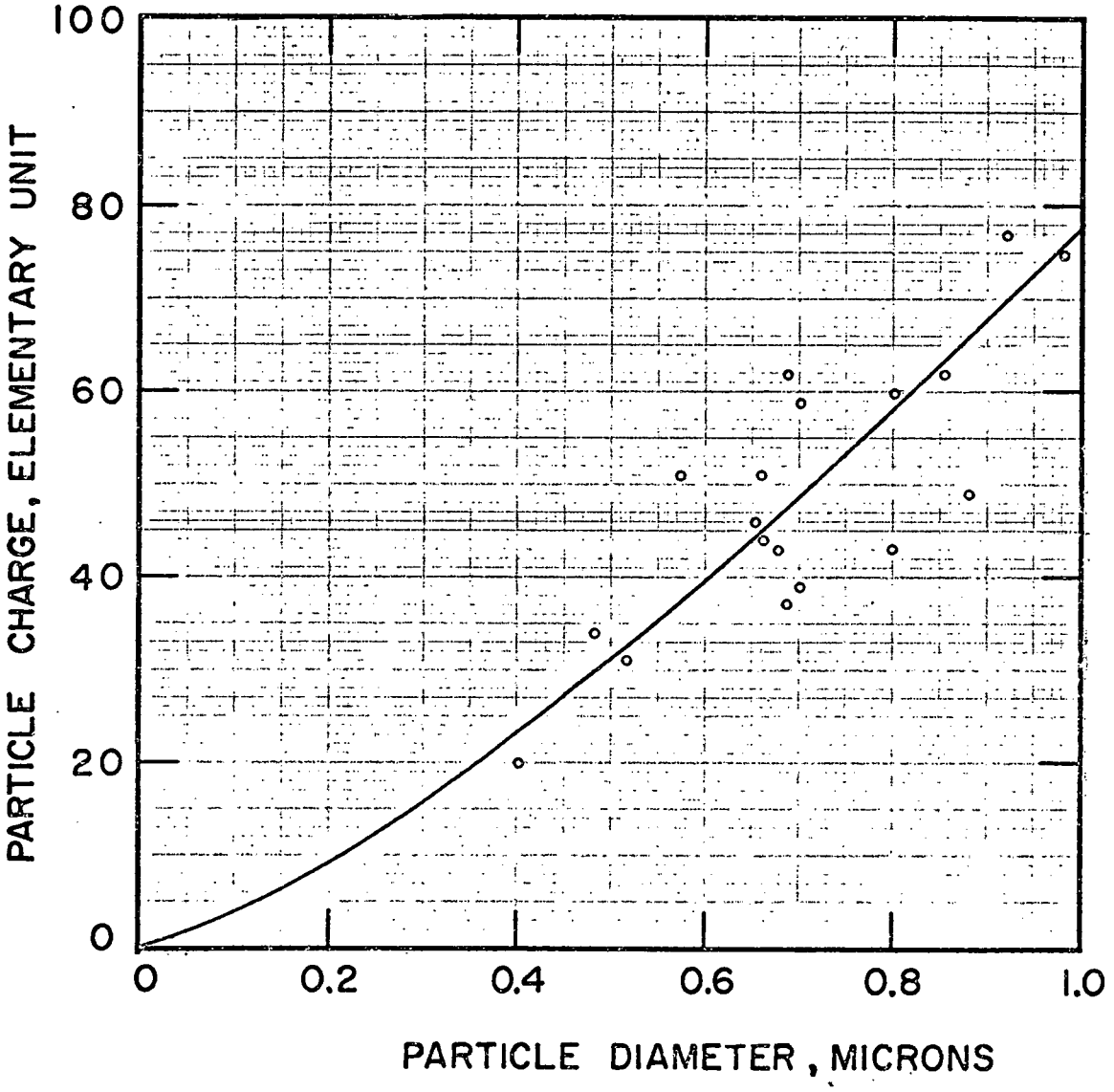

Figure 1. A size-charge bivariate distribution for an aerosol after exposure to an electrical corona.

Data taken from table 1 of H. Schweitzer, Ann. der Phys., series 5, volume 4, page 33 (1930).

linearly related. The correlation coefficient is symmetric in the two variables, showing no preference for either one over the other. The correlation coefficient has the disadvantage that it is not defined in case the aerosol is monodisperse. Nevertheless, it will be used occasionally in the following.

Another method of describing the relationship between size and charge is by means of regression analysis. In this analysis, it is necessary to designate one of the two variables as a random variable and the other as a parameter. The relationship between the two variables is then specified by stating the mean and variance of the random variable. In the usual theory of regression analysis, it is assumed that the mean is a linear function of the parameter and that the variance is independent of the parameter.

In the present study, it seems most natural to regard the particle charge n_p as the random variable and the particle size d_p as the parameter. In some cases, it is preferable to work with the logarithms of the variables rather than with the variables themselves. Thus in figure 1, the curve which has been added to the data points represents the regression of $\ln n_p$ on $\ln d_p$; that is, the curve shown is the geometric mean change as a function of size. The variance of $\ln n_p$ is a measure of the vertical scatter of the points about the line. It is related in a simple way to the geometric standard deviation of the charge. For the data shown in figure 1, the estimate of the geometric standard deviation is 1.20.

1.2 Objectives of this study

The objectives of this study are:

1. To identify the factors which limit the control possible over the charging process,
2. to estimate the contribution of each such factor to the variance of the charge distribution,
3. to measure the mean and (more importantly) the variance of the charge distribution resulting from several practical charging devices and
4. to summarize this information into a clear statement regarding the minimum charge distribution variance attainable in practical charging devices.

1.3 The method of this study

The method employed in this study is partly experimental and partly theoretical. The theoretical part is not intended to provide a highly accurate description of the charging process. Instead it is intended to identify the factors which contribute to the variance of the charge spectrum and to provide some indication of the importance of each. Thus, the theoretical part is limited to a consideration of the simplest models of the charging process. These analyses provide a useful backdrop against which to view experimental results.

The experimental part of this thesis required a series of monodisperse aerosols with size on the range 0.1 and 1.0 microns. After generation, the monodisperse aerosol was passed through a charging device which exposes the particles to a high concentration of unipolar gas ions. The charge thus imparted may be described in terms of a charge distribution function. After charging, the aerosol was passed through an electric mobility

analyzer which physically separates the aerosol into fractions with differing electric mobility. From a measurement of the amount of aerosol in each category, the electric mobility spectrum was determined. The charge distribution then follows from an application of the known relationship between size, charge and electric mobility.

2.0 REVIEW OF THE LITERATURE

The charging of aerosol particles by exposure to gaseous ions has been studied many times since 1920. In practically every study, the primary if not exclusive aim has been to determine the mean charge on aerosol particles as a function of particle size and other parameters. Thus the literature provide very few direct data of value to this thesis, which is primarily concerned with the variance of the charge distribution. This is true of both experimental and theoretical studies of the charging process.

Where the data from an experimental charging study is reported in terms of points in the n_p-d_p plane, as in figure 1, some information regarding the spread of the charge distribution may be extracted by carrying out a regression on the data. To this end, the data points were read from these plots and the regression of ln n_p on ln d_p was determined. The results of this analysis consist of the expression

$$\text{mean of } \ln n_p = \ln\alpha + \beta \ln d_p$$

where α and β are chosen to provide the best fit to the data in the least squares sense and of

$$\text{standard deviation of } \ln n_p.$$

The two results may be expressed equivalently in the form

$$\text{geometric mean of } n_p = \exp(\text{mean of } \ln n_p) = \alpha d_p^{\beta}$$

$$\text{geometric standard deviation of } n_p = \exp(\text{standard deviation of } \ln n_p).$$

The regression of ln n_p on ln d_p is preferred over the regression of n_p on d_p for reasons of homoscedasticity: that is, the variance of ln n_p appears to be more nearly constant over the size range than is the variance of n_p itself.

The more recent studies of particle charging have employed monodisperse aerosols and have measured the charge imparted by means of electric mobility analysis. In this case the width of the mobility spectrum is a direct measure of the spread of the charge spectrum. If the spectrum is reasonably Gaussian in shape, the half-width at half-maximum is about 1.18 times the standard deviation. This fact may be used to estimate the standard deviation.

In viewing the information abstracted from the literature, it must be remembered that the scatter of the data points in an n_p-d_p plot or the width of the mobility spectra is partly a result of the measurement process. In the case of the n_p-d_p plot, random errors in the measurement of size and charge increase the scatter of the data. In the case of mobility analysis, imperfect monodispersity and imperfect analyzer resolution increase the width of the resulting spectra. The amount of increase in each case is very difficult to assess a postiori. Nevertheless the information regarding the charge distribution is considered useful. It will be summarized in the following parts of this section.

2.1 Literature of the 1920's and 1930's

Deutsch(1926) measured the electric charge imparted to cigarette smoke particles in a small coaxial corona. The ion concentration was estimated to be 10^8 ions/cc. The exposure

time was estimated to be .01 to 0.1 sec. The size and charge of several particles was determined by means of a Millikin type cell. A regression of ln n_p on ln d_p applied to the data from the author's figure 7 indicates that

$$\text{geometric mean of } n_p = 594 d_p^{1.65}$$

$$\text{geometric standard deviation of } n_p = 1.24$$

The particle size is expressed in microns; the size range covered is from about 0.5 to 1.3 microns.

Schweitzer(1930) used an apparatus similar to that of Deutsch (1926) to study the charging of paraffin oil droplets. The data from his table 1 has already been presented here as figure 1. For this data,

$$\text{geometric mean of } n_p = 77.8 d_p^{1.31}$$

$$\text{geometric standard deviation of } n_p = 1.20$$

The size range was 0.4 to 1.0 microns. In addition to the particles represented in figure 1, Schweitzer found an occasional particle with much higher charge. These are not considered here.

Further experiments along the lines of that carried out by Deutsch(1926) were done by Sachsse. This work is reported by Ladenburg(1930). The study involved paraffin oil droplets of larger size than those considered by Schweitzer, as well as other particulates. The data from figures 5, 6, 8, 9 and 10 of Ladenburg(1930) are characterized by geometric standard deviations of n_p between 1.26 and 1.33. The size range was 1 to 7 microns. Further information is given in table I.

Fuchs and Petrjanoff(1935) studied the effect of particle charge upon aerosol behavior. The aerosol consisted of mineral oil and was formed by condensation. The ions were formed in an airstream by means of a corona discharge from a wire brush. The charging took place within a 0.4 cubic meter smoke chamber in which the ion-laden and the particle-laden airstreams were allowed to mix. The size and charge of several particles were determined by the "photographic oscillation" method developed by the authors. A regression analysis applied to the data of their figure 3 leads to

$$\text{geometric mean of } n_p = 15.6 d_p^{2.25}$$

$$\text{geometric standard deviation of } n_p = 1.64$$

The range of particle size was 0.7 to 1.5 microns.

Fuchs, Petrjanoff and Rotzeig(1936) studied the charging of particles within a cylinder with a corona wire at its axis. The aerosol was formed by condensation of mineral oil vapor. A small stream of this aerosol was led through the cylinder, parallel to its axis and near its wall. The stream remained intact so that its time of exposure to ions could be calculated. By measuring the ion current, the authors could calculate the ion density and the electric field where the charging took place. The control of charging conditions was therefore more complete than in the earlier studies. The size and charge of several particles were again determined by the authors' "photographic oscillation" method. For three sets of data, the geometric standard deviation of n_p was 1.29, 1.30, and 1.22. The size range was 1 to 6 microns. Further details of this work

are given in table I.

Fuchs, Petrjanoff and Rotzeig comment explicitely on the scatter of the data points in their n_p-d_p plots. They estimate that the uncertainty in the determination of particle charge was 10% for 1.2 micron diameter particles and 3% to 5% for particles larger than 2 microns. The uncertainty in the size determination was about 1/3 as large as that for the charge. The observed scatter is larger than these estimates, indicating that it is at least partly due to unequal charging. The authors say that the scatter is primarily due to tha fact that some particles are exposed to ions for a longer time than others. In connection with the smaller particles, the authors mention also "statistical effects".

2.2 Literature of the 1950's and 1960's

Goyer, Gruen and LaMer(1954) again took up the question of the charge acquired by aerosol particles on exposure to gaseous ions. In this study, the LaMer-Sinclair generator was used to generate monodisperse dioctyl phthalate aerosols. The size could be determined by light scattering methods involving higher order Tyndall spectra. The charging process made use of ions produced within a coaxial corona, but the actual charging took place in a chamber outside the corona cylinder. The size and charge of individual particles was determined by means of a Millikin type cell.

The results reported by the above authors include the relative standard deviation, or coefficient of variation, of n_p. This ratio appeared to be independent of the corona current but

dependent on particle size. For 0.75 micron diameter particles, this ratio was 0.25. The authors note that the aerosols used were not perfectly monodisperse. They suggest that the width of the charge distribution may be closely related to the width of the size distribution. Further details may be found in table I.

Perhaps the most extensive study of particle charging to date is that of Hewitt(1957). He used monodisperse dioctyl phthalate aerosols generated by the LaMer-Sinclair generator. The charging unit designed by him permitted the parameters of the charging process to be varied over a wider range than in the previous studies. For charge measurement, Hewitt employed an electric mobility analyzer. This device separates out the fraction of the aerosol which has electric mobility in the range Z_p to Z_p+dZ_p, where Z_p can be selected at will. The amount of aerosol within this range was determined photometrically. The size of the aerosol particles was determined by light scattering methods based on higher order Tyndall spectra.

Among the data reported by Hewitt are some pertaining to the width of the mobility spectra. For example, the mobility spectrum for a 0.26 micron diameter aerosol given in the author's figure 3 is nearly Gaussian in shape. The mode is equivalent to 20 charges and the full-width at half-maximum is equivalent to 5.4 charges. Since for a Gaussian distribution the full-width at half-maximum is 2.36 times the standard deviation, the latter quantity is estimated to be 2.3 charges. Additional data, read from Hewitt's figures 12 and 15, are shown in table I.

An indication of the mobility analyzer resolution and of the aerosol monodispersity in Hewitt's experiments is provided by his figure 4. This depicts the mobility spectrum for a weakly charged 0.26 micron aerosol. Peaks corresponding to single, double and triple charged particles are evident. For the first two peaks, the full-width at half-maximum is 0.2 times the corresponding mode. This proves that the aerosols used by Hewitt were very nearly monodisperse and that the resolution of his mobility analyzer was also good. The author himself estimates that the effect of imperfect mobility analyzer resolution is to increase the ratio of full-width at half-maximum to mode by 0.1. This correction has not been applied to the data presented in table I.

Drozin and LaMer(1959) considered particle charging as a preliminary to particle size analysis. The aerosols were monodisperse stearic acid. The ions were generated by means of a wire-in-cylinder corona. The particle charge was determined either by observations on individual particles in a Millikin cell or by measurement of the "frontal velocity" of an aerosol cloud. The author's figure 2 is an n_p-d_p diagram. The result of a regression analysis on these data is given in table I. The geometric standard deviation is 1.12. However, it is not clear whether the data points in the author's figure 2 refer to individual particles or to an average charge computed from the moving front of a cloud of charged particles. If the latter is true, the scatter in the data points has nothing to do with the charge distribution; it reflects only measurement errors.

As reported by Whitby and Peterson(1965, p.71), Whitby and McFarland studied the charging of 1.0 micron solid particle aerosols in a large chamber into whose center ions were injected. The charge distribution was ascertained through mobility analysis. The geometric standard deviation was found to be 1.2.

Whitby and Peterson(1965) studied both bipolar and unipolar charging of monodisperse aerosols in a flow system. The aerosols were generated by atomizing solutions of uranine dye, then evaporating off the solvent to leave small solid particles. Ions were generated by means of a sonic jet corona and injected into the aerosol duct. Some distance downstream a sample of the aerosol was removed and subjected to electric mobility analysis. The authors report that for a 1.2 micron aerosol charged by unipolar ions, the geometric standard deviation was 1.92.

Whitby, Liu and Peterson(1965) studied the charging and decay of monodisperse aerosols within a 2000 cubic foot room. The aerosols were formed by atomizing solutions of uranine dye and evaporating the solvent. After the room was filled with aerosol, an ion source at the center of the room was turned on. Starting ten minutes later, an aerosol sample was drawn into an electric mobility analyzer. The authors' table IV reports the average, median and geometric standard deviation of charge for several particle sizes and several charging conditions. These are entered into table I, where the average is taken as the arithmetic mean, and the median is taken as the geometric mean. The geometric standard deviation of n_p is seen to vary from 1.32 to 3.04 for these studies.

Lundgren and Whitby(1965) reported on the charging of particles upon passage through an intense corona discharge. As in the studies just above, the aerosol was formed by atomizing a solution of uranine dye, then evaporating the solvent. After passage through the charging device, a portion of the aerosol was drawn into a parallel plate electric mobility analyzer. The geometric mean and geometric standard deviation of n_p are listed in table I. The latter quantity varied from 1.18 to 1.38 for the conditions studied.

In the charging study of Dötsch, Friedrichs, Knake and Krahe(1969), 1.3 micron diameter dioctyl phthalate particles were charged by exposure to unipolar ions generated by alpha particles. (The ions of opposite sign were drawn away from the charging region by means of an electric field.) The charge on individual particles was determined by means of a Millikin cell. The authors say that the measured charges revealed considerable dispersion even under uniform charging conditions. Typically, 40 particles were measured as to charge at each charging condition and the relative standard deviation was 25%.

In a recent thesis, Bademosi(1971) presented theory and data for the diffusion charging of "Knudsen" aerosols, that is, aerosols for which the particle diameter is of the same order of magnitude as the mean free path of the gaseous ions. The aerosols used in the experiments consisted of polystyrene particles, generated by diluting, atomizing and drying a polystyrene latex. These aerosols were highly monodisperse. The charger used was a modification of Hewitt's(1957) charger. The charge distributions

were determined by means of an electric mobility analyzer. Bademosi was able to operate the mobility analyzer in such a way that the charge distribution could be determined without exact knowledge of the analyzer flow rates, voltage or resolution or of the particle diameter. Thus, several potential sources of error were eliminated.

Bademosi presents data from four carefully conducted tests. His figures I.6.2.4, I.6.2.5, I.6.2.6 and I.6.2.10 show that the experimental charge distributions were Gaussian. The data from three tests of 0.5 micron diameter particles, charged at different total pressure, are given in his tables I.6.2.1, I.6.2.2 and I.6.2.3. From these data, we may calculate that the arithmetic standard deviation of charge is 1.60, 1.54 and 1.73 charge units, respectively. The data from one test on 0.357 micron diameter particles is given in his table I.6.2.4. These data imply the value 1.34 for the arithmetic standard deviation of charge. Bademosi's results are also summarized in our table I.

2.3 Summary of experimental results from the literature

The literature results regarding the charge distribution for aerosols which have been exposed to unipolar gas ions are summarized in table I. If the aerosol used in a particular test was monodisperse, the size of the particles is listed in the particle diameter column. If the aerosol was polydisperse, the range of sizes is given. The center of the charge distribution is given by the arithmetic mean or the geometric mean, or both. In those experiments where a polydisperse aerosol was employed, two numbers

Table I

Summary of experimental information
concerning the width of the charge distribution

reference	comments: nt in sec/cc E in volts/cm	part.dia. microns	arithmetic		geometric	
			mean ch.	st'd dev.	mean charge	st'd dev.
Deutsch(1926), figure 7	nt = 10^6-10^7	0.5-1.3			$594d_p^{1.65}$	1.24
Schweitzer(1930), table I		0.4-1.0			$77.8d_p^{1.31}$	1.20
Sachsse, as figure 5		1.0-3.0			$55.8d_p^{1.91}$	1.26
reported by figure 6		3.0-7.0			$13.4d_p^{1.60}$	1.32
Ladenberg(1930) figure 8		1.0-7.0			$160d_p^{1.82}$	1.33
figure 9		3.0-7.0			$255d_p^{1.86}$	1.29
figure 10 -		3.0-7.0			$157d_p^{2.26}$	1.29
Fuchs and Petrjanoff(1935), figure 3		0.7-1.5			$15.4d_p^{2.25}$	1.64
Fuchs, Petrjanoff figure 3	nt = 3.3×10^5 E = 556	1.5-6.0			$6.37d_p^{1.91}$	1.29
and Rotzeig(1936) figure 4	nt = 4.6×10^5 E = 732	1.0-5.0			$6.59d_p^{1.56}$	1.30
figure 5	nt = 5.1×10^5 E = 940	2.5-4.0			$1.00d_p^{1.87}$	1.22
Goyer, Gruen and LaMer(1954), table II		0.6		25%		
		0.75		25%		
		0.8		20%		
		0.88		15%		
Hewitt(1957), figures 12 and 15	nt = 0.1×10^7 E = 3600	0.28	10	3.1		
	nt = $.25\times10^7$ E = 3600	0.28	13	2.9		
	nt = 0.5×10^7 E = 3600	0.28	18	2.9		
	nt = 1.0×10^7 E = 3600	0.28	23	2.9		
	nt = 2.0×10^7 E = 3600	0.28	27	2.9		
	nt = 4.0×10^7 E = 3600	0.28	32	2.7		
	nt = 5.8×10^7 E = 3600	0.28	34	2.5		
Drozin and LaMer(1959), fig.2		0.8-1.3			$42.4d_p^{2.12}$	1.12
Whitby and Peterson(1965),p71		1.2	30			1.92
Whitby and McFarland, ibid.		1.0	43			1.2

Table I, continued

reference	comments: nt in sec/cc E in volts/cm	part.dia. microns	arithmetic mean ch.	arithmetic st'd dev.	geometric mean charge	geometric st'd dev.
Lundgren and Whitby(1965), table II		0.1			6	1.26
		1.0			90	1.36
		1.0			150	1.38
		1.0			320	1.18
Whitby, Liu and Peterson(1965), table IV		.049	1.29		0.51	1.79
		.049	0.90		0.39	1.80
		0.103	3.58		2.40	1.54
		0.103	2.46		1.20	1.87
		0.26	12.56		7.60	2.42
		0.26	10.83		7.50	2.27
		0.26	3.00		2.40	1.62
		0.26	11.10		9.50	1.40
		0.26	8.90		7.20	1.32
		1.0	101.8		59.0	2.37
		1.0	92.0		48.0	2.25
		1.0	41.5		32.5	1.60
		1.0	87.0		46.0	3.04
		1.0	68.8		42.0	2.67
		2.2	139.0		95.0	2.00
		2.2	127.1		100.0	1.92
		3.6	234.0		142.0	2.18
		3.6	225.0		132.0	2.42
Dötsch, et al(1969), p.27		1.3	25%			
Bademosi(1971) table I.6.2.1	nt=2.4×10^6, 0.15atmos.	0.5	16.56	1.60		
	nt=2.4×10^6, 0.40atmos.	0.5	14.96	1.54		
	nt=2.4×10^6, .934atmos.	0.5	11.19	1.73		
	nt=2.4×10^6, 0.30atmos.	0.357	10.36	1.34		

are given in the geometric mean charge column: These are the values of α and β, respectively, in the expression

$$\text{geometric mean of } n_p = \alpha d_p^{\beta}$$

determined by regression of $\ln n_p$ on $\ln d_p$.

For most entries in table I, the geometric standard deviation is used to characterize the spread of the charge distribution. It is seen that these values range from 1.12 to 3.04, with most values between 1.3 and 2.1. It is difficult, however, to recognize any pattern or trend among the entries in the table.

In some cases, the spread of the charge distribution has been characterized in table I by means of the arithmatic standard deviation, either absolute or relative. It is interesting to compare the results of Hewitt(1957) with those of Bademosi(1971). The particle size was comparable in the two experiments. The charger designs were also similar, although operated under somewhat different conditions. Hewitt's charge distributions have an arithmetic standard deviation of about 3.0 charge units, although this figure may need to be corrected for imperfect monodispersity and imperfect analyzer resolution. Bademosi(1971) finds an arithmetic standard deviation of 1.6 - approximately half that found by Hewitt. Hewitt's value is, in fact, rather similar to that found by Bademosi prior to his modification of the charger.

It is perhaps well to reiterate that, except for the data of Bademosi(1971), the standard deviations listed in table I reflect not only the spread of the charge distribution, but also the dispersive effects of the measurement process.

2.4 Theoretical studies of the distribution of electric charge among the aerosol particles

Theoretical discussions of the electric charging of aerosol particles upon exposure to gaseous ions have mostly concentrated on the mean charge imparted. This is, of course, the most important and difficult part of the charging question. The secondary question of how the net charge of an aerosol is distributed among the individual particles has, however, been discussed in some recent articles. These will be reviewed here. A related aspect of aerosol charging - the charge acquired upon exposure to bipolar gaseous ions - will also be reviewed briefly.

When aerosol particles are exposed to bipolar gaseous ions (as in the atmosphere), some particles acquire negative, and others positive, charge. If the exposure is sufficiently prolonged, a stationary state is reached where the charge distribution no longer changes with time. This distribution has been discussed by Lissowski(1940), Gunn(1955), Keefe, Nolan and Rich (1959) and others. It is generally agreed that under certain conditions the charge distribution is given by a discrete form of the Gaussian distribution:

$$\text{fractional number of particles with charge } n_p = \frac{\exp(-\frac{1}{2}n_p^2/b)}{\sqrt{(2\pi b)}} \qquad (1)$$

where

$b = \frac{1}{2}d_p k_b T_a/\varepsilon^2$, the "electrical size" of the particle

k_b = Boltzmann's constant

T_a = the absolute temperature

The variance of this distribution is just b, which also serves as a dimensionless particle size.

Equation (1) is sometimes referred to as the "Boltzmann equilibrium" charge distribution. It is the simplest of several expressions available for the natural charge of an aerosol. Experiments by Lissowski(1940), Woessner and Gunn(1956) and Whitby and Peterson (1965) indicate that the expression is useful for particles larger than perhaps 0.5 microns. Fuchs(1963) has reviewed the theory of equation (1) and several of its descendents.

In the case of unipolar charging, just as in bipolar charging, a charge distribution arises as a consequence of the discreteness of electric charge. Natanson(1960) pointed out that the proper way to take account of charge disctreteness is to describe the charging process by means of a certain infinite set of ordinary differential equations. Since these equations will be discussed at some length in section 3.2, they will not be written down here. Natanson gave the solution for the first three of these equations, assuming that the aerosol is initially uncharged. Boisdron and Brock(1970) also considered this set of differential equations. They gave the complete solution for the set, again assuming that the aerosol is initially uncharged. They also present some numerical examples which indicate that under some conditions the variance of the charge distribution can be considerable. The authors state that the consequences of charge discreteness have not generally been appreciated.

Bademosi(1971) employed the set of ordinary differential equations mentioned just above in his charging study. He inte-

grated a subset of these equations, as required, for several specific cases using a Runge-Kutta numerical integration method. Several solutions are presented in his thesis. The knowledge of the full distribution of charge, instead of merely the mean charge, proved to be of great value in that work: it provided the clue that the charger was not working as it was intended.

The distribution of charge resulting from unipolar charging has been discussed by Mirzabekyan(1967). He did not employ the infinite set of differential equations mentioned above. Instead, he viewed the problem as a Markov process. Thus, consider an aerosol with r particles which currently carry m charges. The mean charge is then m/r. Now fix attention on a particular one of the r particles and suppose that it carries k charges. Define a parameter j by the equation

$$j = rk - m$$

Since r, k and m are integers, so is j. The value of j is one means of specifying the state of the particle; it is negative if the particle carries below-average charge and positive if the particle carries above-average charge. Now suppose that an additional unit of charge is forced on the aerosol. As regards the one particle under special consideration, one of two things can happen:

1. m increases by 1 but k remains unchanged
2. both m and k increase by 1

If j_o is the state of the particle before the addition of the last

charge, its state after is either

1. $j = rk - (m+1) = j_o - 1$, or
2. $j = r(k+1) - (m+1) = j_o + r - 1$

These are the definitions of the states available to the particle and the two possible transitions which may occur. Mirzabekyan then completes the statement of the Markov process by supplying the probabilities for the two transitions. These are the elements of the Markov matrix for the process. The placing of m charges on the aerosol is represented by the m^{th} power of this matrix.

Mirzabekyan made several calculations for the probability distribution of the state parameter j using a computer to perform the matrix multiplications. He found that after sufficient charge had been imparted to the aerosol, this distribution became stationary. Its shape, as shown by the author's figure 5, is nearly Gaussian. The standard deviation depended on the particle size. The standard deviations (in terms of charge units) reported by the author in table 2 are:

0.926 for a 0.136 micron diameter particle,
1.24 for a 0.34 micron diameter particle,
2.02 for a 1.2 micron diameter particle and
2.97 for a 4.0 micron diameter particle.

The value listed for the 0.34 micron particle compares well with the value 1.34 found experimentally by Bademosi(1971) for 0.357 micron particles.

3.0 THE STATISTICAL ASPECT OF THE CHARGING PROCESS

One consequence of the discrete nature of electricty is that charge cannot accumilate continuously on a particle. Instead, the particle charge must increase in discrete, discontinuous steps of magnitude ε. To say that a particle has acquired k units of charge means that exactly k discrete events have occurred involving that particle.

The charge acquired by an aerosol particle in the type of charger considered in this thesis is related to the availability of ions and to the motions of these ions. In a macroscope device such as a charger, however, it is quite impossible to control precisely the number of ions in the vicinity of any aerosol particle. Nor is it possible to precisely control the paths followed by these ions. It is quite impossible, therefore, to insure that every particle passing through the charger will acquire exactly the same number of charges.

It is the purpose of this chapter to bring together some theoretical information concerning the spread of the charge distribution under the most ideal charging conditions.

In the discussion to follow, attention will be confined to a single aerosol particle. In this way, the question of the distribution of particle size can be avoided for the time being. To simplify notation, let

a = the particle radius

k = the number of units of charge on the particle

These symbols then replace the previous notation d_p and n_p.

3.1 The time required to reach a prescribed number of charges

Consider an aerosol particle of radius a, immersed in air containing n unipolar ions per unit volume. Suppose that the particle currently carries k units of charge. We assume that the probability of acquiring an additional charge in the time interval t to t+dt is given by

$$ng_k dt$$

where g_k is independent of both n and t. ng_k may be called a transition probability and g_k alone is sometimes referred to as a combination coefficient. The determination of g_k as a function of particle radius a and other parameters is really the central problem of the theory of aerosol particle charging. In this thesis, however, we shall consider only a few simple expressions for g_k and focus our attention on the statistical side of the charging problem.

Let the time interval between the acquisition of the k^{th} charge and the $(k+1)^{th}$ charge be denoted by ΔT_k. The capital letter is used here to emphasize that this quantity is a random variable. It follows from the assumed time-independence of g_k that the random variable ΔT_k has a negative exponential distribution:

$$\text{the probability that } \Delta T_k \text{ exceeds the value t is....} \qquad \exp(-ng_k t) \qquad (2)$$

This probability distribution has mean $(ng_k)^{-1}$ and variance $(ng_k)^{-2}$.

Let the time required for an initially uncharged particle

to accumulate k charges be T_k. Obviously, T_k is the sum of the times required for the individual steps:

$$T_k = \Delta T_0 + \Delta T_1 + \ldots + \Delta T_{k-1} = \sum_{j=0}^{k-1} \Delta T_j \qquad (3)$$

T_k is then also a random variable. Its expected value, or mean, is the sum of the expected values of the summands:

$$E(T_k) = \sum_{j=0}^{k-1} E(\Delta T_j) = \sum_{j=0}^{k-1} (ng_j)^{-1} \qquad (4)$$

It may be noted for comparison that if the discreteness of charge is neglected, then the time required to reach k charges is given by the integral

$$\int_0^k (ng_j)^{-1} dj$$

This is very similar to the expression for $E(T_k)$.

It is a simple matter also to determine the variance of T_k. Since the length of time spent by the particle in the charge state j cannot influence the time spent in any other state, the random variables ΔT_j are mutually independent. Therefore the variance of T_k is the sum of the variances of the summands:

$$\mathrm{var}(T_k) = \sum_{j=0}^{k-1} \mathrm{var}(\Delta T_j) = \sum_{j=0}^{k-1} (ng_j)^{-2} \qquad (5)$$

The variance is a purely statistical quantity. It has no counterpart in the continuous approximation to the charging process.

The fact that the terms ΔT_j are mutually independent has a further benefit: the central limit theorem applies. Thus for

suitably large k, the distribution of the random variable T_k approaches the normal distribution. Using this as a guide, one can sketch the distribution for T_k. This is done in figure 2, which applies to the charging of a 1 micron particle by the White mechanism (to be discussed in section 3.2.1).

3.2 The minimum variance charge distribution

In the last section, the objective was to determine the time required to reach a prescribed charge level. While this analysis is simple and indicates clearly the statistical aspect of the charging process, it is not strictly to the point. What is desired instead is the probability p(k;a,t) that the particle will acquire exactly k charges in a prescribed time t. While this distribution could be derived from the distributions of section 3.1, it is easier to start anew.

In the analysis leading to the charge distribution p(k;a,t), the time of exposure to ions t will be considered to be known precisely. In real charging devices, however, the exposure time of individual particles cannot be precisely controlled. Obviously a spread in exposure times will increase the spread of the charge distribution. The distribution p(k;a,t) is therefore an idealized distribution. We shall refer to it as the minimum variance charge distribution.

The first term in the sequence p(k;a,t) may easily be found from the results of section 3.1. The probability p(0;a,t) that an initially uncharged particle is still uncharged at time t is obviously the same as the probability that ΔT_0 (of section 3.1) is greater than t. Hence, from equation (2),

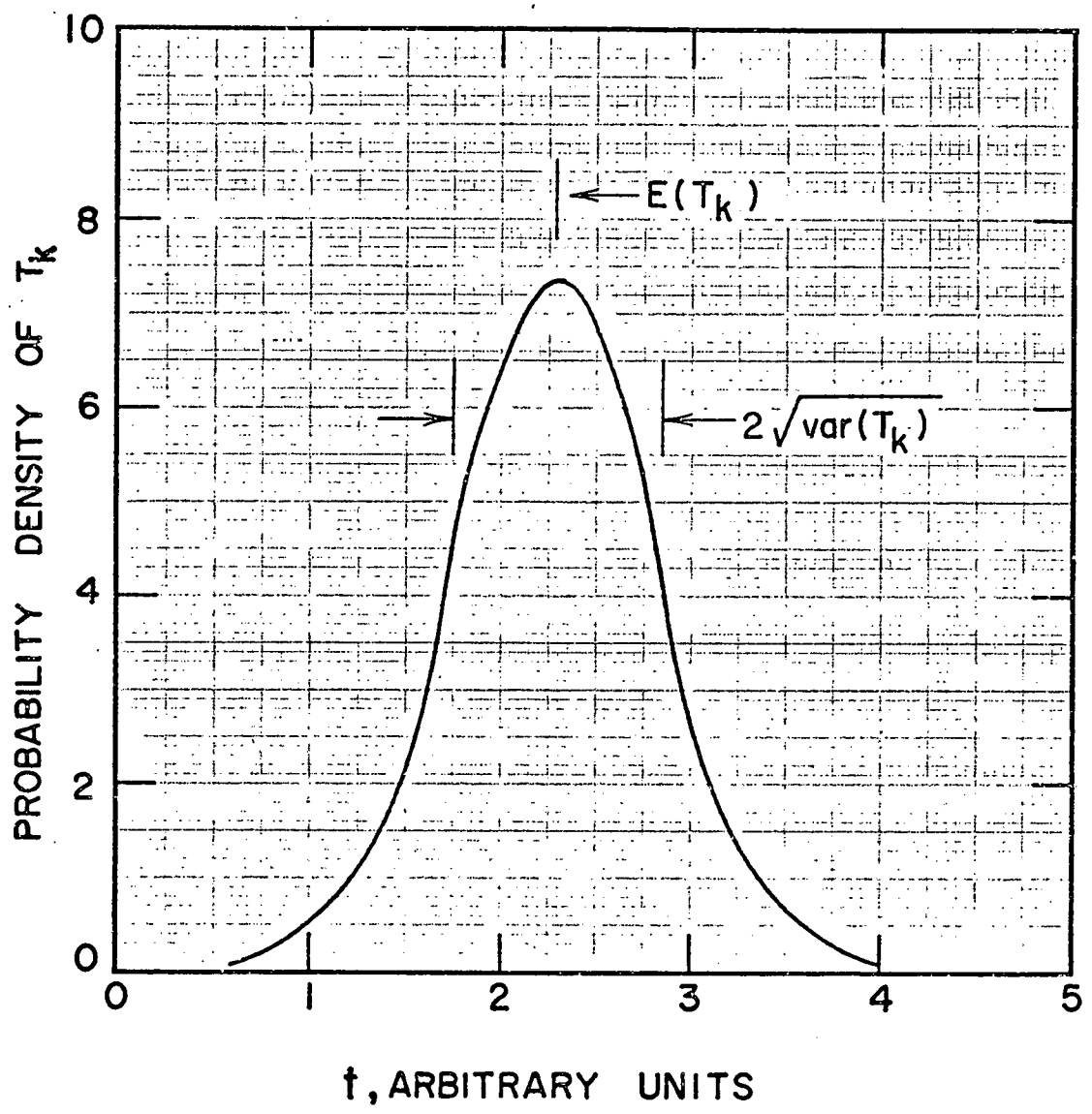

Figure 2. Probability density function for the random variable T_k.

The curve applies to a 1.0 micron particle acquiring 50 charges by the White process, to be described in section 3.2.1. The time scale is left in arbitrary units.

$$p(0;a,t) = \exp(-ng_o t)$$

The remaining p(k;a,t) may be deduced from a set of differential equations discussed by Feller(1950, chap.XVII) under the heading "the pure birth process".

Following Feller, we note that the probability that the particle carries k charges at time t+dt may be written as the sum of two probabilities:

1. the probability that the particle carries k charges at the time t and acquires no additional charge during the interval t to t+dt.
2. the probability that the particle carries k-1 charges at time t and acquires one additional charge during the interval t to t+dt.

In turn, the probability required in item 1 may be expressed as the product of the probability p(k;a,t) that the particle carries k charges at time t and the probability $(1-ng_k dt)$ that no additional charge is acquired during t to t+dt. Similarly, the probability required in item 2 is the product of p(k-1;a,t) and $ng_{k-1}dt$. Thus

$$p(k;a,t+dt) = p(k;a,t)(1-ng_k dt) + p(k-1;a,t)ng_{k-1}dt$$

In the limit as dt tends to zero, this passes over into

$$dp(k;a,t)/dt = ng_{k-1}p(k-1;a,t) - ng_k p(k;a,t) \qquad (6)$$

This is the infinite set of differential equations which has been considered in connection with the charging process by Natanson(1960) and by Boisdron and Brock(1970).

If it is assumed that the particle is known to be uncharged

at t=0, so that $p(0;a,0) = 1$ and $p(1;a,0) = p(2;a,0) = \ldots = 0$, the solution to the set of differential equations is easily found by means of Laplace transforms. Let the transforms of $p(k;a,t)$ be denoted by $P(k;a,s)$. Then

$$P(0;a,s) = \int_0^\infty e^{-ng_o t} e^{-st} dt = 1/(ng_o + s)$$

and (for $k \neq 0$)

$$sP(k;a,s) - p(k;a,0) = ng_{k-1}P(k-1;a,s) - ng_k P(k;a,s)$$

Therefore, noting that $p(k;a,0) = 0$,

$$P(k;a,s) = \frac{ng_{k-1}}{ng_k + s} P(k-1;a,s)$$

$$= \frac{ng_{k-1}}{ng_k + s} \cdot \frac{ng_{k-2}}{ng_{k-1} + s} \cdots \frac{ng_o}{ng_1 + s} \cdot \frac{1}{ng_o + s} \qquad (7)$$

$P(k;a,s)$ is therefore the product of k=1 factors. This product may be expanded in partial fractions:

$$\frac{1}{ng_o + s} \cdot \frac{ng_o}{ng_1 + s} \cdots \frac{ng_{k-1}}{ng_k + s} = \sum_{j=0}^{k} \frac{A_{kj}}{ng_j + s} \qquad (8)$$

On multiplying through by $ng_i + s$, then setting $s = -ng_i$, we find

$$A_{ki} = \frac{1}{g_o - g_i} \cdot \frac{g_o}{g_1 - g_i} \cdots \frac{g_{i-1}}{1} \cdots \frac{g_{k-1}}{g_k - g_i} \qquad (9)$$

$$= \left(\prod_{j=0}^{k-1} g_j\right) \div \left(\prod_{\substack{j=0 \\ j \neq i}}^{k} (g_j - g_i)\right)$$

The expression for P(k;a,s) is then

$$P(k;a,s) = \sum_{j=0}^{k} \frac{A_{kj}}{ng_j + s} \tag{10}$$

The inverse transform is

$$p(k;a,t) = \sum_{j=0}^{k} A_{kj} \exp(-ng_j t) \tag{11}$$

This is the minimum variance charge distribution. It has been given previously by Boisdron and Brock(1970).

From the initial conditions which were adopted in solving the differential equations, it follows that

$$p(k;a,0) = \sum_{j=0}^{k} A_{kj} = 0 \qquad \text{for } k \neq 0$$

This expression provides a check on the arithmetic involved in calculating the coefficients A_{kj}.

At this point it is necessary to consider further the transition probability ng_k. We do not propose in this thesis to present any fundamental discussion of this quantity. Instead, we assume that

> ng_k is identically equal to the steady state flow of ions to a particle carrying k units of charge.

This ion flux has been discussed several times in the literature concerning the theory of aerosol particle charging. The discussions differ in the mechanism assumed for the ion transport. We consider three of the simplest expressions for the ion flux.

3.2.1 White diffusion charging

White(1951) has proposed a simple expression for the ion flux to a particle in the case of no external electric field. Using White's expression, the transition probability ng_k becomes

$$ng_k = n\bar{c}\pi a^2 \exp\left(\frac{-k\varepsilon^2}{ak_bT_a}\right) \tag{12}$$

where

$\bar{c}$ = the mean thermal velocity of the ions

k_b = 1.38054×10^{-16} ergs/deg, Boltzmann's constant

T_a = the absolute temperature

n = the ion concentration

a = the particle radius

ε = 4.8029×10^{-10} statcoul., the elementary unit of charge

The factor $\bar{c}\pi a^2$ is the kinetic theory rate of impingement of ions on the particle for unit concentration of ions. The exponential is a Boltzmann factor which accounts for the repulsion of ions by the charge already on the particle. It has been contended recently that White's expression is valid if the particle radius is much smaller than the mean free path ions (see Fuchs, 1969).

For convenience, let

$b = ak_bT_a/\varepsilon^2$, the "electrical size" of the particle

Then the coefficients in the partial fraction expansion (8) are

$$A_{kj} = \left(\prod_{i=0}^{k-1} \exp(-i/b)\right) \div \left(\prod_{\substack{i=0 \\ i\neq j}}^{k} \{\exp(-i/b) - \exp(-j/b)\}\right)$$

and the minimum variance charge spectrum (11) is

$$p(k;a,t) = \sum_{j=0}^{k} A_{kj} \exp(-n\bar{c}\pi a^2 t e^{-j/b}) \qquad (13)$$

Several charge spectra computed from this expression are shown in figures 3 and 4. The time given in these figures is a dimensionless time given by $n\bar{c}\pi a^2 t/b^2$. The factor b^2 is included to make this parameter independent of particle size.

It is seen in figure 3 that for a given dimensionless time, the spread of the charge spectra increases with increasing particle size. From figure 4 it is seen that for a given particle size the spread of the charge spectrum is practically independent of exposure time. The effect of increasing exposure time is merely to move the entire spectrum rightward. Descriptive statistics for the minimum variance charge distribution assuming White charging are presented in appendix A. The statistics presented are arithmetic mean charge, arithmetic standard deviation, geometric mean charge and geometric standard deviation.

A check on the arithmetic involved in calculating $p(k;a,t)$ was performed by calculating the sum

$$\sum_{j=0}^{k} A_{kj}$$

for a particle diameter of 1 micron and for k = 1 to 130. Although the computer used to evaluate these sums carries about 14 significant digits in all calculations, most of these sums were zero to 4 or 5 places only. The reason for this loss of significance is roundoff: the individual terms of the sum are large and they alternate in sign, creating roundoff difficulties.

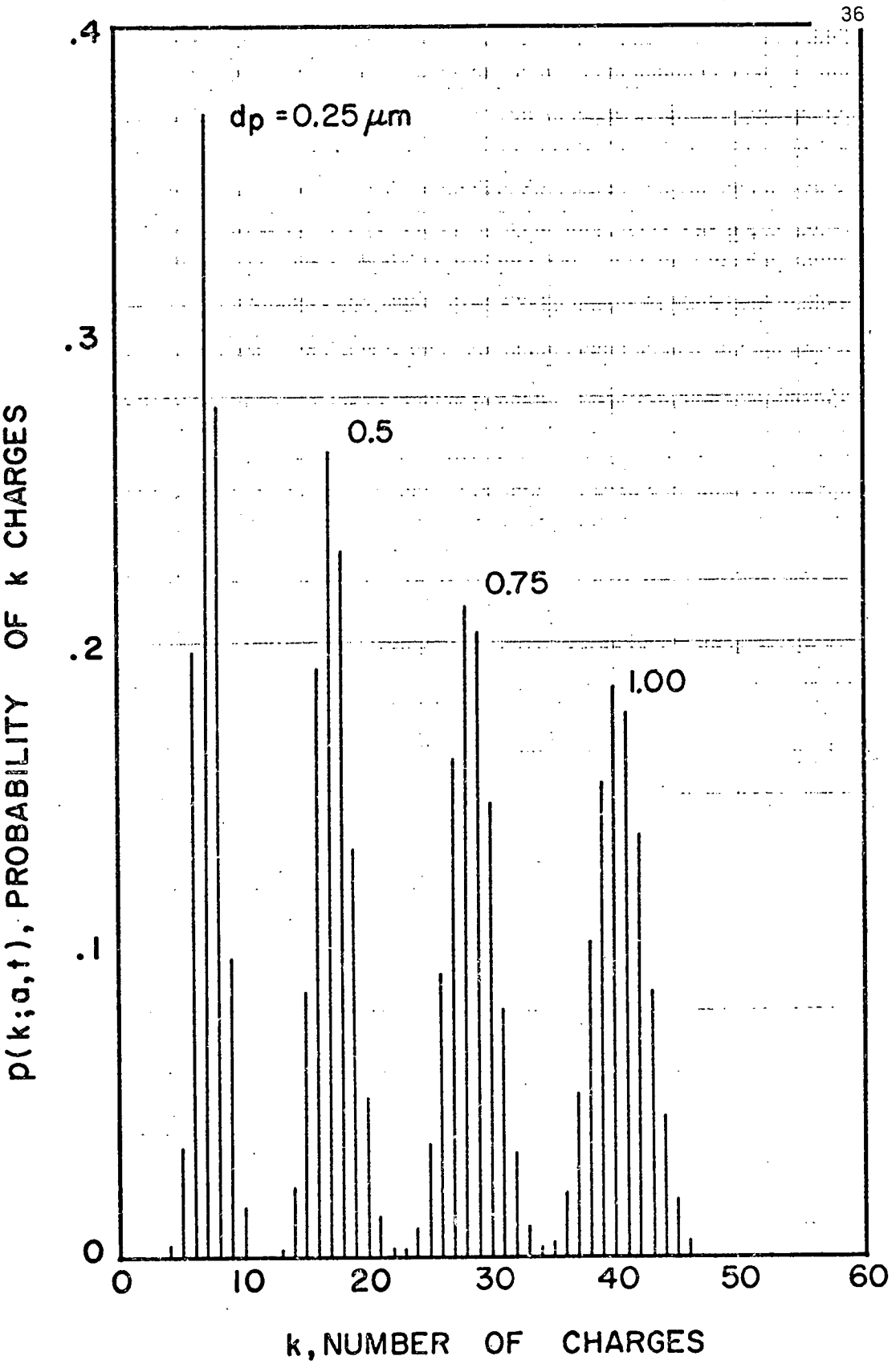

Figure 3. Minimum variance charge spectra based on White charging. The dimensionless charging time $\pi(a/b)^2\bar{c}nt$ is 10.

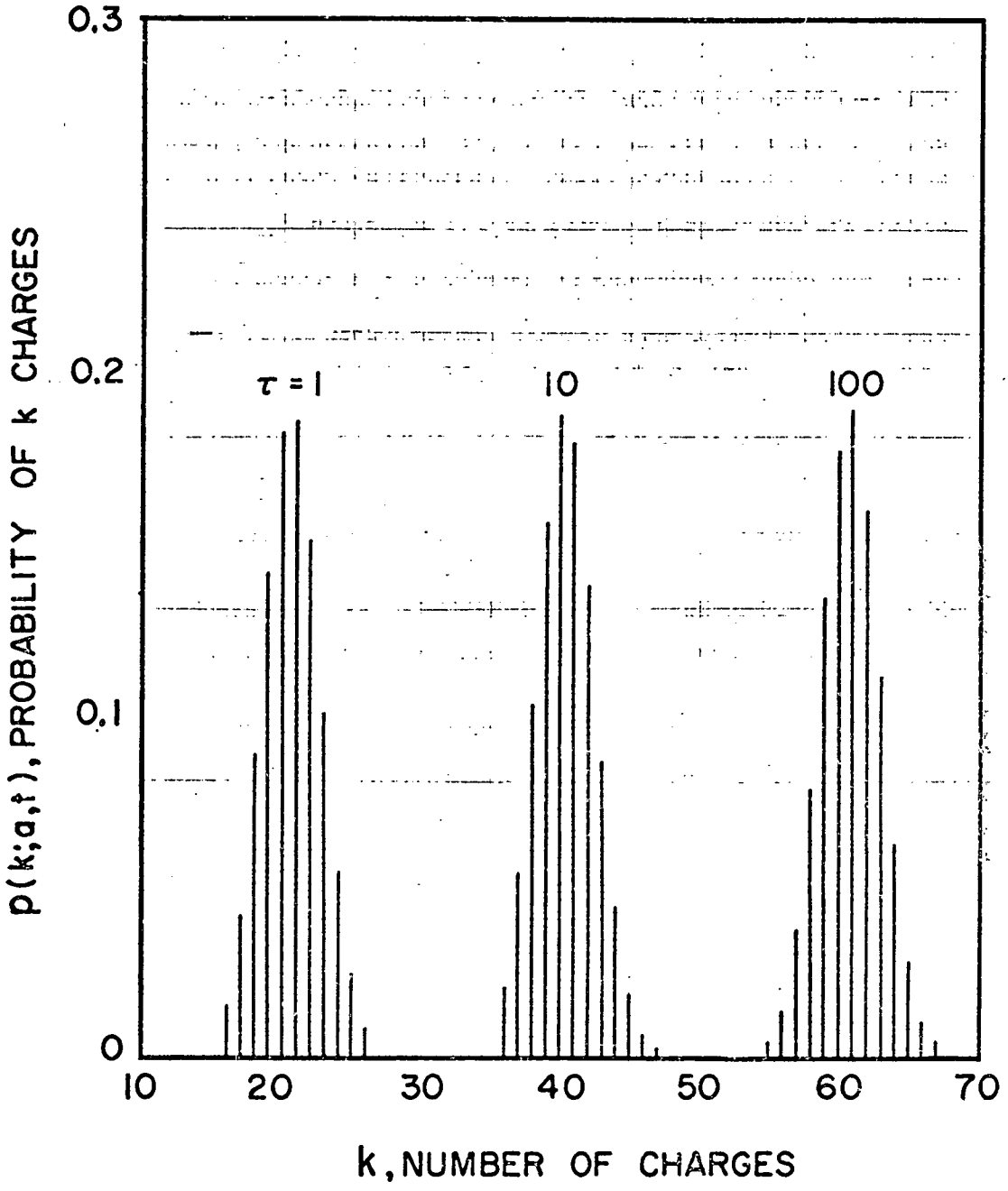

Figure 4. Minimum variance charge distributions based on White charging.

The three distributions pertain to a 1 micron diameter particle. τ is the dimensionless time $\pi(a/b)^2\bar{c}nt$.

We may note that the roundoff problem will be less severe when evaluating $p(k;a,t)$ for $t > 0$, since here each term of the sum is less in absolute value than the corresponding term of the sum just above. It is believed that the values in appendix A are correct to the number of digits given.

3.2.2 Continuum diffusion charging

Another simple expression for the flux of ions to a particle arises from the application of Fick's law to the charging process. Here it is assumed that the ion transport is a continuum diffusion process modified by the electric field due to the particle. Several authors have treated the charging process on this basis. Lissowski(1940) finds

$$ng_k = 4\pi aDn \qquad \text{if } k = 0$$

$$ng_k = \frac{4\pi aDnk}{b(e^{k/b} - 1)} \qquad \text{if } k \neq 0 \tag{14}$$

where

D = the diffusion coefficient of the ions

$b = Da/(\epsilon Z_i)$

Z_i = the electric mobility of the ions

Since Fick's law applies only to macroscopic systems, these expressions can only be expected to be valid if the particle size is much larger than the mean free path of the ions. Several authors have attempted to modify these formulas to extend their range of applicability. Recently, however, Mirzabekyan(1967) has contended that equation (14) does not lead to serious error

for particles larger than 0.1 microns diameter.

In view of Einstein's relation $\varepsilon D = k_b T_a Z_i$, the parameter b may also be written as

$$b = ak_b T_a/\varepsilon^2$$

so that b is again the "electrical size" of the particle.

Several minimum variance charge spectra calculated using the continuum diffusion expression for the ion flux are shown in figures 5 and 6. The dimensionless time reported in these figures is defined as

$$\varepsilon\pi Z_i nt \equiv \pi aDnt/b$$

By comparison to figures 3 and 4, it is seen that continuum diffusion charging leads to charge spectra which are somewhat broader than for White charging. Also, the spectrum width is more dependent on exposure time in the case of continuum diffusion charging than for White charging. Descriptive statistics for the minimum variance charge distribution assuming continuum diffusion charging appear in appendix B.

3.2.3 Field charging

The previous two expressions for the ion flux to a particle have both assumed no applied electric field. If a uniform electric field is applied to the particle and its neighborhood, the motion of the ions will be affected. If the field is strong, the random thermal motion of the ions may be neglected in comparison to their orderly drift along the field lines. This process is called field charging. According to White(1951), the

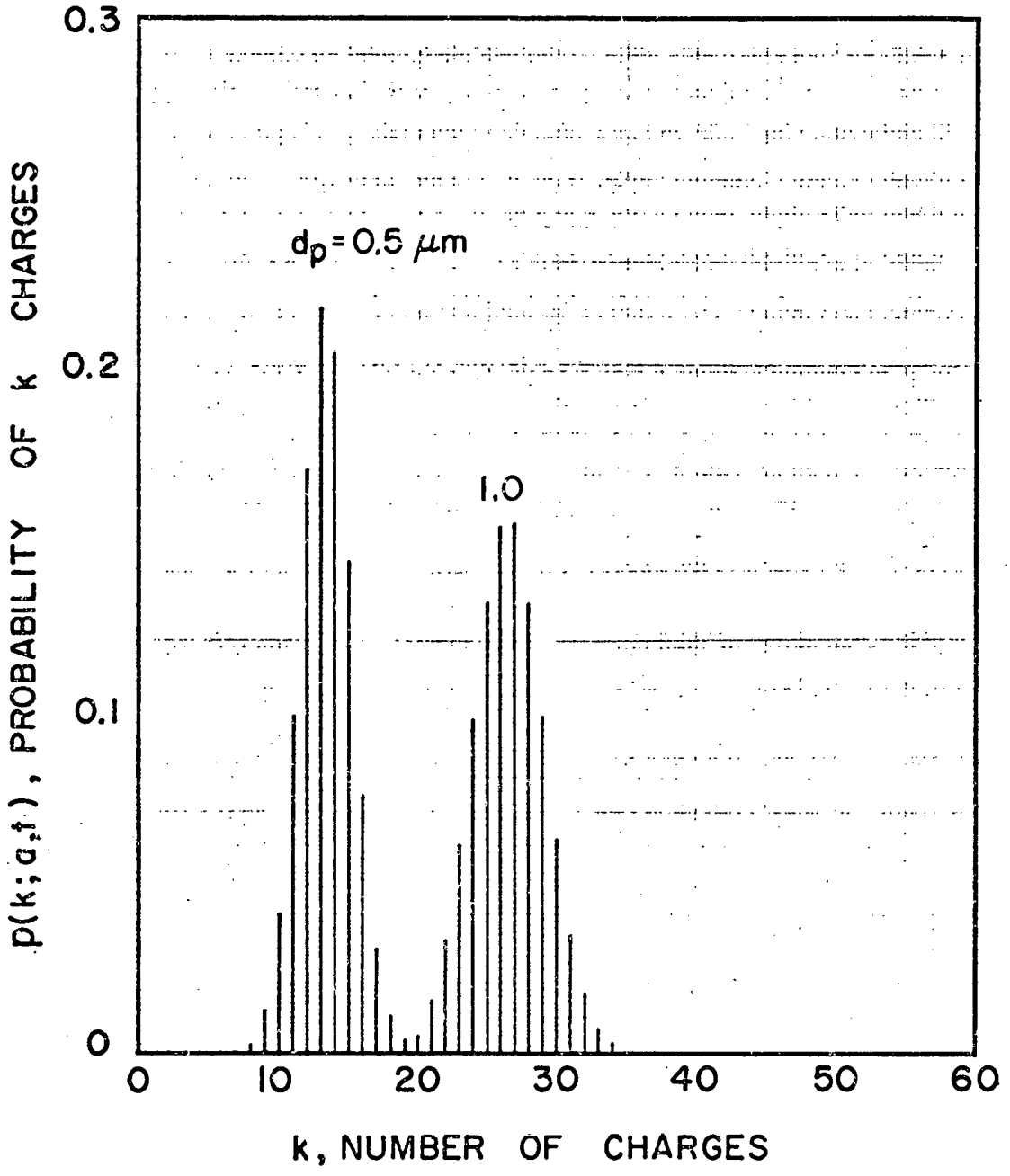

Figure 5. Minimum variance charge distributions based on continuum diffusion charging.

The dimensionless charging time $\pi(a/b)Dnt = \pi\varepsilon Z_i nt$ is 2 units for both spectra.

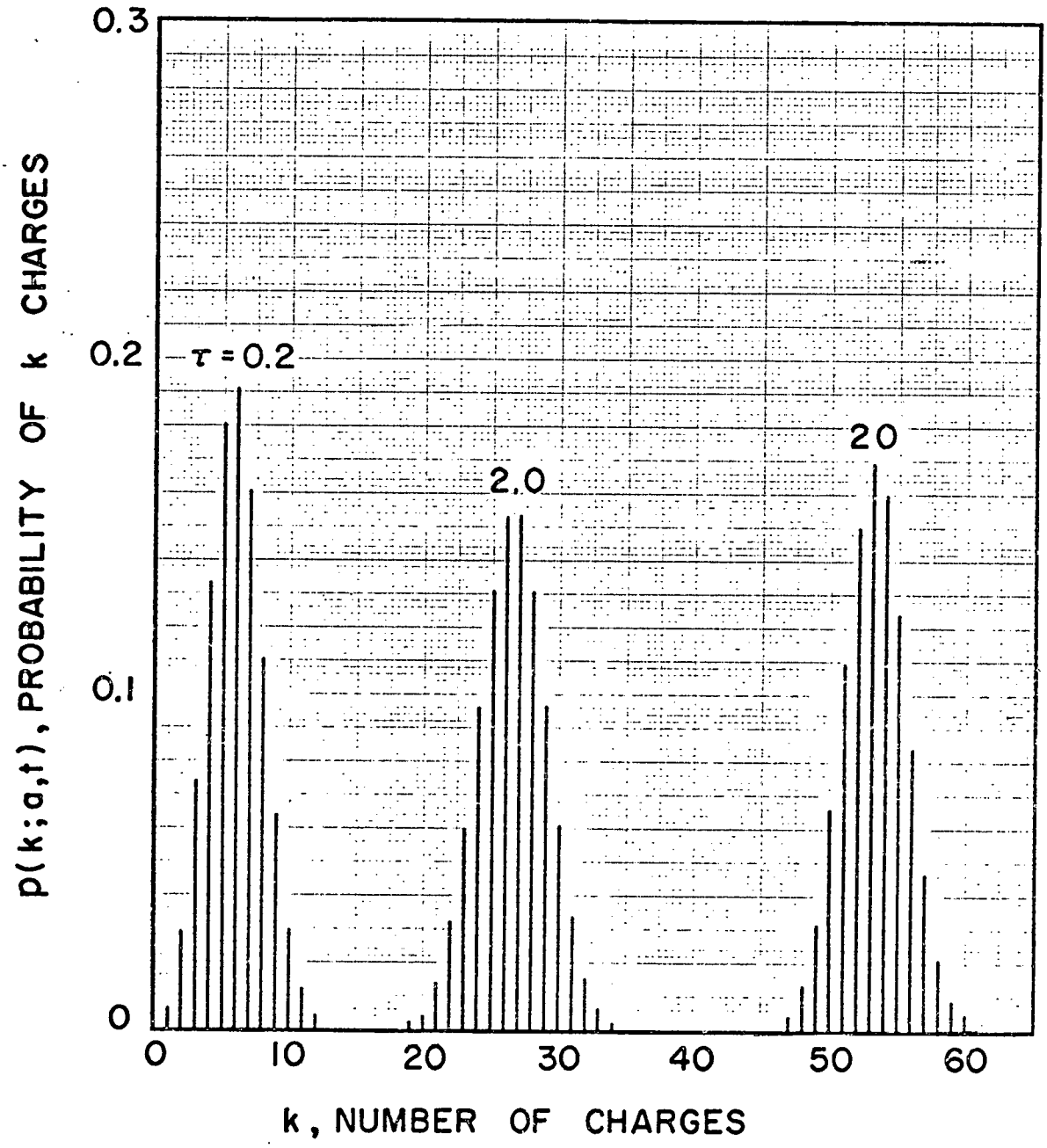

Figure 6. Minimum variance charge distributions based on continuum diffusion charging.

The three distributions all pertain to a 1.0 micron diameter particle. τ is the dimensionless time $\pi(a/b)Dnt = \pi\varepsilon Z_i nt$.

resulting ion flux is

$$ng_k = \pi\varepsilon Z_i n(k_s - k)^2/k_s \qquad (15)$$

where

$k_s = \frac{a^2E_o}{\varepsilon} \cdot \frac{3K}{K+2}$, the saturation charge for the particle

E_o = the applied electric field

K = the dielectric constant of the particle.

The remaining symbols have been defined previously. The saturation charge k_s is the particle charge such that the repulsing field just equals the applied field at the surface of the particle.

Several minimum variance charge spectra based on field charging are presented in figures 7 and 8. Descriptive statistics are presented in appendix C. The dimensionless time in the figures and in the appendix is given by $\pi\varepsilon Z_i nt$. Figure 7 shows how the charge spectra shift and broaden with k_s. Figure 8 shows the dependence of the spectra on exposure time.

The roundoff problem was so severe for field charging that the critical parts of the calculation had to be done in double precision on the computer.

3.3 Approximate expressions for the mean and variance of the minimum variance charge distribution

The exact expression for the minimum variance charge distribution (equation (11) given in section 3.2) is not convenient for calculation. Computations based on it are laborious and

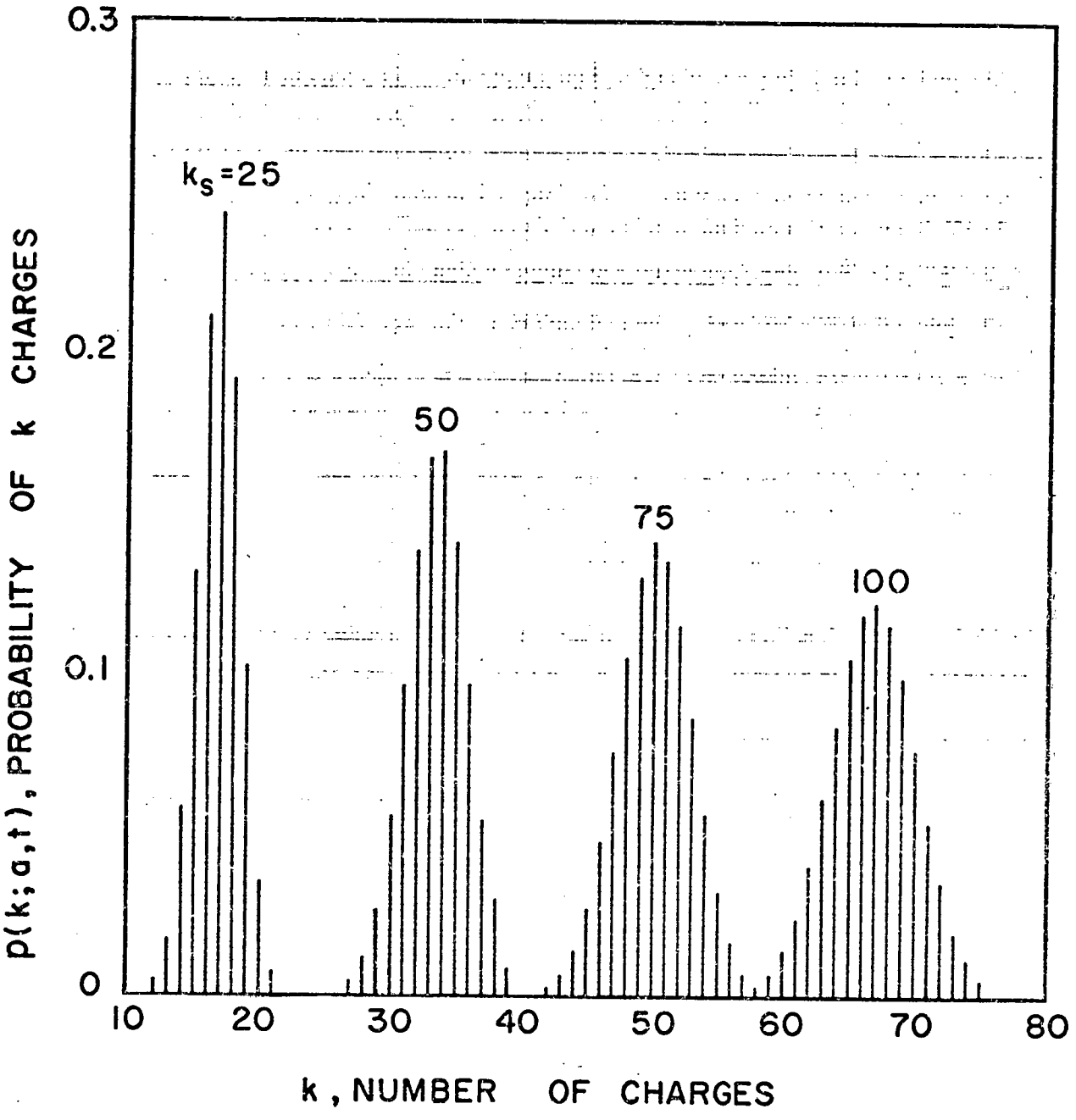

Figure 7. Minimum variance charge distributions based on field charging.

The dimensionless exposure time $\pi\varepsilon Z_i nt$ equals 2 units for each spectrum.

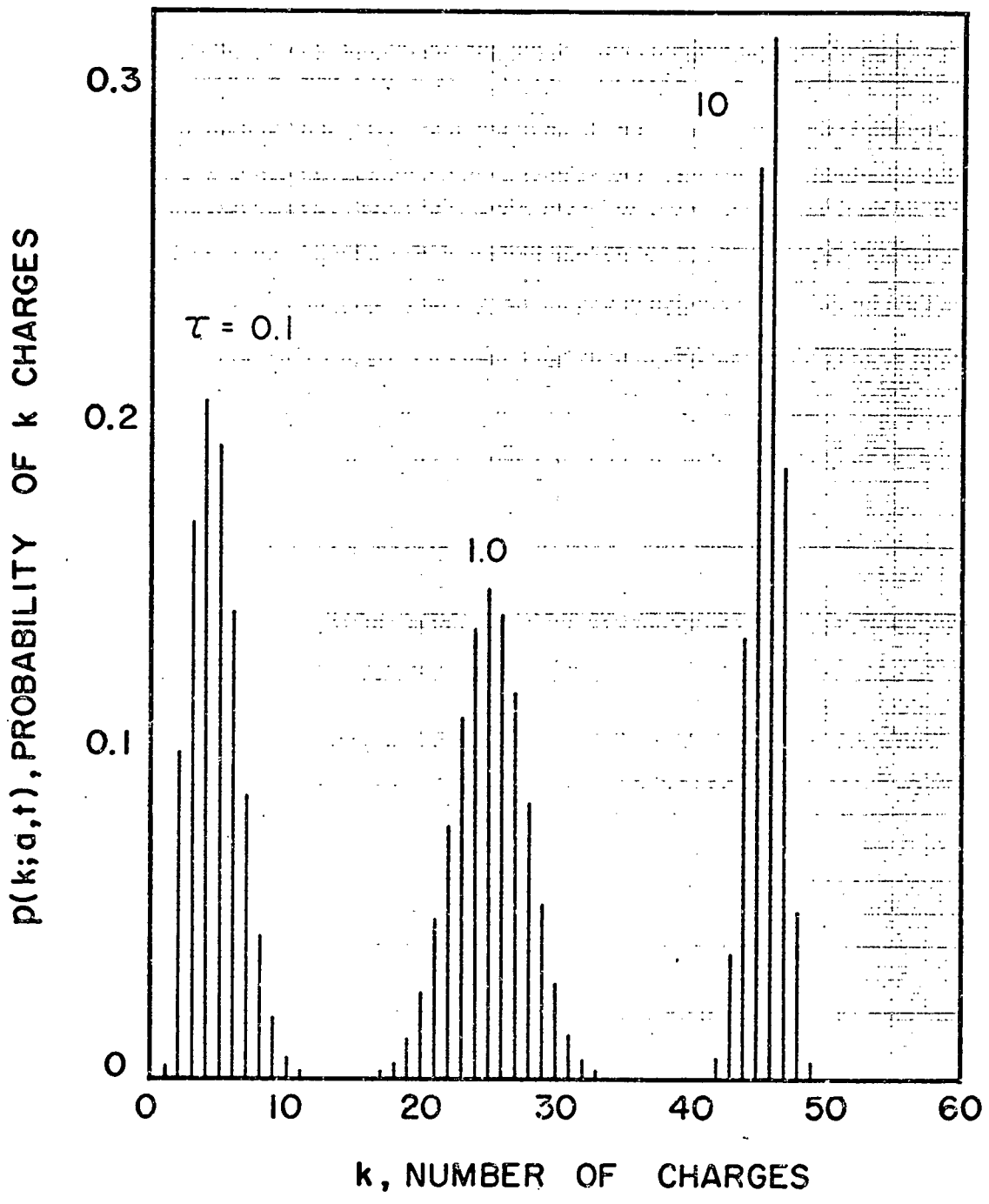

Figure 8. Minimum variance charge distributions based on field charging.

The three distributions pertain to a saturation charge k_s of 50 units. The dimensionless exposure time τ is $\pi\varepsilon Z_i nt$.

they are sometimes afflicted with roundoff errors. Furthermore, this expression gives more information than is really needed in many cases. What is desired now is a shortcut method for computing the mean and variance of the minimum variance charge distribution. Approximate expressions for these two quantities will be proposed in this section.

The mean $\bar{k}$ of the minimum variance charge distribution is defined by

$$\bar{k} = \sum_{k=1}^{\infty} kp(k;a,t)$$

The rate of change of $\bar{k}$ is

$$d\bar{k}/dt = \sum_{k=1}^{\infty} kdp(k;a,t)/dt$$

But according to equation (6) of section 3.2,

$$dp(k;a,t)/dt = ng_{k-1}p(k-1;a,t) - ng_k p(k;a,t) \qquad (6)$$

Hence

$$d\bar{k}/dt = \sum_{j=1}^{\infty} jng_{j-1}p(j-1;a,t) - \sum_{k=1}^{\infty} kng_k p(k;a,t)$$

$$= \sum_{k=0}^{\infty} (k+1)ng_k p(k;a,t) - \sum_{k=0}^{\infty} kng_k p(k;a,t)$$

$$= \sum_{k=0}^{\infty} ng_k p(k;a,t) \qquad (16)$$

Thus the rate of change of $\bar{k}$ is equal to the mean value of ng_k. The mean square $\overline{k^2}$ of the charge distribution is defined by

$$\overline{k^2} = \sum_{k=1}^{\infty} k^2 p(k;a,t)$$

Hence

$$d\overline{k^2}/dt = \sum_{j=1}^{\infty} j^2 n g_{j-1} p(j-1;a,t) - \sum_{k=1}^{\infty} k^2 n g_k p(k;a,t)$$

$$= \sum_{k=0}^{\infty} (k+1)^2 n g_k p(k;a,t) - \sum_{k=0}^{\infty} k^2 n g_k p(k;a,t)$$

$$= \sum_{k=0}^{\infty} (2k+1) n g_k p(k;a,t) \qquad (17)$$

The variance σ^2 of the charge distribution may be expressed as

$$\sigma^2 = \overline{k^2} - (\bar{k})^2$$

Its time derivative is then

$$d\sigma^2/dt = d\overline{k^2}/dt - 2\bar{k}d\bar{k}/dt$$

$$= \sum_{k=0}^{\infty} (2k+1) n g_k p(k;a,t) - 2\bar{k} \sum_{k=0}^{\infty} n g_k p(k;a,t)$$

$$= \sum_{k=0}^{\infty} \{1 + 2(k-\bar{k})\} n g_k p(k;a,t) \qquad (18)$$

Thus far no approximations have been made.

The next step is to expand ng_k in a Taylor's series about $k=\bar{k}$:

$$ng_k = \alpha + \beta(k-\bar{k}) + \tfrac{1}{2}\gamma(k-\bar{k})^2 + \ldots \qquad (19)$$

where

$$\alpha = ng_k\Big|_{k=\bar{k}}, \quad \beta = \frac{d(ng_k)}{dk}\Big|_{k=\bar{k}}, \quad \gamma = \frac{d^2(ng_k)}{dk^2}\Big|_{k=\bar{k}}$$

Making use of this expansion, equations (16) and (18) become

$$d\bar{k}/dt = \sum_{k=0}^{\infty} \{\alpha + \beta(k-\bar{k}) + \tfrac{1}{2}\gamma(k-\bar{k})^2 + \ldots\}p(k;a,t)$$

$$d\sigma^2/dt = \sum_{k=0}^{\infty} \{\alpha + (2\alpha+\beta)(k-\bar{k}) + (2\beta+\tfrac{1}{2}\gamma)(k-\bar{k})^2 + \ldots\}p(k;a,t)$$

Now

$$\sum_{k=0}^{\infty} p(k;a,t) = 1, \qquad \sum_{k=0}^{\infty} (k-\bar{k})p(k;a,t) = 0,$$

$$\sum_{k=0}^{\infty} (k-\bar{k})^2 p(k;a,t) = \sigma^2$$

so that

$$d\bar{k}/dt = \alpha + \tfrac{1}{2}\gamma\sigma^2 + \text{ higher order terms} \qquad (16')$$

$$d\sigma^2/dt = \alpha + (2\beta+\tfrac{1}{2}\gamma)\sigma^2 + \text{higher order terms} \qquad (18')$$

If the higher order terms may be neglected, what remains comprises a pair of differential equations governing the variables $\bar{k}$ and σ^2. These terms will be so neglected, without a priori justification. Justification will come later by comparison to exact calculations.

If the discreteness of charge were neglected, the equation which would be used to determine the particle charge as a function of time is:

$$dk/dt = ng_k \equiv \alpha(k).$$

It is reassuring to note that this is identical to the first part of equation (16'). Thus the deterministic treatment of the charging process gives a particle charge which is approximately equal to the mean charge found in the statistical treatment.

Equation (18'), which describes the width of the charge distribution, has no such counterpart in the deterministic treatment of charging. The charge distribution width is a consequence of charge discreteness.

Equations (16') and (18') will now be applied to three specific charging mechanisms.

3.3.1 White diffusion charging

For White charging, the coefficients in the Taylor's series (19) are

$$\alpha = n\bar{c}\pi a^2 \exp(-\bar{k}/b), \quad \beta = -n\bar{c}\pi a^2 \exp(-\bar{k}/b)/b$$
$$\gamma = n\bar{c}\pi a^2 \exp(-\bar{k}/b)/b^2.$$

The symbols were defined in section 3.2.1. Thus equations (16') and (18') take the form

$$d\bar{k}/dt = n\bar{c}\pi a^2 \exp(-\bar{k}/b)\{1 + \tfrac{1}{2}\sigma^2/b^2\}$$
$$d\sigma^2/dt = n\bar{c}\pi a^2 \exp(-\bar{k}/b)\{1 + (1-4b)\tfrac{1}{2}\sigma^2/b^2\}$$

Let

$$x = \bar{k}/b, \quad y = \sigma^2/b, \quad \tau = n\bar{c}\pi a^2 t/b$$

(The dimensionless time τ given here is b times that given in section 3.2.1.) Then the equations become

$$dx/d\tau = (1 + \tfrac{1}{2}y/b)e^{-x}$$
$$dy/d\tau = (1 + \tfrac{1}{2}y/b - 2y)e^{-x}$$

We consider primarily large particles, so that the parameter b is

large. Thus the terms $\frac{1}{2}y/b$ will be dropped. Under these conditions, the solutions for the two differential equations are

$$x = \ln(\tau+1)$$

$$y = \tfrac{1}{2}\left(1 - \frac{1 - 2y_o}{(\tau+1)^2}\right) \qquad (20)$$

The initial conditions imposed are $x = 0$ and $y = y_o$ when $\tau = 0$. The first equation is the same as that obtained when the discreteness of charge is neglected (see White,1951).

Several values computed from these two expressions are given in table II. Two columns are given for the quantity y. For one of these, the initial value of y is taken as zero. For the other, $y_o = 1$. By comparing the entries in table II to the corresponding entries in appendix A, it is seen that the table II values are accurate to within 2% for particles larger than $\frac{1}{2}$ micron in diameter. The two equations therefore accurately reproduce a substantial part of appendix A.

From the equations it is seen that regardless of its initial value, the variable y quickly tends to the value $\frac{1}{2}$. That is, the variance tends to $\frac{1}{2}b$:

$$\sigma^2 \to \tfrac{1}{2}b = \tfrac{1}{2}ak_bT_a/\varepsilon^2$$

It is interesting to note that this variance is exactly one half that for the Boltzmann equilibrium charge distribution (section 2.4, equation 1).

The two initial conditions chosen for y, 0 and 1, correspond to an uncharged aerosol and to one carrying natural charge, respec-

tively, It is seen in table II that for White charging, the initial condition becomes unimportant rather quickly.

3.3.2 Continuum diffusion charging

In this case, the coefficients in the Taylor's series (19) are:

$$\alpha = 4\pi aDn\frac{1}{e^x - 1}$$

$$\beta = 4\pi aDn/b\left(\frac{1}{e^x - 1} - \frac{xe^x}{(e^x - 1)^2}\right)$$

$$\gamma = 4\pi aDn/b^2\left(\frac{-2e^x}{(e^x - 1)^2} - \frac{xe^x}{(e^x - 1)^2} + \frac{2xe^{2x}}{(e^x - 1)^3}\right)$$

where $x = \bar{k}/b$. The remaining symbols have been defined in section 3.2.2.

If we let $y = \sigma^2/b$ and $\tau = \pi aDnt/b$, the differential equations (16') and (18') for the mean and the variance take the form

$$dx/d\tau = \frac{4x}{e^x - 1} + 2y/b\left(\frac{-2e^x}{(e^x - 1)^2} - \frac{xe^x}{(e^x - 1)^2} + \frac{2xe^{2x}}{(e^x - 1)^3}\right)$$

$$dy/d\tau = dx/d\tau + 8y\left(\frac{1}{e^x - 1} - \frac{xe^x}{(e^x - 1)^2}\right)$$

We again consider large particles, so that the term divided by the "electrical size" b may be dropped. The solution corresponding to $x = 0$ and $y = y_o$ at $\tau = 0$ is

$$\tau = \int_0^x \frac{e^x - 1}{4x}\,dx$$

$$y = \frac{x^2}{(e^x - 1)^2}\left(y_o + \int_0^x \frac{(e^x - 1)^2}{x^2}\,dx\right) \qquad (21)$$

The expression for τ as a function of x is the same as that obtained if charge discreteness is neglected (see Natanson, 1960).

Several values computed from the above expressions are given in table II. Again, two y-columns are presented, one corresponding to $y_o = 0$ and the other corresponding to $y_o = 1$. By comparing the entries in table II to the corresponding entries in appendix B, it is again seen that the table II values are accurate to within 2% for particles larger than ½ micron in diameter.

In contrast to the case of White charging, the variance for continuum diffusion charging does not appear to approach a constant value as time increases. Instead (for the initial condition $y_o = 0$) the variable y first increases to the value 0.74 at $\tau = 1$, then decreases slowly. It may be seen directly from the differential equation for y, however, that for very large τ (or x) the variable y again approaches ½.

3.3.3 Field charging

For field charging the Taylor's series expansion for ng_k has only three terms. The expansion coefficients are:

$$\alpha = \pi\varepsilon Z_i n(k_s - \bar{k})^2/k_s, \quad \beta = -2\pi\varepsilon Z_i n(k_s - \bar{k})/k_s$$

$$\gamma = 2\pi\varepsilon Z_i n/k_s$$

The only higher order term in the differential equations for $\bar{k}$ and σ^2 is the one involving

$$\sum_{k=0}^{\infty} (k-\bar{k})^3 p(k;a,t)$$

that is, the third moment about the mean. Since the charge distri-

butions are known from section 3.2 to be nearly symmetric, odd moments about the mean are expected to be small. This is a partial a priori justification for dropping the one higher order term.

The differential equations for $\bar{k}$ and σ^2 are

$$dx/d\tau = (1-x)^2 + y/k_s$$
$$dy/d\tau = (1-x)^2 + y/k_s - 4y(1-x)$$

where $x = \bar{k}/k_s$, $y = \sigma^2/k_s$ and $\tau = \pi\varepsilon Z_i nt$. We consider again large particles so that the parameter k_s is large. The term y/k_s will therefore be dropped. The solution corresponding to $x = 0$ and $y = y_o$ at $\tau = 0$ is

$$x = \frac{\tau}{\tau + 1}$$
$$y = \frac{1}{3}\left(\frac{1}{\tau + 1} - \frac{1 - 3y_o}{(\tau + 1)^4}\right) \qquad (22)$$

The first equation is the familiar expression for the charge accumulated during field charging.

Several values computed from the above expressions are presented in table II. The cases $y_o = 0$ and $y_o = 1$ are both tabulated. By comparing the entries in table II to the corresponding entries in appendix C, it is seen that the expressions are accurate to within 2% for k_s larger than 25.

For the initial condition $y_o = 0$, the variable y reaches a maximum value of $(4)^{-4/3} = 0.1575$ at the time $\tau = (4)^{-1/3} - 1 = 0.588$. Thereafter, y decreases gradually to zero as time increases.

Table II

Approximate values of the mean and variance for the minimum variance charge distribution

White diffusion charging				Continuum diffusion charging				Field charging			
$n\bar{c}\pi a^2 t/b$	$x=\bar{k}/b$	$y = \sigma^2/b$		$\pi a D n t/b$	$x=\bar{k}/b$	$y = \sigma^2/b$		$\pi \epsilon Z_i n t$	$x=\bar{k}/k_s$	$y = \sigma^2/k_s$	
0	0.0	0.0	1.0	0.0	0.0	0.0	1.0	0.0	0.0	0.0	1.0
4	1.609	.4800	.5200	.2	.669	.4769	.9704	.1	.0909	.0754	.7584
8	2.197	.4938	.5062	.5	1.357	.6840	.9055	.2	.1667	.1170	.5993
20	3.045	.4989	.5011	1.0	2.096	.7426	.8289	.5	.3333	.1564	.3539
40	3.714	.4997	.5003	2.0	2.959	.7258	.7520	1.0	.5000	.1458	.2083
80	4.394	.4999	.5001	5.0	4.163	.6720	.6763	2.0	.6667	.1070	.1193
200	5.298	.5000	.5000	10.0	5.066	.6381	.6392	5.0	.8333	.0553	.0561
400	5.994	.5000	.5000	20.0	5.945	.6136	.6138	10.0	.9091	.0303	.0303
800	6.686	.5000	.5000								

3.4 The minimum variance charge distribution - concluding remarks and comparison to data

The minimum variance charge distribution defined and discussed in sections 3.2 and 3.3 exhibits a few general features which are worth mentioning. This will be done now. Also, this distribution will be compared to some of the available data.

The minimum variance charge distribution takes on a different form for each different charging mechanism. It is noteworthy, however, that for the three mechanisms (White, continuum diffusion, field) considered above, the charge distribution is nearly always symmetric about its mean. This may be seen from figures 3 through 8. The appearance of these plots suggests, in fact, that these distributions may be approximated rather well by the Gaussian distribution.

The mean of the minimum variance charge distribution depends strongly upon the mechanism assumed for the charging process, as well as on the exposure time. In this thesis, we are more concerned with the variance of the charge distribution. In this connection, it may be noted that for diffusion charging (either White or continuum), the variance σ^2 is almost always on the range $\frac{1}{2}b$ to b:

$$\tfrac{1}{2}b < \sigma^2 < b \qquad \text{for diffusion charging.}$$

For field charging, the situation is more complicated. The variance σ^2 is very nearly proportional to the parameter k_s, but it also depends strongly on exposure time as well as initial conditions.

A detailed comparison of the minimum variance charge distribution to data from the literature is possible only in those cases

where sufficient information regarding the charging conditions is available. One case is the study of Fuchs, Petrjanoff and Rotzeig (1936). In this study, the charging mechanism appears to be pure field charging. At any rate, this is the conclusion reached by the authors from the agreement between the mean charge and the corresponding field charging expression. What is desired now is a comparison of the variance as well as the mean to the appropriate expressions from theory.

The data presented by Fuchs, Petrjanoff and Rotzeig consist of observations on a limited number of particles. There is the possibility that the particles observed are not representative of the cloud as a whole. Therefore, the question of agreement between data and theory must be formulated in terms of a statistical test of hypothesis. Let the null hypothesis be:

> the data conform to the minimum variance charge distribution based on field charging.

We now develop some consequences of this hypothesis and compare them to data.

If the null hypothesis is true, then it is also true (at least approximately) that the particle charge k is a normal random variable. The mean $\bar{k}$ and the variance σ^2 both depend on the parameter k_s, which in turn depends on particle size. From section 3.3.3, equations (22),

$$\bar{k} = k_s\tau/(\tau + 1), \qquad \sigma^2 = (k_s/3)/(\tau + 1)$$

(We have assumed that $\sigma^2 = k_s/3$ at $\tau = 0$.)

A random variable whose mean and variance both depend on an

external parameter is awkward. Consider instead the quantity $(k-\bar{k})/\sigma$, which under the null hypothesis is a standard normal variable with mean and variance independent of k_s. Therefore, if m particles are observed,

$\sum_{1}^{m}(k-\bar{k})/\sigma$ is a normal variable with mean zero and variance m

$\sum_{1}^{m}(k-\bar{k})^2/\sigma^2$ is a chi-square variable with m degrees of freedom.

These are two consequences of the null hypothesis. They may easily be compared to data.

Figure 3 of the article by Fuchs, Petrjanoff and Rotzeig depicts observations on 43 particles. Under the null hypothesis, therefore, the first sum above is 95% certain to fall in the interval (-12.85, +12.85) and the second sum is 95% certain to fall within (26.4, 62.5). The values actually found for the two sums are 46.7 and 143.8, respectively. The null hypothesis may be rejected with 95% confidence.

The authors' figure 4 depicts 64 particles. 95% probability intervals for the first and second sums above are (-15.86, +15.68) and (43.3, 87.5) respectively. The sums actually found from the data are 10.24 and 188.1, respectively. Again, the null hypothesis must be rejected, in spite of the fact that the first sum falls within its prescribed range.

For the authors' figure 5, which represents 23 particles, the 95% intervals for the first and second sums are (-9.37, +9.37) and (11.7, 38.1), respectively. The actual values for the sums are 24.7 and 121.5, respectively. These values again call for the re-

jection of the null hypothesis.

Unfortunately, the statistical test employed does not provide any information as to why or in what respect the null hypothesis is false. It does appear, however, that the minimum variance charge distribution underestimates both the mean and the variance.

The other set of data which is suitable for comparison to the minimum variance charge distribution is that of Hewitt(1957, figures 12 and 15). Since these data were obtained by observation of the collective behavior of large number of particles, the problem of small-sample statistics does not arise here. Furthermore, since the aerosols used were nearly monodisperse (0.28 microns diameter) the mobility distribution is a more or less direct reflection of the charge distribution. Although the charging was carried out in a moderately strong electric field, the mean charge observed was 2 to 3 times that predicted by the field charging mechanism of section 3.2. The diffusion charging mechanisms, either White or continuum, provide slightly better fit as to mean charge. As to the variance, the quantity σ^2/b decreased from 3.85 to 2.48 with increasing exposure time. This is 3 to 6 times as large as the value predicted for σ^2/b by either of the diffusion charging mechanisms.

As has been stated previously, the experimental values for the charge distribution variance abstracted from the literature are certain to be inflated by the measurement process. Hewitt(1957) suggests a method of "deflating" the spread of the charge distributions determined by him. However, in the light of the discussion in the present chapter 5, it seems that the correction required is not as large as that suggested by Hewitt. No correction was used

here.

In the experiment of Bademosi(1971), the conditions were such that he could determine not only the mean and standard deviation of charge, but also the frequency of occurance of each number of charges. That is, Bademosi measured all members of the sequence p(0;a,t), p(1;a,t),...., p(k;a,t),.... . His theory of the charging process was based on a much more comprehensive expression for the ion flux ng_k than those considered here. (His expression includes the White and continuum diffusion expressions as limiting cases.) He found good agreement between the experimental and theoretical values of the sequence p(k;a,t). Thus the charger used by him achieved the minimum variance possible for a charge distribution.

To compare Bademosi's experimental results to the present theories, we may note that for his four tests the ratio σ^2/b had the values 0.574, 0.535, 0.673 and 0.564. All these are on the range ½ to 1, indicating again that the charge distribution widths were near the minimum.

The agreement between Bademosi's experimental value for σ and Mirzabekyan's(1967) theoretical value has already been noted at the end of section 2.4.

4 THE EFFECT OF NONUNIFORM PARTICLE EXPOSURE TIME

In the previous section, it was assumed that the time of exposure of the particle to the ion cloud was known precisely. This is not the case in real charging devices. Various factors contrive to introduce uncertainty into the length of time which an individual particle is exposed.

As an example of the impossibility of precisely controlling the time of exposure, one may cite the work of Fuchs, Petrjanoff and Rotzeig(1936). In this work the aerosol was admitted into the charging region through a 3.5 mm tube at a mean linear velocity of about 3 m/sec. After a travel of about 7 cm, the entire aerosol stream was collected in a 8 mm tube which faced the inlet tube. The stream was observed to remain intact. Nevertheless, the authors suggest that there is a distribution of velocities across the jet, with the result that particles near the centerline were exposed for a shorter time than the others. The authors attribute the scatter in their charge vs. size diagram to this nonuniform exposure time.

In this section, we shall regard the time of exposure of the particle to the ions as a random variable T_e. Its distribution will be described in terms of the density function h(t).

$$h(t)dt = \text{the probability that } t < T_e < t + dt$$

A few explicit forms for h(t) will be considered below.

4.1 Mathematical formalism for incorporating the particle exposure time distribution into the charge spectrum

If it is accepted that the particle exposure time T_e is a random variable, then it must be accepted that the charge distributions

$p(k;a,t)$ discussed in the previous section are in fact conditional distributions. That is, $p(k;a,t)$ represents the probability that the particle acquires k charges given that its exposure time is t. We must now lift this condition. This is easily done as follows: note that the product

$$p(k;a,t)h(t)$$

represnts the joint probability that the particle's exposure time is t and its charge is k. (This follows from the definition of conditional probability.) What we seek is the marginal distribution of k, which may be obtained by summing over t.

$$p(k;a) = \int_0^\infty p_k(t)h(t)dt$$

$$= \int_0^\infty \Big(\sum_{j=0}^{k} A_{kj}\exp(-ng_j t)\Big)h(t)dt$$

$$= \sum_{j=0}^{k} A_{kj}\int_0^\infty \exp(-ng_j t)h(t)dt \cdot \qquad (23)$$

The last integral is essentially the Laplace transform (or moment generating function) of h(t). Therefore, tables of Laplace transforms may be useful in this section. Some specific expressions for h(t) will now be considered.

4.2 The negative exponential exposure time

Suppose that the charging process takes place within a vessel of volume V. A stream of ions and an aerosol stream are injected into this vessel at a constant rate. Suppose that the turbulence

within the vessel is so intense as to uniformly mix the contents. In this case the trajectory of a particle which enters the vessel is very disorderly, and one cannot be sure just when the particle will leave the vessel through its outlet. What one can say is that, assuming the particle to be in the vessel at time t, the probability that it will escape during the interval t to t + dt is

$$Qdt/V$$

where Q is the total flow rate through the vessel. This leads immediately to the negative exponential distribution

$$h(t) = (Q/V)\exp(-Qt/V) \tag{24}$$

The mean exposure time is of course V/Q. The standard deviation is also V/Q. With this distribution,

$$\int_0^\infty \exp(-ng_k t)h(t)dt = \frac{Q/V}{ng_k + Q/V}$$

Thus equation (23) becomes

$$p(k;a) = \frac{Q}{V}\sum_{j=0}^{k}\frac{A_{kj}}{ng_j + Q/V}$$

The summation is recognized to be the partial fraction expansion (8) encountered in section 3.2, with Q/V in place of s. Therefore

$$p(k;a) = \frac{Q}{V}\cdot\frac{ng_{k-1}}{ng_k+Q/V}\cdot\frac{ng_{k-2}}{ng_{k-1}+Q/V}\cdots\frac{ng_0}{ng_1+Q/V}\cdot\frac{1}{ng_0+Q/V}$$

The terms in the sequence p(k;a) may conveniently be calculated

from the recursion formula.

$$p(0;a) = \frac{1}{ng_0V/Q+1}, \quad p(k;a) = \frac{ng_{k-1}V/Q}{ng_kV/Q+1}p(k-1;a) \qquad (25)$$

Again, a specific choice for the "reaction rate constant" g_k must be made in order to make the expression more explicit.

It is hard to imagine a physical situation in which the exposure time is more uncertain than in the turbulent charging vessel considered here. Therefore it is legitimate to regard the charge distribution resulting from the negative exponential exposure time as an extreme case. We shall call it the "maximum variance charge spectrum", in contrast to the minimum variance charge spectrum of section 3.2. Real devices are expected to produce charge spectra with variance intermediate to these two.

4.2.1 White diffusion charging

A typical maximum variance charge spectrum based on White's expression (12) for ng_k is shown in figure 9. The corresponding minimum variance spectrum, with exposure time equal to V/Q, is shown in the same figure. It is seen that the two distributions have the same mode, but the former is much broader than the latter. The maximum variance charge distribution is not symmetric: its long tail extends to the left.

Descriptive statistics for the maximum variance charge distribution according to White's expression for ng_k are given in appendix A. The same statistics are given as for the minimum variance charge distribution. The time cited in appendix A, as well as in figure 9, is a dimensionless value given by $n\bar{c}\pi(a/b)^2V/Q$.

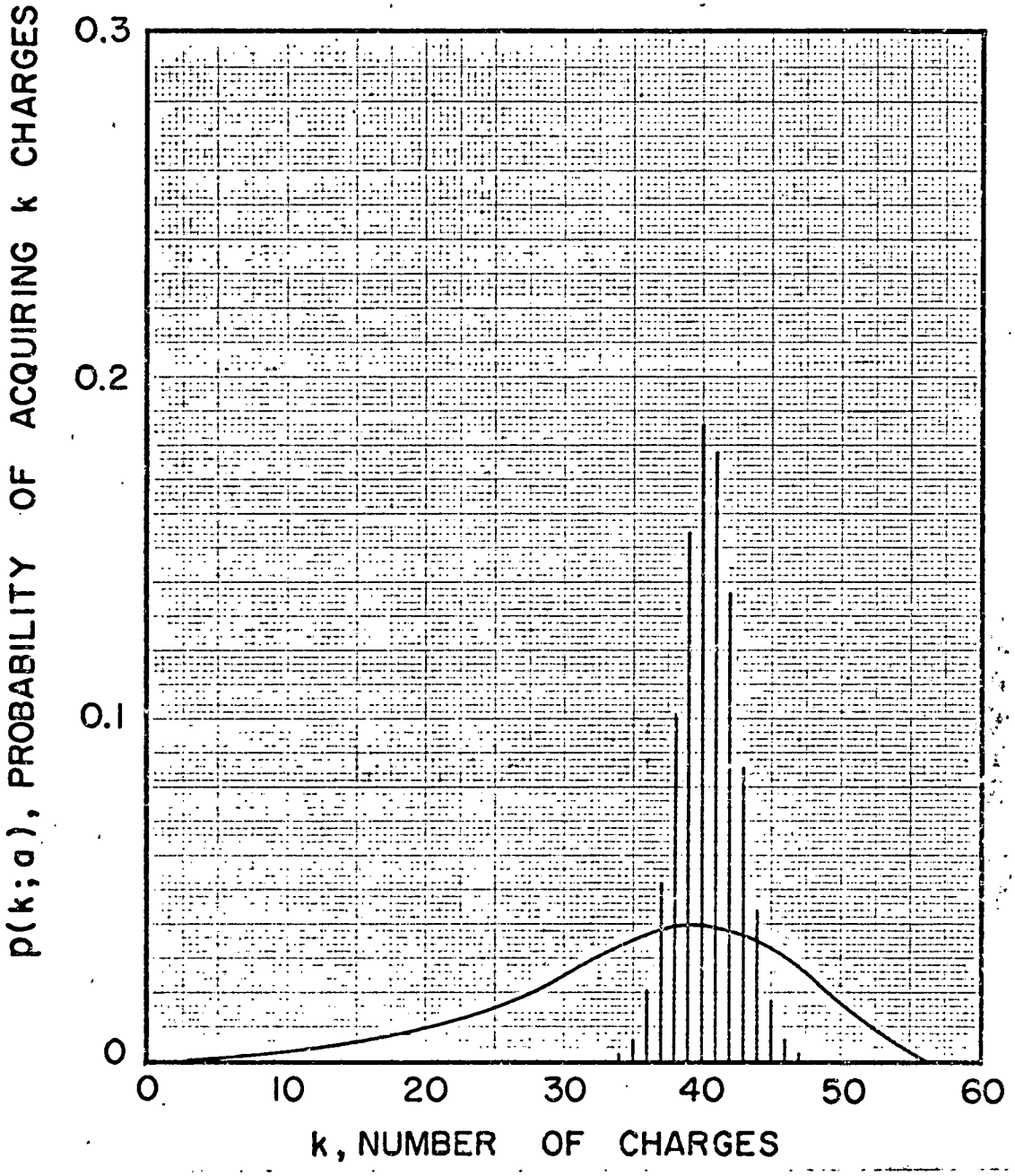

Figure 9. Charge distributions for a 1.0 micron diameter particle, based on White charging.

The bar graph is the minimum variance charge distribution. The solid curve is the envelope of the maximum variance charge distribution. For both, the dimensionless exposure time $\pi(a/b)^2\bar{c}nt$ or $\pi(a/b)^2\bar{c}nV/Q$ is 10.

It is seen in appendix A that for a given exposure time the arithmetic standard deviation is approximately equal to b, the electrical size of the particle. The ratio σ/b changes slowly with both particle size and mean exposure time. It is noteworthy also that the geometric standard deviation is nearly independent of particle size provided that the size is greater than about 0.3 microns diameter. It decreases with increasing exposure time, however.

4.2.2 Continuum diffusion charging

Figure 10 shows a typical maximum variance charge spectrum based on the continuum diffusion expression (14) for ng_k. Also shown is the corresponding minimum variance charge distribution. The comments made above in connection with White charging apply here as well.

Descriptive statistics for the maximum variance charge distribution are given in appendix B. The dimensionless time cited there, as well as in figure 10, is $n\pi D(a/b)V/Q = \pi\varepsilon Z_i nV/Q$. Again it is seen that the ratio σ/b has a value nearly independent of particle size. It increases markedly with increasing exposure time, however. A typical value for σ/b is 1.3. The geometric standard deviation is again nearly independent of particle size, for size greater than 0.3 microns diameter. Its change with exposure time is less pronounced than for White charging.

4.2.3 Field charging

A typical maximum variance charge distribution based on field charging (expression 15) is shown in figure 11. Descriptive statis-

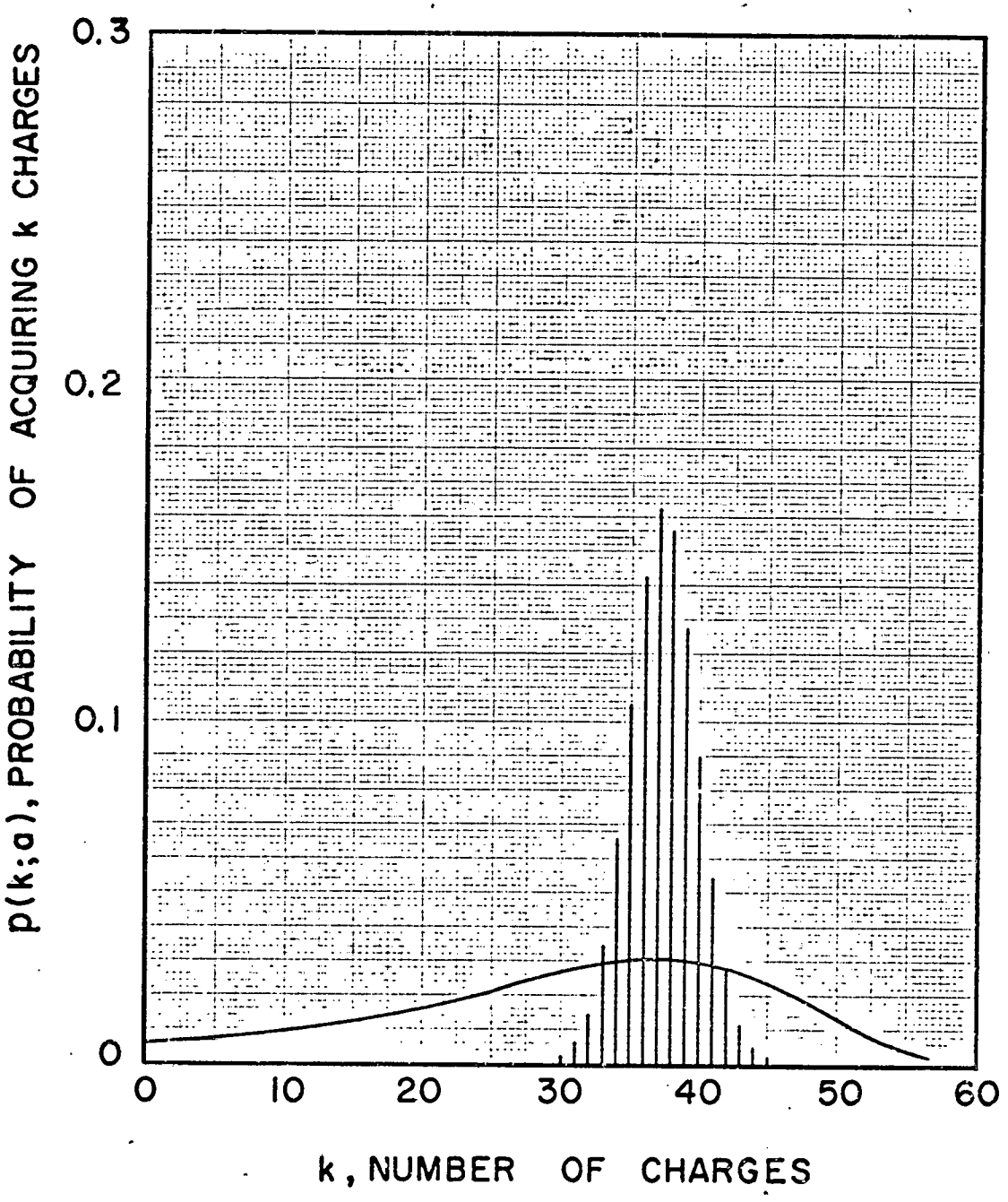

Figure 10. Charge distributions for a 1.0 micron diameter particle, based on continuum diffusion charging.

The bar graph is the minimum variance charge spectrum. The solid curve is the envelope of the maximum variance charge distribution. For both, the dimensionless exposure time $\pi(a/b)Dnt$ or $\pi(a/b)DnV/Q$ is 5.0.

tics are given in appendix C. The dimensionless time is defined as $\pi\varepsilon Z_i nV/Q$.

For a given mean exposure time, the arithmetic standard deviation σ is roughly proportional to the parameter k_s. As regards time dependence, σ passes through a maximum at about two dimensionless time units. The maximum value of σ is about $0.22k_s$. The geometric standard deviation is reasonably independent of both k_s and exposure time, provided that the mean dimensionless exposure time is less than about 2. A typical value for the geometric standard deviation is 2.2.

4.3 Other expesure time distributions

As mentioned in section 4.2, the negative exponential exposure time is considered to be an extreme case. This point, together with its mathematical simplicity, commends it for study. However, if the charging device employs laminar aerosol throughflow, rather than turulent mixing, other exposure time distributions will be more appropiate. Some simple alternatives will be mentioned now.

In the charging device used by Goyer, Gruen and LaMer(1954), the aerosol flows through a rectangular channel. The charging ions cross this channel at right angles to the aerosol flow. The authors mention that the time of exposure to ions is a function of the height at which the particles travel in the channel. They calculate that particles traveling on the median plane of the channel have the shortest exposure time (.008 sec) and they use the value .012 sec as the mean exposure time. The exposure time distribution is characterized by the existance of a definite minimum

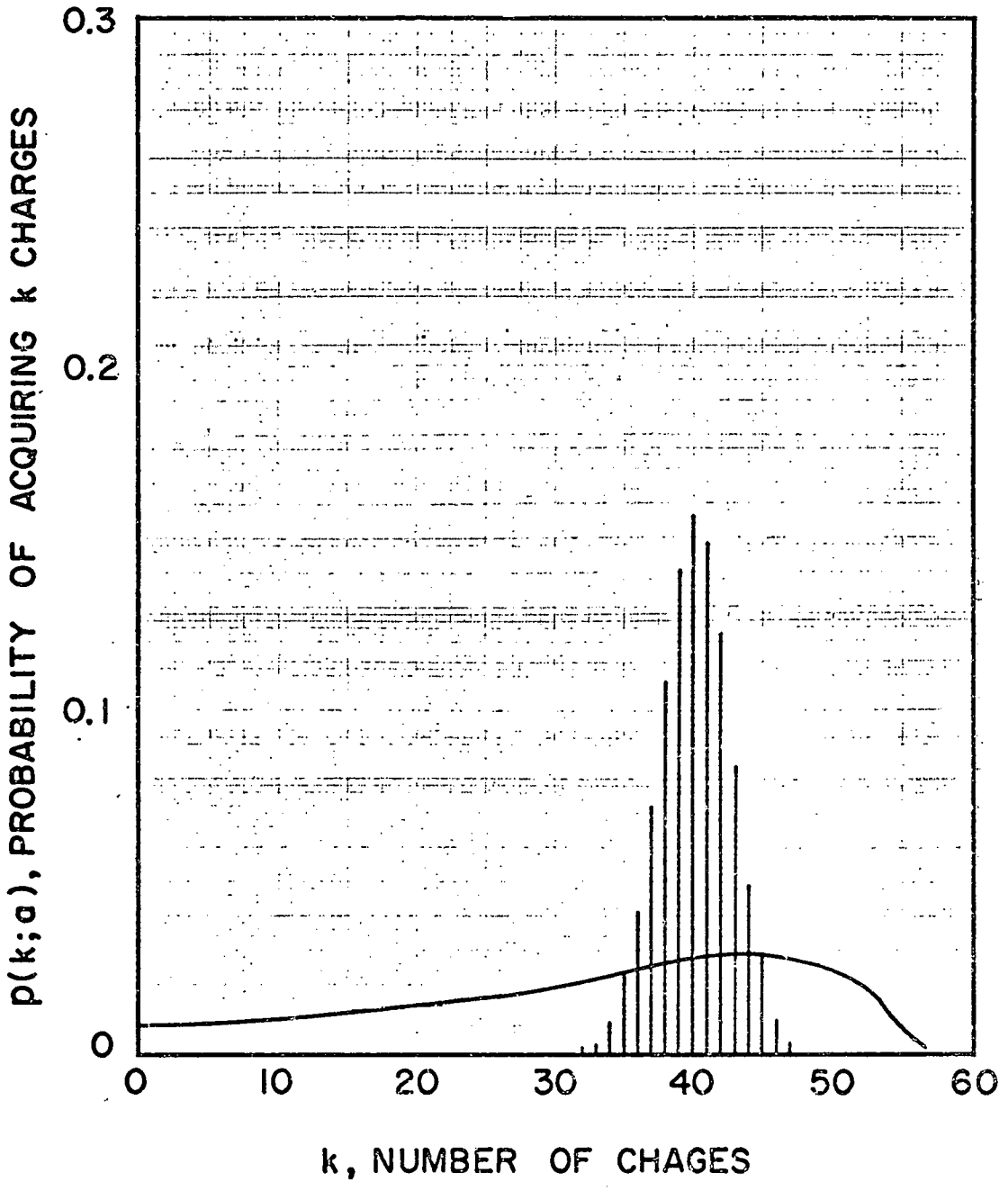

Figure 11. Charge distributions based on field charging, for a particle with saturation charge $k_S = 60$.

The bar graph is the minimum variance charge spectrum. The solid curve is the envelope of the maximum variance charge spectrum. For both, the dimensionless exposure time $\pi\varepsilon Z_i nt$ or $\pi\varepsilon Z_i nV/Q$ is 2.0.

exposure time.

The full exposure time distribution for a device of the type used by Goyer, Gruen and LaMer (that is, fully developed two-dimensional flow between parallel plates) may be found by a simple proability analysis. It is

$$h(t) = 0 \qquad \text{for } t < t^* \tag{26}$$

$$h(t) = \frac{3t^{*2}}{4t^3(1 - t^*/t)^{\frac{1}{2}}} \qquad \text{for } t \geq t^*$$

where t^* is the minimum exposure time, equal to the length of the charging region in the direction of aerosol flow divided by the centerline velocity. The mean of this distribution is $3t^*/2$. The distribution is unusual in that its variance does not exist.

Fuchs, Petrjanoff and Rotzeig(1936) suggest that in their charging device, the flow of aerosol through the charging region was similar to fully developed laminar flow in a pipe. If this is true, then the exposure time distribution is

$$h(t) = 0 \qquad \text{for } t < t^* \tag{27}$$

$$h(t) = 2t^{*2}/t^3 \qquad \text{for } t \geq t^*$$

where t^* is again the minimum exposure time. This distribution has mean $2t^*$. Its variance does not exist.

The two exposure time distributions just above, together with the negative exponential distribution, are shown in figure 12. In each case, the time is given in multiples of the corresponding mean exposure time. It is clear that the two distributions considered in this section entail considerably less spread in exposure time

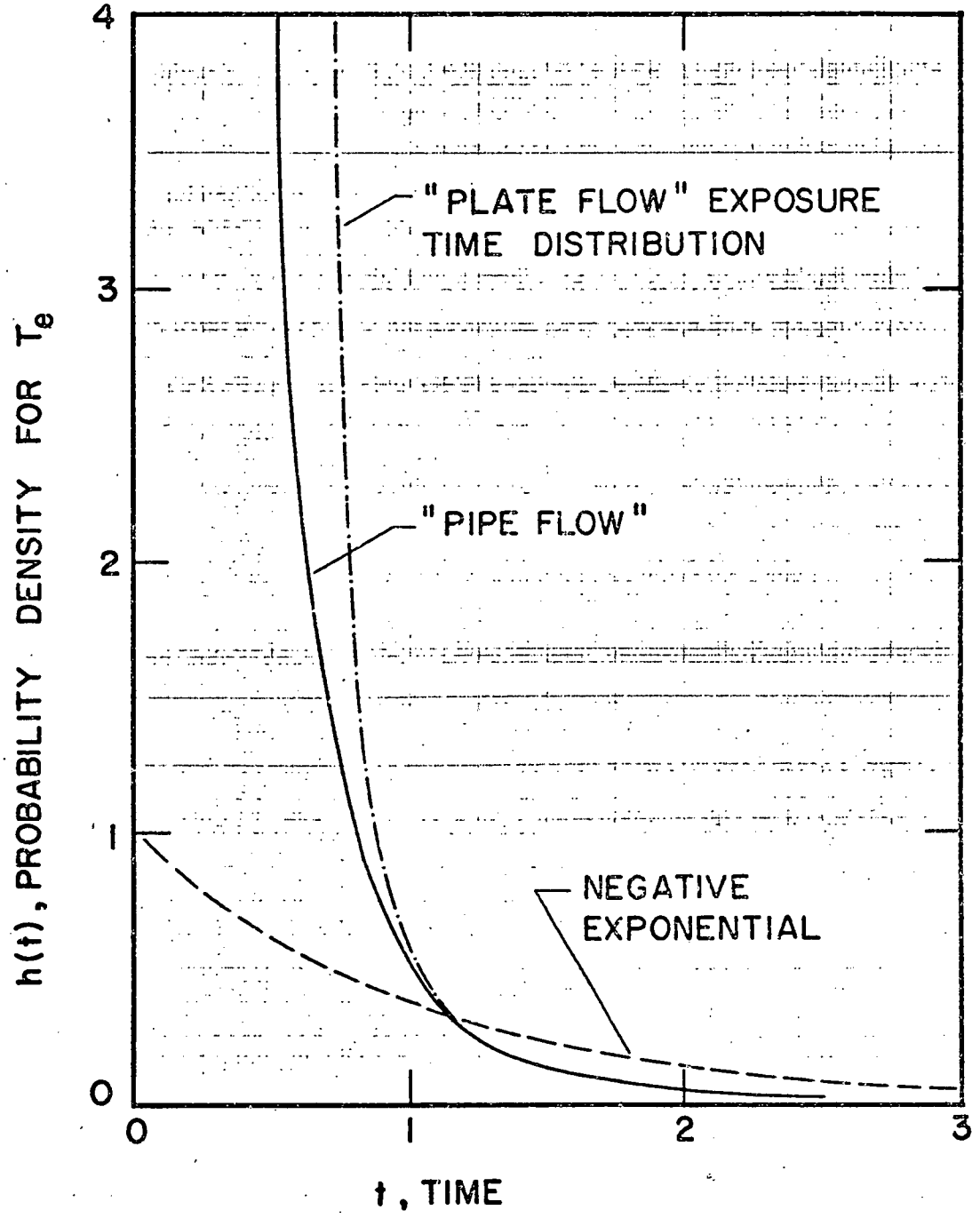

Figure 12. Comparison of three exposure time distributions.

The mean exposure time for each distribution has been chosen equal to unity.

than the negative exponential distribution. This will also reduce the variance of the resulting charge distribution.

The two exposure time distributions just above are not of sufficiently general interest to warrant extensive tabulation of the resulting charge distributions. One spectrum has been computed on the basis of the pipe flow exposure time distribution and White charging. The expression for p(k;a) is the same as that for p(k;a,t) (equation 13 of section 3.2.1) except that the factors $\exp(-ng_j t)$ are replaced by

$$\int_{t^*}^{\infty} 2t^{*2}\exp(-ng_j t)dt/t^3 = 2E_3(ng_j t^*)$$

Here E_3 is one of the exponential integrals (see Abramowitz and Stegun, 1964). The resulting charge spectrum at a minimum exposure time t^* such that $\pi\bar{c}n(a/b)^2t^* = 5$ is shown in figure 13. For comparison, the minimum variance charge distribution at the time $t = 2t^*$ is also shown. The particle diameter in both cases is 0.5 microns. It is seen that the "pipe flow" charge distribution is displaced from and is broader than the minimum variance charge distribution. The former distribution is slightly asymmetric, with the long tail to the right.

4.4 Comparison of the maximum variance charge distribution to data

We consider only those data from the literature for which the information on the charging conditions is most complete.

Hewitt's(1957) data on the spread of the charge spectrum pertains to 0.28 micron diameter particles. The charging took place in a 3600 volt/cm electric field. The particle dielectric constant was 5.1. The product nt had values ranging from 0.13×10^7 to

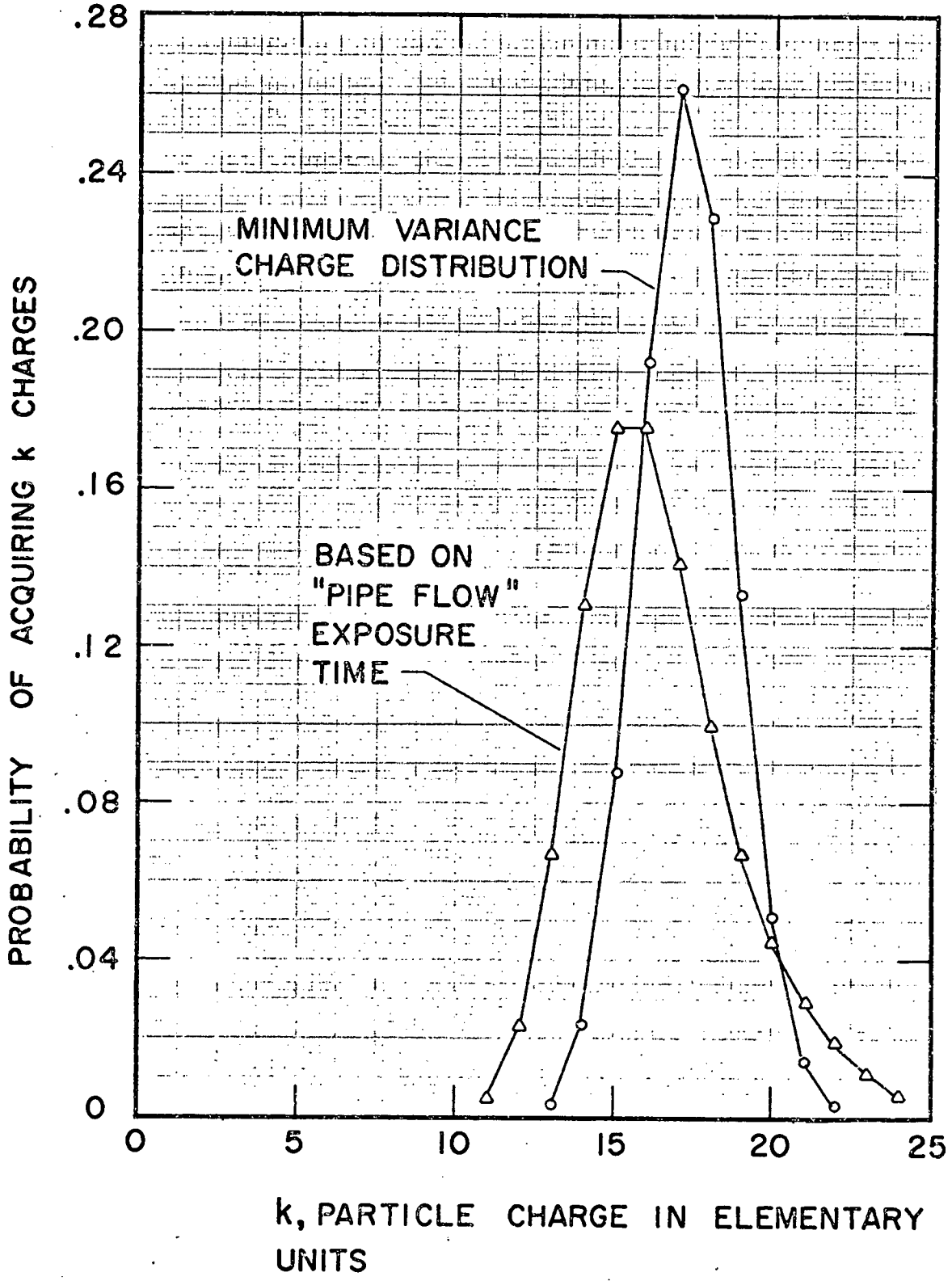

Figure 13. Two charge distributions based on White charging.

For both, the particle diameter is 1.0 microns and the dimensionless mean exposure time $\pi(a/b)^2\bar{c}n\bar{t}$ is 10.

5.8×10^7 sec/cc. Using Hewitt's values for Z_i, $\bar{c}$ and T_a, we have

$$b = 2.52, \quad k_s = 10.6, \quad \pi\bar{c}n(a/b)^2t = 6.5 \text{ to } 290$$

$$\pi\varepsilon Z_i nt = 0.94 \text{ to } 43$$

As to the mean charge, Hewitt's data (figure 12) agrees slightly better with White charging than with the other two charging mechanisms which have been considered. We therefore use appendix A for the comparison. From table I of section 2.3, it is seen that the arithmetic standard deviation of Hewitt's charge distributions decreased from 3.1 to 2.5 with increasing exposure time. Correspondingly the ratio σ/b decreased from 1.2 to 1.0. From appendix A, the maximum variance charge distribution has σ/b increasing from 1.1 to 1.3 as $\pi a^2\bar{c}nb^2t$ increases from 5 to 100. Hewitt's data regarding σ therefore roughly agrees with that from the maximum variance charge distribution based on White charging.

Fuchs, Petrjanoff and Rotzeig(1936) provide data on particle charging in electric fields of strength 556, 732 and 940 volts/cm. The aerosols used were polydisperse, with particle size between 1 and 6 microns diameter. The authors contend that the mean charge found by them agrees well with that found from field charging theory. We therefore compare their data on the spread of the charge spectrum to the tabulation in appendix C. The dimensionless exposure times $\pi\varepsilon Z_i nt$ for three sets of data were 0.26, 0.37 and 0.40. According to appendix C, the geometric standard deviation of the maximum variance charge distribution is nearly independent of both particle size and exposure time, in this range of exposure times. Its value is 2.2 to 2.6. This is much larger than the values 1.22 to

1.30 found from the data and given in table I. Thus, the charge distributions of Fuchs, Petrjanoff and Rotzeig show considerably less spread than the maximum variance charge distribution.

Perhaps the only other set of data from table I suitable for comparison to theory is that of Whitby, Liu and Peterson(1965). They studied charging within a chamber (2000 cu. ft.). We may assume that the charging mechanism was diffusion. The exposure times are not known, but the particle size together with the geometric mean charge may be used as means of entry into appendix A or B. As an example, one of the 0.26 micron diameter aerosols was found to have a geometric mean charge of 7.6 units and a geometric standard deviation of 2.42. The best corresponding entry in the maximum variance section of appendix A has a geometric standard deviation of 1.58. In appendix B, the geometric standard deviation of the best corresponding entry is 1.76. Thus the observed spread of the charge distribution is much larger than that of the distribution which we have proposed as the broadest possible. This is true of several of the distributions reported by Whitby, Liu and Peterson.

The data of Bademosi(1971) imply a standard deviation which is about 1/3 of the value expected according to maximum variance charge distribution.

5.0 METHOD AND APPARATUS FOR THE EXPERIMENTAL STUDY OF THE CHARGE DISTRIBUTION

The electric charge carried by an individual aerosol particle can seldom be measured directly. Usually it is necessary to first measure a related quantity, such as the electric mobility or the charge-to-mass ratio. The particle charge may then be calculated if the particle size is known, either *a priori* or by concurrent measurement.

During the 1920's and 1930's, the method usually employed to determine particle charge was to observe individual particles in motion in a combined electric and gravity field. In this way both the gravity settling speed and the electric mobility of the particle could be measured. From these two data, both the size and charge of that particle could be determined. In this way the bivariate size-charge distribution can be constructed particle-by-particle, as in figure 1.

The above individual particle method of determining the charge spectrum is not well suited for accumulating large amounts of data. Therefore conclusions regarding the size and charge of billions of aerosol particles must often be based on the observations on 50 particles or less. This raises questions regarding the adequacy of small samples. Less tedious methods of constructing the bivariate size-charge distribution, still based on individual particle observations, have been developed since. (See Gillespie and Langstroth, 1952.)

The study of the distribution of electric charge among the particles of an aerosol was considerably simplified by the advent of monodisperse aerosols. For such aerosols the size of individual

particles is known, at least approximately, from a prior measurement on a sample of the aerosol. A single measurement per particle is therefore sufficient to determine the particle charge.

Hewitt(1957) made full use of the advantages of monodisperse aerosols. His method requires an aerosol generator which produces a monodisperse aerosol continuously at a constant rate and particle size. This aerosol is passed through the charging device, then into an electric mobility analyzer. The latter device passes those aerosol particles whose mobility lie on a narrow range. The relative number of particles in this range was then determined photometrically. By adjusting the mobility analyzer to pass various mobility fractions, the mobility spectrum could be determined. Since the particles all have a known common size, the charge spectrum can then be obtained by a simple calculation.

The method to be used to determine charge spectra in this study is similar to that employed by Hewitt. The heart of the system is the electric mobility analyzer. This is of the type sometimes referred to as the "air blast" or "winnowing" type of mobility analyzer, wherein the electric field is applied substantially at right angles to the air flow. The mobility analyzer used in this study is described in section 5.2.

In Hewitt's study, the primary objective was to locate the center of the mobility distribution, for various conditions of charging. This center was defined as the average of the two half-maximum points on the mobility analyzer response curve.

In the present study, the mobility analyzer is called upon not only to determine the center of the mobility distribution, but also to provide accurate information concerning its width. In

effect, we require accurate values of both the first and the second moments of the mobility distribution; higher moments, or a detailed plot of the distribution function, would also be welcome. This, in turn, requires a deeper understanding of the mobility analyzer as a measuring instrument than has been the case in the past.

Sections 5.3 and 5.4 are devoted to developing a "theory of operation" for the mobility analyzer. It is perhaps worthwhile to preview these sections here, in a qualitative way.

One of the ingredients of the theory of operation for the mobility analyzer is an accurate knowledge of the motion of particles once they are inside. This is taken up in section 5.3. The assumptions made in section 5.3 are standard ones:

> incompressible, laminar, axisymmetric airflow;
> negligible electric space charge and image forces;
> negligible particle inertia and diffusion.

The particle motion is described in terms of the streamfunction ψ and the electric flux function ϕ, rather than in terms of the traditional cylindrical polar coordinates r and z. In terms of ψ and ϕ, the particle path is a straight line. Furthermore, this approach shows that the relation between the initial and terminal points of the particle path is quite independent of the details of the airflow.

Although the path of the particle within the mobility analyzer is deterministic, its point of entrance into the analyzer is not known exactly. The uncertainty in its initial position (in terms of ψ) is related to the volumetric flow of aerosol into the analyzer. We assume that its initial position is governed by chance. Thus, the second ingredient of the theory of mobility analyzer operation

is a probabilistic one. This aspect of the theory is taken up in section 5.4.

Since the theory of the mobility analyzer operation rests on several assumptions, some explicit, some implicit, it is advisable to check the theory by experiment. Such experiments are described in section 5.5.

5.1 The relationship between the particle electric mobility and the particle attributes size and charge

The electric mobility of an aerosol particle depends on its size and charge and on certain properties of the suspending gas. In this study, we shall accept that expression for the mobility which is based on the Stokes-Cunningham law for the air-drag on an aerosol particle. This law applies to spherical particles and is semi-empirical. The history of this expression is discussed by Fuchs (1964, p.27).

The electric mobility Z_p of an aerosol particle may be written as $Z_p = n_p Z_1$, where n_p is the number of charges carried by the particle and Z_1 is the mobility of a singly charged particle. Z_1 is given by

$$Z_1 = \frac{\varepsilon C}{3\pi\mu d_p} \tag{28}$$

where C is the Cunningham slip correction

$$C = 1 + 2A(\lambda/d_p) + 2Q(\lambda/d_p)\exp(-\tfrac{1}{2}bd_p/\lambda) \tag{29}$$

and

ε = 4.803×10^{-10} statcoulomb = 1.601×10^{-10} coulomb

d_p = the particle diameter

λ = the mean free path of the air molecules

μ = the air viscosity

According to Fuchs(1964), the preferred value for the mean free path is

$$\lambda = (6.53 \times 10^{-6})/p, \qquad \lambda \text{ in cm, } p \text{ in atmospheres}$$

where p is the air pressure. The parameters A, Q and b have been determined by experiment to be

$$A = 1.25, \qquad Q = 0.44, \qquad b = 1.09$$

These values are based primarily on data for oil droplets.

For given air temperature and pressure, the single-charge mobility Z_1 is uniquely related to the particle diameter d_p. This relationship is shown in table III, which was calculated for the conditions 25°C and 736 mm Hg. These values are considered typical for the laboratory in which the experiments were done.

5.2 The mobility analyzer

As used here, the term mobility analyzer means a device for separating an aerosol into components which differ in electric mobility. We consider especially those devices which employ a continuous and steady flow of aerosol.

There are several possible configurations, or geometries, which may be employed in constructing mobility analyzers. The articles of Gillespie and Langstroth(1952), Hurd and Mullins(1962), Whitby and Peterson(1965), Whitby and Clark(1966) and Megaw and Wells(1969) describe some of the geometries which may be used. The unit used in the present study is very similar to the one used

Table III

The electric mobility of singly charged particles
at 25°C and 736 mmHg

Part A Particle diameter .010 to 0.119 microns
Electric mobility in cm^2/kilovolt-sec

	.000	.001	.002	.003	.004	.005	.006	.007	.008	.009
.01	21.15	17.53	14.77	12.63	10.92	9.538	8.407	7.468	6.681	6.013
.02	5.442	4.951	4.524	4.151	3.823	3.534	3.276	3.047	2.841	2.656
.03	2.489	2.338	2.201	2.075	1.960	1.855	1.759	1.670	1.588	1.512
.04	1.441	1.376	1.315	1.258	1.205	1.155	1.109	1.065	1.024	.9853
.05	.9490	.9148	.8824	.8519	.8230	.7956	.7696	.7449	.7215	.6992
.06	.6780	.6579	.6386	.6203	.6027	.5860	.5700	.5546	.5400	.5259
.07	.5124	.4995	.4871	.4752	.4637	.4527	.4421	.4319	.4220	.4126
.08	.4035	.3946	.3862	.3780	.3700	.3624	.3550	.3478	.3409	.3342
.09	.3277	.3215	.3154	.3095	.3038	.2982	.2928	.2876	.2825	.2776
.10	.2728	.2682	.2637	.2593	.2550	.2509	.2468	.2429	.2390	.2353
.11	.2317	.2281	.2247	.2213	.2180	.2148	.2117	.2087	.2057	.2028

Part B Particle diameter 0.10 to 1.19 microns
Electric mobility in cm^2/megavolt-sec

	.00	.01	.02	.03	.04	.05	.06	.07	.08	.09
0.1	272.8	231.7	199.9	174.9	154.8	138.3	124.7	113.2	103.5	95.15
0.2	87.93	81.64	76.11	71.22	66.88	62.99	59.50	56.35	53.50	50.90
0.3	48.53	46.35	44.35	42.51	40.81	39.23	37.76	36.40	35.12	33.93
0.4	32.81	31.76	30.77	29.84	28.97	28.14	27.35	26.61	25.90	25.23
0.5	24.60	23.99	23.41	22.86	22.33	21.82	21.34	20.88	20.44	20.01
0.6	19.60	19.21	18.83	18.47	18.12	17.78	17.46	17.14	16.84	16.55
0.7	16.26	15.99	15.73	15.47	15.22	14.98	14.75	14.52	14.30	14.09
0.8	13.88	13.68	13.49	13.30	13.11	12.93	12.76	12.59	12.42	12.26
0.9	12.10	11.95	11.80	11.65	11.51	11.37	11.23	11.10	10.97	10.84
1.0	10.72	10.60	10.48	10.36	10.25	10.14	10.03	9.992	9.818	9.716
1.1	9.616	9.518	9.422	9.328	9.235	9.145	9.056	8.969	8.884	8.800

by Hewitt(1957). The same unit, with a slightly different exit fixture, was also used previously by Bademosi(1971).

The mobility analyzer consists of four main parts, or sub-assembles. These are:

the head, shown in figure 14

the housing, shown in figure 15

the exit fixture, shown in figure 16

the center rod, shown in figure 17.

Schematic views of the analyzing region proper, along with the flow and electric fields, are provided by figures 18 and 19.

The head (figure 14) is shown full scale in a half-sectional view. Clean air flows into the head through the axial hole in the two delrin pieces at the top. The axial hole in the lower delrin piece is blocked at its bottom by a brass button. The clean air flows out through the right 3/32" radial holes just above the brass button. Thereafter, the clean air flows downward through the 200 mesh nylon screen stretched across the annulus at the plane indicated in figure 14. This screen serves to smooth the air and distribute it evenly around the annulus. A high voltage lead is also brought out through the axial hole in the delrin piece.

Aerosol enters the head through the two opposed inlet pipes. A large passage is provided to allow the aerosol to freely distribute around the circumference of the head. The aerosol then flows downward through the narrow annular gap adjacent to the outer wall. Thus the head provides a core flow of clean air surrounded by a thin layer of aerosol.

Figure 14. The head of the mobility analyzer.

Half-sectional view of assembly, full scale.

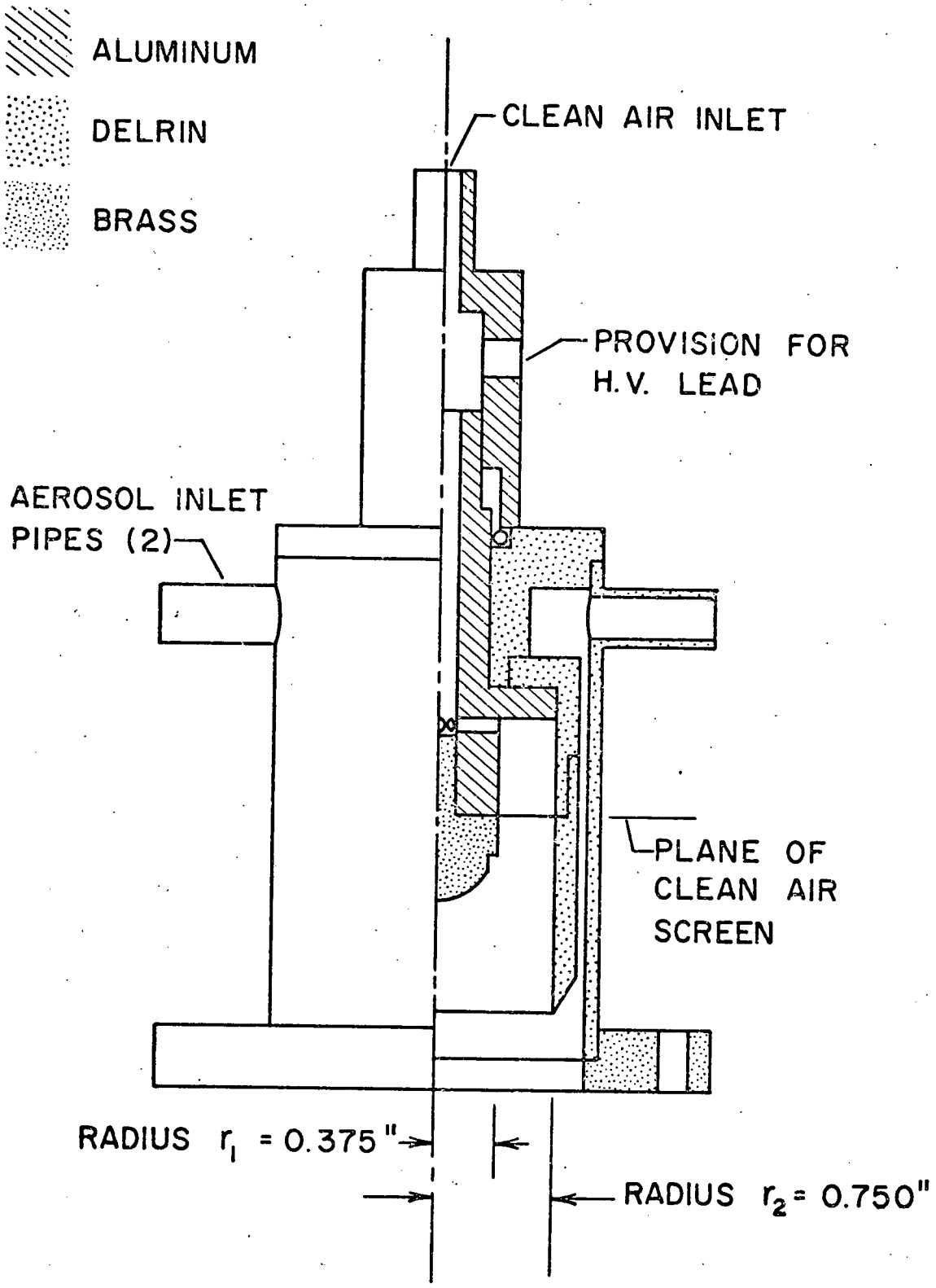

The housing (figure 15) joins to the head by means of a flange at its upper end. A lip on this flange fits snugly into the flange on the head, insuring alignment of these two parts. The lip also serves as an edge of the entrance slit. The housing itself forms one boundary of the analyzing region proper. Its internal diameter was measured and found to be 1.5019" ± .0007". The width of the entrance slit is 0.3112".

The exit fixture is shown twice full scale in figure 16. The upper web of this fixture fits snugly into the bore of the housing (at its lower end), providing alignment of these two parts. It has two outlet ports, one for drawing out the bulk of the airflow of the mobility analyzer, the other for drawing out a small portion of it. A groove for an O-ring gasket is provided.

The center rod (figure 17, twice full scale) has a socket in its upper end which fits snugly over a shoulder on the brass button in the head. At the bottom of the center rod is a delrin piece with a conical end, which fits the corresponding socket in the outlet fixture. The exit fixture may be moved slightly in the axial direction to provide compressive stress on the center rod. This aligns the center rod within the housing. The diameter of the center rod is 0.7481" ± .0005". Electrical connection to the center rod is provided by means of its contact with the brass button.

When the mobility analyzer is assembled and in operation, clean air and aerosol enter the head as just described and flow into the annular space between the center rod and the housing. With a suitable electric potential applied to the center rod (the housing is grounded), charged particles drift across the clean air

Figure 15. The housing of the mobility analyzer.

Two views, both full scale.

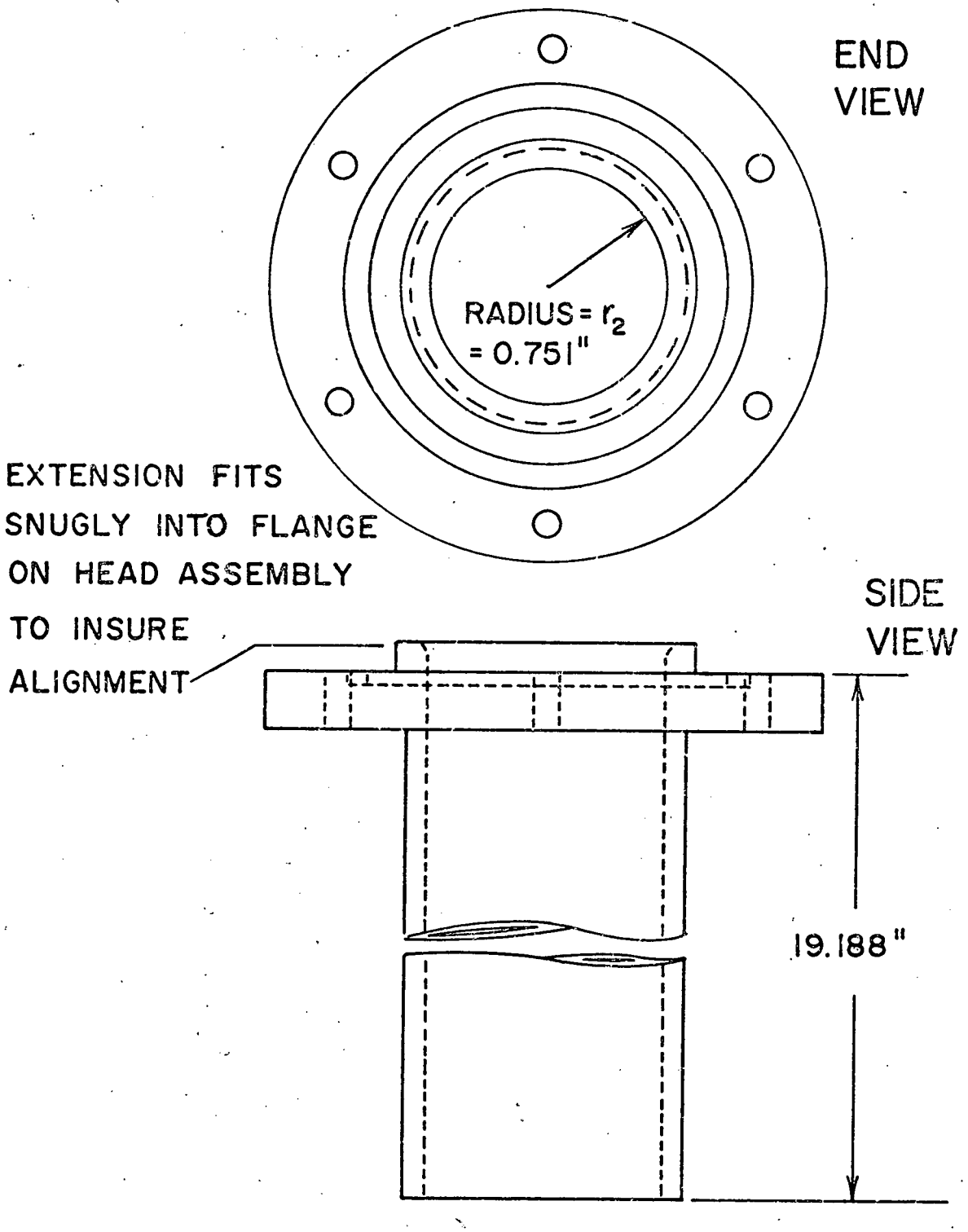

Figure 16. The exit fixture of the mobility analyzer.

Two views, twice full scale.

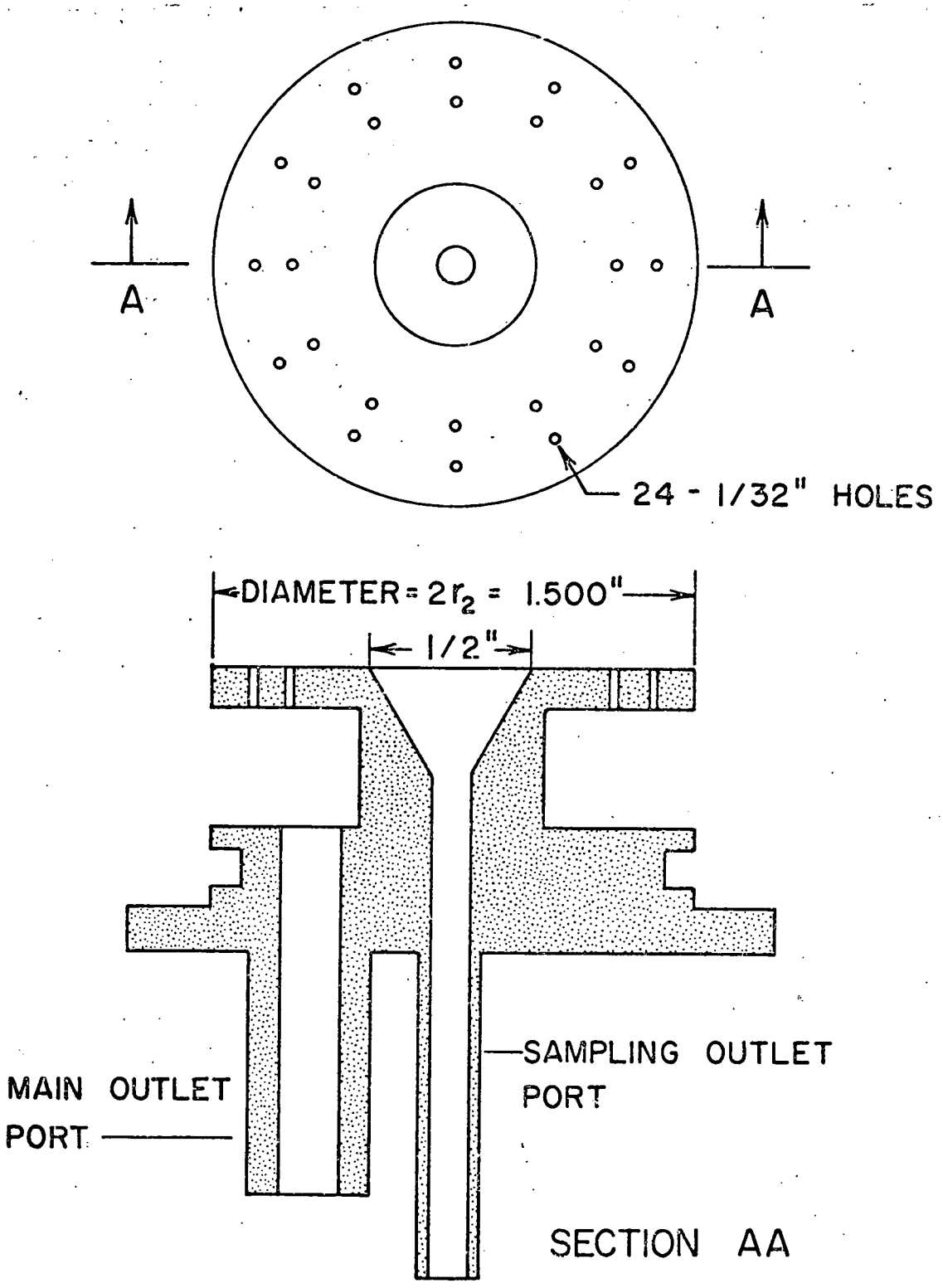

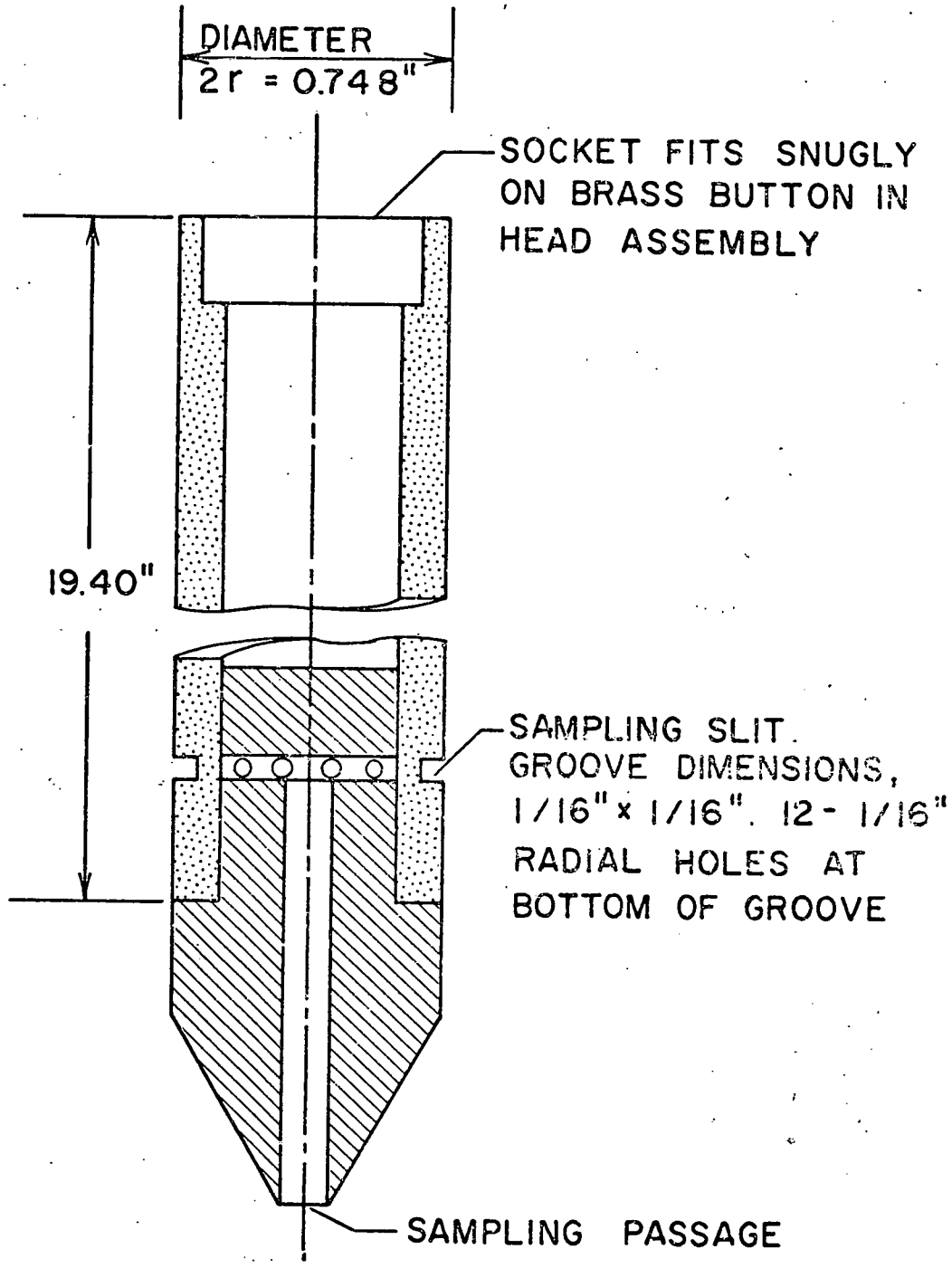

Figure 17. The center rod for the mobility analyzer.

Shown twice full scale.

flow toward the center rod. Particles with high electric mobility will deposit on the rod upstream of the sampling slit. Particles with low mobility will not reach the rod and therefore will be carried off by the main outlet flow. In between, there is a narrow range of mobilities which will land in the sampling slit and be carried out of the analyzer by the sampling flow.

The sampling slit on the center rod consists of a 1/16" x 1/16" circumferential groove, with twelve 1/16" radial holes drilled at its bottom. The purpose of the groove is to help distribute the suction evenly around the circumference. After passing through these holes, the sampling flow leaves through the axial hole in the conical delrin piece, which connects to an axial hole in the exit fixture. A header plug is inserted in the center rod just above the sampling slit to keep the dead volume of the sampling circuit to a minimum.

The bulk of the analyzer airflow is removed through the twenty-four 1/32" holes in the web of the exit fixture. These holes draw air equally from all sectors of the mobility analyzer.

5.3 Particle trajectories within the electric mobility analyzer

The following discussion of particle trajectories within the electric mobility analyzer is based on the observation that under many conditions, the motion of the particle is described by an exact differential equation. This observation greatly facilitates the solution of the equation of motion. The key idea in the discussion is taken from Fuchs(1964, p.111), who discusses particle trajectories in a parallel plate device.

The analyzing region of the electric mobility analyzer is

shown schematically in figure 18. The boundaries of the analyzing region are the cylindrical surfaces at distance r_1 and r_2 from the symmetry axis. The length L of the analyzing region is measured from the mid-plane of the entrance slit to the mid-plane of the exit slit. For the mobility analyzer described in section 5.2, $r_1 = 0.9501 \pm .0006$ cm, $r_2 = 1.9074 \pm .0009$ cm and $L = 45.52 \pm .02$ cm.

Within the analyzing region, the air velocity has components $v_r(r,z)$ and $v_z(r,z)$ in the radial and axial direction, respectively. We shall assume that the flow is axisymmetric, so that the velocity components are independent of the angular coordinate. Furthermore, we shall assume that the flow is steady and incompressible. Therefore the equation of continuity takes the form

$$\partial(rv_r)/\partial r + r\partial v_z/\partial z = 0 \qquad (30)$$

Note that we do <u>not</u> assume that the flow is fully developed.

The electric field within the analyzing region also has components $E_r(r,z)$ and $E_z(r,z)$. We assume perfect axial symmetry so that these two components are independent of the angular coordinate. According to Poisson's equation from electrostatics, the divergence of the electric field is proportional to the space charge density. We shall assume that the space charge may be neglected within the analyzing region. Then

$$\partial(rE_r)/\partial r + r\partial E_z/\partial z = 0 \qquad (31)$$

The field component E_z differs from zero only in the immediate vicinity of the entrance and exit slits.

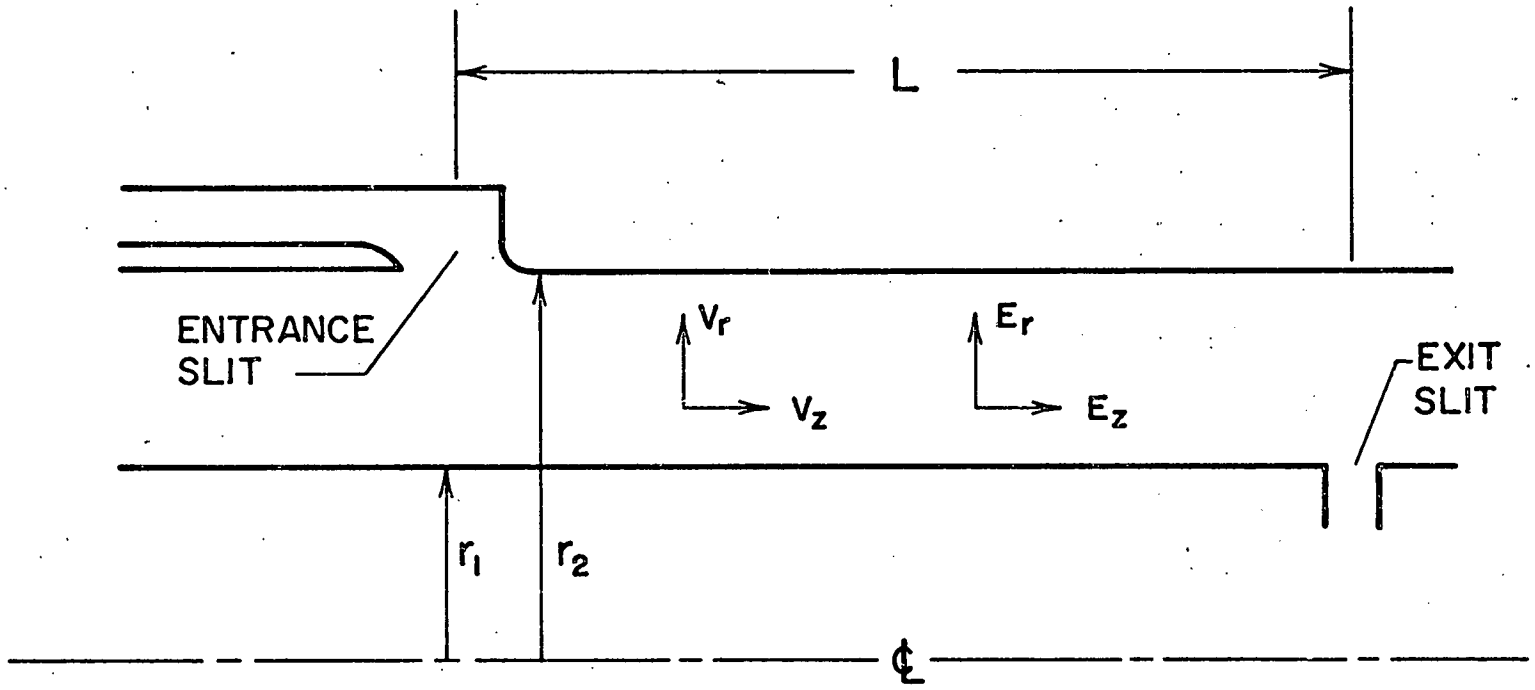

Figure 18. Analyzing region of the mobility analyzer.

As a preliminary to discussing particle trajectories within the mobility analyzer, it is useful to introduce the stream function ψ and the electric flux function ϕ. ψ is defined through the line integral

$$\psi(r,z) = -\int^{(r,z)} [rv_z(r,z)dr - rv_r(r,z)dz] \tag{32}$$

The lower limit of the integral is any agreed-upon reference point. The integral is independent of the path of integration by virtue of the assumed incompressibility of the flow. The function ϕ is defined in a similar way.

$$\phi(r,z) = \int^{(r,z)} [rE_z(r,z)dr - rE_r(r,z)dz] \tag{33}$$

This line integral is independent of path by virtue of the assumption that the space charge is negligible.

The sign chosen in the definition of ψ is the most commonly accepted one. The sign of ϕ is chosen purely for convenience. Note that the function ϕ is <u>not</u> the potential of the electric field, a quantity which is sometimes denoted by the same symbol.

Several streamlines (lines of constant ψ) have been indicated schematically in figure 19. Four streamlines have particular significance. ψ_1 is the streamline which adheres to the outer tube downstream of the entrance slit. The streamline ψ_1' forms the boundary between the clean air, which enters from the left in figure 19, and the aerosol flow, which enters through the entrance slit. Thus the flow bounded by the streamlines ψ_1 and ψ_1' is the flow which originally contained the aerosol particles. ψ_2 is the streamline which adheres to the center rod upstream of the exit slit.

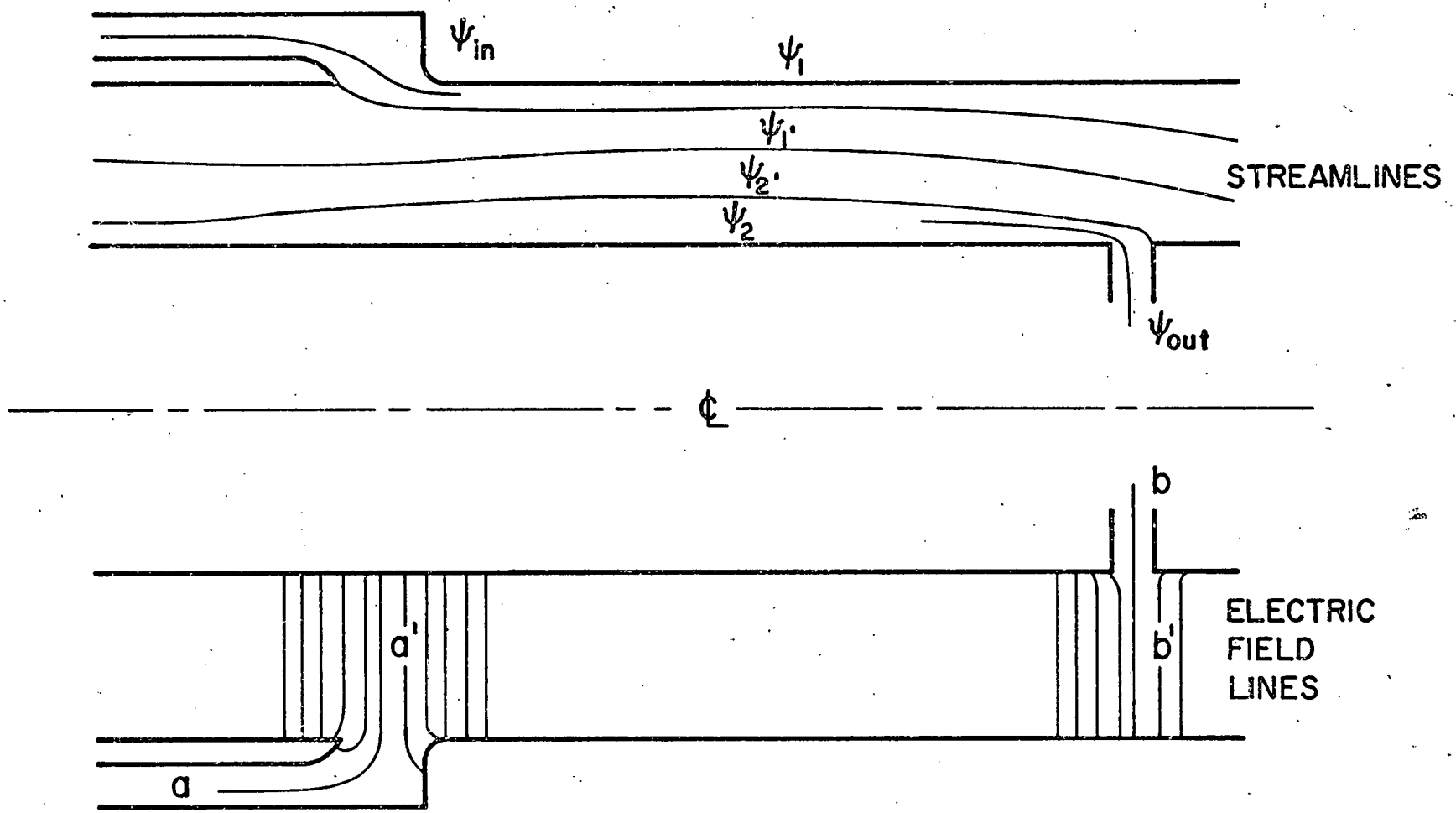

Figure 19. The key streamlines and electric field lines in the mobility analyzer.

ψ_2' forms the boundary between the air which leaves through the exit slit and the air which leaves through the main outlet, at the right of figure 19. It is the flow between ψ_2' and ψ_2 which eventually reaches the aerosol monitor connected to the mobility analyzer.

As is well known, the stream function is closely related to the volumetric flow. Let

q_c = the volumetric clean air flow

q_a = the volumetric aerosol flow

q_s = the volumetric sampling flow (the exit slit flow)

q_o = the volumetric main outlet flow.

The total flow rate in the analyzing region between the slits is then $q_c + q_a = q_o + q_s$. From the relationship between the stream function and the flow, it is seen that

$$q_a = 2\pi(\psi_1' - \psi_1)$$
$$q_s = 2\pi(\psi_2 - \psi_2')$$
$$q_c + q_a = q_o + q_s = 2\pi(\psi_2 - \psi_1) \qquad (34)$$

Thus the values of the key streamlines, relative to the streamline ψ_1, are completely determined by three airflow values.

Some electric field lines (lines of constant ϕ) are shown schematically, also in figure 19. It is expected that throughout most of the analyzing region, the electric field lines are almost perfectly radial. The electric field here is given quite accurately by the expression

$$E_r(r) = V/[r\ln(r_2/r_1)]$$

appropriate for coaxial cylinders of infinite length. Here V is the voltage on the analyzer center rod. Near the entrance and exit slits, the electric field will become curved and weaken considerably, owing to penetration into the slits.

One particular increment in the flux function ϕ is of importance in the subsequent discussion. Let

$$\Delta\phi = \int_a^b [rE_z dr - rE_r dz]$$

be the increment in ϕ between a point a, well back in the entrance slit, and a point b, well down into the exit (see figure 19). The integral is independent of the path followed from a to b. Starting at a, integrate along an electric field line to the point a', midway between the two cylinders. Since a and a' are located on the same field line, this leg of the integration path contributes nothing to the value of $\Delta\phi$. Next integrate along a path parallel to the axis of the mobility analyzer from the point a' to the point b', adjacent to the exit slit. Along this leg, E_z is very nearly zero and E_r is given quite accurately by the expression cited just above. Hence the contribution to $\Delta\phi$ is

$$+\int_{a'}^{b'} \frac{-rVdz}{r\ln(r_2/r_1)} = +\frac{-V\,\overline{a'b'}}{\ln(r_2/r_1)} = +\frac{-VL}{\ln(r_2/r_1)}$$

In the last member of this equation, we have assumed that the distance $\overline{a'b'}$ is very nearly equal to the distance L. Finally, the integration from b' to b is along an electric field line so that there is no contribution to $\Delta\phi$ from this leg. Thus

$$\Delta\phi = -VL/[\ln(r_2/r_1)] \qquad (35)$$

For the mobility analyzer described in section 5.2, the combination $L/[\ln(r_2/r_1)]$ has the value 65.31 cm.

It is important to note that the increment $\Delta\phi$ is independent of the exact positions of the points a and b. This follows from the fact that the electric field is vanishingly small in the regions where these points are located. It is believed that the above expression for $\Delta\phi$ is accurate to within 1%. To obtain an improved value, either by experiment or by theoretical analysis, would require a great deal of work. One of the design considerations in the mobility analyzer of section 5.2 was to make it easy to determine $\Delta\phi$ accurately by elementary methods.

We may now take up the particle trajectories within the mobility analyzer. In addition to the assumptions made regarding the flow and electric fields (incompressible flow, no space charge), it will be assumed that:

1. the particle inertia may be neglected,
2. the particle Brownian motion may be neglected,
3. electrical image forces due to the charge on the particle may be neglected,
4. the particle velocity relative to the air is accurately given by $Z_p\vec{E}$,
5. the flow and electric fields are steady.

Under these conditions, the equations of motion for the particle are

$$dr/dt = v_r(r,z) + Z_pE_r(r,z)$$

$$dz/dt = v_z(r,z) + Z_pE_z(r,z)$$

In these equations, Z_p is regarded as a signed quantity; its sign is that of the charge carried by the particle. Since the right hand sides are independent of the time t, this variable may be

eliminated to give

$$[v_z + Z_p E_z]dr - [v_r + Z_p E_r]dz = 0$$

It is readily seen that under the assumptions made regarding the velocity and electric fields, this differential equation has r as an integrating factor. After multiplying through by r, the solution is most easily found by rearranging:

$$-[rv_z dr - rv_r dz] = Z_p[rE_z dr - rE_r dz]$$

The terms in the square brackets are recognized to be the differentials of the stream function ψ and the electric flux function ϕ, respectively. That is, the above differential equation may be expressed as

$$d\psi = Z_p d\phi \tag{36}$$

It is seen that if Z_p is zero, then $d\psi = 0$ so that the particle moves along a path on which ψ is constant - that is, along a streamline. Conversely, if Z_p tends to infinity, the particle moves along a path with constant ϕ (an electric field line). For finite Z_p, the particle path is a compromise between these two extremes. The solution of the above differential equation is simply

$$\psi = Z_p \phi + \text{constant} \tag{37}$$

In terms of the "coordinates" ψ and ϕ, the particle path is always a straight line.

If one requires a detailed knowledge of the particle trajectory, it is still necessary to know the flow field ψ in detail. However, the information required in this study may be extracted

from the trajectory equation without a detailed knowledge of the flow field or the particle path. To do this, consider a particle which enters the mobility analyzer from a point well back in the entrance slit, traverses the analyzing region, and leaves the analyzer through the exit slit. Let ψ_{in} be the streamline on which the particle is carried prior to entering. The exact value of ψ_{in} is not known, but it is known that

$$\psi_1 \leq \psi_{in} \leq \psi_1'$$

Let ψ_{out} be the streamline on which the particle leaves the analyzer. Its value is known only to the extent indicated by the double inequality

$$\psi_2' \leq \psi_{out} \leq \psi_2$$

The increment $\Delta\psi = \psi_{out} - \psi_{in}$, which is the number of streamlines crossed by the particle in passing through the mobility analyzer, is therefore known to lie on the interval

$$\psi_2' - \psi_1' \leq \Delta\psi \leq \psi_2 - \psi_1$$

On the other hand, the increment in ϕ for the same particle is $-VL/\ln(r_2/r_1)$, as has already been computed. But according to the trajectory equation (37), $\Delta\psi$ is always equal to $Z_p\Delta\phi$. Thus

$$\psi_2' - \psi_1' \leq Z_p\Delta\phi \leq \psi_2 - \psi_1$$

This is the basic operating equation for the mobility analyzer. In it, the ψ differences are related in a simple way to the three independent airflows and $\Delta\phi$ is related to the center rod voltage and the geometry of the mobility analyzer (equations 34 and 35).

The double inequality just above incorporates the correct sign for Z_p and $\Delta\phi$. When solving for Z_p, the sense of the inequalities must be adjusted in accordance with the sign of $\Delta\phi$. To avoid this nuisance, it is better to use the absolute values of Z_p and $\Delta\phi$. When this is done, and when the ψ-differences and $\Delta\phi$ are expressed in terms of the more familiar quantities, the result is

$$\frac{(q_o-q_a)\ln(r_2/r_1)}{2\pi VL} \leq Z_p \leq \frac{(q_o+q_s)\ln(r_2/r_1)}{2\pi VL}, \quad \begin{array}{l}\text{use absolute}\\ \text{values of (38)}\\ Z_p \text{ and } V\end{array}$$

To summarize, it has been demonstrated that

> no particle with mobility outside the range just above may pass through the mobility analyzer.

Note, however, that it has <u>not</u> been demonstrated that

> all particles with mobility within the above range will pass through the mobility analyzer.

The latter statement is, in fact, false, as will be seen in the next section.

The mid-point Z_p^* of the mobility interval just above is

$$Z_p^* = [q_o + \tfrac{1}{2}(q_s - q_a)]\ln(r_2/r_1)/(2\pi VL) \qquad (39)$$

The width ΔZ_p of the interval is

$$\Delta Z_p = (q_s + q_a)\ln(r_2/r_1)/(2\pi VL) \qquad (40)$$

A simple and logical way to define the resolution of the instrument is to consider its application to a monodisperse aerosol carrying low charge. Such an aerosol will have a mobility spectrum

with singularities or "spikes" at the mobilities 0, Z_1, $2Z_1$,..... n_pZ_1, $(n_p+1)Z_1$.... . The two successive peaks n_p and n_p+1 will be completely resolved if, with Z_p^* adjusted to the value $(n_p+\frac{1}{2})Z_1$, the interval ΔZ_p is less than the interval $(n_p+1)Z_1 - n_pZ_1 = Z_1$:

$$\Delta Z_p < Z_1 \text{ , when } Z_p^* = (n_p+\tfrac{1}{2})Z_1 \text{ .}$$

That is, if

$$\frac{\Delta Z_p}{Z_p^*} < \frac{1}{n_p+\frac{1}{2}}$$

or, bringing in equations (39) and (40),

$$\frac{q_s + q_a}{q_o + \frac{1}{2}(q_s - q_a)} < \frac{1}{n_p+\frac{1}{2}}$$

or

$$n_p < \frac{q_o - q_a}{q_s + q_a} \tag{41}$$

The ratio on the right of equation (41) may be called the resolution of the instrument. For example, if $q_o = 50$ and $q_s = q_a = 3$, the resolution is 7.83. The first seven spikes in the mobility spectrum will be completely resolved. Higher spikes will either be incompletely resolved or not resolved at all.

A natural sequence for the voltage settings is suggested by the following consideration: consecutive members of the sequence should be chosen in such a way that the corresponding mobility intervals are contiguous. Thus if V' is one member of the sequence, the upper end of the corresponding interval is

$$(q_o + q_s)\ln(r_2/r_1)/(2\pi V'L)$$

If V" is the next member of the sequence, the lower end of the corresponding interval is

$$(q_o - q_a)\ln(r_2/r_1)/(2\pi V"L)$$

On equating these two it is seen that

$$V" = V'(q_o - q_a)/(q_o + q_s) \tag{42}$$

Thus the voltage settings form a geometric progression with common ratio $(q_o - q_a)/(q_o + q_s)$. In some cases, it might be advisable to overlap the mobility intervals somewhat by taking a common ratio nearer unity.

One of the assumptions underlying the above development is that the center rod is perfectly concentric with the housing. The effect of relaxing this condition somewhat is considered in appendix E.

5.4 The passage function for the mobility analyzer and the determination of moments of the mobility distribution

Section 5.3 culminated in a compact expression for the paths of particles within the mobility analyzer and in a definition of the instrument resolution. No method was given, however, for retrieving information concerning the mobility spectrum from the mobility analyzer data. Such methods are proposed in this section.

It will be demonstrated that the output of the mobility analyzer is related to the input mobility spectrum by means of an integral equation. The equation is not easy to solve exactly, but a simple approximate solution will be proposed which is more accurate

the higher the mobility analyzer resolution. In addition, an exact method will be proposed for determining moments of the mobility spectrum.

The discussion following hinges on the passage function Ω of the mobility analyzer. We define this function as follows:

> Ω = the probability that a particle entering the mobility analyzer via the aerosol flow q_a will leave via the sampling flow q_s.

Obviously, Ω depends on the particle mobility as well as on the operating parameters of the analyzer. This function may be given explicit form by a more careful consideration of the particle trajectory equation (equation 37).

As indicated in the last section, it is convenient to discuss the particle trajectory in terms of the "coordinates" ψ and ϕ. These coordinates are represented in figure 20 by means of a ψ-ϕ plane. The four key streamlines ψ_1, $\psi_{1'}$, $\psi_{2'}$ and ψ_2, explained in the last section, are shown. We have assumed that the center rod of the analyzer carries a negative potential, so that ϕ increases in the downstream direction. ϕ_{in} and ϕ_{out}, the initial and final values of ϕ for a particle which passes completely through the analyzer, are both known except for an arbitrary additive constant. The distance $\Delta\phi$ between ϕ_{in} and ϕ_{out} has already been given (equation 35). It is indicated again in figure 20.

The trajectory of the particle in the ψ-ϕ plane is the straight line

$$\psi = \psi_{in} + Z_p(\phi - \phi_{in})$$

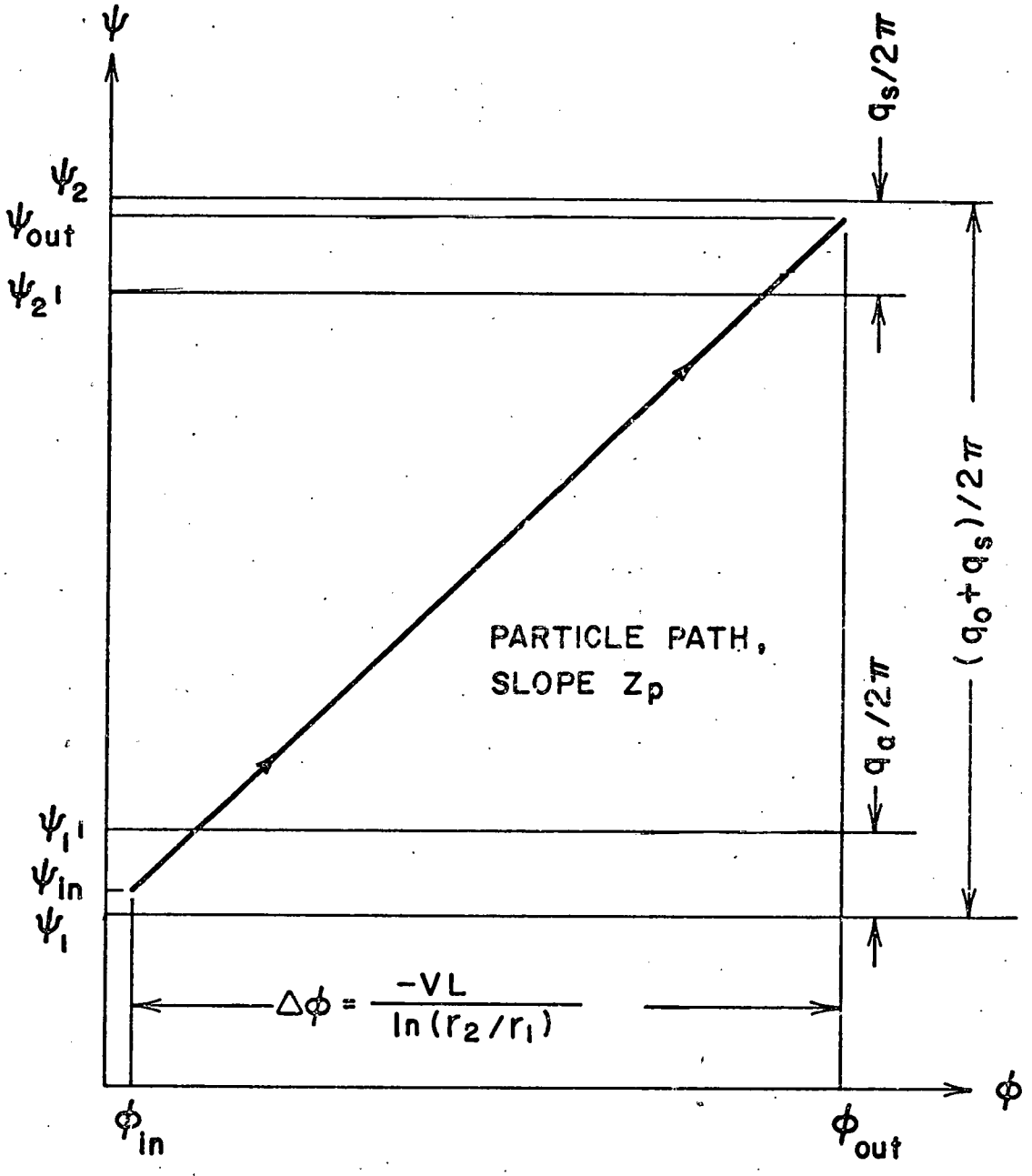

Figure 20. The particle trajectory in the ϕ-ψ plane.

where ψ_{in} is the streamline on which the particle resides prior to entry. From figure 20, it is seen that the particle will pass through the exit slit only if

$$\psi_{2'} < \psi_{in} + Z_p\Delta\phi < \psi_2.$$

In terms of ψ_{in}, the condition is

$$\psi_{2'} - Z_p\Delta\phi < \psi_{in} < \psi_2 - Z_p\Delta\phi.$$

Let this interval for ψ_{in} be denoted by H_2. It is required to determine the probability that ψ_{in} meets this condition.

It is known that ψ_{in} is on the interval $[\psi_1,\psi_{1'}]$, which we denote by H_1. Hence the probability of passage Ω is closely related to the way in which H_1 and H_2 overlap. There are five distinct possibilities for this overlap.

If there is no overlap between H_1 and H_2, the passage function must be zero:

$\Omega = 0$ if $\psi_{1'} < \psi_{2'} - Z_p\Delta\phi$ or $\psi_2 - Z_p\Delta\phi < \psi_1$

i.e., if $Z_p\Delta\phi$ lies outside the interval

$[\psi_{2'}-\psi_{1'}, \psi_2-\psi_1] = [(q_o-q_a)/2\pi, (q_o+q_s)/2\pi]$

This result was mentioned at the end of section 5.3.

If H_1 lies wholly within H_2, the particle is certain to pass through the exit slit. Hence,

$\Omega = 1$ if $\psi_{2'} - Z_p\Delta\phi < \psi_1$ and $\psi_{1'} < \psi_2 - Z_p\Delta\phi$

i.e., if $Z_p\Delta\phi$ lies within the interval

$[\psi_{2'}-\psi_1, \psi_2-\psi_{1'}] = [q_o/2\pi, (q_o+q_s-q_a)/2\pi]$

This case is possible only if $q_s > q_a$.

If H_2 lies wholly within H_1, the transfer function Ω must be less than unity. H_2 is now a subinterval of H_1. The probability that the particle will pass through H_2 is proportional to the volumetric aerosol flow which corresponds to the interval H_2. But this aerosol flow is equal to 2π times the length of H_2. Hence the required probability is proportional to the length of H_2. The constant of proportionality is chosen to make this probability equal unity when the length of H_2 equals the length of H_1. Thus

$$\Omega = (\psi_2 - \psi_{2'})/(\psi_{1'} - \psi_1) = q_s/q_a$$

if $\psi_1 < \psi_{2'} - Z_p\Delta\phi$ and $\psi_2 - Z_p\Delta\phi < \psi_{1'}$,

i.e., if Z_p lies within the interval

$$[\psi_2 - \psi_{1'}, \psi_{2'} - \psi_1] = [(q_o + q_s - q_a)/2\pi, q_o/2\pi]$$

This case arises only if $q_a > q_s$.

In the remaining two cases, neither interval completely contains the other. Ω in each case is the ratio of the length of the overlapping part of H_1 and H_2 to the length of H_1. The results are:

$$\Omega = (\psi_{1'} - \psi_{2'} + Z_p\Delta\phi)/(\psi_{1'} - \psi_1) = (2\pi Z_p\Delta\phi - q_o + q_a)/q_a$$

if $Z_p\Delta\phi$ is within the interval

$$[(q_o - q_a)/2\pi, \min\{q_o/2\pi, (q_o + q_s - q_a)/2\pi\}]$$

$$\Omega = (\psi_2 - \psi_1 - Z_p\Delta\phi)/(\psi_{1'} - \psi_1) = (q_o + q_s - 2\pi Z_p\Delta\phi)/q_a$$

if $Z_p\Delta\phi$ lies within the interval

$$[\max\{q_o/2\pi, (q_o - q_a + q_s)/2\pi\}, (q_o + q_s)/2\pi]$$

These expressions apply to both the cases $q_s > q_a$ and $q_a > q_s$.

It appears most convenient to regard the passage function Ω

as a function of the product $Z_p\Delta\phi$. Ω is shown in figure 21, where the cases $q_s > q_a$, $q_s = q_a$ and $q_a > q_s$ are given separately.

The passage function Ω is used as follows. Suppose that the mobility analyzer is set up with a particular set of flowrates and that N particles, each with mobility Z_p, enter per unit time. (For the time being, we assume that N is a very large integer.) Let $N^*(\Delta\phi)$ denote the number of particles emerging via the sampling flow q_s per unit time at the voltage setting V. From the definition of Ω, it follows that

$$N^*(\Delta\phi) = N\cdot\Omega(Z_p\Delta\phi) \tag{43}$$

If the N particles have mobility described by the distribution function $f(Z_p)$, the output must be

$$N^*(\Delta\phi) = N\int_0^\infty \Omega(Z_p\Delta\phi)f(Z_p)dZ_p \tag{44}$$

In the usual application, the unknown function in this integral relation is f. The relation therefore constitutes a Fredholm integral equation of the first kind. After determining the function $N^*(\Delta\phi)$ by experiment, the mobility distribution $f(Z_p)$ may be found by solving the integral equation. It appears, however, that there exists no simple analytical method for solving this particular integral equation.

An approximate solution for the integral equation may be obtained by applying the first mean value theorem for integrals. To do this, first note that the range of integration may be reduced to $Z_p^* \pm \frac{1}{2}\Delta Z_p$ because the integrand is zero outside this interval. (Z_p^* and ΔZ_p are given by equations 39 and 40, respectively.) Then by

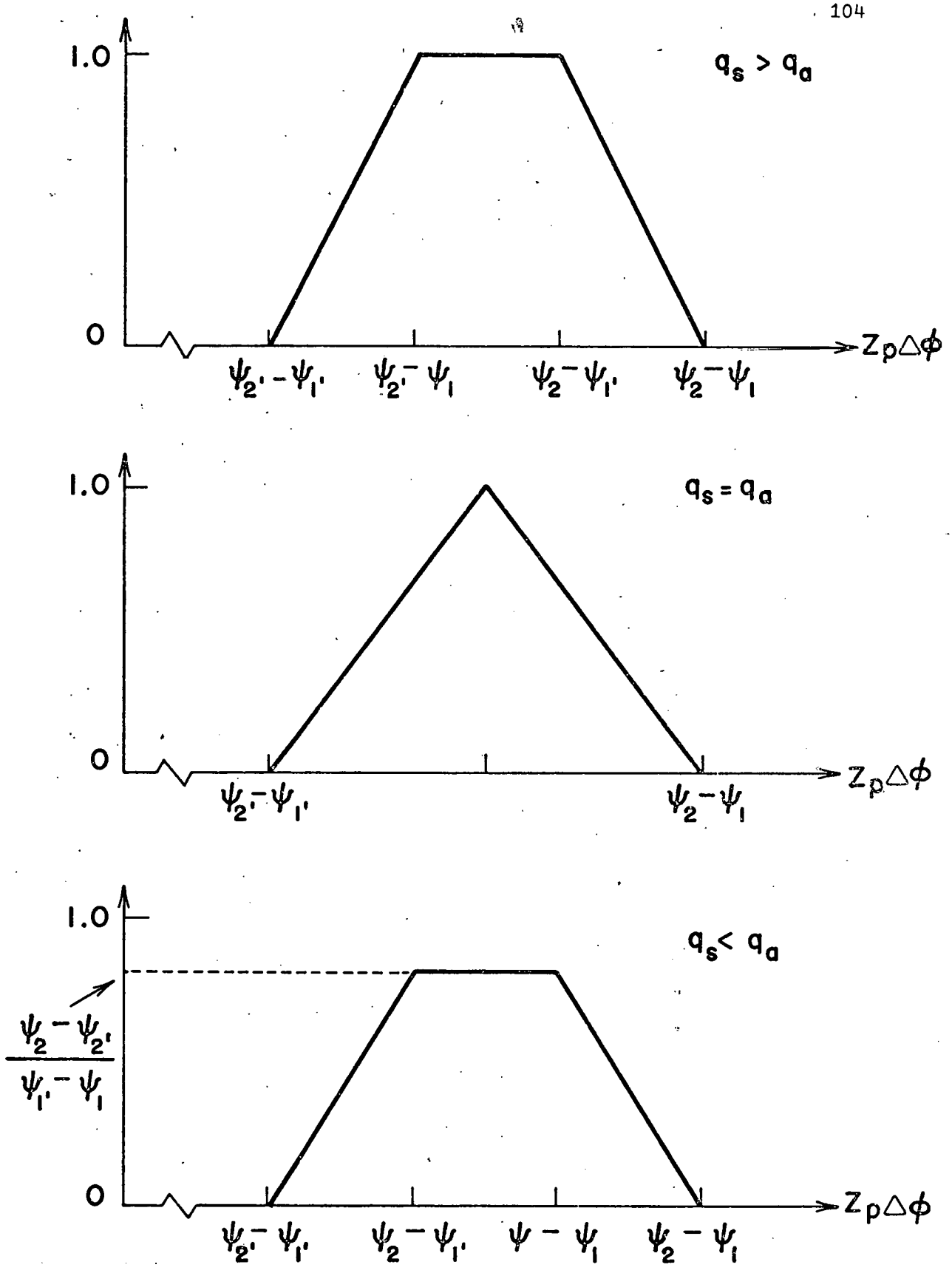

Figure 21. The passage function $\Omega(Z_p\Delta\phi)$.

the first mean value theorem for integrals,

$$\int_0^\infty \Omega(Z_p\Delta\phi)f(Z_p)dZ_p = f(Z_p^\dagger)\int_{Z_p^* - \Delta Z_p/2}^{Z_p^* + \Delta Z_p/2} \Omega(Z_p\Delta\phi)dZ_p$$

where $Z_p^\dagger$ is an unknown point on the interval $Z_p^* \pm \frac{1}{2}\Delta Z_p$. The integral over Ω on the right has the value $q_s/(2\pi\Delta\phi)$. (This holds for both of the cases $q_s > q_a$ and $q_s < q_a$.) Collecting these expressions, we find that

$$f(Z_p^\dagger) = \frac{2\pi\Delta\phi}{q_s} \cdot \frac{N^*(\Delta\phi)}{N} \tag{45}$$

This equation is exact; the approximation comes in when the unknown point $Z_p^\dagger$ is replaced by the interval midpoint Z_p^*. The error thus incurred will obviously decrease with decreasing width of the interval ΔZ_p, that is, with increasing mobility analyzer resolution.

In this thesis, we are particularly concerned with the first several moments of the mobility distribution. Fortunately, the fact that Ω depends only on the product of Z_p and $\Delta\phi$ may be used to devise a simple method of extracting any desired moment of $f(Z_p)$ from the data $N^*(\Delta\phi)$. To do this, divide both members of the integral equation (44) by $(\Delta\phi)^{m+1}$, then integrate over $\Delta\phi$.

$$\int_0^\infty \frac{N^*(\Delta\phi)d(\Delta\phi)}{(\Delta\phi)^{m+1}} = N\int_0^\infty \left(\int_0^\infty \frac{\Omega(Z_p\Delta\phi)}{(\Delta\phi)^{m+1}} d(\Delta\phi)\right) f(Z_p)dZ_p \tag{46}$$

On the right, the order of integration has been interchanged. The inside integral on the right may be evaluated and expressed in the form

$$\int_0^\infty \frac{\Omega(Z_p\Delta\phi)}{(\Delta\phi)^{m+1}}d(\Delta\phi) = (2\pi Z_p/q_o)^m I_m \tag{47}$$

where I_m depends only on the two quantities q_s/q_o and q_a/q_o. Therefore,

$$\begin{aligned}\int_0^\infty \frac{N^*(\Delta\phi)d(\Delta\phi)}{(\Delta\phi)^{m+1}} &= N(2\pi/q_o)^m I_m \int_0^\infty (Z_p)^m f(Z_p)dZ_p \\ &= (2\pi/q_o)^m N I_m \overline{(Z_p)^m}\end{aligned} \tag{48}$$

If we denote the integral on the left by I_m^*, the expression takes the compact form

$$I_m^* = (2\pi/q_o)^m N I_m \overline{(Z_p)^m} \tag{49}$$

where $\overline{(Z_p)^m}$ denotes the m-th moment of Z_p. The cases m = 0, 1 and 2 are especially important.

$$\begin{aligned}I_o^* &= NI_o \\ I_1^* &= (2\pi/q_o)NI_1\overline{Z_p} \\ I_2^* &= (2\pi/q_o)^2 NI_2\overline{(Z_p)^2}\end{aligned} \tag{50}$$

These three equations may be solved for N and the first two moments of the mobility distribution.

In theory, the above procedure provides exact values for the moments of the mobility distribution. In practice, the moment determination is made uncertain by two obvious factors, and perhaps a host of subtle factors. The two factors have to do with the data N^* and the integrals I_m^*. Since N^* is determined empirically, its values are only available at a discrete set of points. Therefore the integrals-over-data I_m^* have to be evaluated numerically. We

use the trapezoid rule, so that the $\Delta\phi$ values (or the voltages) need not be equally spaced. As is well known, an error is incurred in such integration; it increases rapidly with the point spacing. It is wise therefore to include several measurements of N* near any interesting feature of the mobility spectrum.

A more serious cause for uncertainty in the moment determination is the fact that N and N* are usually integers which are not always large. This situation is due to apparatus limitations. Without any lengthy analysis, it seems obvious that both N and N* are Poisson random variables. Therefore any quantity computed from a particular set of data is uncertain. As regards the integrals I^*_m, it may be noted that these involve a weighted sum of the data N*. Since the relative uncertainty of the sum is less than the relative uncertainty of the summands, the I^*_m may be rather well determined in spite of the uncertainty in the data N*.

These two sources of error - the finite data available and the statistical fluctuations in these data - are investigated briefly by a simulation technique in appendix D.

Explicit forms for the integrals I_o, I_1 and I_2 may be obtained by carrying out the required integrations. The two cases $q_s > q_a$ $q_a > q_s$ must be treated separately. It is found that I_o and I_1 have the same value in the two cases:

$$I_o = [(1-q'_a)\ln(1-q'_a) - (1+q'_s-q'_a)\ln(1+q'_s-q'_a) + (1+q'_s)\ln(1+q'_s)]/q'_a$$

$$I_1 = (1/q'_a)\ln\frac{1+q'_s-q'_a}{(1-q'_a)(1+q'_s)} \qquad (51)$$

where $q'_a = q_a/q_o$ and $q'_s = q_s/q_o$. The form of I_2 is different for the two cases:

$$I_2 = \tfrac{1}{2}\left(\frac{q'_a}{1-q'_a} + 1 - \frac{1}{(1+q'_s)(1+q'_s-q'_a)}\right) \qquad \text{for } q'_s > q'_a$$

$$I_2 = \tfrac{1}{2}(q'_s/q'_a)\left(\frac{1}{(1-q'_a)(1-q'_a+q'_s)} - 1 + \frac{q'_s}{1+q'_s}\right) \qquad \text{for } q'_a > q'_s \tag{52}$$

These three integrals contain the effect of the imperfect resolution of the mobility analyzer on the first two moments of the mobility distribution.

It may be noted in closing that similar techniques may be applied to determining the moments of $\ln Z_p$. These moments are required for the determination of the geometric mean and standard deviation of Z_p. The integrals corresponding to the I_m, however, are much more complicated than those above. They will not be given here.

5.5 Experimental check of the mobility analyzer performance

In view of the several assumptions made in section 5.3, it is advisable to check the theory of sections 5.3 and 5.4 by experiment. Such experiments are described in this section.

The arrangement of apparatus for these experiments is shown in the diagram below. The mobility analyzer has already been discussed in detail. The other two major components of the system will be discussed in section 5.5.1 and 5.5.2. The ancillary equipment is discussed in section 5.5.3. The test procedure and results are presented in section 5.5.4.

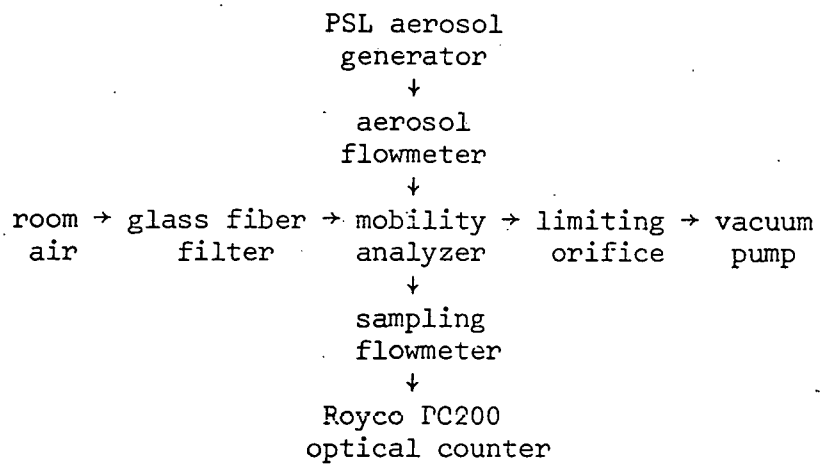

The downward arrows represent aerosol or sampling flow. The rightward arrows depict clean air or main outlet flow.

5.5.1 The aerosol generator

The aerosols for these experiments were generated by the familiar method which involves a polystyrene latex (PSL) produced by the Dow Chemical Co. of Midland, Michigan. These latices (several are available) contain spherical polystyrene particles of highly uniform size. The procedure is to dilute the latex with water, atomize this suspension, and mix the resulting mist with sufficient dry air to permit evaporation of the water. This leaves an aerosol which consists of polystyrene particles and other non-volatile residue from the evaporating drops.

The system used to form the aerosol has been described by Whitby and Liu(1968). It consists of a Collison atomizer; a dessicant bed, filter, flowmeter and suitable valves for providing the diluting air; and a chamber containing a radioactive krypton-85 source for neutralizing the charge on the particles. Whitby and Liu give several data concerning the size distribution and the electric charge of the aerosols produced by this generator. A

striking feature is the large amount of residue in these aerosols. These residue particles, which result from the evaporation of droplets not containing a polystyrene particle, outnumber the polystyrene by about 10^5 to 1. As to the electric charge, it was found that this may amount to several hundreds of unit charges per particle unless the aerosol is properly neutralized. Whitby and Liu found that the Kr-85 neutralizer was quite effective, reducing the particle charge to a level near the Boltzmann equilibrium mentioned in section 2.4 (equation 1).

The operating data for the generator as used in these experiments are as follows:

the latex: Dow run no. LS-1117-B,
stated mean diameter = 0.79 microns
stated standard deviation = .0044 microns

the suspension: 4 drops PSL in ½ pint of demineralized water (approx. dilution = 2000:1),
treated for 5 minutes in an ultrasonic bath.

the Collison: operated at 35 psig, airflow = 10.1 l/min,
liquid output = approx. 0.32 g/min.

diluting air: flowrate = 19.0 l/min.

In one respect, the configuration of the aerosol generator as used here differed from that described by Whitby and Liu(1968). In these tests, the aerosol flow requirement never exceeded 0.5 l/min. The generator was set up so that the excess aerosol (28.5 l/min or more) was dumped upstream of the charge neutralizer. That is, only the aerosol actually needed was passed through the neutralizer. Since the neutralizer volume is 2.0 l, the particle residence time was more than 4 min., depending on flow rate.

No special steps were taken in these experiments to suppress

the residue aerosol. Since these residue particles should have electric mobility far higher than the single or double charged polystyrene particles, they are not expected to interfere with the present experiments. (The higher mobility is a consequence of the smaller size of the residue particles. See Whitby and Liu(1968).)

It may be important to note that the entire aerosol generator, and particularly the Collison atomizer, cools by evaporation during operation. In one test, the suspension temperature dropped from 24°C to 16°C in 1½ hours of operation. However, the temperature at the output of the generator (downstream of the charge neutralizer) settled at 23°C, even with the full output passing through the neutralizer.

5.5.2 The aerosol monitor

The device used in these experiments to determine the amount of aerosol passing through the mobility analyzer at the various voltage settings was the Royco PC 200 particle counter (Royco Instruments, Inc., Menlo Park, Cal.). In this device, the aerosol to be monitored is drawn into a narrow thread which passes at right angles through a narrow light beam. If the aerosol is suitably dilute, only one particle at a time is within the light beam. The geometry is such that all particles must pass through the light beam and each particle that passes through gives rise to a pulse of scattered light. Part of the scattered light is intercepted by a photomultiplier tube, which converts the light pulses into electrical pulses. These pulses are then sorted and counted electronically.

The Royco PC 200 is adequately described in its operating

manual. The instrument used in these experiments, however, incorporates one important modification: a clean air sheath has been provided to surround the aerosol thread. This sheath prevents diffusion of the aerosol particles from the aerosol thread into the dead volume of the optical chamber, where they move around randomly and may be counted several times. This modification is described by Whitby(1967). The sheath arrangement is similar to one pictured in Green and Lane(1964, p.247).

The Royco PC 200 may be operated in such a way as to obtain the size distribution, as well as the amount, of the aerosol. In these experiments, however, the sizing capability of the Royco was not used. Instead, the instrument was set up to count all particles with diameter greater than 0.6 microns. This choice of lower size limit is a further attempt to insure that the residue particle aerosol will not interfere with the experiments. It should be noted, however, that this discriminator setting does not guarantee the non-interference of the residue aerosol. It has been found (Whitby and Liu, 1967) that a high concentration of sub-optical particles may register in optical counters, giving the impression of an aerosol of larger size and lower concentration. Experimental results on PSL aerosols have to be interpreted with caution.

5.5.3 Ancillary equipment

The aerosol flowmeter consists of a glass capillary and an oil manometer. The glass capillary is about 8" long and is joined smoothly at either end to a section of larger ID glass tubing. Pressure taps for connection to the manometer are provided in each end section. This flowmeter was calibrated by means of a water

displacement method. Water is syphoned out of a reservoir (approx. volume = 5 gal.) at a controlled rate. Air is drawn from the room through the flowmeter into the reservoir, where it takes up the volume vacated by the water. The flow rate was determined by timing the discharge of a standard volume of water (½ or 1 liter). The humidification of the air upon entering the reservoir may cause the water flowrate to exceed the air flowrate by 3%. No correction was made for this.

Two other capillary flowmeters were calibrated by the water displacement method. These were then available as secondary standards.

It is vital in the operation of the mobility analyzer that the total air flow through it remain constant, free of pulsations, sudden shifts or long term drifts. The most effective method of establishing a constant flow is to use a constriction and a vacuum source downstream of the mobility analyzer. Then according to the theory of choked flow, the volumetric flow upstream of the constriction is independent of both the upstream and downstream pressures, provided that the ratio of these pressures (in absolute terms) exceeds approximately 2. In line with these considerations, a limiting orifice (Millipore Filter Corporation, Bedford, Mass.) and a vacuum pump (0322-V103. G8D, Gast Manufacturing Corp., Benton Harbor, Mich.) were used to establish the main outlet flow q_o of the mobility analyzer. Depending on the size of the orifice used, the vacuum pump gauge indicated 23 to 25 inches Hg. Each orifice used was calibrated by using the pump/orifice combination to draw air through one of the secondary standard flowmeters. One of the

orifices (3.0 l/min, nominal) was also checked directly by water displacement. In this last case, the arrangement of apparatus was such that no correction is required for humidification of the air. The flow rate found in this way was 50.5 ± 1.3% (90% confidence limits).

The power supply used to establish the voltage on the mobility analyzer center rod was either a Fluke 10 kv supply (model 410-B, John Fluke Manufacturing Co., Inc., Seattle, Wash.) or a Honeywell 6 kv supply (model 6K-20, Honeywell, Denver, Colo.). In both of these, the potential can be set to the nearest volt by means of click-stop dials and fractions of a volt can be set on a continuous dial. No check was made on the accuracy of the dial settings, however.

5.5.4 Test procedure and results

Preliminary experiments indicated that the mobility analyzer should be operated with its axis vertical, rather than horizontal. In one pair of tests where the axis orientation was the only difference, the results were more nearly in accord with theory when the axis was vertical. Also, the tests seemed to be more reproducible when the axis was vertical. The difference in performance for the two orientations is probably due to a bouyancy effect, arising from a difference in density between the clean air and aerosol. These forces, if acting perpendicular to the axis, may destroy the axial symmetry of the flow. The vertical orientation was used for the 16 tests to be described in this section.

The PSL suspension was generally prepared fresh each day, although in some cases a day-old suspension was used. It is impor-

tant in these tests that the generator output remain constant, both as to particle size and as to aerosol concentration, for the duration of each test. In the 16 tests to be described in this section, the generator output was checked directly by duplicating each set of data. That is, the desired sequence of airflow and voltage settings were swept through twice without stopping the aerosol generator, each sweep requiring ½ to 1 hour. In each of these 16 tests, the data duplicated very well indicating that the generator output was stable over the time periods involved.

The Royco particle counter was generally run for ½ hour and the aerosol generator was run for 10 to 15 minutes prior to the start of data-taking. During the tests, it is necessary to allow sufficient time after each change in voltage setting for fresh aerosol to completely fill the mobility analyzer and the sampling line to the Royco. Usually this requirement was met by skipping one cycle in the Royco's automatic scanning sequence.

Since the aerosol is expected to be nearly monodisperse, the contibution of singly charged particles to the output $N^*(\Delta\phi)$ of the mobility analyzer should be closely approximated by $N \cdot \Omega(Z_1 \Delta\phi)$, where N is the input of singly charged particles and Z_1 is the mobility of a singly charged particle. Z_1 may be determined from table III, making use of the stated particle size. Thus the range of voltages for which the singly charged particles contribute to the output may be computed in advance, at least approximately. The procedure was then to measure the output N^* for several voltage settings in and near the expected range of single charge output.

The raw data N^* - vs. - voltage for one test is shown in

figure 22. Also shown is the function $N \cdot \Omega$, where N has been chosen to fit the data but Ω is completely theoretical. In this particular test, the range of voltage settings used was broader than actually necessary to define the single charge peak, for reasons that will be mentioned later. It is seen that the experimental and theoretical peaks are displaced from one another by 100 to 150 volts, out of 6000 volts. The experimental peak appears also to be slightly broader at its base than the theoretical. The air flows for the data in figure 22 were q_o = 34.4 cc/sec, q_a = 4.0 cc/sec and q_s = 3.4 cc/sec. The remaining air flow q_c may be determined from the conservation equation $q_c + q_a = q_o + q_s$.

Figure 22 is typical of the raw data in the 16 tests to be described. The peak displacement, as well as the relative peak widths, varied somewhat from test to test, however. The 16 tests involved various combinations of the three independent flow rates q_a, q_s and q_o. The combinations used are shown in table IV.

As may be seen in figure 22, the single charge peak of the PSL aerosol is well separated from any other feature of the mobility spectrum. Therefore the singly charged particles may be considered as an aerosol onto themselves. The method of section 5.4 may be applied to determine N, the number of single charged particles entering the analyzer during one Royco cycle, the arithmetic mean mobility of the singly charged particles and the corresponding arithmetic standard deviation.. These quantities are listed also in table IV.

The aerosols used in these tests should be very nearly identical. Therefore, the column for N in table IV should be directly

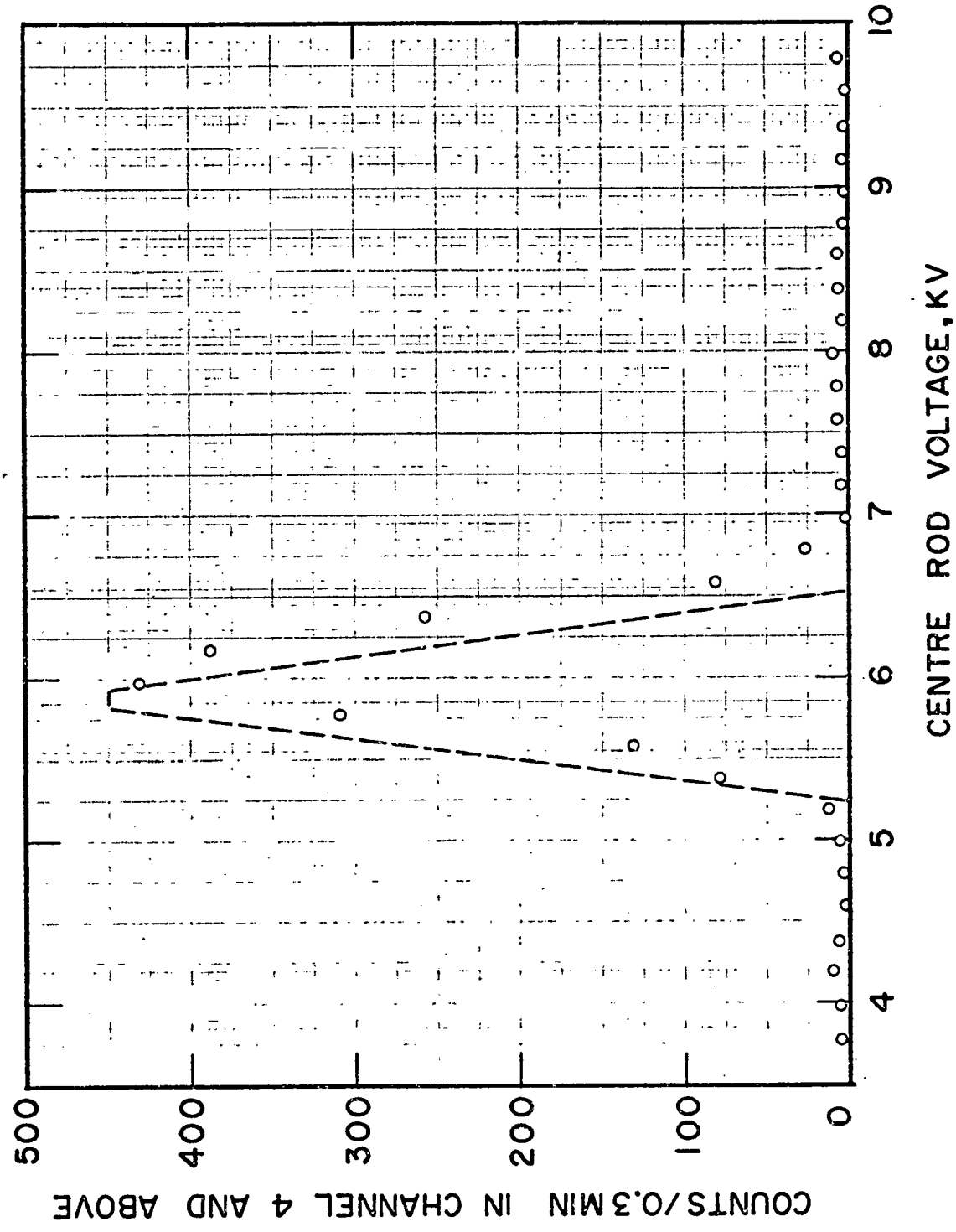

Figure 22. A typical counts-vs.-voltage curve for a polystyrene latex aerosol carrying single charge.

The dashed line is the passage function for monodisperse 0.79 micron diameter particles.

proportional to the value of the aerosol flow q_a. This does not hold true. Even when tests from a given data book page, such as p. 174, are compared among themselves, the values found for N are not strictly proportional to q_a. This indicates that the mobility analyzer is not working in strict accordance with the theory of sections 5.3 and 5.4.

The mean mobility column in table IV should be independent of the flow rates. It is seen in the table that this column is, in fact, very nearly constant. All but one of the 14 tests for the single charged peak are within 1% of 13.85 cm^2/megavolt-sec. This mobility corresponds to a mean particle size of 0.80 microns. If the mean mobilities found for the different q_o are considered separately, the constancy of values is improved, indicating some systematic differences in the measurements of q_o.

The standard deviation columns, both absolute and relative, in table IV should also be independent of flow rate. It is seen, however, that these range over a factor of approximately two. There seems to be some correlation between the standard deviation found and the flow rates, particularly q_s. This again indicates that the mobility analyzer is not working in strict accordance with the theory of section 5.3 and 5.4.

It should be pointed out that the present tests are rather severe ones for the mobility analyzer. The standard deviation is found from the difference of the mean square mobility and the mean mobility squared. For the tests in table IV, these quantities were apparently very nearly equal, differing only in the fourth significant figure. One feels, therefore, that the standard deviation

might be strongly affected by statistical fluctuations in the data, at least when the relative standard deviation is small. (Incidentally, this points up the need for very accurately computed values for the integrals I_o, I_1 and I_2.) A typical value for the standard deviation in table IV is 4.0×10^{-7} cm^2/volt-sec. This is equivalent to a standard deviation of .019 microns for the particle diameter. The corresponding relative standard deviations are 0.029 for the mobility and 0.024 for the diameter.

The fact that the computed mean and standard deviation of the particle diameter differ somewhat from the values stated by the manufacturer does not, of itself, imply that the mobility analyzer is malfunctioning. As pointed out by Fuchs and Sutugin(1965), it is difficult to aerosolize PSL in such a way that the aerosol particles are identical to the particles in the latex.

Although the mobility analyzer performance is not quite up to expectations, it is nevertheless very good. Its performance is such that it is capable of measuring, at least approximately, the relative standard deviation of mobility for an aerosol for which this quantity is of the order 0.03. A further conclusion from these tests is that the aerosol generator produced an extremely high quality aerosol, at least during the period when these tests were run.

One other item of interest concerning the quality of the aerosol is the possible presence of double particles. According to Ströber, et al(1969), a singly charged doublet will have mobility equal to 0.7 times that for a singly charged single particle. Thus, singly charged doublets, if present, should pass through the mo-

Table IV

Moment determination for mobility data
from single and double charged 0.79 micron PSL

particle charge	flowrates, cc/sec outlet q_o	aerosol q_a	sampling q_s	date	data book page	N, number of particles per 0.3min	mobility, cm^2/megavolt-sec arithmetic mean	standard deviation	relative st'd dev.
1	25.2	2.0	1.7	3/9/71	163	1099	14.16	0.145	.0102
1	25.2	2.0	1.7	3/18/71	177	390	13.94	0.293	.0210
1	25.2	2.0	3.4	3/25/71	180	177	13.93	0.435	.0312
1	25.2	4.0	3.4	3/18/71	177	1263	13.96	0.382	.0273
1	34.4	2.0	1.7	3/18/71	177	317	13.75	0.327	.0238
1	34.4	2.0	3.4	3/25/71	180	174	13.84	0.426	.0308
1	34.4	4.0	3.4	3/15/71	173	586	13.78	0.420	.0305
1	50.5	2.0	1.7	3/10/71	170	219	13.81	0.347	.0251
1	50.5	2.0	3.4	3/10/71	170	319	13.83	0.390	.0282
1	50.5	2.0	3.4	3/15/71	174	244	13.89	0.371	.0267
1	50.5	2.0	4.8	3/10/71	170	342	13.94	0.472	.0339
1	50.5	4.0	3.4	3/15/71	174	511	13.81	0.398	.0288
1	50.5	6.0	3.4	3/15/71	174	870	13.82	0.430	.0311
1	50.5	8.0	3.4	3/15/71	174	1185	13.83	0.443	.0321
2	77.3	2.0	3.4	3/25/71	180	120	27.17	0.836	.0308
2	77.3	4.0	3.4	3/25/71	180	350	27.32	0.808	.0258

bility analyzer at a voltage 1/0.7 = 1.4 times the voltage for which singly charged singlets appear. This would be 8400 volts in figure 22. Doubly charged doublets should appear at 4200 volts. One does, in fact, see small bumps in figure 22 at approximately these voltages. Their amplitude is about 1/100 of that for the main peak. Thus it appears that the doublet concentration is of the order 1% of the total for the PSL aerosols used here.

The scatter observed in the mean and standard deviation of mobility for the singly charged PSL is due in part to the small number of particles counted. (The peak count rate in figure 22, for example, was about 430 counts per 0.3 minute cycle.) An estimate of the scatter due to this effect alone is available in appendix D, where comparable cases have been treated by simulation methods. From the results in appendix D, it appears that the scatter in table IV is in large measure due to the small-sample statistics effect.

6.0 EXPERIMENTAL DETERMINATION OF MOBILITY DISTRIBUTIONS FOR ARTIFICIALLY CHARGED AEROSOLS

As discussed in chapters 3 and 4, the width of the charge distribution for an artificially charged aerosol certainly depends on the particle size and upon the manner in which the particles are exposed to ions. Several other factors may also be involved. An experimental program was therefore designed for investigating the effect on the charge distribution of the following factors:

1. charger design
2. particle size
3. aerosol initial charge
4. flow rate through charger
5. aerosol concentration
6. aerosol material.

The apparatus, test procedure and test results are discussed in this chapter.

Obviously, the most important piece of apparatus in these experiments is the aerosol charger. The design of this charger determines to a large extent whether or not all particles will have an equal opportunity to acquire charge. Two essentially different charger designs were studied in the experiments. These chargers are discussed in section 6.1.

The particle sizes which could be employed in the experiments were dictated to some extent by the capabilities of the apparatus. The sizes studied were approximately 0.4, 0.7 and 1.0 microns.

Two states of initial charge for the aerosol were considered to be of special interest. One was the case where all particles were uncharged initially. The other was the case where the aerosol was in equilibrium with bipolar ions prior to entry into the

charger. This latter case - the Boltzmann equilibrium charge state - is considered appropriate for any well aged aerosol. These two initial charge states, as well as a few aerosols with higher initial charge, were tried in the experiments.

Changing the flow rate through the charger changes primarily the particle residence time within the charger. It may appear, therefore, that the effect of flow rate on the charge distribution is completely predictable. However, changing the flow rate changes the Reynolds number of the flow, so that it is conceivable that the flow patterns could also change. For this reason, it was considered advisable to determine the charge distribution for each charger at two flow rates. These differed by a factor of three.

The concentration of aerosol within the charger is not expected to affect the charge distribution at all. However, Dötsch, et al(1969) found that at very high concentrations, the mean charge acquired depended on the concentration. It was therefore considered worthwhile in the present tests to check the charge distribution at two aerosol concentrations. These differed by a factor of nine.

The aerosol properties other than particle size are not expected to influence the charging process noticeably. The physical state - solid or liquid - is not expected to be important, for example. Nevertheless, it was found valuable in the present experiments to compare the test results based on one aerosol with those from a totally different aerosol. The two aerosols used were polystyrene latex and dioctyl phthalate. The two aerosol generators are discussed in section 6.2.

The test procedure is dictated to some extent by the capabi-

lities and versatility of the aerosol generator. Different test procedures were devised for the two different aerosols. Test procedures and results for the dioctyl phthalate aerosol are presented in section 6.4. The corresponding presentation for the polystyrene latex aerosol is in section 6.5.

The test procedures were designed so that the effect of a given factor may be seen directly by comparing an appropriate pair of test results. In this chapter, the discussion of test results is limited to making such comparisons. The test results are presented primarily in terms of mobility distributions and moments of these distributions. Comparison of test results with theory, which requires establishing the connection between mobility distributions and charge distributions, is deferred until chapter 7.

6.1 The charger designs studied

Two essentially different charger designs were studied in these experiments. In one (the sonic jet charger), the charging is accomplished by mixing an ion-laden airstream with the particle-laden airstream. Intense turbulence is probably present in the mixing zone. In the other design (the triode corona charger), charging is accomplished by using a weak electric field to draw ions through the aerosol stream. An attempt is made to secure laminar flow. These two chargers are described in the following pages.

6.1.1 The sonic jet charger

The sonic jet charger tested in the present experiments has been described by Whitby and Clark(1966). It is shown also in

figure 23.

The ion generator portion of the jet charger is of the type described by Whitby(1961). In it, air flows at sonic velocity through a nominal .0135" diameter square-edged orifice, which is supplied with dried air at 35 psig. A tungsten needle with tip diameter 5 microns or less is positioned upstream of this orifice, perpendicular to the orifice plate. The point-to-plane spacing is 2 to 3 mm. The orifice plate is grounded and the needle is maintained at about 3500 volts negative. A corona discharge occurs at the point of the needle and the negative ions are ejected towards the orifice plate. The air flowing into the orifice at high velocity entrains some of these ions with the result that the emerging jet carries a high concentration of negative ions.

The aerosol charging is accomplished by causing the ion-laden air jet to mix with the aerosol stream. The aerosol is brought in radially at the base of the jet and the two streams form a co-current flow through a throat section. In this section, the two streams presumably mix thoroughly. At the exit of the throat section is placed a reservoir to permit further contact between ions and particles.

Three different charging reservoirs were tried in the present experiments. The charging reservoir shown by Whitby and Clark(1966) has a volume of 22 liters. This will be referred to as the large kettle. Recently, a 1.2 liter reservoir has been used instead, as shown in figure 23. This will be called the small kettle. A third type of reservoir was also tested in the present experiments. It consisted of a 91 cm length of brass tube with 1.27 cm internal

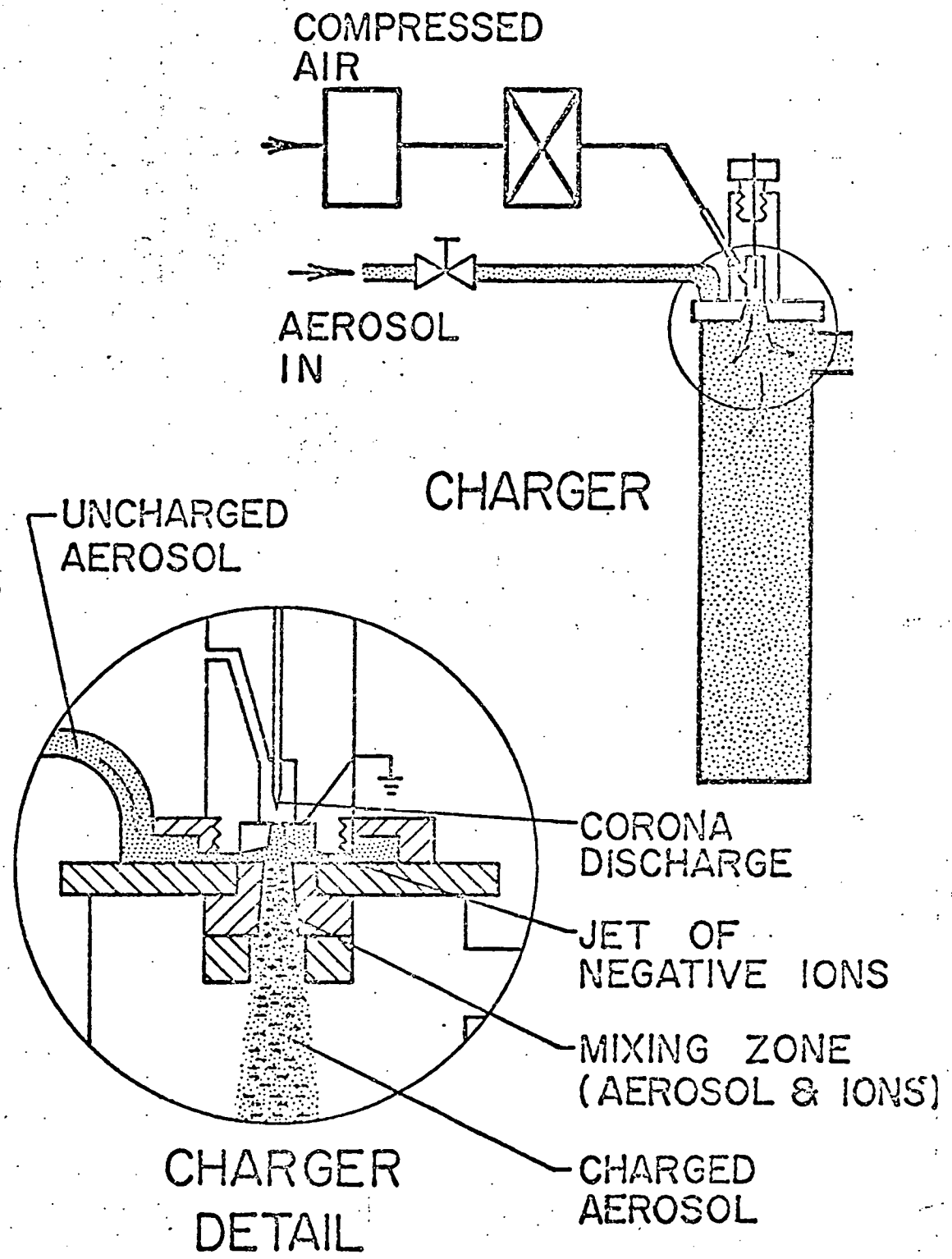

Figure 23. The sonic jet charger.

The mixing reservoir depicted is the small kettle.

diameter. This diameter fairs in smoothly with the throat section of the charger. The tube was aligned with the jet axis, and the aerosol was taken out through the end opposite the jet. This will be called the tube reservoir.

The operation of the sonic jet charger is monitored by grounding the charging reservoir through an electrometer. The current flow was kept near 30 nanoamps by adjusting the needle spacing and/or voltage.

The ionizer airflow is listed by Whitby and Clark(1966) as 3.4 l/min. The unit used in these tests, however, was found to pass 7.5 l/min. Probably, the orifice had become worn due to repeated cleaning.

Since no external electric field is applied in the region where charging occurs, the sonic jet charger is expected to act as a diffusion charger.

6.1.2 The triode corona charger

The second type of charger considered in the present tests was a scaled-up version of the charger studied by Bademosi(1971). It is similar in many respects to the charger used by Goyer, Gruen and LaMer(1954). It also has several points of similarity to Hewitt's(1957) charger. We shall call it the triode corona charger. It is shown in figure 24.

The electrical elements of the triode corona charger are similar to a triode vacuum tube. The three electrodes of the charger are the corona wire, the ion screen and the collecting plate. These are analagous to the cathode, the grid and the plate, respectively, of the triode vacuum tube. In the charger used here, how-

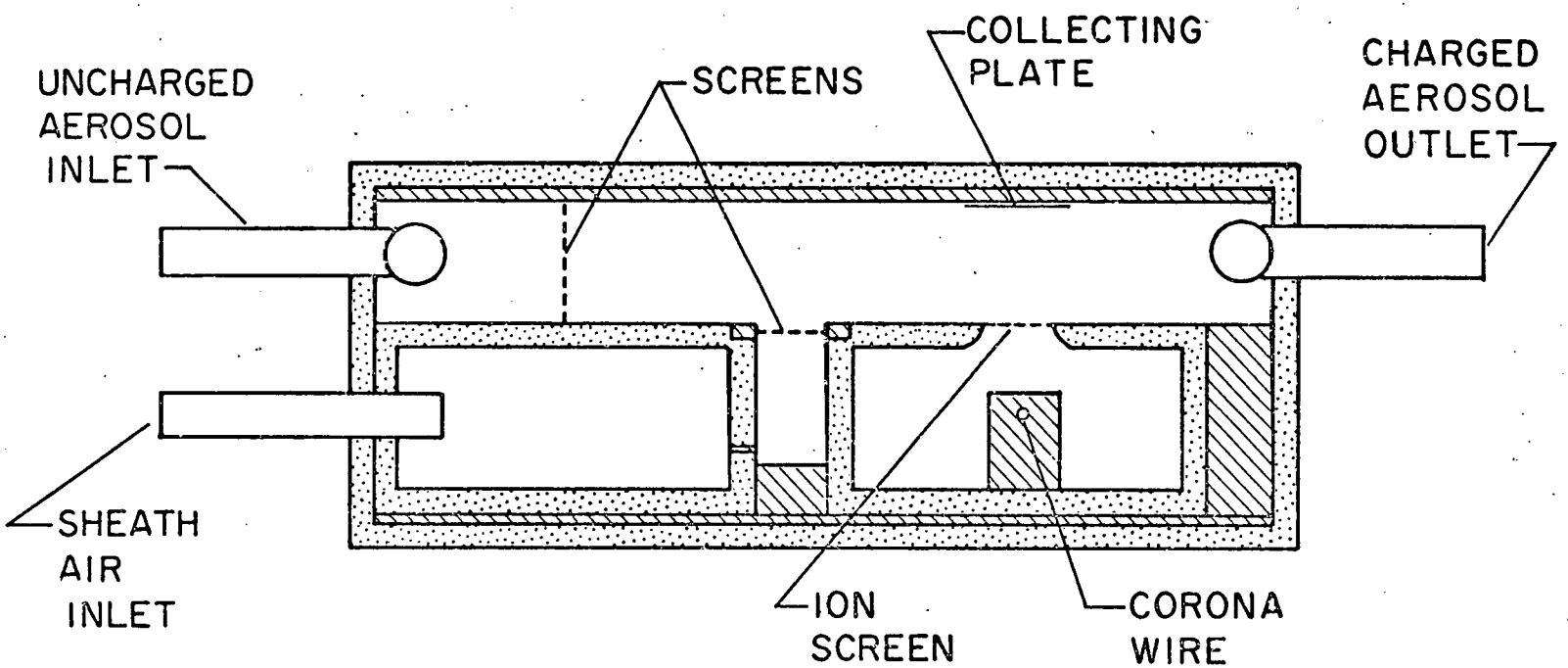

Figure 24. The triode corona charger.

ever, the polarities of the electrodes were reversed from those in the vacuum tube; positive ions, rather than electrons, were the charge carriers.

The aerosol flow in the triode corona charger occupies part of a rectangular channel, whose dimensions are width(w) = 5" and height(h) = 9/16". Adjacent to one of the 5" walls of the channel is mounted a chamber for the generation of ions. A rectangular opening, 5" by 3/8", in the channel wall permits ions to pass from the chamber into the channel. On the channel wall opposite the screen is mounted a collecting electrode. When a modest potential is applied to this electrode, ions from the vicinity of the screen are drawn across the channel through the aerosol flow. This provides the opportunity for aerosol particles to capture ions. The dimensions of the charging region are:

h = dimension in the direction of ion flow = 9/16"
l = dimension in the direction of aerosol flow = 3/8"
w = the remaining demension = 5"

The ion-generating chamber is in the form of a rectangular parallelopiped whose long dimension is equal to the width w of the channel. At the axis of this box is placed a .001" diameter tungsten wire. In normal operation this wire is held at about 5 kilovolts positive, yeilding a corona current of 60 μamps. The collecting electrode is held at 90 volts negative. The ion current flowing through the screen and across the channel to the collecting electrode is 9.1 nanoamps.

The part of the channel which is not occupied by aerosol flow is taken up by a clean air sheath. This sheath is admitted to the

channel just upstream of the ion screen. It prevents aerosol particles from penetrating the ion screen into the corona chamber. It was found by Bademosi(1971) that this air sheath greatly improved the uniformity of charging.

In normal operation, the flow through the charger is about 3 l/min, of which 20% is sheath air. Since the electric field in the charging region is only 63 volts/cm, the charging is due to ionic diffusion.

The charger used here differs from the Goyer, Gruen and LaMer (1954) unit in that the present unit incorporates an ion screen, an air sheath and uses a much lower electric field. It differs from Hewitt's(1957) charger in the use of an air sheath and in that a low DC potential is applied to the collecting electrode, instead of a high square-wave AC potential.

6.2 The test aerosols employed

Two aerosols were used in these tests. One is solid and the other is liquid. The differences between them, however, are more profound than their physical state. They differ in dispersity, concentration and the amount of extraneous particles in the aerosol.

6.2.1 Dioctyl phthalate (DOP)

The DOP aerosol used in these experiments was generated by means of the condensation apparatus described by Tomaides, Liu and Whitby(1971). Figures 1, 2 and 3 of that article show the device in drawing and photograph.

In the condensation aerosol generator, DOP (Union Carbide Corp., South Charleston, W. Va.) diluted as desired with denatured alcohol

is atomized by means of a single-jet Collison atomizer. The Collison is operated at 35 psig. The atomizing airflow was measured at 50.4 cc/sec. The mist from the Collison is passed downward through a 19 mm glass tube. The upper portion of this tube is heated by means of an electrical heating tape. In this region of the tube, the alcohol and DOP evaporate, leaving residual particles composed of the nonvolatile impurities in the alcohol or the DOP. In the lower portion of the glass tube, which is cooled by air currents, the DOP recondenses on the residue particles. The resulting aerosol is more nearly monodisperse than the original mist. The droplets are smaller because the alcohol component of the original mist does not recondense. The size of the droplets may therefore be controlled by the percentage of DOP in the original solution.

At the bottom of the glass tube, a small portion (1 to 2 cc/sec in these experiments) of the flow is removed from the center of the glass tube by means of a peristaltic pump. The remaining aerosol is discarded. The small portion of aerosol is pumped into a charge neutralizing chamber, where it is mixed with 55 cc/sec of air carrying a high concentration of bipolar ions. Within this chamber (volume = 4 liters), the aerosol charge is brought to a level near the Boltzmann equilibrium (equation 1).

From the charge neutralizer, the aerosol is led through a concentric tube electrical condenser. When the high voltage to this condenser is turned on, it removes all charged particles from the aerosol, provided the particle diameter is less than about 1.2 microns. In these experiments, additional diluting air, as re-

quired, was added to the aerosol downstream of the condenser - not upstream as shown by Tomaides, et al(1971).

6.2.2 Polystyrene latex (PSL)

The PSL aerosol generator used in these tests has already been described in section 5.4 of this thesis. The charger tests in chapter 6, however, required much larger aerosol flow than the tests in section 5.4. Therefore, the full aerosol flow (29.1 l/min) was passed through the K_r^{85} neutralizer and made available for the charger. This reduced the residence time to about 4 sec. Difficulties were encountered in neutralizing the particles. The neutralizer previously used had to be replaced by a more active unit.

6.3 The arrangement of apparatus

The arrangement of apparatus for these experiments differed in some details according to which aerosol and which charger was in use. In general, however, the arrangement was as depicted by the "crossroads" below.

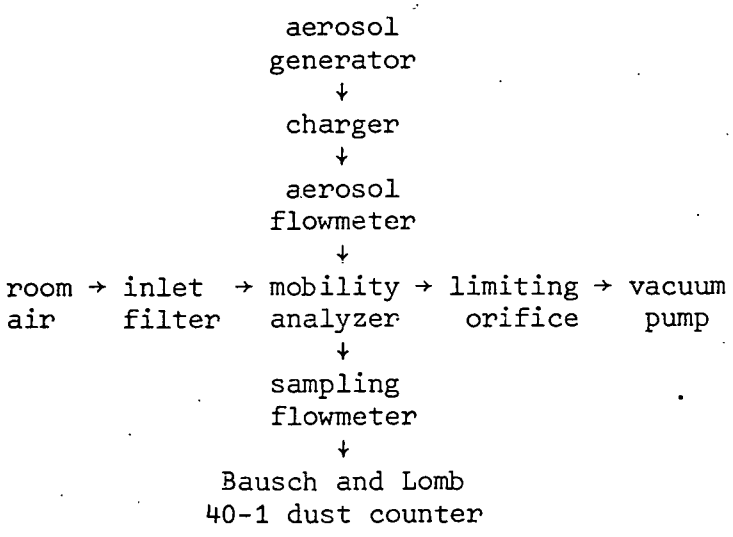

The downward arrows indicate either aerosol or sampling flow. The

rightward arrows indicate clean air or main outlet flow.

The aerosol generator was either the DOP or the PSL unit, already described. The standard output flow of the DOP condensation generator is 3.4 l/min. If a higher aerosol flow rate to the charger is desired, it is obtained by adding clean, dry, diluting air at a point between the generator and the charger. The PSL generator, as used here, has a standard output flow of 29.1 l/min. If this was more than required for the charger, the excess was dumped at the same point.

The aerosol provided by the DOP generator has a very high concentration (of the order 10^5/cc). This had to be reduced considerably to be acceptable to the apparatus that follows. The reduction in concentration was accomplished by splitting the aerosol flow into two streams, passing the larger flow through a high efficiency filter, then rejoining the streams. This can be accomplished compactly by puncturing the element of the filter and sealing into the hole a short piece of small bore tubing. The tubing acts as a controlled leak through the filter. One or two such denuders, as required, were used in the DOP experiments.

The charger was either the triode corona charger or one of the three versions of the sonic jet charger.

The aerosol flowmeter and its method of calibration were described in section 5.5.3. For all tests described in this chapter, the aerosol flow was set at 2.83 cc/sec. The excess aerosol from the charger was discarded just upstream of the aerosol flowmeter.

The mobility analyzer was described in section 5.2.

For the tests described in this chapter, the aerosol counting

was accomplished with a Bausch and Lomb 40-1 dust counter together with the Bausch and Lomb digital read-out (Bausch and Lomb, Inc., Rochester, N.Y.). Since the 40-1 dust counter does not have an integral flowmeter, a sampling flowmeter was made up of a 16.4 cm length of 1/16" ID stainless steel tubing. This tubing was sealed into a similar length of larger, more rigid, tubing. A tee was fitted at either end of the larger tubing. This assembly was fit between the sampling port of the mobility analyzer and the inlet of the dust counter. A slant manometer (1" H_2O full scale) was used to read the pressure drop across the flowmeter. For all tests described in this chapter, the sampling flow rate was 2.83 cc/sec. The flowmeter was calibrated by the syphon method as described in section 5.5.3.

The filter at the clean air inlet of the mobility analyzer was an MSA "Ultra Filter" cartridge (Mine Safety Appliances Co., Pittsburg, Pa.). For some tests, two of these were used in series.

The limiting orifice and vacuum pump used to establish the main outlet flow from the mobility analyzer have been described in section 5.5.3. The flow rates, however, were re-measured by means of a "bubble meter" of the type described by Levy(1964). The meter was made up from a 3 ft. length of 1.708" ID glass tube. Two marks, separated by 1 liter of volume (determined by a volumetric flask), were scribed on the tube. This tube was set vertically with its top connected to the inlet filter of the mobility analyzer. Thus the clean air for the mobility analyzer was drawn first through the glass tube. When a suitable soap solution is touched to the bottom end of the glass tube, a soap film forms across it

and travels up the tube. The travel time between the two marks was determined with a stop watch. The readings are repeatable to within 1/10 sec.

For the calibration of the limiting orifii, the aerosol inlet and sampling outlet of the mobility analyzer were blocked, so that the clean air flow and main outlet flow were identical. The results were

orifice nominal flow	measured flow
0.5 and 1.0 l/min in parallel	25.30 cm/sec ± 0.26%
1.0 and 1.0 l/min in parallel	34.14 cm/sec ± 0.23%
3.0 l/min	50.10 cm/sec ± 0.43%

The ± figures represent the 90% confidence limits based on 5 time readings.

The power supply used to establish the potential of the center rod in the mobility analyzer was the Fluke 10 kilovolt unit already mentioned in section 5.5.3.

6.4 Test procedure and results for the DOP aerosol

Eight tests were done with the DOP aerosol. Each test involved a different combination of charger and droplet size. The combinations used are shown in table V, part A.

Each test with the DOP aerosol was run according to an agenda designed to present the charger with a variety of aerosol conditions. One scan through the appropriate sequence of voltage settings for the mobility analyzer was devoted to each item on the agenda. (That is, the mobility spectrum was determined for each item.) Six scans were made for each test. The operating conditions for the charger and the aerosol generator for each of the

Table V

Operating conditions for the charger tests with the DOP aerosol

Part A The charger, droplet size, and corresponding test number, data book page and date for the DOP tests.

	% DOP and approx. drop size		
	1%,0.4μ	4%,0.7μ	10%,1 μ
sonic jet, large kettle	I,358 8/5/71	II,356 8/5/71	III,354 8/5/71
sonic jet, small kettle		IV,350 8/2/71	
sonic jet tube reservoir		V,348 8/2/71	
triode corona charger	VI,342 7/31/71	VII,340 7/31/71	VIII,338 7/31/71

Part B The test agenda

Each DOP test consisted of six scans in rapid succession. The data under sonic jet charger apply only to tests I through V. The triode corona charger data apply only to the remaining tests.

scan number	1	2	3	4	5	6
DOP generator:						
tubing pump(cc/sec)	2.12	2.12	2.12	2.12	0.59	2.12
neutralizer airflow(cc/sec)	53.4	53.4	53.4	53.4	53.4	53.4
neutralizer voltage	on	on	on	on	on	on
condenser voltage	zero	6000	6000	6000	zero	zero
location of denuder in relation to charger	before	before	before	after	before	before
sonic jet charger						
aerosol flow(l/min)	29.1	29.1	10.0	29.1	29.1	29.1
ionizer air(l/min)	7.5	7.5	7.5	7.5	7.5	7.5
charging current (nanoamps)	zero	30	30	30	30	zero
triode corona charger						
total airflow(l/min)	3.4	3.4	10.0	3.4	3.4	3.4
sheath air	20%	20%	20%	20%	20%	20%
charging current (nanoamps)	zero	9.1	9.1	9.1	9.1	zero

six scans are shown in part B of table V.

In scan 1, the electrical condenser within the DOP generator cabinet was turned off. Therefore, the entire Boltzmann-equilibrated aerosol from the neutralizer was allowed to reach the charger. But the charging current was also turned off. Thus the aerosol was passed along unchanged to the mobility analyzer. The scan was made covering that range of voltage settings necessary to map out the mobility peaks corresponding to the single and double charged particles. The double charge peak was taken only to corroborate the single charge peak. Data from the single charge peak, however, was used to determine the mean and standard deviation of mobility, and the corresponding values for the DOP droplet size. The number of particles carrying the single unit of charge (of one sign only) was also determined.

In scan 2, the condenser was turned on, so that only the uncharged particles from the neutralizer were allowed to reach the charger. The charger current was also turned on. Thus the output of the charger consisted of the originally uncharged particles from the neutralizer, now charged by unipolar ions. Scan 2 was considered to be the standard operating condition for the charger.

In scan 3, the flow rate through the charger was altered by a factor of three. This was accomplished by charging the amount of diluting air added at the generator output. (The flow through the condenser, which remained on, was not changed.) The charger remained on. Thus the residence time in the charger and/or the mixing ratio in the charger were altered. Incidentally, the concentration was also altered.

In all tests, at least one denuder was used. This denuder passed approximately 1 particle out of every 9 that approached. It was normally placed immediately upstream of the charger. In scan 4, the apparatus was first returned to the conditions in scan 2, then the denuder was moved to immediately downstream of the charger. Thus, relative to scan 2, the concentration of aerosol in the charger was increased about 9 fold.

In scan 5, the conditions differed from those in scan 2 in that the condenser was turned off and that the tubing pump rate was decreased. With the condenser off, all particles - charged and uncharged - from the neutralizer were passed on to the charger. (the increase in number of particles was partly offset by the decrease in pumping rate.) Thus the aerosol reaching the charger approximated a well aged aerosol with the Boltzmann equilibrium charge distribution.

Scan 6 was a duplication of scan 1. It was made to check on drifts in the size or concentration of DOP aerosol. Each scan required about 15 minutes; the complete test (six scans) took about 1½ hours.

In summary, the purpose of each of the six scans was:

scan	purpose
1	to determine the DOP size
2	to determine the mobility distribution of the aerosol for "standard" operation of the charger
3	to determine the effect of charger flow-rate on the mobility distribution
4	to determine the effect of aerosol concentration on the mobility distribution

scan	purpose
5	to determine the effect of nonzero initial charge on the mobility distribution
6	to recheck the DOP droplet size.

Scan 2 is regarded as the benchmark to which scans 3, 4 and 5 may be compared.

6.4.1 Characteristics of the DOP aerosol

For each test, the size of the DOP droplets was determined from the data of scans 1 and 6. Specifically, the procedure was to apply the calculation scheme described in section 5.4 to that portion of the mobility spectrum which is due to singly charged particles. This determines the mean and standard deviation of mobility for the singly charged particles, as well as the number of them which enter the mobility analyzer during one counting interval. These quantities (denoted by $\bar{Z}_p$, σ_{Z_p} and N, respectively) are entered in table VI under scans 1 and 6.

It is seen from table VI that for each test the single charge mobility in scan 6 is less than that in scan 1. The largest shift occurred in test II, where the two mean mobilities were:

17.7 cm^2/megavolt-sec for scan 1
15.3 cm^2/megavolt-sec for scan 6.

These shifts indicate that, in every test, the droplet size increased in the course of the test. The drop sizes corresponding to the mean single charged mobility may be found in table III. Thus for test II, the initial and final drop sizes were 0.65 microns and 0.74 microns, respectively.

Table VI

Experimental values of mobility distribution moments
for the DOP tests

$\overline{N}$=number of particles/30 sec $\overline{Z}_p$,σZ_p=mean and st'd dev. of mobility in cm^2/megavolt-sec rsd = relative st'd dev.	test I	test II	test III	test IV	test V	test VI	test VII	test VIII
	1% DOP	4% DOP	10% DOP	4% DOP	4% DOP	1% DOP	4% DOP	10% DOP
	sonic		jet	charger		triode	corona	
	large	kettle		sm.kettle	tube res.	charger		
scan 1 - Condenser off, charging current off. Determination of single charge mobility.	$\overline{N}$ = 3806	2724	909	2005	3311	1942	1824	2069
	$\overline{Z}_p$ = 31.6	17.7	10.8	16.2	17.3	31.1	18.2	10.8
	σZ_p= 3.97	2.62	1.31	2.30	2.73	3.57	2.61	1.54
	rsd= .126	.148	.121	.142	.158	.115	.143	.143
scan 2 - Condenser on, charging current on. "Standard" operation of the charger.	4473	2802	980	2095	2414	1732	1342	1837
	565	518	498	394	310	517	451	450
	124	105	93	82	52	68	54	51
	.220	.202	.187	.208	.169	.131	.121	.114
scan 3 - Condenser on, charging current on. "Nonstandard" flow rate through charger	12197	6491	3340	5764	7043	698	580	525
	601	555	544	457	397	336	306	299
	107	88	79	75	70	67	59	52
	.179	.159	.146	.165	.176	.200	.194	.173
scan 4 - Condenser on, charging current on. High aerosol concentration in the charger.	3794	1911	694	1586	2575	4392	3393	3003
	560	519	506	402	312	499	459	454
	124	103	94	80	51	69	53	47
	.221	.199	.185	.198	.164	.137	.116	.103
scan 5 - Condenser off, charging current on. Initial charge distribution is Boltzmann.	2309	2429	882	1183	1180	2181	2330	3119
	564	518	499	405	313	508	484	451
	123	103	90	83	56	63	55	47
	.219	.199	.179	.204	.177	.124	.113	.104
scan 6 - Condenser off, charging current off, Duplication of scan 1.	4262	2209	815	1888	2278	2463	1871	1506
	30.3	15.3	10.2	15.4	16.0	30.5	17.4	10.2
	4.38	2.13	1.29	2.33	2.33	3.77	2.67	1.24
	.144	.139	.126	.151	.146	.124	.153	.122

The shifting of droplet size, which is probably due to the distilling away of alcohol from the DOP-alcohol solution, is one disadvantage of the DOP aerosol. Fortunately, the mobility spectrum for the charged aerosol proves to be only weakly dependent on particle size, so that perfect size-stability is not required in the present tests.

Another disadvantage of the DOP aerosol is that it is not particularly monodisperse. This is seen from the standard deviation of the single charged mobility, listed also under scans 1 and 6 in table VI. The relative standard deviations range from 0.12 to 0.15. The relative standard deviations for size will be slightly smaller, due to the form of the relationship between size and single charge mobility. The aerosol, however, cannot be considered highly monodisperse. Fortunately, high monodispersity is not required in these experiments. The effect of aerosol polydispersity will be considered further in chapter 7.

The final computed quantity for the singly charged particles is the number N which enter the analyzer during one counting cycle. Since the aerosol flow q_a was 2.83 cc/sec and the counting time was 30 sec for all the DOP tests, the number N may be converted to concentration (of singly charged particles of one sign) by dividing by 2.83x30 = 85 cc. Thus in test I, the concentration in scans 1 and 6 were 44.8 and 50.1 particles/cc, respectively. Such changes in concentration, both up and down, were common in the DOP tests, as may be seen from table VI.* However, if we assume that

*The value of N in test V, scan 1, should not be compared to scan 6 because the neutralizer voltage was inadvertantly left off during scan 1. Also, the N-values for the triode corona charger tests are erratic because two denuders in series were required for these tests.

these 10% to 20% changes may be divided up among five scans, the change during any given scan is small. The conclusions regarding the mobility distributions are therefore believed to be unaffected by the concentration drifts.

The aerosol formed from the 1% DOP solution requires special comment. It is believed that the smallest droplets in this aerosol were too small to be detected by the dust counter. Hence the aerosol was probably more polydisperse than the results here indicate. However, if the dust counter ignores these small droplets in every scan, their presence should have no effect on the conclusions drawn regarding the aerosol charge distribution.

A further indication of the aerosol quality may be provided by plotting the mobility distributions from scans 1 and 6. This is done in figure 25. In this graph, we have chosen to plot the distribution of $\log Z_p^*$ rather than that of Z_p^* itself. Let these two distributions be denoted by $\hat{f}(\log Z_p^*)$ and $f(Z_p^*)$ respectively. Then

$$\hat{f}(\log Z_p^*)\,d(\log Z_p^*) = f(Z_p^*)\,dZ_p^*$$

or

$$\begin{aligned}\hat{f}(\log Z_p^*) &= f(Z_p^*) \div [d(\log Z_p^*)/dZ_p^*] \\ &= Z_p^* f(Z_p^*)/\log(e)\end{aligned} \tag{53}$$

$f(Z_p^*)$ is determined from data by mean of equation (45), replacing Z_p^T by Z_p^*. Z_p^* is determined from data by means of equation (39).

(continued)It was learned later that this is bad practice: the penetration through a series of denuders may change with their relative orientation. However such changes should occur only between scans, so that conditions during each scan should be constant.

Combining these,

$$\hat{f}(\log Z^*) \simeq \frac{q_o + \frac{1}{2}(q_s - q_a)}{q_s \log(e)} \cdot \frac{N^*(\Delta\phi)}{N}$$

All factors except N^* are constant for a given spectrum. Hence, if the normalization is not important, we may write simply:

$$\hat{f}(\log Z_p^*) \propto N^*(\Delta\phi). \qquad (54)$$

Thus we obtain a non-normalized distribution of $\log Z_p^*$ by simply plotting the raw data N^* versus $\log Z_p^*$. This is what is presented in figure 25.

The two mobility spectra shown in figure 25 are scans 1 and 6 from test II. For each scan, the peak corresponding to single charged particles is clearly defined. (That it is, in fact, the single charge peak is made clear by the location of the next peak, which has mobility twice that of the first.) It is seen that the single and double charge peaks are not completely separated. This is not due to poor resolution in the mobility analyzer (the resolution for this test was 5.5; see equation 41). The lack of separation is due to aerosol polydispersity.*

The shift in location and amplitude of the single charge peak during the course of test II is seen clearly in figure 25.

6.4.2 Mobility distributions for the charged DOP aerosols

For each test, the mobility analyzer data for the charger-on scans was processed by the methods of section 5.4 (equations 50)

*Figure 25 here may be contrasted to Hewitt's(1957) figure 4. The DOP aerosol used by Hewitt was obviously much more nearly monodisperse than that used here.

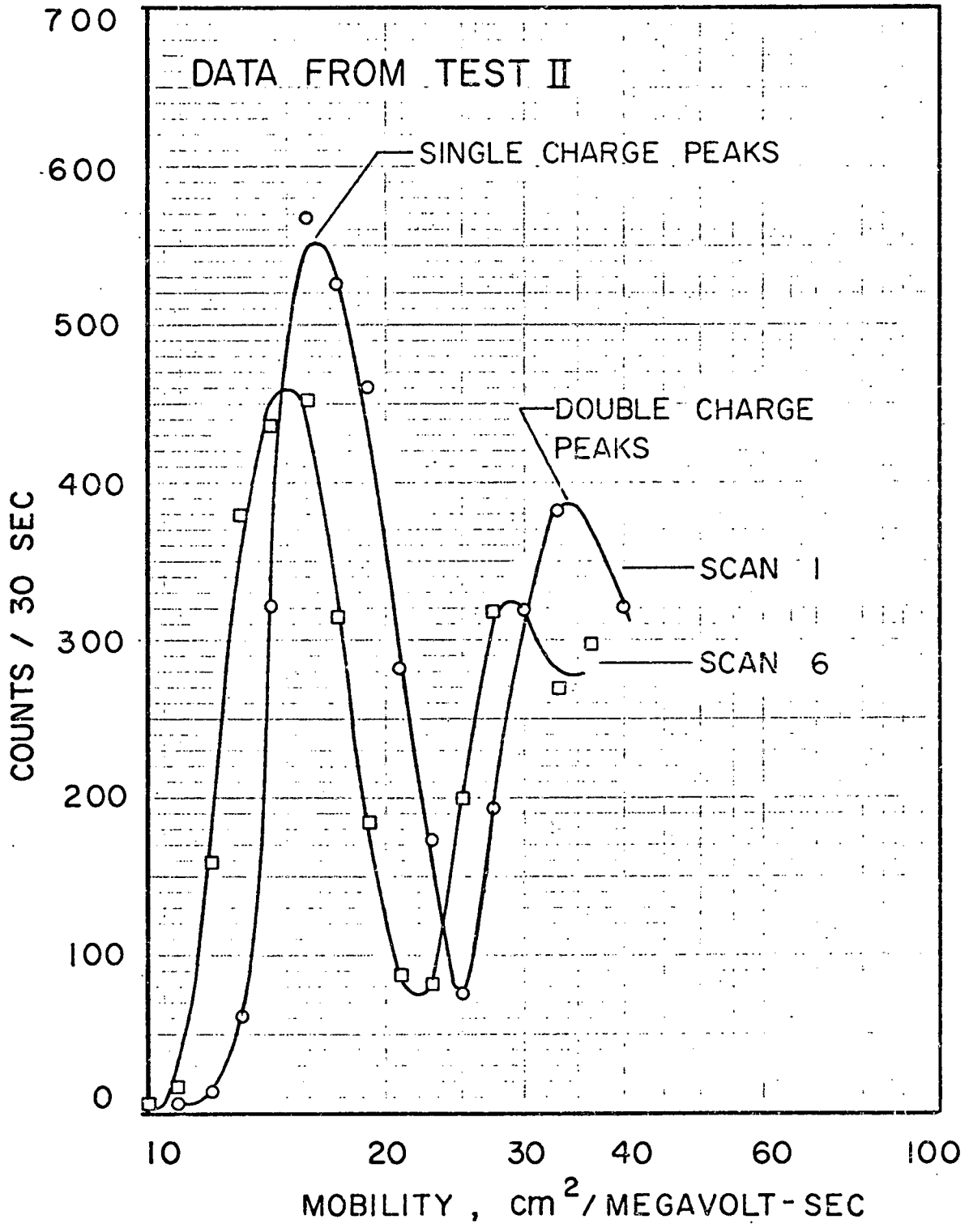

Figure 25. Duplicate mobility spectra for natural charged DOP.

to yield the quantities N, $\bar{Z}_p$ and σ_{Z_p}. These are entered into table VI. Scan 2 represents the standard operating condition for the charger. Scans 3, 4 and 5 were each intended to check the effect of one particular factor on the mobility distribution.

Consider first the effect of aerosol concentration within the charger. In scan 2, the concentration was dropped nine-fold prior to charging. In scan 4, the drop was after charging. Thus the concentration within the charger differed by a factor of nine in the two scans. Yet, according to table VI, there was virtually no change in either the mean or standard deviation of mobility. In test I, for example, the mean and standard deviations were 565 and 124 cm^2/megavolt-sec for scan 2 and 560 and 124 cm^2/megavolt-sec for scan 4. The duplication is equally remarkable in the other tests. (The number N, however, does not duplicate well; the reason for this is not known.) It may be concluded that the charging process is unaffected by concentration, at least for concentrations of the order 10 to 100 particles/cc.

Consider next the effect of initial charge on the mobility distribution. In scan 2, only uncharged particles were admitted to the charger. In scan 5, the aerosol passed to the charger was Boltzmann-equilibrated. Yet it is seen in table VI that the mean and standard deviation for these two scans were virtually identical, test by test. We may conclude that the initial charge, if no greater than the Boltzmann equilibrium level, has no effect on the resultant mobility distribution.

Scans 2 and 3 of each test differed in the flow rate through the charger. For the sonic jet charger in its three versions, the two flowrates were 29.1 l/min and 10.0 l/min. For the triode

corona charger, the flowrates were 3.4 l/min and 10.0 l/min. As may be seen in table VI, a decrease in flowrate leads to an increase in the mean mobility in every test. This is to be expected from the increased residence time in the charger. The effect on the width of the mobility distribution, however, is quite unexpected. In tests I through IV, a decrease in flowrate causes a decrease in standard deviation. In test V, there was an increase. In the remaining tests, there was virtually no change. In summary:

charger	effect of decrease in flowrate on st'd dev.
sonic jet, lg. kettle	decrease
sonic jet, sm. kettle	decrease
sonic jet, tube res.	increase
triode corona charger	no change.

Whether or not these trends would continue upon further change of flow rate is an interesting question which must remain unanswered.

The effect of particle size upon the mobility distribution may be seen by comparing scan 2 of tests I, II and III or of tests VI, VII and VIII. Both the mean and standard deviation of mobility decrease with increasing size. The standard deviation decreases somewhat more rapidly than the mean.

The effect of charger design, as well as charger flowrate, on the mobility distribution of the aerosol may be seen graphically in figures 26 and 27. These figures show scans 2 and 3 for the four tests involving the 4% DOP aerosols. The distributions were computed by application of equation (45), after N had been determined by use of equation (50). The size reported on figures 26 and 27 is the average of the sizes determined from scans 1 and 6 of

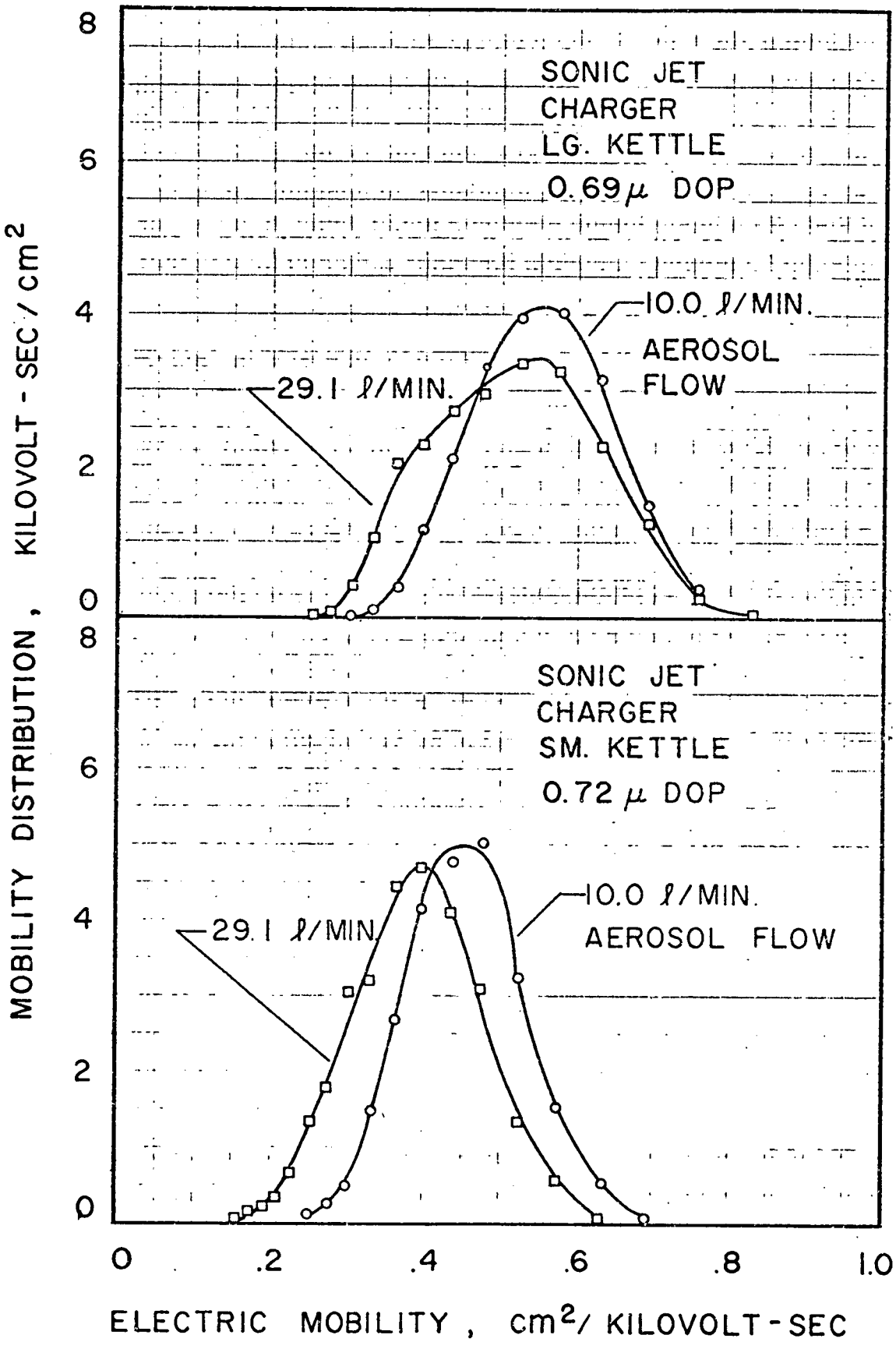

Figure 26. Mobility spectra from the sonic jet charger.

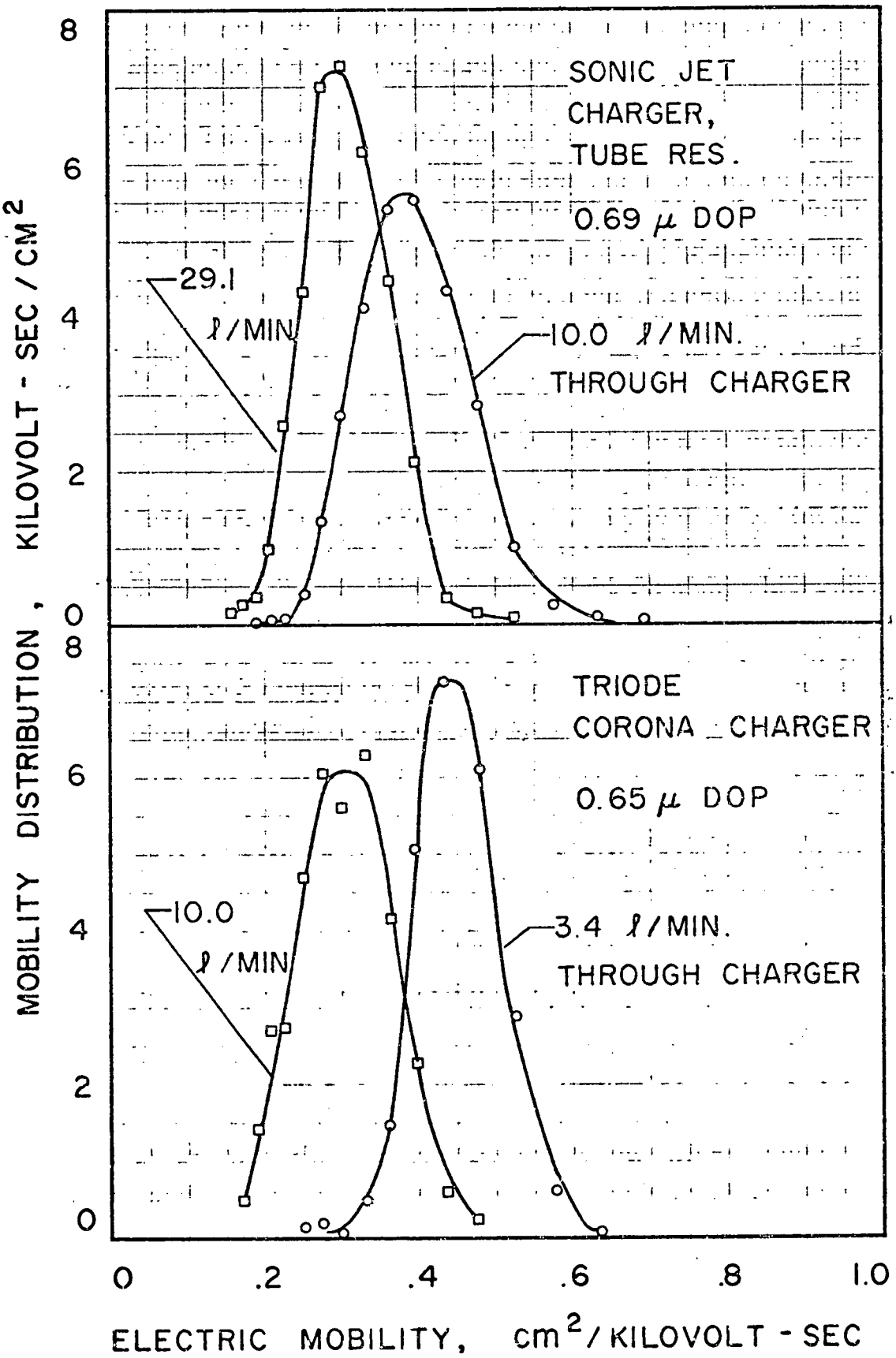

Figure 27. Mobility spectra from the tube and triode chargers.

the corresponding test.

The curves in figures 26 and 27 are arranged in order of increasing uniformity of mobility. The broadest mobility distribution is that for the sonic jet charger, large kettle, at the top of figure 26. When the large kettle is replaced by the small kettle, both the mode and the width of the distribution decrease, as seen at the bottom of figure 26. This trend is continued when the small kettle is replaced by the tube reservoir (top of figure 27). Finally, at the bottom of figure 27, the narrowest mobility spectrum is achieved with the triode corona charger.

It may be noted that the mobility distributions in figures 26 and 27 are all nearly symmetric. One exception is that for the sonic jet, large kettle, at 29.1 l/min. This peculiar shape was noted also in tests I and II (not shown in the graphs). Figures 26 and 27 again show the effect of altering the charger flow rate.

It may be worthwhile to mention that the distributions shown in figures 25, 26 and 27 are distorted copies of the real mobility distributions, owing to imperfect mobility analyzer resolution. It is believed, however, that the distortion is negligible for these particular figures. In any case, the values listed in table VI are completely and automatically corrected for imperfect resolution.

6.5 Test procedure and results for the PSL aerosol

As described in section 5.5, the experimental checks of the mobility analyzer performance were done with a polystyrene latex aerosol. Those tests indicated not only that the mobility analyzer functioned well, but also that the PSL aerosol was of high quality.

It was then planned that the same aerosol would be used for the experimental study of charge distributions for artificially charged aerosols. However, when the tests with the PSL aerosol commenced, a sequence of difficulties was encountered which eventually led to the adoption of DOP as the test aerosol. Selected results from the PSL tests are presented here for comparison to the DOP results. All tests employed the 0.79 micron diameter PSL mentioned in section 5.5.

No fixed test agenda was followed in the PSL tests. As a general rule, however, each data set was done in duplicate to check on repeatability (there were few exceptions). Frequently, the duplicate data sets did not agree perfectly: either the amplitude or the mode of the charged aerosol mobility spectrum changed slightly. Only one of the two data sets was used in the computations. Also as a general rule, the mobility peak for the single or double charged particles was checked at least once in every test.*

The charging tests with the PSL aerosol commenced after a one month lapse from the tests of section 5.5. The only changes required in apparatus were to increase the aerosol flow through the Kr^{85} neutralizer and to insert the sonic jet charger between the generator and the aerosol flowmeter. It was found that the original Kr^{85} neutralizer was ineffective at the higher flowrate

*The mean mobility for single charged particles during these tests was mostly on the range 13.45 to 13.55 cm /megavolt-sec. This is about 2½% below the value 13.85 found repeatedly in section 5.5. The reason for this difference is not known. The standard deviations were generally similar to those found in section 5.5.

(29.1 l/min.) and it had to be replaced by a more active unit. A portion of the mobility distribution for the aerosol emerging from the new neutralizer is shown in figure 28.

Clearly visible in figure 28 are mobility peaks corresponding to particle charges 1 through 6. (The small peak at 20 cm^2/megavolt-sec is believed to be due to doubly charged double particles. See discussion at the end of section 5.5.) By comparing with equation (1), it may be seen that the peak amplitudes do not decrease quite as rapidly with charge as expected for the Boltzmann equilibrium. We conclude that the aerosol charge is not quite reduced to the Boltzmann equilibrium level.*

As a further check on the charge of the "neutralized" aerosol, the mean absolute charge was measured by the method of Thomas and Rimberg(1967). The value found was 4.2 charge units. The value expected for a 0.79 micron diameter aerosol on the basis of equation (1) is 2.1. This again indicates that the aerosol was not fully neutralized. There is indirect evidence, also, that the charge level of the aerosol emerging from the neutralizer changed from day to day; the mean charge was often higher than 4.2 units.

In order to further reduce the charge level of the PSL aerosol before its presentation to the charger, a parallel plate precipi-

*Figure 28 is of interest also in connection with section 5.5. First note that the amplitude of the peak tentatively identified as doubly charged doublets suggests that 1 particle in 15 is a doublet. The proportion of doublets is higher than indicated in section 5.5. Note also that the width and shape of the peaks is due mostly to imperfect analyzer resolution. The resolution (see equation 41 and following) for this spectrum was 8.06. Thus, in theory, the first eight peaks should be fully resolved. In figure 28, however, only five peaks are fully resolved. The discrepancy between theory and practice is believed to be due to aerosol polydispersity.

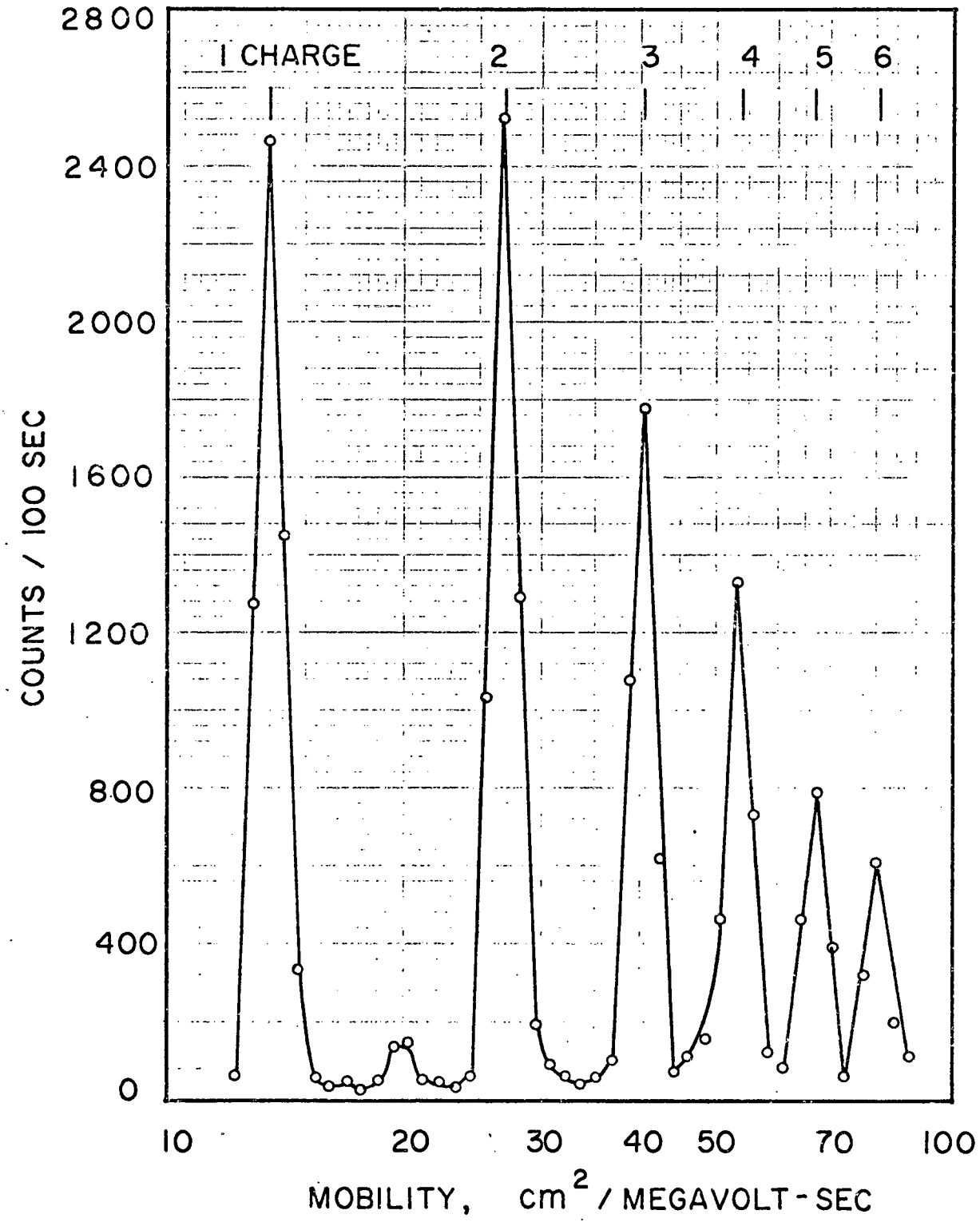

Figure 28. Mobility spectrum for natural charged 0.79 micron PSL.

tator was installed between the generator and the charger. The geometry and operating conditions for this precipitator were:

plate spacing	= 2.6 cm
plate width	= 21.6 cm
plate length	= 67.4 cm
flow rate	= 29.1 l/min
applied potential	= 10 kv

Under these conditions, it may be calculated (assuming laminar flow) that all 0.79 micron particles with charge greater than six units will be precipitated. A fraction of the lower charged ones will also be precipitated.

The results of selected PSL tests are shown in table VII. Consider first the results from data book page 263, pertaining to the sonic jet charger with the large kettle. For the first data set, the parallel plate precipitator voltage was left off. For the second, it was on at 10 kv. It is seen that turning on the voltage diminishes the number of particles reaching the mobility analyzer by a factor of three, due to the removal of charged particles in the precipitator. Also the mean and standard deviation of mobility are reduced 10-15%. The "precipitator on" values are 668 and 178 cm^2/megavolt-sec for the mean and standard deviation, respectively. Since the single charge mobility for the PSL particles is 13.5 cm^2/megavolt-sec, the corresponding mean and standard deviation for the charge distribution are 49.4 and 12.8 charge units, respectively. Rather similar values are obtained for the "precipitator on" test of the triode corona charger (data book page 260).

The mean charges determined from the PSL tests described above were higher than expected from past experience and from charging theories. At this point, it was decided to try a DOP aerosol of

Table VII

Experimental values of mobility distribution moments for the PSL tests

$\underline{N}$ = the number of particles entering analyzer per count time.
$\overline{Z}_p$, σ_{Z_p} = the mean and st'd dev. of mobility, cm^2/megavolt - sec.
rsd = the relative standard deviation.

Sonic jet, large kettle

aerosol flow = 29.1 l/min charging current = 30 nanoamps	data book page, date and count time 263 6/30/71 100 sec	 278 7/8/71 100 sec	 307 7/21/71 30 sec
Direct aerosol flow precipitator out or off, silica bed bypassed, no Triton added	$\underline{N}$ = 30768 $\overline{Z}_p$ = 722 σ_{Z_p} = 209 rsd =.289	30248 682 198 .291	9868 644 176 .274
Parallel plate precipitator inserted between generator and charger. Flow rate through PPP = 29.1 l/min.	10887 668 173 .259		
Silica gel dessicant bed inserted between PSL generator and charger.		8344 654 178 .271	
Triton X100 added to PSL suspension.			8921 516 100 .194

Triode corona charger

total flow rate = 3.0 l/min charging current = 9.1 nanoamps	data book page, date and count time 260 6/29/71 100 sec	 310 7/21/71 30 sec	 311 7/21/71 30 sec
Direct aerosol flow precipitator out or off, no Triton added	$\underline{N}$ = 33168 $\overline{Z}_p$ = 672 σ_{Z_p} = 195 rsd =.290		
Parallel plate precipitator inserted between generator and charger. Flow rate through PPP = 29.1 l/min.	12748 666 188 .283		
Triton X100 added to PSL suspension		6946 490 44 .091	5385 488 44 .090
Triton X100 added and PPP on Flow rate through PPP = 29.1 l/min for page 310 3.0 l/min for page 311		4315 501 41 .082	2670 526 48 .091

roughly equal size. Not only was the mean charge less for the DOP, but the width of the distribution was also reduced dramatically. This indicated that the PSL aerosol was not as simple as previously believed. It was thought that the anomalous results with the PSL aerosol were due to interference by the residue particles in the aerosol. It is emphasized, however, that in every test with the charger turned off, the single charge mobility indicated a highly monodisperse aerosol.

In another PSL test (data book page 278), the parallel plate precipitator was replaced by a silica gel bed. This had a dual purpose:

1. to dry the aerosol
2. to remove a large fraction of the small residue particles by diffusion.

The sonic jet charger was used in this test. It is seen in table VII, which shows the results both with and without the bed, that the number of particles reaching the mobility analyzer was reduced 3½ fold by the action of the bed. The mean and standard deviation of charge, however, were reduced only slightly. The single charge mobility peaks for the two conditions (not included in table VII) were identical except in number; this was in the ratio 2½:1.

In the final PSL tests, a small amount of Triton X-100 dispersing agent (Rohn and Hass Company, Philidelphia, Pa.) was added to the PSL suspension. One small drop suspended on the point of a needle was added to the approximately ½ pint of water in the Collison reservoir. Before and after tests using the sonic jet charger are shown in table VII (data book page 307). The addition

of Triton to the PSL suspension dramatically reduced both the mean and the standard deviation of the particle charge. The number of particles decreased slightly. The corresponding single charge mobility peaks (not included in table VII) were identical except for a 25% increase in number upon addition of the Triton.

The mobility distributions for the sonic jet charger before and after Triton are shown also in figure 29. The absissa and ordinate values were computed from the data by means of equations (39) and (45), respectively. (Z_p^+ was replaced by Z_p^*; N was computed from equation 50.) The "after Triton" distribution is seen to be very nearly the same as the best corresponding case for the DOP aerosol, at the top of figure 26. Thus the differences between the PSL and DOP aerosols are resolved by the addition of Triton.

For the triode corona charger, the addition of Triton had an even more dramatic effect: the standard deviation of the charge distribution was reduced four-fold. This is shown in table VII under data book page 310. Also shown is the result of a test in which the parallel plate precipitator was turned on. This appeared to further decrease the standard deviation of mobility.

For the test listed in table VII under data book page 311, the flow rate through the parallel plate precipitator was reduced from 29.1 to 3.0 l/min. Under these conditions, the precipitator should remove all charged 0.79 micron particles (when it is turned on). According to table VII, the mean and standard deviation of the mobility distribution increased upon removal of the charged particles from the feed aerosol. This is not comprehensible. It may be the result of statistical fluctuations.

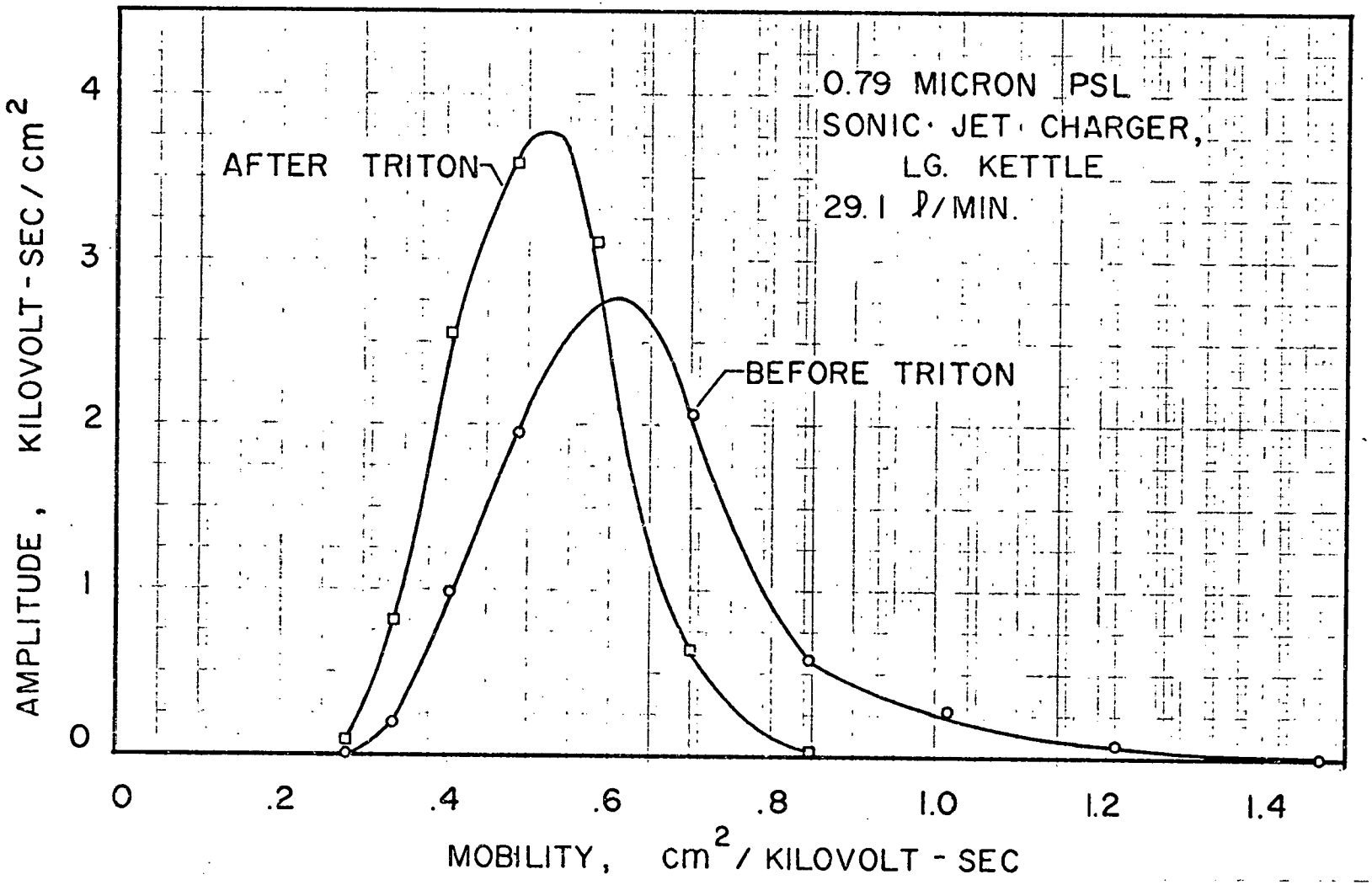

Figure 29. Mobility spectra for charged PSL, before and after Triton.

The explanation for the effect of Triton on the PSL aerosol is not known. One might suppose that it would reduce the number of multiple particles in the aerosol, but this was shown to be small even without Triton. Furthermore, a decrease in the number of clusters in the aerosol should increase the mean mobility, not decrease it as was found. Another possible effect of Triton would be an alteration of the residue aerosol. However, to explain the change in mobility distribution the residue aerosol must have decreased in size and/or number. This is unreasonable. Finally, there is evidence that the addition of Triton reduced the initial charge of the PSL particles. This is seen by comparing the number of particles reaching the mobility analyzer for the precipitator "on" and the precipitator "off" runs, with and without Triton. (Data book pages 260 vs. 310 in table VII.) Without Triton, 2/3 of the particles were precipitated (page 260); with Triton, 1/3 were precipitated (page 310). In both cases, however, this removal of charged particles from the aerosol fed to the charger had little effect on the resulting mobility distribution. This indicates that the initial charge is unimportant in any case. It is emphasized again that the addition of Triton had no effect on the mobility of singly charged particles.

The effect of Triton on the PSL aerosol will be left unexplained. Further comment on the results of the PSL tests is deferred until chapter 7.

7.0 DISCUSSION OF EXPERIMENTAL MOBILITY DISTRIBUTIONS

Chapters 3 and 4 of this thesis presented a theoretical treatment of the charge distribution of an aerosol after its exposure to unipolar gas ions. Several simplifying assumptions were necessary is those chapters. Chapter 6 of this thesis presented experimentally determined mobility spectra for aerosols which had been passed through one of several real charging devices. The purpose of chapter 7 is to form comparisons between experiment and theory. We are particularly interested in the uniformity of charging, as measured by the standard deviation of the charge or mobility spectra. By comparing experiment to theory, we hope to determine how and why the real charging devices differ from the abstract model devices.

This chapter is arranged somewhat in parallel to chapters 3 and 4. In section 7.1, the results of experiment are compared to the minimum variance charge distributions of chapter 3. Section 7.2 takes up the effect of non-uniform particle size in the test aerosols. In section 7.3, comparison is made between the experimental results and the maximum variance charge distributions of chapter 4. The charge distributions resulting from other exposure time distributions are compared to experiment in section 7.4. Concluding remarks are offered in section 7.5.

7.1 Comparison to the minimum variance charge distribution

The process of charging aerosol particles by exposure to gaseous ions was discussed theoretically in chapters 3 and 4. In chapter 3, it was assumed that all particles have equal exposure to ions, and therefore equal opportunity to acquire charge. The

charge distribution which resulted from this assumption was called the minimum variance charge distribution. It was claimed in chapter 3 that this distribution represents the ultimate in uniformity of particle charge.

The detailed form of the minimum variance charge distribution depends on the details of the mechanism assumed for the capture of ions by the particles. Three mechanisms were considered in chapter 3. These were:

1. White diffusion charging
2. Continuum diffusion charging
3. Field charging.

In the experimental tests of chapter 6, neither charging unit employed a high electric field in the charging region. Therefore the experimental results should be compared to one of the diffusion charging mechanisms. Furthermore, since the particle size in the experiments was always greater than 0.4 microns, the continuum diffusion charging mechanism is expected to be nearer the truth than the White mechanism.

In section 3.3, approximate expressions were developed for the standard deviation σ of the minimum variance charge distribution. For the diffusion charging models, it was found that

$$\sigma = [by(\tau)]^{\frac{1}{2}}$$

where

b = the electrical size of the particle

$y(\tau)$ = a function given in table II.

For White charging, the function $y(\tau)$ is virtually independent of exposure time t; its value is ½. For continuum charging, it varies slowly with time. Over a broad range of exposure times, its value is within 10% of 0.7. Thus

$$\sigma = 0.707\sqrt{b} \qquad \text{for White charging}$$

$$\sigma \approx 0.84\sqrt{b} \qquad \text{for continuum charging}$$

The point we make here is that for the minimum variance charge distribution, the standard deviation is virtually independent of exposure time and only weakly dependent on the charging mechanism. It depends on the square root of the particle size. This makes comparison to experiment simple.

The standard deviation of mobility for the minimum variance charge distribution is

$$\sigma_{Z_p} = Z_1\sigma = Z_1[by(\tau)]^{\frac{1}{2}}$$

This relation has been plotted in figure 30, using the value 0.7 for $y(\tau)$. It is plotted in the form σ_{Z_p} versus Z_1, for easy comparison to data. Also shown in figure 30 are the experimental values of σ_{Z_p} and the mean single charge mobility $\overline{Z_1}$ for the DOP tests. Figure 30 shows clearly that the standard deviations of the experimental mobility distributions are larger than that expected from the minimum variance charge distribution. Furthermore, for the sonic jet charger in its three versions, σ_{Z_p} is found to depend on exposure time (that is, flowrate). In the remaining parts of this chapter we shall try to determine why the chargers studied by experiment do not conform to the ideal one of chapter 3.

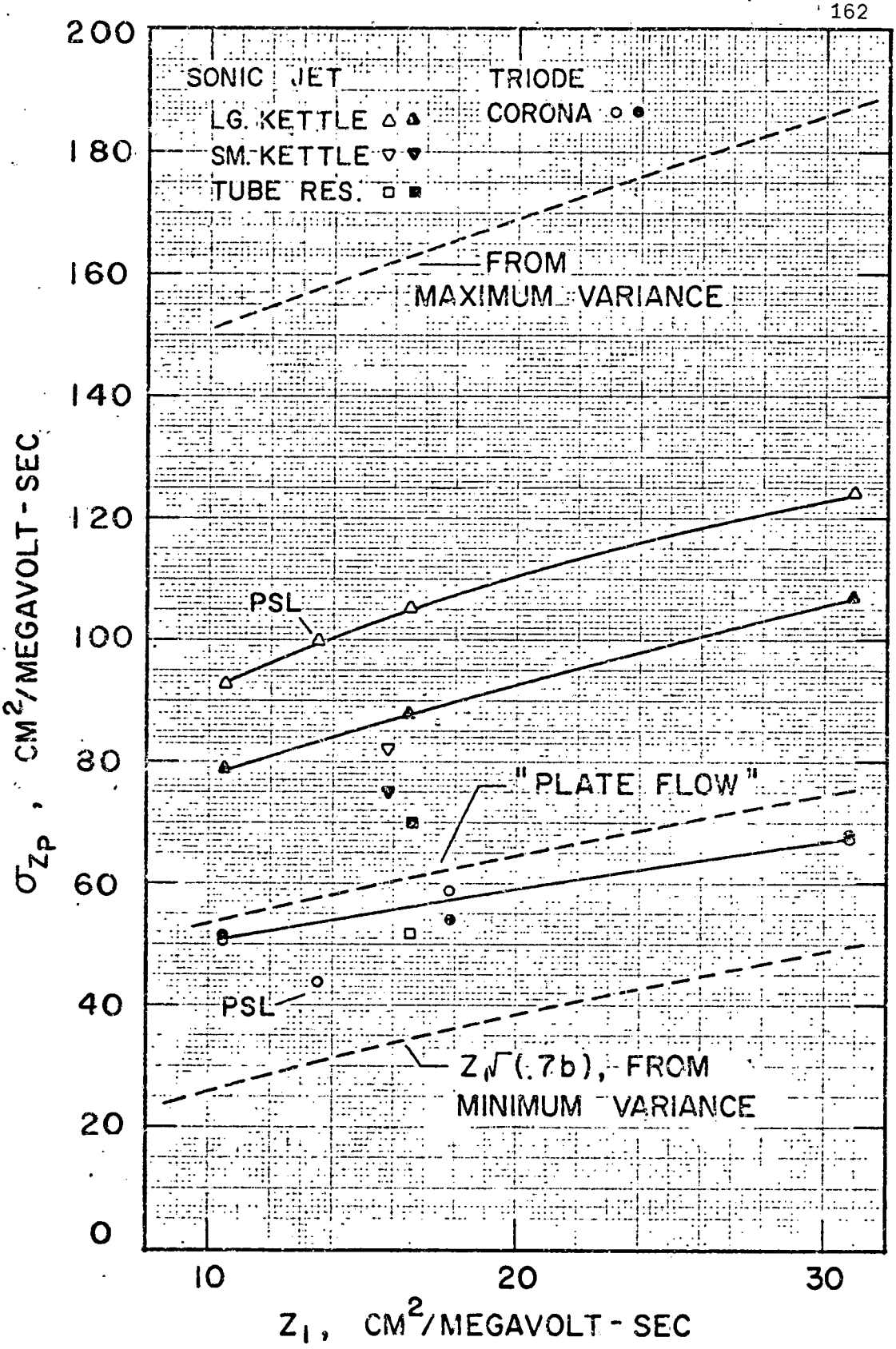

Figure 30 Experimental and theoretical mobility distribution width

The open points are the high flowrate.
The filled-in points are the low flowrate.

There is no need at this time to compare the experimental and theoretical mean mobilities.

7.2 The question of aerosol polydispersity

The charging theories of chapters 3 and 4 were written for monodisperse aerosols. Due to practical limitations, however, the experiments had to be done with slightly polydisperse aerosols. It is obvious that non-uniformity of particle size will cause an increase in the width of the charge distribution, and of the mobility distribution. The question here is whether its effect is so large as to account for the discrepancy between theory and experiment in figure 30.

There is some direct experimental evidence on the contribution of polydispersity to the mobility distribution width. This comes from a comparison of the DOP and PSL tests. These two aerosols differ considerably in their uniformity of size. The PSL results are shown also in figure 30.

For the sonic jet charger, the charged aerosol mobility standard deviation fits in well with the curve through the DOP results. This indicates that aerosol polydispersity has no effect on the mobility distribution width, at least for this charger and this size particle.

For the triode corona charger, the PSL result shown in figure 30 is the average of four test results. These test results are somewhat questionable, because they did not duplicate well. It is seen in figure 30 that standard deviation of the charged aerosol mobility distribution is smaller for the PSL aerosol than for the DOP tests. This indicates that aerosol polydispersity is a factor

in the DOP tests on the triode corona charger. There is still a considerable gap between theory and experiment however.

It is of interest also to explore the matter of aerosol polydispersity from a theoretical angle. We shall make use of the approximate expressions for the mean and variance of the minimum variance charge distribution (section 3.3).

$$\text{mean charge:} \quad \bar{k} = bx(\tau)$$

$$\text{variance of charge:} \quad \sigma^2 = by(\tau)$$

Also, by definition of σ^2, the mean square charge $\overline{k^2}$ is

$$\text{mean square charge:} \quad \overline{k^2} = \sigma^2 + \bar{k}^2 = by(\tau) + [bx(\tau)]^2$$

These expressions apply to any monodisperse aerosol. For the case of continuum diffusion charging, τ and therefore x and y are independent of particle size; the size dependence is concentrated in the factor b, the electrical size of the particle.

The mean, mean square and variance of the mobility distribution for the monodisperse aerosol are

$$\text{mean mobility:} \quad Z_1\bar{k} = Z_1 bx(\tau)$$

$$\text{variance of mobility:} \quad Z_1^2\sigma^2 = Z_1 by(\tau)$$

$$\text{mean square mobility:} \quad Z_1^2[\sigma^2 + \bar{k}^2] = Z_1^2 by(\tau) + [Z_1 bx(\tau)]^2$$

For a polydisperse aerosol, the mean mobility may be expressed as an average of the mean mobility for its component monodisperse aerosols (see Lindgren, 1962, p.102). The same is true of the

mean square mobility. The average is taken with respect to the aerosol size distribution $f_s(d_p)$.

$$\text{mean mobility:} \quad \overline{Z_p} = \int Z_1 \bar{k} f_s(d_p) dd_p$$
$$= x(\tau) \int Z_1 b f_s(d_p) dd_p$$

$$\text{mean square mobility:} \quad \overline{Z_p^2} = \int [(Z_1\sigma)^2 + (Z_1\bar{k})^2] f_s(d_p) dd_p$$
$$= y(\tau) \int Z_1 b f_s(d_p) dd_p + x^2(\tau) \int Z_1^2 b^2 f_s(d_p) dd_p$$

Then the variance $\sigma_{Z_p}^2$ of the mobility distribution is

$$\sigma_{Z_p}^2 = y(\tau) \int Z_1^2 b f_s(d_p) dd_p + x^2(\tau) \cdot \text{var}(Z_1 b)$$

where (55)

$$\text{var}(Z_1 b) = \int Z_1^2 b^2 f_s(d_p) dd_p - \left[\int Z_1 b f_s(d_p) dd_p\right]^2$$

The first term in equation (55) is an average variance of the component monodisperse aerosols. The second term, as evidenced by the presence of $x(\tau)$, derives from the mean mobility of the component aerosols.

The value of $\text{var}(Z_1 b)$ for the test aerosols may be easily estimated from the data. To do this, note that the product $Z_1 b$ is uniquely related to Z_1 itself. Therefore,

$$[\text{var}(Z_1 b)]^{\frac{1}{2}} \simeq \frac{d(Z_1 b)}{dZ_1} \sigma_{Z_1}$$

The quantity σ_{Z_1} is determined for each test aerosol in the experiments. The derivative $d(Z_1 b)/dZ_1$ may be evaluated from a table of $Z_1 b$ versus Z_1, or by direct differentiation. Thus $\text{var}(Z_1 b)$ is determined. For example, for a few of the DOP test aerosols:

test	var(Z_1b), (cm^2/megavolt-sec)^2
VI	10.78
VII	6.96
VIII	2.56

Also, to fit the mean mobility observed in the experiments, the function $x(\tau)$ must have a value of about 5.0. When these values are combined into equation (55), it is found that polydispersity should increase the value of σ_{Z_p} by 3 to 7% in these tests. The theoretical estimate, then, is that aerosol polydispersity has a negligible effect in the present experiments.

The theoretical and experimental evidence regarding the effect of aerosol polydispersity do not agree completely. In any case, however, its effect is too small to account for the discrepancy between theory and experiment in figure 30. It is clear, then, that none of the chargers studied charge aerosols in accordance with the minimum variance charge distribution.

7.3 Comparison of experimental results to the maximum variance charge distribution

The maximum variance charge distribution was defined in section 4.2. This resulted when the time of particle exposure to ions obeyed the negative exponential distribution. Superficially, it seems that this model could be applicable to the sonic jet charger, particularly with the large kettle.

The maximum variance charge distribution based on continuum diffusion charging was discussed in section 4.2.2, and tabulated in appendix B. The standard deviation of charge is approximately proportional to particle size and changes slowly with exposure

time.

The mean mobilities found by experiment for the charged aerosols are best duplicated by the entries in appendix B corresponding to 20 units dimensionless exposure time. The mobility standard deviation for this maximum variance distribution is plotted against Z_1 in figure 30. It is seen that the broadest experimental mobility distributions (sonic jet charger, large kettle, 29.1 l/min.) have width about 62% of that for the maximum variance distribution. The sonic jet charger therefore does not conform to the uniform mixing model from which the maximum variance distribution was derived. This conclusion is supported also by the experimental observation that σ_{Z_p} changes markedly with flowrate for the sonic jet charger.

An indication of the way in which the sonic jet charger differs from the uniform mixing model is provided by comparing the experimental mobility distribution (top of figure 26 or figure 29) to the maximum variance charge distribution (figure 10, solid curve). The long tail to the left in figure 10 is missing in the experimental distributions. The long tail is due to particles which pass through the charger very quickly, acquiring little charge. For the real charger, there is apparently a certain minimum residence time or minimum charging. Probably, this minimum charging occurs in the throat section of the sonic jet charger. It is clear from the experiments, however, that not all the charging occurs in the throat section. The mixing reservoir size has a strong effect on charge acquired, indicating that some charging occurs in the reservoir.

7.4 Comparison of experimental results to the "plate flow" charge distribution

It has been established that all the experimental mobility spectra have widths which lie well within the boundaries set by the minimum and maximum variance charge distributions. Both these models have been recognized as extreme cases. The triode corona charger has a charging region with such simple geometry that one is tempted to devise a more specific model for this charger. We are encouraged in this effort by the theoretical results pictured in figure 13. There, adoption of a "pipe flow" exposure time distribution increased the spectrum width by about 50% relative to the minimum variance spectrum. (Note also a substantial change in the mode.) An increase of this magnitude would largely close the gap between theory and experiment in figure 30.

In the triode corona charger the aerosol flows in a rectangular channel. This channel has aspect ratio 5:9/16 ≈ 9. The aerosol flow in this channel may be similar to fully developed flow between infinite parallel plates. Then the distribution of exposure times for particles in the charger is given by equation (26), the "plate flow" exposure time distribution. (For the moment, we will neglect the sheath air in the triode corona charger.)

The mean dimensionless exposure time $\pi\varepsilon Z_i n\bar{t}$ (continuum diffusion charging) for the triode corona charger may be computed by means of the following considerations. The dimensions h, l and w of the charging region have been given in section 6.1.2. The charging current I may be expressed as

$$I = n\varepsilon Z_i E_o l w.$$

where E_o is the electric field in the charging region. The mean particle residence time in the charging region is $\bar{t} = lwh/Q$, where Q is the charger flowrate. Thus the mean dimensionless exposure time τ is

$$\tau = \pi\varepsilon Z_i n l w h/Q$$

Combining these expressions, we find

$$\tau = \frac{\pi h I}{E_o Q}$$

The ion mobility conveniently cancels out. The operating conditions for the triode charger were:

I = 9.1 nanoamps = 27.3 statc/sec

E_o = 90 volts/(9/16") = 0.210 statv/cm

h = 9/16" = 1.43 cm

Q = 57 or 167 cc/sec for DOP tests

= 50 cc/sec for PSL tests

Thus

τ = 10.2 or 3.5 for the DOP tests

= 11.7 for the PSL tests

We shall base our calculations on $\tau = 7\frac{1}{2}$. Then the quantity τ^* in the plate flow exposure time distribution (equation 26) has the value 5.

The theoretical values for the mean and variance of mobility based on the plate flow exposure time distribution will be obtained by the same methods as used in section 7.2. All that is necessary

is to take the averages with respect to the exposure time distribution $h(t)$ or $h(\tau)$, rather than with respect to the size distribution $f_s(d_p)$. Thus equation (55) becomes

$$\sigma^2_{Z_p} = Z_1^2 b^2 \int_0^\infty y(\tau)h(t)dt + Z_1^2 b^2 \text{var}[x(\tau)] \qquad (56)$$

where

$$\text{var}[x(\tau)] = \int x^2(\tau)h(t)dt - \left(\int x(\tau)h(t)dt\right)^2$$

The two integrals in $\text{var}[x(\tau)]$ present difficulties. For one thing, the function $x(\tau)$ is not available in closed form. It has to be generated from its differential equation as required. Secondly, the function $h(t)$ has a singularity at t^*, which complicates the integration.

Specifically, the integrals to be evaluated are

$$\int_{\tau^*}^{\infty} \frac{y(\tau)\cdot 3\tau^{*2}d\tau}{4\tau^3\sqrt{(1-\tau^*/\tau)}} = \bar{y}$$

$$\int_{\tau^*}^{\infty} \frac{x(\tau)\cdot 3\tau^{*2}d\tau}{4\tau^3\sqrt{(1-\tau^*/\tau)}} = \bar{x}$$

$$\int_{\tau^*}^{\infty} \frac{x^2(\tau)\cdot 3\tau^{*2}d\tau}{4\tau^3\sqrt{(1-\tau^*/\tau)}} = \overline{x^2}$$

The variables x, y and τ are interrelated by means of equations (21), or by the differential equations immediately preceeding these equations. The last two integrals were evaluated numerically, with $\tau^* = 5$. Special consideration was given to the neighborhood of the singularity. The values found were:

$$\bar{x} = 4.528 \pm .003$$

$$\bar{x}^2 = 20.76 \pm .02$$

The uncertainty arises from the mathematical difficulties in integration. The variance of $x(\tau)$ is therefore

$$\text{var}[x(\tau)] = \overline{x^2} - \bar{x}^2 = 0.254 \pm .05$$

There is, therefore, a 20% uncertainty in the calculated value of $\text{var}[x(\tau)]$.

As regards the integral $\bar{y}$, it will not be necessary to determine its value with high accuracy. As may be seen in table II, y varies slowly with τ. The value of $\bar{y}$ is probably near y(10), that is, about 0.638. It is certainly no larger than 0.672. With these numerical values, equation (56) becomes

$$\sigma_{Z_p}^2 = 0.638 Z_1^2 b + 0.254 Z_1^2 b^2$$

The quantity σ_{Z_p} computed from this equation is plotted in figure 30, where it is identified by "plate flow".

The increase in width of the mobility distribution due to the spread in exposure times is unexpectedly large. The "plate flow" curve in figure 30 lies just above the experimental values for the triode corona charger. That is, the triode corona charger provides more uniform charging than is expected on the basis of the plate flow exposure time distribution. This could be the effect of the 20% sheath air used in this charger.

7.5 Concluding remarks

Neither the triode corona charger nor the sonic jet charger

(in its three versions) achieved the minimum variance charge distribution. For the triode corona charger, the width of the experimental mobility distributions can be explained by assuming a parabolic velocity profile through the charging region, resulting in a spread of particle exposure times. This suggests that its charging could be made more uniform by the use of two airsheaths, which would narrow the exposure time distribution more than the single air sheath. There is reason to expect that its uniformity of charging could be improved 30% to 50%.

The experiments of Bademosi(1971) have shown that the minimum variance charge distribution is not idle concept. It can be attained by careful control of the charging conditions. The data of Fuchs, et al(1936) also come close to the minimum variance charge distribution. In those experiments, the charge attained was rather low and the initial charge distribution of the aerosol may have been reflected in the width of the final distribution.

For the sonic jet charger, the width of the charged aerosol mobility distribution is affected both by flowrate and by the shape and size of the reservoir. No explanation is known for these effects. It is possible, however, that these effects could be exploited to achieve highly uniform charging.

BIBLIOGRAPHY

Abramowitz, M. and I. A. Stegun (1964)
Handbook of Mathematical Functions, National Bureau of Standards Applied Mathematics Series 55
U. S. Government Printing Office, Washington, D. C.

Bademosi, F. (1971)
Diffusion Charging and Related Transfer Processes in Knudsen Aerosols
Ph.D. Thesis, University of Minnesota, Minneapolis, Minnesota

Boisdron, Y. and J. R. Brock (1970)
"On the stochastic nature of the acquisition of electrical charge and radioactivity by aerosol particles"
Atmospheric Envir., 4:35-50

Bricard, J. and J. Pradel (1966)
"Electric charge and radioactivity of naturally occurring aerosols" in Aerosol Science, edited by C. N. Davies, Academic Press, N. Y.

Deutsch, W. (1926)
"Die Reinigung der Gase durch Stossionisation"
Z. f. Technische Physik, 7:623-630

Dötsch, E. and H. A. Friedrichs (1969)
"The kinetics of electrical charging of an aerosol"
Staub, 29(7):24

Drozin, V. G. and V. K. LaMer (1959)
"The determination of the particle size distribution of aerosols by precipitation of charged particles"
J. Coll. Sci., 14:74-90

Feller, W. (1950)
An Introduction to Probability Theory and Its Applications, 2nd ed.
John Wiley and Sons, Inc., New York

Fuchs, N. A. and I. Petrjanoff (1935)
"Uber die Stabilitat und Aufladung der Aerosole. II Experimenteller Teil"
Acta Physica Chemica URSR, 3:827-38

Fuchs, N. , I. Petrjanoff and B. Rotzeig (1936)
"On the rate of charging of droplets by an ionic current"
Trans. Faraday Soc., 32:1131

Fuchs, N. A. (1963)
"On the stationary charge distribution on aerosol particles in a bipolar ionic atmosphere"
Geofis. Pura Appl., 56:185-93

Fuchs, N. A. (1964)
The Mechanics of Aerosols
the Macmillan Company, NewYork

Fuchs, N. A. and A. G. Sutugin (1966)
"Generation and use of monodisperse aerosols"
Aerosol Science, C. N. Davies, Academic Press, New York

Fuchs, N. A. (1969)
"Comments on the theory of charging of aerosol particles by unipolar ions in the absence of an applied electric field"
J. Colloid Interface Sci., 29(1):176

Gillespie, T. and G. O. Langstroth (1952)
"An instrument for determining the electric charge distribution in Aerosols"
Canad. J. Chem., 30:1056-1068

Goyer, G. G., R. Gruen and V. K. LaMer (1954)
"Filtering of monodisperse electrically charged aerosols"
J. Phys. Chem., 58:137-142

Green, H. L. and W. R. Lane (1964)
Particulate Clouds: Dusts, Smokes and Mists, 2nd ed.
D. Van Nostrand Company, Inc., Princeton, New Jersey

Gunn, R. (1955)
"The statistical electrification of aerosols by ionic diffusion"
J. Coll. Sci., 10:107-19

Hewitt, G. W. (1957)
"The charging of small particles for electrostatic precipitation"
Trans. Amer. Inst. Elect. Engrs., 76:300-306

Hurd, F. K. and J. C. Mullins (1962)
"Aerosol size distribution from ion mobility"
J. Coll. Sci., 17:91-100

Junge, C. E. (1963)
Air Chemistry and Radioactivity
Academic Press, New York

Keefe, D., P. J. Nolan and T. A. Rich (1959)
"Charge equilibrium in aerosols according to the Boltzmann law"
Proc. Roy. Irish Acad. A., 60(4):27-45

Ladenburg, R. (1930)
"Research on the physical basis of electrical gas purification"
Ann. Phys. Lpz., 4:863-97

Levy, A. (1964)
"The accuracy of the bubble meter method for gas flow measurement"
J. Sci. Instrum. 41:449-53

Lindgren, B. W. (1962)
Statistical Theory, The Macmillan Company, New York

Lissowski, P. (1940)
"Das laden von aerosolteilchen im einer bipolaren ionenatmosphare"
Acta Physico Chemica URSR, 13:157-92

Lundgren, D. and K. T. Whitby (1965)
"Effect of particle electrostatic charge on filtration by fibrous filters"
Ind. Eng. Chem. Proc. Des. Dev., 4(4):345

Megaw, W. J. and A. C. Wells (1969)
"A high resolution charge and mobility spectrometer for radioactive submicrometer aerosols"
J. Sci. Instrum., 2(12):1013-1016

Mirzabekyan, G. Z. (1967)
"The charging of conducting spherical particles with a radius of the order of a free path length for ions in air"
Soviet Phys. Tech. Phys., 11(7):935-41

Natanson, G. L. (1960)
"Theory of charging submicroscopic aerosol particles as a result of capturing gas ions"
Soviet Phys. Tech. Phys., 5(5):538-52

Rohmann, H. (1923)
"Method of size measurement for suspended particles"
Z. Phys., 17:253-65

Schweitzer, H. (1930)
"Uber die Aufladung kleiner schwebteilchen in der Korona-entladung"
Ann. Phys. Lpz., 4:33

Strober, W., A. Berner and R. Blaschke (1969)
"The aerodynamic diameter of aggregates of uniform spheres"
J. Coll. Interface Sci., 29(4):710-9

Thomas, J. W. and D. Rimberg (1967)
"A simple method for measuring the average charge on a monodisperse aerosol"
Staub(in English), 27(8):18-22

Tomaides, M., B. Y. H. Liu and K. T. Whitby (1971)
"Evaluation of the condensation aerosol generator for producing monodispersed aerosols"
J. Aerosol Sci., 2:39-46

Whitby, K. T. (1961)
"Generator for producing high concentrations of small ions"
Rev. Sci. Instr., 32:351-55

Whitby, K. T., B.Y.H. liu and C. M. Peterson (1965)
"Charging and decay of some monodispersed aerosols in the presence of unipolar ion sources"
J. Coll. Sci., 20:585-601

Whitby, K. T. and C. M. Peterson (1965)
"Electrical neutralization and particle size measurement of dye aerosols"
Ind. Engr. Chem. Fund., 4(1):66-72

Whitby, K. T. and W. E. Clark (1966)
"Electric aerosol particle counting and size distribution measuring system for the 0.015 to 1 μ size range"
Tellus, 18:573-86

Whitby, K. T. and B.Y.H. Liu (1966)
"The electrical behavior of aerosols"
in Aerosol Science edited by C. N. Davies, Academic Press, N. Y.

Whitby, K. T. (1967)
Evaluation of Optical Particle Counters, Particle Laboratory Publication No. 110
Particle technology laboratory, Mechanical Engineering Dept., University of Minnesota, Minneapolis, Minnesota

Whitby, K. T. and B.Y.H. Liu (1967)
"Generation of countable pulses by high concentrations of sub-countable sized particles in the sensing volume of optical counters"
J. Coll. Interface Sci., 25(4):537-46

Whitby, K. T. and B.Y.H. Liu (1968)
"Polystyrene aerosols. Electrical charge and residue size distribution"
Atmos. Envir., 2(2):103

White, H. J. (1951)
"Particle charging in electrostatic precipitation"
Trans. Amer. Inst. Elect. Engrs., 70:1186-1191

White, H. J. (1963)
Industrial Electrostatic Precipitation
Addison-Wesley Publishing Company, Inc., Reading, Massachusetts

Woessner, R. H. and R. Gunn (1956)
"Measurements related to the fundamental processes of aerosol electrification"
J. Coll. Sci., 11:69-76

Yoshikawa, H. H., G. A. Swartz and W. L. Fite (1956)
"Electrostatic Particle Size Analyzer"
Rev. Sci. Instr., 27:359-62

Appendix A

CHARGE DISTRIBUTION STATISTICS FOR WHITE CHARGING

The descriptive statistics arithmetic mean charge, geometric mean charge, arithmetic standard deviation and geometric standard deviation are given for the minimum variance and the maximum variance charge distributions, both based on the White charging mechanism. The parameters in these distributions are the particle diameter d_p and the dimensionless mean exposure time $\pi(a/b)^2\bar{c}n\bar{t}$. The values of these parameters covered by the table are d_p = 0.05(0.05)1.00 microns and dimensionless time = 1, 2, 5, 10, 20, 50, 100 and 200.

The geometric mean of the resulting electric mobility distribution is also given in the table. The electric mobility is calculated for the conditions 25°C and 736 mmHg. The geometric standard deviation applies to the mobility distribution as well as to the charge distribution.

The tabulated values are believed to be accurate to the number of digits shown.

The relationship between the dimensionless time and the nt product is:

$\pi(a/b)^2\bar{c}n\bar{t}$	nt, sec/cc	
1	0.219×10^6	assuming
2	0.438	
5	1.095	$\bar{c} = 4.63\times10^4$ cm/sec
10	2.19	
20	4.38	$T_a = 298°K$
50	10.95	
100	21.9	
200	43.8	

CHARGE DISTRIBUTION STATISTICS FOR WHITE CHARGING. DP IS THE PARTICLE DIAMETER IN MICRONS. AMC(GMC) IS THE ARITHMETIC(GEOMETRIC) MEAN CHARGE, ASD(GSD) IS THE ARITHMETIC(GEOMETRIC) STANDARD DEVIATION, GMM IS THE GEOMETRIC MEAN MOBILITY IN (CM/SEC)/(10000 VOLTS/CM). THE TIME INDICATED IS DIMENSIONLESS.

DP	MINIMUM AMC	MINIMUM ASD	MINIMUM GMC	MINIMUM GSD	MINIMUM GMM	MAXIMUM AMC	MAXIMUM ASD	MAXIMUM GMC	MAXIMUM GSD	MAXIMUM GMM
TIME =	1.000									
.050	.18222	.39104	1.00752	1.07432	9.55973	.16923	.38396	1.01439	1.10351	9.62492
.100	.62414	.62481	1.09907	1.27325	2.99816	.54134	.67827	1.16093	1.34651	3.16692
.150	1.22112	.78494	1.35626	1.46624	1.87591	1.03441	.98070	1.45867	1.56519	2.01756
.200	1.93257	.91796	1.83870	1.55194	1.61660	1.62136	1.35621	1.86438	1.68345	1.63917
.250	2.73661	1.03490	2.55123	1.51146	1.60685	2.28511	1.68439	2.35205	1.77820	1.48140
.300	3.61832	1.13935	3.42436	1.42111	1.66153	3.01394	2.04057	2.90697	1.84339	1.41049
.350	4.56654	1.23518	4.38648	1.34299	1.72062	3.79930	2.45175	3.51967	1.88844	1.38051
.400	5.57311	1.32400	5.40669	1.28808	1.77375	4.63466	2.86546	4.18337	1.91956	1.37242
.450	6.63142	1.40708	6.47558	1.24942	1.82182	5.51485	3.26991	4.89292	1.94085	1.37656
.500	7.73623	1.48542	7.58869	1.22082	1.86624	6.43570	3.66359	5.64418	1.95513	1.38804
.550	8.88350	1.55971	8.74277	1.19854	1.90788	7.39373	4.05532	6.43373	1.96430	1.40399
.600	10.06932	1.63060	9.93421	1.18086	1.94710	8.38630	4.45436	7.25895	1.96969	1.42275
.650	11.29101	1.69834	11.16080	1.16621	1.98434	9.41049	5.00951	8.11699	1.97232	1.44316
.700	12.54561	1.76363	12.41950	1.15417	2.01970	10.46431	5.46026	9.00587	1.97287	1.46456
.750	13.83130	1.82626	13.70897	1.14369	2.05350	11.54620	5.91631	9.92403	1.97181	1.48654
.800	15.14583	1.88683	15.02683	1.13473	2.08580	12.65401	6.37676	10.86930	1.96960	1.50871
.850	16.48741	1.94568	16.37125	1.12709	2.11672	13.78673	6.84159	11.84070	1.96644	1.53094
.900	17.85477	2.00251	17.74133	1.12018	2.14644	14.94263	7.31007	12.83642	1.96265	1.55302
.950	19.24616	2.05823	19.13493	1.11439	2.17496	16.12096	7.78225	13.85578	1.95831	1.57491
1.000	20.66086	2.11185	20.55196	1.10883	2.20251	17.32022	8.25753	14.89713	1.95363	1.59649
TIME =	2.000									
.050	.33532	.48731	1.01550	1.10758	9.63542	.29603	.48120	1.02854	1.14693	9.75913
.100	1.02494	.67831	1.21435	1.38193	3.31264	.85532	.85068	1.29342	1.44488	3.52833
.150	1.88204	.82437	1.77992	1.52156	2.46189	1.56191	1.19268	1.77590	1.63072	2.45633
.200	2.86817	.95087	2.70217	1.44459	2.37576	2.37952	1.59092	2.39398	1.73651	2.10480
.250	3.95596	1.06263	3.80275	1.33850	2.39510	3.28567	2.00923	3.11169	1.79797	1.95984
.300	5.12704	1.16365	4.98849	1.27089	2.42046	4.26517	2.44319	3.90982	1.83389	1.89708
.350	6.36882	1.25654	6.24059	1.22766	2.44791	5.30798	2.88966	4.77624	1.85442	1.87351
.400	7.67173	1.34294	7.55118	1.19752	2.47728	6.40579	3.34617	5.70187	1.86535	1.87059
.450	9.02845	1.42411	8.91385	1.17527	2.50780	7.55279	3.81127	6.68032	1.87010	1.87942
.500	10.43353	1.50075	10.32385	1.15789	2.53888	8.74377	4.28338	7.70601	1.87082	1.89509
.550	11.88216	1.57362	11.77657	1.14400	2.56992	9.97509	4.76175	8.77499	1.86882	1.91491
.600	13.37052	1.64323	13.26842	1.13282	2.60061	11.24300	5.24530	9.88324	1.86506	1.93711
.650	14.89540	1.70998	14.79632	1.12312	2.63072	12.54516	5.73369	11.02629	1.86004	1.96078

CHARGE DISTRIBUTION STATISTICS FOR WHITE CHARGING. DP IS THE PARTICLE DIAMETER IN MICRONS. AMC(GMC) IS THE ARITHMETIC(GEOMETRIC) MEAN CHARGE, ASD(GSD) IS THE ARITHMETIC(GEOMETRIC) STANDARD DEVIATION. GMM IS THE GEOMETRIC MEAN MOBILITY IN (CM/SEC)/(10000 VOLTS/CM). THE TIME INDICATED IS DIMENSIONLESS.

DP	MINUS AMC	MINUS ASD	MINUS GMC	MINUS GSD	MINUS GMM	MAX AMC	MAX ASD	MAX GMC	MAX GSD	MAX GMM
TIME =	2.000									
.700	16.45391	1.77455	16.35730	1.11530	2.66008	13.87897	6.25618	12.20721	1.85423	1.98518
.750	18.04404	1.83646	17.94981	1.10830	2.68874	15.24184	6.72225	13.41748	1.84795	2.00984
.800	19.66354	1.89634	19.57142	1.10222	2.71662	16.63273	7.22179	14.65779	1.84130	2.03458
.850	21.31061	1.95439	21.22040	1.09689	2.74369	18.04964	7.72431	15.92602	1.83447	2.05915
.900	22.98366	2.01076	22.89517	1.09216	2.76998	19.49113	8.22956	17.22 63	1.82757	2.08344
.950	24.68126	2.06559	24.59434	1.08794	2.79551	20.95565	8.73721	18.53981	1.82073	2.10732
1.000	26.40215	2.11900	26.31667	1.08415	2.82030	22.44263	9.24727	19.88322	1.81386	2.13084
TIME =	5.000									
.050	.66723	.54504	1.04191	1.17814	9.88597	.54656	.58743	1.06884	1.22800	10.14153
.100	1.69579	.69407	1.60237	1.48344	4.37111	1.40054	.99916	1.59210	1.54906	4.34310
.150	2.92710	.83941	2.79774	1.36768	3.86969	2.43652	1.43051	2.40191	1.67345	3.32220
.200	4.30057	.96327	4.18811	1.26516	3.68221	3.60067	1.89420	3.37146	1.72449	2.96421
.250	5.78219	1.07297	5.68004	1.21092	3.57747	4.86411	2.37329	4.45640	1.74473	2.80679
.300	7.35105	1.17244	7.25589	1.17701	3.52062	6.20876	2.86375	5.63312	1.75040	2.73324
.350	8.99301	1.26410	8.90301	1.15355	3.49225	7.62203	3.36284	6.88632	1.74870	2.70119
.400	10.69783	1.34953	10.61186	1.13627	3.48139	9.09457	3.86866	8.20498	1.74318	2.69177
.450	12.45781	1.42987	12.37509	1.12296	3.48157	10.61978	4.38013	9.58150	1.73559	2.69563
.500	14.26689	1.50596	14.18687	1.11238	3.48888	12.19190	4.89620	11.00931	1.72699	2.70745
.550	16.12022	1.57846	16.04245	1.10378	3.50084	13.80647	5.41615	12.48337	1.71795	2.72416
.600	18.01380	1.64792	17.93792	1.09670	3.51583	15.45981	5.93945	13.99953	1.70881	2.74390
.650	19.94458	1.71384	19.87064	1.09026	3.53291	17.14881	6.46558	15.55432	1.69975	2.76548
.700	21.90932	1.77786	21.83688	1.08504	3.55118	18.87082	6.99427	17.14478	1.69090	2.78814
.750	23.90574	1.83983	23.83458	1.08058	3.57024	20.62357	7.52520	18.76838	1.68232	2.81136
.800	25.93171	1.90014	25.86158	1.07683	3.58972	22.40543	8.05814	20.42353	1.67393	2.83489
.850	27.98579	1.95711	27.91713	1.07280	3.60954	24.21401	8.59285	22.10721	1.66594	2.85835
.900	30.06576	2.01370	29.99799	1.06977	3.62932	24.04806	9.13917	23.81821	1.65826	2.88165
.950	32.17034	2.06930	32.10321	1.06728	3.64900	27.90619	9.64696	25.55500	1.65090	2.90470
1.000	34.29871	2.12139	34.23286	1.06416	3.66866	26.78715	10.20610	27.31619	1.64384	2.92741
TIME =	10.000									
.050	.97428	.49953	1.09315	1.26240	10.37218	.78374	.64144	1.13010	1.30659	10.72279
.100	2.26236	.69694	2.14682	1.40326	5.85632	1.89110	1.09304	1.92671	1.58369	5.25587
.150	3.79014	.84194	3.69313	1.26143	5.10816	3.20080	1.57367	3.03017	1.65284	4.19118
.200	5.46543	.96546	5.37843	1.19862	4.72875	4.64765	2.07310	4.30200	1.67016	3.78234

CHARGE DISTRIBUTION STATISTICS FOR WHITE CHARGING. DP IS THE PARTICLE DIAMETER IN MICRONS. AMC(GMC) IS THE ARITHMETIC(GEOMETRIC) MEAN CHARGE. ASD(GSD) IS THE ARITHMETIC(GEOMETRIC) STANDARD DEVIATION. GMM IS THE GEOMETRIC MEAN MOBILITY IN (CM/SEC)/(10000 VOLTS/CM). THE TIME INDICATED IS DIMENSIONLESS.

DP	MIXTURE AMC	MIXTURE ASD	MIXTURE GMC	MIXTURE GSD	MIXTURE GMM	MAXIMUM AMC	MAXIMUM ASD	MAXIMUM GMC	MAXIMUM GSD	MAXIMUM GMM
TIME =	10.000									
.250	7.25129	1.07471	7.17061	1.16268	4.51629	6.19912	2.58414	5.69490	1.66966	3.58684
.300	9.12572	1.17403	9.04947	1.13917	4.39088	7.83525	3.16340	7.18329	1.66222	3.48539
.350	11.07425	1.26534	11.00148	1.12223	4.31539	9.54251	3.69879	8.75070	1.65204	3.43251
.400	13.08608	1.35072	13.01598	1.10965	4.27009	11.31109	4.15894	10.38558	1.64094	3.40715
.450	15.15357	1.43078	15.08575	1.09964	4.24418	13.13358	4.69289	12.07934	1.62975	3.39837
.500	17.27036	1.50686	17.20436	1.09174	4.23096	15.00414	5.25997	13.82530	1.61885	3.39997
.550	19.43150	1.57988	19.36683	1.08554	4.22629	16.91839	5.76967	15.61865	1.60832	3.40835
.600	21.63345	1.64835	21.57043	1.07962	4.22780	18.87198	6.31157	17.45427	1.59840	3.42103
.650	23.87238	1.71446	23.81066	1.07475	4.23342	20.86186	6.85540	19.32883	1.58903	3.43658
.700	26.14540	1.77878	26.08463	1.07086	4.24197	22.88566	7.40085	21.23995	1.58008	3.45411
.750	28.45040	1.84006	28.39074	1.06709	4.25272	24.94042	7.94780	23.18395	1.57173	3.47278
.800	30.78484	1.90067	30.72577	1.06433	4.26490	27.02466	8.49600	25.15960	1.56376	3.49228
.850	33.14741	1.95785	33.08937	1.06120	4.27829	29.13604	9.04540	27.16392	1.55632	3.51216
.900	35.53574	2.01611	35.47781	1.05949	4.29230	31.27314	9.59587	29.19545	1.54932	3.53222
.950	37.94935	2.06951	37.89250	1.05668	4.30704	33.43512	10.14717	31.25385	1.54253	3.55246
1.000	40.38630	2.12210	40.33029	1.05433	4.32210	35.62017	10.69934	33.33662	1.53611	3.57261
TIME =	20.000									
.050	1.25499	.48767	1.21152	1.36872	11.49533	1.04635	.68315	1.23476	1.38779	11.71581
.100	2.85346	.69870	2.76449	1.29349	7.54127	2.42860	1.17115	2.35086	1.57777	6.41293
.150	4.66436	.84264	4.60716	1.20244	6.37239	4.02570	1.60572	3.77063	1.60225	5.21535
.200	6.60511	.96592	6.59440	1.15840	5.79783	5.76597	2.26749	5.36096	1.59763	4.71338
.250	8.75768	1.07515	8.69125	1.13197	5.47403	7.61424	2.74055	7.07389	1.58556	4.45537
.300	10.93950	1.17439	10.87615	1.11425	5.27720	9.54950	3.27934	8.88337	1.57177	4.31029
.350	13.19579	1.26570	13.13487	1.10127	5.15223	11.55733	3.83227	10.77227	1.55817	4.22548
.400	15.51578	1.35088	15.45682	1.09139	5.07085	13.62753	4.36840	12.72877	1.54536	4.17587
.450	17.89137	1.43151	17.83386	1.08387	5.01733	15.75281	4.91704	14.74474	1.53337	4.14825
.500	20.31669	1.50721	20.26061	1.07740	4.98256	17.92655	5.46776	16.81246	1.52242	4.13458
.550	22.78657	1.57936	22.73171	1.07206	4.96059	20.14463	6.02011	18.92774	1.51220	4.13048
.600	25.29697	1.64838	25.24317	1.06756	4.94765	22.40267	6.57389	21.08551	1.50279	4.13275
.650	27.84421	1.71646	27.79078	1.06452	4.94107	24.69716	7.12898	23.28167	1.49420	4.13937
.700	30.42612	1.77997	30.37362	1.06100	4.93946	27.02592	7.68501	25.51439	1.48612	4.14923
.750	33.03985	1.84139	32.98816	1.05796	4.94137	29.38619	8.24198	27.78036	1.47861	4.16129
.800	35.68328	1.90091	35.63231	1.05529	4.94595	31.77551	8.79993	30.07651	1.47176	4.17478
.850	38.35457	1.95867	38.30423	1.05293	4.95254	34.19291	9.35842	32.40268	1.46519	4.18950

CHARGE DISTRIBUTION STATISTICS FOR WHITE CHARGING. DP IS THE PARTICLE DIAMETER IN MICRONS. AMC(GMC) IS THE ARITHMETIC(GEOMETRIC) MEAN CHARGE, ASD(GSD) IS THE ARITHMETIC(GEOMETRIC) STANDARD DEVIATION. GMM IS THE GEOMETRIC MEAN MOBILITY IN (CM/SEC)/(10000 VOLTS/CM). THE TIME INDICATED IS DIMENSIONLESS.

DP	MEAN CHARGE AMC	STANDARD DEVIATION ASD	MEAN CHARGE GMC	STANDARD DEVIATION GSD	MEAN MOBILITY GMM	MEAN CHARGE AMC	STANDARD DEVIATION ASD	MEAN CHARGE GMC	STANDARD DEVIATION GSD	MEAN MOBILITY GMM
TIME =	20.000									
.900	41.05208	2.01482	41.00231	1.05082	4.96068	36.63630	9.91756	34.75613	1.45904	4.20498
.950	43.77434	2.06952	43.72509	1.04893	4.97000	38.10425	10.47729	37.13534	1.45327	4.22097
1.000	46.52007	2.12285	46.47127	1.04723	4.98022	41.59550	11.03756	39.53895	1.44783	4.23730
TIME =	50.000									
.050	1.64518	.54665	1.54842	1.42892	14.69199	1.42255	.72316	1.45788	1.45868	13.83285
.100	3.65465	.69772	3.58704	1.21574	9.78511	3.18547	1.24922	3.02221	1.52763	8.24430
.150	5.89006	.84282	5.82930	1.15585	8.06280	5.17527	1.78113	4.87413	1.51638	6.74165
.200	8.27709	.96508	8.22048	1.12476	7.22749	7.31307	2.32731	6.89412	1.49784	6.06135
.250	10.77676	1.07529	10.72298	1.10547	6.75368	9.56141	2.87848	9.03541	1.48009	5.69080
.300	13.36617	1.17440	13.31450	1.09219	6.46031	11.89839	3.43298	11.27240	1.46426	5.46947
.350	16.03022	1.26579	15.98018	1.08243	6.26831	14.30915	3.99986	13.58819	1.45036	5.33004
.400	18.75814	1.35106	18.70943	1.07491	6.13792	16.78318	4.56852	15.97113	1.43813	5.23958
.450	21.54192	1.43134	21.49428	1.06895	6.04714	19.31263	5.16858	18.41254	1.42731	5.18014
.500	24.37530	1.50754	24.32853	1.06416	5.98296	21.89134	5.66075	20.90577	1.41767	5.14122
.550	27.25328	1.58045	27.20716	1.06031	5.93724	24.51443	6.23184	23.44551	1.40900	5.11636
.600	30.17213	1.64844	30.12705	1.05629	5.90489	27.17785	6.79476	26.02743	1.40117	5.10137
.650	33.12794	1.71502	33.08344	1.05337	5.88208	29.87827	7.35825	28.64794	1.39405	5.09347
.700	36.11804	1.77950	36.07395	1.05096	5.86646	32.61285	7.95230	31.30400	1.38753	5.09076
.750	39.13992	1.84261	39.09598	1.04915	5.85628	35.37913	8.49688	33.99303	1.38155	5.09190
.800	42.19195	1.90021	42.14903	1.04631	5.85051	38.17502	9.05191	36.71277	1.37604	5.09592
.850	45.27153	1.95894	45.22882	1.04475	5.84786	40.99866	9.61735	39.46124	1.37093	5.10214
.900	48.37722	2.01749	48.33438	1.04377	5.84775	43.84840	10.18316	42.23669	1.36620	5.11002
.950	51.50819	2.06927	51.46639	1.04136	5.84991	46.72334	10.74885	45.03899	1.36157	5.11934
1.000	54.66219	2.12417	54.62036	1.04047	5.85354	49.62122	11.31520	47.86433	1.35742	5.12951
TIME =	100.000									
.050	1.97699	.49970	1.90538	1.33037	18.07888	1.71897	.73837	1.68442	1.46597	15.98239
.100	4.26756	.69796	4.20984	1.18100	11.48406	3.77910	1.27840	3.58873	1.47517	9.78971
.150	6.81048	.84284	6.75814	1.13278	9.34753	6.07164	1.82681	5.76892	1.45119	7.97914
.200	9.50580	.96611	9.45662	1.10749	8.31432	8.51418	2.38478	8.11354	1.42939	7.13356
.250	12.31400	1.07544	12.26698	1.09162	7.72614	11.06845	2.94404	10.57818	1.41132	6.66248
.300	15.21199	1.17517	15.16641	1.08090	7.35887	13.71187	3.50645	13.13711	1.39632	6.37424
.350	18.18500	1.26588	18.14091	1.07227	7.11587	16.42952	4.06838	15.77402	1.38368	6.18744
.400	21.22169	1.35198	21.17848	1.06619	6.94793	19.21075	4.63246	18.47737	1.37288	6.06179

CHARGE DISTRIBUTION STATISTICS FOR WHITE CHARGING. DP IS THE PARTICLE DIAMETER IN MICRONS. AMC(GMC) IS THE ARITHMETIC(GEOMETRIC) MEAN CHARGE. ASD(GSD) IS THE ARITHMETIC(GEOMETRIC) STANDARD DEVIATION. GMM IS THE GEOMETRIC MEAN MOBILITY IN (CM/SEC)/(10000 VOLTS/CM). THE TIME INDICATED IS DIMENSIONLESS.

DP	MINUS IONS AMC	MINUS IONS ASD	MINUS IONS GMC	MINUS IONS GSD	MINUS IONS GMM	MINUS AND POSITIVE IONS AMC	MINUS AND POSITIVE IONS ASD	MINUS AND POSITIVE IONS GMC	MINUS AND POSITIVE IONS GSD	MINUS AND POSITIVE IONS GMM
TIME =	100.000									
.450	24.31449	1.43125	24.27233	1.06077	6.82871	22.04757	5.19746	21.23857	1.36354	5.97520
.500	27.45672	1.50793	27.41511	1.05691	6.74202	24.93417	5.76291	24.05185	1.35515	5.91492
.550	30.64385	1.57949	30.60309	1.05305	6.67831	27.86501	6.32913	26.91066	1.34784	5.87253
.600	33.87131	1.64987	33.83080	1.05055	6.63082	30.83623	6.89590	29.81116	1.34134	5.84298
.650	37.13626	1.71517	37.09653	1.04752	6.59559	33.84492	7.46274	32.75085	1.33528	5.82295
.700	40.43515	1.78145	40.39529	1.04611	6.56921	36.88751	8.03023	35.72503	1.32994	5.80972
.750	43.76638	1.84138	43.72737	1.04345	6.55003	39.96176	8.59817	38.73163	1.32512	5.80170
.800	47.12724	1.90027	47.08880	1.04138	6.53617	43.06626	9.16579	41.77025	1.32042	5.79793
.850	50.51565	1.96074	50.47696	1.04060	6.52642	46.19800	9.73425	44.83596	1.31635	5.79706
.900	53.93072	2.01535	53.89272	1.03862	6.52023	49.35651	10.30236	47.93012	1.31231	5.79884
.950	57.37049	2.06919	57.33298	1.03703	6.51673	52.53913	10.87121	51.04799	1.30883	5.80235
1.000	60.83333	2.12638	60.79523	1.03695	6.51528	55.74583	11.43959	54.19168	1.30529	5.80760
TIME =	200.000									
.050	2.26808	.49020	2.21767	1.23589	21.04207	2.01914	.74974	1.94457	1.44593	18.45076
.100	4.88246	.69908	4.83223	1.15542	13.18186	4.38313	1.30166	4.18644	1.42102	11.42021
.150	7.73423	.84285	7.68826	1.11568	10.63402	6.98110	1.86016	6.69219	1.39209	9.25630
.200	10.73821	.96618	10.69472	1.09445	9.40286	9.73025	2.42234	9.35947	1.37031	8.22890
.250	13.85527	1.07533	13.81355	1.08086	8.70022	12.59169	2.98667	12.14473	1.35357	7.64914
.300	17.06215	1.17500	17.02159	1.07168	8.25902	15.54291	3.55224	15.02373	1.34009	7.28965
.350	20.34399	1.26605	20.30456	1.06440	7.96457	18.56840	4.11899	17.97961	1.32912	7.05260
.400	23.68976	1.35112	23.65122	1.05881	7.75915	21.65787	4.68610	21.00191	1.31977	6.88997
.450	27.09112	1.43340	27.05275	1.05531	7.61095	24.80288	5.25403	24.08105	1.31189	6.77490
.500	30.54257	1.50852	30.50502	1.05126	7.50190	27.99770	5.82217	27.21184	1.30489	6.69203
.550	34.03865	1.58035	34.00175	1.04797	7.41998	31.23676	6.39099	30.38764	1.29891	6.63129
.600	37.57530	1.64919	37.53894	1.04521	7.35762	34.51675	6.95970	33.60598	1.29338	6.58676
.650	41.14914	1.71535	41.11325	1.04285	7.30974	37.83383	7.52869	36.86228	1.28843	6.55394
.700	44.75732	1.77911	44.72183	1.04080	7.27281	41.18478	8.09839	40.15262	1.28417	6.52975
.750	48.39737	1.84069	48.36224	1.03900	7.24430	44.56803	8.66770	43.47678	1.28004	6.51249
.800	52.06717	1.90031	52.03237	1.03739	7.22236	47.98097	9.23721	46.83125	1.27629	6.50042
.850	55.76432	1.96439	55.72846	1.03783	7.20541	51.42173	9.80688	50.21414	1.27282	6.49244
.900	59.48825	2.02080	59.45264	1.03654	7.19290	54.88815	10.37743	53.62218	1.26990	6.48750
.950	63.23695	2.07593	63.20151	1.03542	7.18378	58.37993	10.94727	57.05725	1.26689	6.48539
1.000	67.00911	2.12997	66.97376	1.03449	7.17742	61.89515	11.51725	60.51619	1.26409	6.48538

Appendix B

CHARGE DISTRIBUTION STATISTICS FOR CONTINUUM DIFFUSION CHARGING

The descriptive statistics arithmetic mean charges, geometric mean charge, arithmetic standard deviation and geometric standard deviation are given for the minimum variance and the maximum variance charge distributions, both based on the continuum diffusion charging mechanism. The parameters in these distributions are the particle diameter d_p and the dimensionless exposure time $\pi aDnt/b = \pi\varepsilon Z_i nt$. The parameters values covered are d_p = 0.05(0.05)1.00 microns and $aDnt/b$ = 0.2, 0.5, 1.0, 2.0, 5.0, 10.0, 20.0 and 50.0.

The geometric mean of electric mobility for the charged aerosol is also given in the table following. The mobility is calculated at 25°C and 736 mmHg. The geometric standard deviation applies to the mobility distribution as well as to the charge distribution.

The relationship between the dimensionless exposure time and the nt product is:

$\pi\varepsilon Z_i nt$	nt, sec/cc	
0.2	0.316×10^6	assuming
0.5	0.79	
1.0	1.58	Z_i = 1.4 cm^2/volt-sec
2.0	3.16	
5.0	7.90	
10.0	15.8	
20.0	31.6	
50.0	79.0	

CHARGE DISTRIBUTION STATISTICS FOR CONTINUUM DIFFUSION CHARGING. DP IS THE PARTICLE DIAMETER IN MICRONS, AMC(GMC) IS THE ARITHMETIC(GEOMETRIC) MEAN CHARGE, ASD(GSD) IS THE ARITHMETIC(GEOMETRIC) STANDARD DEVIATION, GMM IS THE GEOMETRIC MEAN MOBILITY IN (CM/SEC)/(10000 VOLTS/CM). THE TIME INDICATED IS DIMENSIONLESS.

DP	MINIMUM AMC	MINIMUM ASD	MINIMUM GMC	MINIMUM GSD	MINIMUM GMM	MAXIMUM AMC	MAXIMUM ASD	MAXIMUM GMC	MAXIMUM GSD	MAXIMUM GMM
TIME = .200										
.050	.31471	.49524	1.03447	1.16176	9.81544	.28612	.50150	1.06265	1.21869	10.08475
.100	.61310	.67580	1.14616	1.33076	3.12661	.55248	.75017	1.23657	1.42170	3.37326
.150	.91138	.81790	1.28621	1.44687	1.77902	.81914	.98227	1.42349	1.55781	1.96690
.200	1.20967	.93884	1.44643	1.53052	1.27171	1.08585	1.20699	1.61147	1.66190	1.41082
.250	1.50797	1.04593	1.62490	1.58999	1.02342	1.35264	1.42790	1.79872	1.74644	1.13489
.300	1.80620	1.14290	1.82045	1.63002	.88330	1.61939	1.64635	1.98483	1.81749	.96305
.350	2.10455	1.23247	2.03201	1.65432	.79707	1.88610	1.86316	2.16981	1.87862	.85112
.400	2.40288	1.31593	2.25817	1.66588	.74083	2.15296	2.07927	2.35387	1.93221	.77222
.450	2.70120	1.39439	2.49743	1.66741	.70262	2.41969	2.29430	2.53695	1.97970	.71374
.500	2.99947	1.46858	2.74817	1.66131	.67584	2.68656	2.50908	2.71929	2.02231	.66874
.550	3.29781	1.53931	3.00884	1.64962	.65660	2.95330	2.72314	2.90085	2.06082	.63303
.600	3.59605	1.60679	3.27778	1.63403	.64244	3.22016	2.93715	3.08183	2.09593	.60404
.650	3.89441	1.67172	3.55371	1.61593	.63183	3.48691	3.15061	3.26218	2.12809	.58000
.700	4.19275	1.73418	3.83521	1.59640	.62369	3.75363	3.36380	3.44199	2.15772	.55975
.750	4.49101	1.79438	4.12115	1.57626	.61732	4.02052	3.57721	3.62143	2.18518	.54246
.800	4.78936	1.85272	4.41067	1.55610	.61222	4.28725	3.79009	3.80035	2.21069	.52751
.850	5.08763	1.90919	4.70285	1.53637	.60805	4.55414	4.00321	3.97897	2.23451	.51446
.900	5.38597	1.96412	4.99717	1.51734	.60458	4.82088	4.21588	4.15715	2.25679	.50295
.950	5.68426	2.01749	5.29300	1.49919	.60163	5.08776	4.42879	4.33505	2.27773	.49275
1.000	5.98286	2.06988	5.59027	1.48198	.59910	5.35450	4.64190	4.51263	2.29744	.48361
TIME = .500										
.050	.66519	.61273	1.09165	1.26162	10.35800	.56581	.66524	1.14619	1.32623	10.87541
.100	1.26773	.82159	1.40385	1.48528	3.82957	1.07653	1.03596	1.51200	1.56713	4.12459
.150	1.87186	.98924	1.82021	1.57482	2.51763	1.58874	1.39574	1.89196	1.71238	2.61087
.200	2.47639	1.13272	2.30999	1.58898	2.03095	2.10129	1.75096	2.27129	1.81671	1.99693
.250	3.08102	1.26002	2.85071	1.56442	1.79547	2.61397	2.10386	2.64854	1.89744	1.66813
.300	3.68571	1.37563	3.42340	1.52446	1.66106	3.12672	2.45543	3.02373	1.96271	1.46714
.350	4.29043	1.48228	4.01423	1.48185	1.57460	3.63951	2.80617	3.39715	2.01708	1.33255
.400	4.89518	1.58176	4.61443	1.44239	1.51384	4.15231	3.15635	3.76906	2.06339	1.23050
.450	5.49994	1.67536	5.21901	1.40801	1.46830	4.66514	3.50614	4.13969	2.10350	1.16465
.500	6.10471	1.76401	5.82538	1.37880	1.43260	5.17797	3.85564	4.50923	2.13871	1.10893
.550	6.70950	1.84842	6.43231	1.35416	1.40368	5.69082	4.20492	4.87783	2.16997	1.06446
.600	7.31429	1.92914	7.03926	1.33330	1.37969	6.20367	4.55404	5.24560	2.19796	1.02614
.650	7.91909	2.00662	7.64603	1.31549	1.35943	6.71652	4.90303	5.61265	2.22324	.99790

CHARGE DISTRIBUTION STATISTICS FOR CONTINUUM DIFFUSION CHARGING. DP IS THE PARTICLE DIAMETER IN MICRONS, AMC(GMC) IS THE ARITHMETIC(GEOMETRIC) MEAN CHARGE, ASD(GSD) IS THE ARITHMETIC(GEOMETRIC) STANDARD DEVIATION, GMM IS THE GEOMETRIC MEAN MOBILITY IN (CM/SEC)/(10000 VOLTS/CM). THE TIME INDICATED IS DIMENSIONLESS.

DP	MINUS AMC	MINUS ASD	MINUS GMC	MINUS GSD	MINUS GMM	MAXIMUM AMC	MAXIMUM ASD	MAXIMUM GMC	MAXIMUM GSD	MAXIMUM GMM
TIME =	.500									
.700	9.52389	2.08122	8.25256	1.30013	1.34206	7.22938	5.25191	5.97907	2.24621	.97234
.750	9.12870	2.15324	8.85886	1.28674	1.32699	7.74224	5.60071	6.34492	2.26722	.95042
.800	9.73351	2.22292	9.46496	1.27495	1.31379	8.25511	5.94944	6.71026	2.28652	.93142
.850	10.33831	2.29049	10.07087	1.26448	1.30211	8.76797	6.29811	7.07515	2.30434	.91478
.900	10.94300	2.35611	10.67649	1.25516	1.29170	9.28084	6.64672	7.43962	2.32086	.90008
.950	11.54794	2.41996	11.28235	1.24661	1.28240	9.79371	6.99530	7.80371	2.33623	.88701
1.000	12.15297	2.48214	11.88827	1.23875	1.27404	10.30634	7.34350	8.16728	2.35059	.87527
TIME =	1.000									
.050	1.05282	.63347	1.19894	1.36513	11.37591	.86454	.77472	1.26394	1.41332	11.99474
.100	1.98084	.85528	1.87594	1.52210	5.11738	1.63436	1.24473	1.85574	1.64415	5.06429
.150	2.91344	1.03029	2.73143	1.48123	3.77798	2.40691	1.70747	2.45856	1.77301	3.40056
.200	3.84705	1.17989	3.64969	1.41140	3.20883	3.18016	2.16738	3.05948	1.86148	2.68992
.250	4.78099	1.31261	4.58416	1.35450	2.88725	3.95359	2.62576	3.65767	1.92771	2.30372
.300	5.71507	1.43310	5.52123	1.31301	2.67895	4.72708	3.08328	4.25348	1.97993	2.06382
.350	6.64919	1.54424	6.45798	1.28252	2.53318	5.50083	3.54053	4.84752	2.02254	1.90147
.400	7.58352	1.64794	7.39436	1.25918	2.42583	6.27446	3.99724	5.43984	2.05822	1.78462
.450	8.51777	1.74548	8.33011	1.24076	2.34357	7.04826	4.45390	6.03098	2.08868	1.69674
.500	9.45199	1.83789	9.26546	1.22578	2.27859	7.82195	4.91024	6.62091	2.11509	1.62824
.550	10.38647	1.92581	10.20094	1.21307	2.22608	8.59561	5.36641	7.20987	2.13829	1.57336
.600	11.32078	2.00994	11.13599	1.20238	2.18265	9.36950	5.82272	7.79822	2.15884	1.52945
.650	12.25506	2.09074	12.07084	1.19316	2.14614	10.14320	6.27874	8.38569	2.17726	1.49094
.700	13.18957	2.16839	13.00598	1.18490	2.11507	10.91687	6.73466	8.97252	2.19388	1.45914
.750	14.12392	2.24345	13.94076	1.17772	2.08822	11.69081	7.19082	9.55905	2.20894	1.43187
.800	15.05825	2.31612	14.87543	1.17134	2.06479	12.46451	7.64668	10.14487	2.22271	1.40816
.850	15.99258	2.38662	15.81002	1.16561	2.04416	13.23818	8.10248	10.73023	2.23536	1.38737
.900	16.92716	2.45481	16.74508	1.16016	2.02591	14.01215	8.55855	11.31549	2.24698	1.36901
.950	17.86155	2.52136	17.67972	1.15538	2.00956	14.78584	9.01431	11.90014	2.25777	1.35262
1.000	18.79672	2.58529	18.61592	1.15015	1.99503	15.55951	9.47003	12.48442	2.26781	1.33793
TIME =	2.000									
.050	1.49304	.61923	1.43403	1.44879	13.60660	1.22182	.85700	1.44592	1.48088	13.71937
.100	2.80495	.83947	2.66988	1.39324	7.28317	2.30541	1.41580	2.33237	1.67004	6.36250
.150	4.12154	1.01396	3.98781	1.30414	5.51575	3.39302	1.96983	3.22598	1.76983	4.46201
.200	5.43933	1.16256	5.30859	1.25338	4.66734	4.48156	2.52201	4.11715	1.83593	3.61982

CHARGE DISTRIBUTION STATISTICS FOR CONTINUUM DIFFUSION CHARGING. DP IS THE PARTICLE DIAMETER IN MICRONS, AMC(GMC) IS THE ARITHMETIC(GEOMETRIC) MEAN CHARGE, ASD(GSD) IS THE ARITHMETIC(GEOMETRIC) STANDARD DEVIATION, GMM IS THE GEOMETRIC MEAN MOBILITY IN (CM/SEC)/(10000 VOLTS/CM). THE TIME INDICATED IS DIMENSIONLESS.

DP	MONO-MODAL AMC	MONO-MODAL ASD	MONO-MODAL GMC	MONO-MODAL GSD	MONO-MODAL GMM	BI-MODAL AMC	BI-MODAL ASD	BI-MODAL GMC	BI-MODAL GSD	BI-MODAL GMM
TIME =	2.000									
.250	6.75777	1.29426	6.62880	1.22129	4.17503	5.57045	3.07331	5.00569	1.88419	3.15275
.300	8.07647	1.41374	7.94864	1.19877	3.85675	6.65952	3.62412	5.89209	1.92151	2.85890
.350	9.39532	1.52388	9.26828	1.18165	3.63553	7.74869	4.17462	6.77678	1.95150	2.65823
.400	10.71425	1.62658	10.58780	1.16855	3.47349	8.83777	4.72481	7.65993	1.97633	2.51496
.450	12.03324	1.72317	11.90723	1.15775	3.34995	9.92707	5.27501	8.54213	1.99727	2.40322
.500	13.35215	1.81477	13.22640	1.14890	3.25268	11.01640	5.82510	9.42339	2.01527	2.31743
.550	14.67125	1.90177	14.54583	1.14120	3.17424	12.10573	6.37511	10.30385	2.03095	2.24854
.600	15.99036	1.98499	15.86520	1.13458	3.10957	13.19487	6.92492	11.18339	2.04480	2.19194
.650	17.30931	2.06515	17.18419	1.12902	3.05527	14.28427	7.47485	12.06263	2.05707	2.14468
.700	18.62849	2.14193	18.50363	1.12382	3.00912	15.37366	8.02474	12.94134	2.06809	2.10456
.750	19.94765	2.21611	19.82297	1.11922	2.96933	16.46305	8.57460	13.81960	2.07804	2.07007
.800	21.26664	2.28828	21.14190	1.11535	2.93461	17.55220	9.12427	14.69715	2.08713	2.04004
.850	22.58586	2.35773	22.46135	1.11152	2.90414	18.64163	9.67410	15.57469	2.09538	2.01373
.900	23.90478	2.42596	23.78007	1.10848	2.87704	19.73106	10.22391	16.45190	2.10297	1.99044
.950	25.22411	2.49131	25.09974	1.10512	2.85295	20.82015	10.77350	17.32840	2.11002	1.96963
1.000	26.54349	2.55477	26.41955	1.10192	2.83132	21.90962	11.32340	18.20511	2.11649	1.95100
TIME =	5.000									
.050	2.08173	.58271	1.99243	1.36301	18.90491	1.74343	.91791	1.78852	1.51178	16.97014
.100	3.92703	.80360	3.84180	1.23774	10.48008	3.29867	1.56131	3.14659	1.63043	8.58359
.150	5.78053	.97228	5.69684	1.18860	7.87959	4.85867	2.20164	4.50856	1.69044	6.23601
.200	7.63539	1.11576	7.55246	1.16074	6.64016	6.41971	2.84084	5.86851	1.72913	5.15962
.250	9.49076	1.24281	9.40827	1.14230	5.92563	7.98114	3.47953	7.22649	1.75685	4.55148
.300	11.34635	1.35815	11.26409	1.12906	5.46543	9.54304	4.11805	8.58327	1.77790	4.16468
.350	13.20226	1.46417	13.12027	1.11869	5.14650	11.10487	4.75634	9.93864	1.79466	3.89049
.400	15.05814	1.56321	14.97629	1.11058	4.91320	12.66675	5.39452	11.29301	1.80839	3.70485
.450	16.91406	1.65646	16.83225	1.10400	4.73554	14.22890	6.03269	12.64694	1.81984	3.55805
.500	18.76998	1.74495	18.68811	1.09858	4.59585	15.79091	6.67076	13.99997	1.82965	3.44292
.550	20.62622	1.82826	20.54467	1.09343	4.48333	17.35291	7.30878	15.35244	1.83815	3.35026
.600	22.48228	1.90857	22.40074	1.08932	4.39054	18.91490	7.94677	16.70439	1.84561	3.27406
.650	24.33833	1.98573	24.25676	1.08575	4.31274	20.47721	8.58482	18.05642	1.85214	3.21035
.700	26.19438	2.06013	26.11273	1.08265	4.24654	22.03927	9.22277	19.40772	1.85803	3.15615
.750	28.05041	2.13209	27.96863	1.07994	4.18949	23.60132	9.86072	20.75869	1.86334	3.10949
.800	29.90679	2.20027	29.82544	1.07683	4.13993	25.16335	10.49864	22.10934	1.86815	3.06889
.850	31.76291	2.26748	31.68154	1.07451	4.09626	26.72536	11.13655	23.45971	1.87255	3.03322

CHARGE DISTRIBUTION STATISTICS FOR CONTINUUM DIFFUSION CHARGING. DP IS THE PARTICLE DIAMETER IN MICRONS, AMC(GMC) IS THE ARITHMETIC(GEOMETRIC) MEAN CHARGE, ASD(GSD) IS THE ARITHMETIC(GEOMETRIC) STANDARD DEVIATION, GMM IS THE GEOMETRIC MEAN MOBILITY IN (CM/SEC)/(10000 VOLTS/CM). THE TIME INDICATED IS DIMENSIONLESS.

DP	MINIMUM AMC	MINIMUM ASD	MINIMUM GMC	MINIMUM GSD	MINIMUM GMM	MAXIMUM AMC	MAXIMUM ASD	MAXIMUM GMC	MAXIMUM GSD	MAXIMUM GMM
TIME =	5.000									
.900	33.61902	2.33287	33.53758	1.07243	4.05756	28.28781	11.77454	24.81059	1.87647	3.00172
.950	35.47514	2.39644	35.39366	1.07051	4.02301	29.84987	12.41245	26.16064	1.88016	2.97354
1.000	37.33115	2.45906	37.24936	1.06901	3.99193	31.41192	13.05035	27.51048	1.88356	2.94823
TIME =	10.000									
.050	2.49615	.57653	2.42898	1.26659	23.04699	2.14995	.93427	2.11022	1.49451	20.02446
.100	4.75088	.78266	4.68533	1.18326	12.78116	4.08343	1.61379	3.86214	1.56689	10.53555
.150	7.00698	.94717	6.94226	1.14693	9.60219	6.02191	2.29144	5.61704	1.60367	7.76921
.200	9.26439	1.08705	9.20009	1.12590	8.08877	7.96159	2.96839	7.37077	1.62727	6.48042
.250	11.52231	1.21085	11.45828	1.11180	7.21679	9.90162	3.64500	9.12312	1.64413	5.74604
.300	13.78049	1.32312	13.71664	1.10152	6.65543	11.84207	4.32147	10.87472	1.65687	5.27051
.350	16.03869	1.42701	15.97480	1.09387	6.26620	13.78262	4.99784	12.62552	1.66696	4.95243
.400	18.29718	1.52325	18.23346	1.08740	5.98177	15.72308	5.67413	14.37543	1.67526	4.71608
.450	20.55569	1.61384	20.49208	1.08212	5.76519	17.66383	6.35039	16.12518	1.68212	4.53061
.500	22.81405	1.70040	22.75026	1.07809	5.59482	19.60428	7.02662	17.87397	1.68806	4.39563
.550	25.07270	1.78170	25.00912	1.07410	5.45757	21.54515	7.70281	19.62307	1.69308	4.28221
.600	27.33132	1.85964	27.26785	1.07073	5.34449	23.48599	8.37899	21.37178	1.69749	4.18886
.650	29.58979	1.93529	29.52612	1.06816	5.24961	25.42652	9.05517	23.11967	1.70147	4.11057
.700	31.84848	2.00702	31.78500	1.06539	5.16898	27.36743	9.73132	24.86799	1.70492	4.04411
.750	34.10692	2.07779	34.04310	1.06356	5.09940	29.30831	10.40746	26.61604	1.70804	3.98688
.800	36.36568	2.14441	36.30216	1.06115	5.03893	31.24889	11.08362	28.36335	1.71093	3.93098
.850	38.62408	2.21132	38.56008	1.05987	4.98562	33.18982	11.75975	30.11115	1.71348	3.89322
.900	40.88292	2.27354	40.81934	1.05765	4.93854	35.13035	12.43590	31.85803	1.71592	3.85436
.950	43.14124	2.33761	43.07695	1.05691	4.89632	37.07133	13.11201	33.60565	1.71804	3.81977
1.000	45.40015	2.39600	45.33644	1.05480	4.85860	39.01226	13.78812	35.35307	1.72001	3.78871
TIME =	20.000									
.050	2.90441	.56568	2.84672	1.22641	27.01066	2.55303	.93264	2.46626	1.45564	23.40091
.100	5.54446	.76772	5.49090	1.15041	14.97865	4.86987	1.62967	4.62382	1.49439	12.61334
.150	8.19238	.92912	8.13942	1.12114	11.25803	7.19174	2.32507	6.78436	1.51496	9.38379
.200	10.84165	1.06612	10.78904	1.10396	9.48578	9.51482	3.02005	8.94440	1.52837	7.86397
.250	13.49134	1.18753	13.43892	1.09247	8.46427	11.83838	3.71483	11.10377	1.53799	6.99352
.300	16.14128	1.29768	16.08897	1.08410	7.80651	14.16218	4.40951	13.26257	1.54531	6.43512
.350	18.79134	1.39923	18.73909	1.07768	7.35051	16.48612	5.10414	15.42092	1.55112	6.04694
.400	21.44150	1.49395	21.38927	1.07255	7.01708	18.81015	5.79872	17.57889	1.55587	5.76703

CHARGE DISTRIBUTION STATISTICS FOR CONTINUUM DIFFUSION CHARGING. DP IS THE PARTICLE DIAMETER IN MICRONS. AMC(GMC) IS THE ARITHMETIC(GEOMETRIC) MEAN CHARGE. ASD(GSD) IS THE ARITHMETIC(GEOMETRIC) STANDARD DEVIATION. GMM IS THE GEOMETRIC MEAN MOBILITY IN (CM/SEC)/(10000 VOLTS/CM). THE TIME INDICATED IS DIMENSIONLESS.

DP	MINUS MONOMER AMC	MINUS MONOMER ASD	MINUS MONOMER GMC	MINUS MONOMER GSD	MINUS MONOMER GMM	MAXIMUM MONOMER AMC	MAXIMUM MONOMER ASD	MAXIMUM MONOMER GMC	MAXIMUM MONOMER GSD	MAXIMUM MONOMER GMM
TIME =	20.000									
.450	24.09171	1.58305	24.03948	1.06834	6.76320	21.13424	6.49328	19.73657	1.55984	5.55263
.500	26.74196	1.66740	26.68973	1.06479	6.56363	23.45837	7.18782	21.89399	1.56323	5.38425
.550	29.39225	1.74769	29.34002	1.06175	6.40268	25.78253	7.88234	24.05120	1.56615	5.24853
.600	32.04257	1.82444	31.99033	1.05909	6.27009	28.10671	8.57686	26.20823	1.56871	5.13580
.650	34.69291	1.89806	34.64067	1.05675	6.15895	30.43091	9.27136	28.36511	1.57097	5.04318
.700	37.34327	1.96890	37.29104	1.05465	6.06439	32.75513	9.96586	30.52185	1.57298	4.96356
.750	39.99365	2.03726	39.94143	1.05276	5.98292	35.07935	10.66035	32.67847	1.57479	4.89499
.800	42.64403	2.10337	42.59183	1.05104	5.91197	37.40359	11.35484	34.83499	1.57643	4.83528
.850	45.29443	2.16744	45.24225	1.04947	5.84960	39.72783	12.04933	36.99141	1.57792	4.78280
.900	47.94483	2.22963	47.89269	1.04802	5.79431	42.05208	12.74381	39.14776	1.57928	4.73631
.950	50.59524	2.29009	50.54314	1.04668	5.74497	44.37633	13.43829	41.30402	1.58053	4.69481
1.000	53.24567	2.34893	53.19362	1.04542	5.70064	46.70059	14.13276	43.46022	1.58169	4.65753
TIME =	50.000									
.050	3.40433	.54995	3.36092	1.17339	31.88960	3.07184	.91791	2.96155	1.39266	28.10025
.100	6.55284	.75426	6.50935	1.12272	17.75689	5.89202	1.61690	5.65375	1.40363	15.42290
.150	9.70182	.91258	9.65885	1.09900	13.35964	8.71680	2.31565	8.34875	1.41126	11.54757
.200	12.85202	1.04710	12.80933	1.08512	11.26204	11.54298	3.01416	11.04418	1.41657	9.71011
.250	16.00263	1.16651	15.96002	1.07594	10.05214	14.36940	3.71271	13.73903	1.42066	8.65329
.300	19.15359	1.27435	19.11115	1.06898	9.27290	17.19636	4.41107	16.43422	1.42371	7.97403
.350	22.30444	1.37502	22.26177	1.06425	8.73230	20.02313	5.10958	19.12861	1.42631	7.50330
.400	25.45572	1.46702	25.41335	1.05959	8.33724	22.85033	5.80787	21.82352	1.42831	7.15955
.450	28.60663	1.55631	28.56375	1.05696	8.03605	25.67725	6.50636	24.51759	1.43015	6.89771
.500	31.75810	1.63731	31.71571	1.05328	7.79964	28.50455	7.20462	27.21229	1.43157	6.69214
.550	34.90944	1.71542	34.86723	1.05051	7.60884	31.33155	7.90310	29.90614	1.43295	6.52622
.600	38.06061	1.79148	38.01821	1.04863	7.45155	34.15890	8.60135	32.60068	1.43403	6.38972
.650	41.21160	1.86638	41.16852	1.04766	7.31957	36.98594	9.29982	35.29437	1.43512	6.27517
.700	44.36322	1.93329	44.32081	1.04500	7.20759	39.81287	9.99839	37.98768	1.43614	6.17768
.750	47.51427	2.00295	47.47124	1.04430	7.11083	42.64039	10.69653	40.68235	1.43684	6.09391
.800	50.66587	2.06526	50.62350	1.04204	7.02681	45.46736	11.39508	43.37559	1.43769	6.02076
.850	53.81699	2.13043	53.77409	1.04146	6.95272	48.29487	12.09323	46.07013	1.43826	5.95664
.900	56.96856	2.18928	56.92621	1.03959	6.88724	51.12187	12.79176	48.76332	1.43897	5.89965
.950	60.11974	2.25056	60.07697	1.03905	6.82863	53.94938	13.48992	51.45775	1.43945	5.84893
1.000	63.27076	2.31237	63.22709	1.03913	6.77590	56.77641	14.18844	54.15090	1.44006	5.80323

Appendix C

CHARGE DISTRIBUTION STATISTICS BASED ON FIELD CHARGING

The descriptive statistics arithmetic mean charge, geometric mean charge, arithmetic standard deviation and geometric standard deviation are given for the minimum and the maximum variance charge distributions, both based on field charging. The parameters in these distributions are the particle saturation charge k_s and the dimensionless exposure time $\pi\varepsilon Z_i nt$. The values covered in the table are k_s = 5(5)100 and $\pi\varepsilon Z_i nt$ = 0.1, 0.2, 0.5, 1.0, 2.0, 5.0 and 10.0.

Also shown in the table is the fraction charged PNC.

The relationship between the dimensionless time $\pi\varepsilon Z_i nt$ and the nt product is:

$\pi\varepsilon Z_i nt$	nt, sec/cc
0.1	0.158×10^6
0.2	0.316
0.5	0.790
1.0	1.58
2.0	3.16
5.0	7.90
10.0	15.8

assuming

Z_i = 1.4 cm^2/volt-sec

CHARGE DISTRIBUTION STATISTICS FOR FIELD CHARGING. SC IS THE SATURATION CHARGE FOR THE PARTICLE. AMC(GMC) IS THE ARITHMETIC(GEOMETRIC) MEAN CHARGE. ASD(GSD) IS THE ARITHMETIC(GEOMETRIC) STANDARD DEVIATION OF THE CHARGE DISTRIBUTION. PNC IS THE PROBABILITY OF NONZERO CHARGE. THE TIME INDICATED IS DIMENSIONLESS.

SC	MEAN AMC	MEAN ASD	MEDIAN GMC	MEDIAN GSD	PNC	MAXIMUM AMC	MAXIMUM ASD	MAXIMUM GMC	MAXIMUM GSD	PNC
TIME = .100										
5.00	.45849	.62140	1.11821	1.30117	.39347	.42740	.67917	1.20181	1.39651	.33333
10.00	.91300	.87337	1.32607	1.48184	.63212	.84914	1.08440	1.49412	1.62214	.50000
15.00	1.36752	1.06743	1.57232	1.59406	.77687	1.27093	1.46793	1.78234	1.77401	.60000
20.00	1.82202	1.23126	1.85526	1.66165	.86466	1.69266	1.84307	2.06635	1.88900	.66667
25.00	2.27653	1.37572	2.17267	1.69592	.91792	2.11449	2.21452	2.34713	1.98125	.71429
30.00	2.73106	1.50641	2.52106	1.70547	.95021	2.53633	2.58368	2.62532	2.05786	.75000
35.00	3.18559	1.62665	2.89604	1.69756	.96980	2.95817	2.90143	2.90143	2.12305	.77778
40.00	3.64013	1.73851	3.29286	1.67821	.98168	3.37988	3.31784	3.17576	2.17952	.80000
45.00	4.09468	1.84379	3.70691	1.65212	.98889	3.80173	3.68400	3.44974	2.22919	.81818
50.00	4.54924	1.94330	4.13407	1.62272	.99326	4.22358	4.04966	3.72051	2.27334	.83333
55.00	5.00380	2.03796	4.57086	1.59241	.99591	4.64527	4.41451	3.99115	2.31296	.84615
60.00	5.45835	2.12841	5.01450	1.56271	.99752	5.06713	4.77956	4.26098	2.34882	.85714
65.00	5.91291	2.21518	5.46286	1.53454	.99850	5.48899	5.14437	4.53001	2.38148	.86667
70.00	6.36747	2.29867	5.91440	1.50835	.99909	5.91067	5.50851	4.79825	2.41139	.87500
75.00	6.82188	2.37906	6.36784	1.48436	.99945	6.33254	5.87303	5.06596	2.43894	.88235
80.00	7.27646	2.45702	6.82272	1.46248	.99966	6.75440	6.23740	5.33310	2.46444	.88889
85.00	7.73104	2.53257	7.27835	1.44265	.99980	7.17607	6.60117	5.59964	2.48810	.89474
90.00	8.18561	2.60593	7.73438	1.42470	.99988	7.59794	6.96539	5.86582	2.51017	.90000
95.00	8.64018	2.67727	8.19060	1.40845	.99993	8.01981	7.32952	6.13157	2.53082	.90476
100.00	9.09460	2.74663	8.64669	1.39375	.99995	8.44167	7.69358	6.39694	2.55018	.90909
TIME = .200										
5.00	.84601	.78055	1.25003	1.41872	.63212	.75417	.90949	1.37246	1.51552	.50000
10.00	1.67919	1.09265	1.73447	1.61094	.86466	1.49327	1.51643	1.89686	1.77465	.66667
15.00	2.51245	1.33371	2.34606	1.66316	.95021	2.23261	2.10716	2.41216	1.93673	.75000
20.00	3.34576	1.53747	3.05464	1.64278	.98168	2.97192	2.69213	2.92030	2.05318	.80000
25.00	4.17900	1.71714	3.82638	1.59275	.99326	3.71137	3.27473	3.42343	2.14290	.83333
30.00	5.01237	1.87996	4.63381	1.53690	.99752	4.45068	3.85559	3.92271	2.21504	.85714
35.00	5.84561	2.02944	5.45880	1.48569	.99909	5.19017	4.43594	4.41921	2.27486	.87500
40.00	6.67901	2.16888	6.29166	1.44216	.99966	5.92947	5.01534	4.91330	2.32557	.88889
45.00	7.51227	2.29976	7.12727	1.40624	.99988	6.66898	5.59476	5.40566	2.36931	.90000
50.00	8.34567	2.42359	7.96376	1.37668	.99995	7.40827	6.17346	5.89633	2.40756	.90909
55.00	9.17895	2.54151	8.80003	1.35224	.99998	8.14780	6.75241	6.38585	2.44140	.91667
60.00	10.01221	2.65409	9.63591	1.33177	.99999	8.88708	7.33073	6.87409	2.47162	.92308
65.00	10.84564	2.76218	10.47164	1.31429	1.00000	9.62662	7.90941	7.36154	2.49883	.92857

CHARGE DISTRIBUTION STATISTICS FOR FIELD CHARGING. SC IS THE SATURATION CHARGE FOR THE PARTICLE. AMC(GMC) IS THE ARITHMETIC(GEOMETRIC) MEAN CHARGE. ASD(GSD) IS THE ARITHMETIC(GEOMETRIC) STANDARD DEVIATION OF THE CHARGE DISTRIBUTION. PNC IS THE PROBABILITY OF NONZERO CHARGE. THE TIME INDICATED IS DIMENSIONLESS.

SC	MINIMUM AMC	MINIMUM ASD	MINIMUM GMC	MINIMUM GSD	MINIMUM PNC	MAXIMUM AMC	MAXIMUM ASD	MAXIMUM GMC	MAXIMUM GSD	MAXIMUM PNC
TIME = .200										
70.00	11.67893	2.86613	11.30682	1.29928	1.00000	10.36590	8.48750	7.84797	2.52350	.93333
75.00	12.51220	2.96644	12.14170	1.28620	1.00000	11.10544	9.06601	8.33384	2.54599	.93750
80.00	13.34546	3.06347	12.97630	1.27468	1.00000	11.84472	9.64395	8.81886	2.56663	.94118
85.00	14.17893	3.15756	13.81106	1.26429	1.00000	12.58427	10.22234	9.30347	2.58563	.94444
90.00	15.01222	3.24890	14.64538	1.25507	1.00000	13.32354	10.80018	9.78736	2.60322	.94737
95.00	15.84550	3.33774	15.47954	1.24674	1.00000	14.06309	11.37849	10.27096	2.61955	.95000
100.00	16.67877	3.42429	16.31358	1.23917	1.00000	14.80236	11.95625	10.75393	2.63478	.95238
TIME = .500										
5.00	1.71218	.91264	1.70120	1.54487	.91792	1.42696	1.22594	1.76896	1.64325	.71429
10.00	3.37765	1.26993	3.14184	1.52706	.99326	2.81237	2.14132	2.80916	1.89439	.83333
15.00	5.04383	1.54717	4.78036	1.41674	.99945	4.19856	3.04810	3.83388	2.03616	.88235
20.00	6.71035	1.78197	6.45138	1.34022	.99995	5.58518	3.95233	4.84900	2.13156	.90909
25.00	8.37695	1.98927	8.12334	1.29181	1.00000	6.97170	4.85512	5.85758	2.20169	.92593
30.00	10.04344	2.17692	9.79345	1.25907	1.00000	8.35817	5.75716	6.86159	2.25613	.93750
35.00	11.71014	2.34964	11.46268	1.23508	1.00000	9.74502	6.65915	7.86260	2.29996	.94595
40.00	13.37669	2.51054	13.13097	1.21670	1.00000	11.13160	7.56061	8.86079	2.33628	.95238
45.00	15.04321	2.66180	14.79873	1.20205	1.00000	12.51813	8.46184	9.85689	2.36700	.95745
50.00	16.71001	2.80475	16.46671	1.18976	1.00000	13.90502	9.36327	10.85167	2.39338	.96154
55.00	18.37660	2.94089	18.13408	1.17958	1.00000	15.29161	10.26434	11.84480	2.41640	.96491
60.00	20.04316	3.07105	19.80125	1.17089	1.00000	16.67817	11.16529	12.83671	2.43670	.96774
65.00	21.70972	3.19597	21.46825	1.16337	1.00000	18.06468	12.06616	13.82758	2.45477	.97015
70.00	23.37658	3.31582	23.13584	1.15646	1.00000	19.45167	12.96741	14.81807	2.47093	.97222
75.00	25.04320	3.43177	24.80282	1.15055	1.00000	20.83824	13.86824	15.80738	2.48558	.97403
80.00	26.70980	3.54396	26.46972	1.14528	1.00000	22.22477	14.76902	16.79598	2.49890	.97561
85.00	28.37640	3.65273	28.13655	1.14052	1.00000	23.61174	15.67016	17.78445	2.51102	.97701
90.00	30.04300	3.75838	29.80333	1.13622	1.00000	24.99832	16.57093	18.77199	2.52220	.97826
95.00	31.70960	3.86117	31.47007	1.13230	1.00000	26.38487	17.47166	19.75901	2.53252	.97938
100.00	33.37619	3.96132	33.13677	1.12871	1.00000	27.77139	18.37234	20.74556	2.54207	.98039
TIME = 1.000										
5.00	2.58927	.88548	2.44414	1.46141	.99326	2.08806	1.40031	2.21982	1.67469	.83333
10.00	5.08616	1.22891	4.92265	1.30542	.99995	4.10330	2.50237	3.82463	1.88157	.90909
15.00	7.58512	1.49619	7.42807	1.23338	1.00000	6.12067	3.60106	5.41331	1.99105	.93750
20.00	10.08470	1.72257	9.93077	1.19549	1.00000	8.13851	4.69842	6.99243	2.06193	.95238

CHARGE DISTRIBUTION STATISTICS FOR FIELD CHARGING. SC IS THE SATURATION CHARGE FOR THE PARTICLE. AMC(GMC) IS THE ARITHMETIC(GEOMETRIC) MEAN CHARGE. ASD(GSD) IS THE ARITHMETIC(GEOMETRIC) STANDARD DEVIATION OF THE CHARGE DISTRIBUTION. PNC IS THE PROBABILITY OF NONZERO CHARGE. THE TIME INDICATED IS DIMENSIONLESS.

SC	MINIMUM AMC	MINIMUM ASD	MINIMUM GMC	MINIMUM GSD	MINIMUM PNC	MAXIMUM AMC	MAXIMUM ASD	MAXIMUM GMC	MAXIMUM GSD	MAXIMUM PNC
TIME = 1.000										
25.00	12.58433	1.92265	12.43209	1.17147	1.00000	10.15652	5.79518	8.56550	2.11265	.96154
30.00	15.08423	2.10362	14.93318	1.15432	1.00000	12.17453	6.89157	10.13433	2.15127	.96774
35.00	17.58406	2.27036	17.43376	1.14149	1.00000	14.19273	7.98783	11.70031	2.18187	.97222
40.00	20.08392	2.42573	19.93413	1.13140	1.00000	16.21093	9.08394	13.26394	2.20689	.97561
45.00	22.58378	2.57178	22.43435	1.12321	1.00000	18.22897	10.17991	14.82554	2.22787	.97826
50.00	25.08366	2.71003	24.93448	1.11640	1.00000	20.24728	11.27590	16.38600	2.24570	.98039
55.00	27.58356	2.84159	27.43456	1.11061	1.00000	22.26514	12.37170	17.94464	2.26120	.98214
60.00	30.08347	2.96735	29.93460	1.10562	1.00000	24.28359	13.46765	19.50305	2.27467	.98361
65.00	32.58339	3.08799	32.43463	1.10124	1.00000	26.30192	14.56354	21.06044	2.28660	.98485
70.00	35.08333	3.20408	34.93467	1.09736	1.00000	28.31984	15.65927	22.61647	2.29732	.98592
75.00	37.58329	3.31608	37.43471	1.09388	1.00000	30.33827	16.75515	24.17260	2.30687	.98684
80.00	40.08326	3.42440	39.93477	1.09074	1.00000	32.35601	17.85079	25.72714	2.31563	.98765
85.00	42.58324	3.52937	42.43484	1.08789	1.00000	34.37456	18.94668	27.28237	2.32347	.98837
90.00	45.08323	3.63128	44.93492	1.08527	1.00000	36.39299	20.04252	28.83696	2.33067	.98901
95.00	47.58323	3.73038	47.43502	1.08286	1.00000	38.41040	21.13815	30.39020	2.33738	.98958
100.00	50.08323	3.82689	49.93512	1.08064	1.00000	40.42931	22.23400	31.94416	2.34346	.99010
TIME = 2.000										
5.00	3.46843	.76270	3.37561	1.27446	.99995	2.79750	1.46380	2.77403	1.63806	.90909
10.00	6.79551	1.05428	6.70957	1.17635	1.00000	5.48345	2.64916	5.04975	1.78775	.95238
15.00	10.12697	1.28264	10.04307	1.13938	1.00000	8.17431	3.83630	7.31339	1.86372	.96774
20.00	13.45939	1.47635	13.37644	1.11868	1.00000	10.86617	5.02344	9.56950	1.91160	.97561
25.00	16.79216	1.64758	16.70974	1.10506	1.00000	13.55840	6.21046	11.82087	1.94525	.98039
30.00	20.12512	1.80268	20.04302	1.09524	1.00000	16.25080	7.39741	14.06902	1.97050	.98361
35.00	23.45819	1.94547	23.37632	1.08773	1.00000	18.94330	8.58429	16.31482	1.99031	.98592
40.00	26.79133	2.07844	26.70965	1.08172	1.00000	21.63585	9.77114	18.55884	2.00638	.98765
45.00	30.12453	2.20338	30.04299	1.07678	1.00000	24.32845	10.95796	20.80148	2.01972	.98901
50.00	33.45775	2.32158	33.37635	1.07261	1.00000	27.02068	12.14483	23.04228	2.03113	.99010
55.00	36.79059	2.43630	36.70847	1.06996	1.00000	29.71350	13.33159	25.28319	2.04080	.99099
60.00	40.12397	2.54322	40.04217	1.06660	1.00000	32.40625	14.51835	27.52318	2.04924	.99174
65.00	43.45734	2.64588	43.37578	1.06369	1.00000	35.09896	15.70510	29.76243	2.05669	.99237
70.00	46.79069	2.74478	46.70933	1.06114	1.00000	37.79166	16.89186	32.00108	2.06331	.99291
75.00	50.12402	2.84030	50.04282	1.05889	1.00000	40.48436	18.07861	34.23922	2.06925	.99338
80.00	53.45694	2.93561	53.37489	1.05779	1.00000	43.17657	19.26545	36.47593	2.07472	.99379
85.00	56.79040	3.02440	56.70876	1.05567	1.00000	45.86944	20.45215	38.71359	2.07954	.99415

CHARGE DISTRIBUTION STATISTICS FOR FIELD CHARGING. SC IS THE SATURATION CHARGE FOR THE PARTICLE. AMC(GMC) IS THE ARITHMETIC(GEOMETRIC) MEAN CHARGE. ASD(GSD) IS THE ARITHMETIC(GEOMETRIC) STANDARD DEVIATION OF THE CHARGE DISTRIBUTION. PNC IS THE PROBABILITY OF NONZERO CHARGE. THE TIME INDICATED IS DIMENSIONLESS.

SC	MINIMUM AMC	MINIMUM ASD	MINIMUM GMC	MINIMUM GSD	MINIMUM PNC	MAXIMUM AMC	MAXIMUM ASD	MAXIMUM GMC	MAXIMUM GSD	MAXIMUM PNC
TIME = 2.000										
90.00	60.12381	3.11092	60.04245	1.05382	1.00000	48.56225	21.63887	40.95077	2.08396	.99448
95.00	63.45661	3.19978	63.37397	1.05350	1.00000	51.25501	22.82560	43.18757	2.08801	.99476
100.00	66.79016	3.28062	66.70817	1.05158	1.00000	53.94776	24.01232	45.42404	2.09175	.99502
TIME = 5.000										
5.00	4.35185	.57773	4.31187	1.14767	1.00000	3.65837	1.36323	3.54798	1.51902	.96154
10.00	8.49959	.76728	8.46410	1.09656	1.00000	7.15193	2.48844	6.72076	1.60371	.98039
15.00	12.66181	.92801	12.62723	1.07718	1.00000	10.65333	3.61476	9.89019	1.64556	.98684
20.00	16.82646	1.06590	16.79227	1.06613	1.00000	14.15756	4.74301	13.05659	1.67157	.99010
25.00	20.99196	1.18819	20.95799	1.05876	1.00000	17.66288	5.87206	16.22073	1.68964	.99206
30.00	25.15788	1.29914	25.12405	1.05339	1.00000	21.16870	7.00146	19.38320	1.70307	.99338
35.00	29.32385	1.40274	29.28981	1.04982	1.00000	24.67479	8.13102	22.54440	1.71353	.99432
40.00	33.49026	1.49693	33.45655	1.04605	1.00000	28.18103	9.26068	25.70463	1.72196	.99502
45.00	37.65665	1.58636	37.62304	1.04325	1.00000	31.68737	10.39039	28.86409	1.72892	.99558
50.00	41.82299	1.67213	41.78921	1.04129	1.00000	35.19377	11.52013	32.02292	1.73479	.99607
55.00	45.98954	1.75208	45.95597	1.03905	1.00000	38.70023	12.64990	35.18123	1.73982	.99638
60.00	50.15589	1.83095	50.12199	1.03788	1.00000	42.20671	13.77968	38.33911	1.74418	.99668
65.00	54.32255	1.90353	54.28900	1.03590	1.00000	45.71323	14.90947	41.49661	1.74802	.99693
70.00	58.48894	1.97697	58.45495	1.03519	1.00000	49.21976	16.03928	44.65380	1.75142	.99715
75.00	62.65566	2.04380	62.62211	1.03341	1.00000	52.72631	17.16909	47.81070	1.75445	.99734
80.00	66.82207	2.11264	66.78807	1.03295	1.00000	56.23288	18.29890	50.96736	1.75719	.99751
85.00	70.98811	2.18515	70.95251	1.03397	1.00000	59.73945	19.42873	54.12380	1.75966	.99765
90.00	75.15528	2.23981	75.12132	1.03101	1.00000	63.24603	20.55855	57.28005	1.76192	.99778
95.00	79.32144	2.30747	79.28618	1.03177	1.00000	66.75263	21.68838	60.43612	1.76398	.99790
100.00	83.48852	2.35991	83.45465	1.02933	1.00000	70.25922	22.81821	63.59204	1.76588	.99800
TIME = 10.000										
5.00	4.77380	.42065	4.75360	1.09872	1.00000	4.16602	1.17791	4.05935	1.41008	.98039
10.00	9.28087	.59525	9.26151	1.06704	1.00000	8.15220	2.17665	7.81484	1.46427	.99010
15.00	13.81440	.70074	13.79644	1.05252	1.00000	12.13734	3.16404	11.56497	1.48980	.99338
20.00	18.35530	.79832	18.33779	1.04478	1.00000	16.12527	4.15174	15.31446	1.50559	.99502
25.00	22.89833	.88684	22.88103	1.03973	1.00000	20.11499	5.14045	19.06354	1.51654	.99602
30.00	27.44226	.96780	27.42509	1.03608	1.00000	24.10575	6.12986	22.81222	1.52469	.99668
35.00	31.98666	1.04270	31.96958	1.03328	1.00000	28.09712	7.11971	26.56049	1.53103	.99715
40.00	36.53135	1.11268	36.51433	1.03105	1.00000	32.08886	8.10983	30.30840	1.53613	.99751

CHARGE DISTRIBUTION STATISTICS FOR FIELD CHARGING. SC IS THE SATURATION CHARGE FOR THE PARTICLE. AMC(GMC) IS THE ARITHMETIC(GEOMETRIC) MEAN CHARGE. ASD(GSD) IS THE ARITHMETIC(GEOMETRIC) STANDARD DEVIATION OF THE CHARGE DISTRIBUTION. PNC IS THE PROBABILITY OF NONZERO CHARGE. THE TIME INDICATED IS DIMENSIONLESS.

SC	MINIMUM AMC	MINIMUM ASD	MINIMUM GMC	MINIMUM GSD	MINIMUM PNC	MAXIMUM AMC	MAXIMUM ASD	MAXIMUM GMC	MAXIMUM GSD	MAXIMUM PNC
TIME = 10.000										
45.00	41.07622	1.17857	41.05925	1.02921	1.00000	36.09085	9.10014	34.05599	1.54034	.99778
50.00	45.62122	1.24101	45.60428	1.02766	1.00000	40.07299	10.09056	37.80329	1.54389	.99800
55.00	50.16630	1.30048	50.14939	1.02634	1.00000	44.06524	11.08106	41.55035	1.54692	.99819
60.00	54.71145	1.35737	54.69456	1.02519	1.00000	48.05757	12.07161	45.29719	1.54955	.99834
65.00	59.25639	1.41684	59.23880	1.02555	1.00000	52.04997	13.06221	49.04384	1.55186	.99846
70.00	63.80179	1.46640	63.78466	1.02378	1.00000	56.04240	14.05284	52.79032	1.55391	.99857
75.00	68.34711	1.51601	68.33017	1.02265	1.00000	60.03488	15.04349	56.53666	1.55574	.99867
80.00	72.89243	1.56470	72.87556	1.02180	1.00000	64.02738	16.03416	60.28287	1.55738	.99875
85.00	77.43713	1.62563	77.41840	1.02425	1.00000	68.01990	17.02485	64.02896	1.55886	.99882
90.00	81.98283	1.66391	81.96525	1.02178	1.00000	72.01245	18.01555	67.77494	1.56022	.99889
95.00	86.52832	1.70561	86.51121	1.02044	1.00000	76.00500	19.00625	71.52083	1.56145	.99895
100.00	91.07373	1.74812	91.05681	1.01961	1.00000	79.99758	19.99697	75.26663	1.56259	.99900

APPENDIX D

SIMULATION OF MOBILITY ANALYZER PERFORMANCE AND THE ENSUING DATA TREATMENT

In section 5.4, a scheme was devised for extracting moments of the mobility distribution from the mobility analyzer data. It was mentioned there that the scheme cannot provide exact results in practice for two major reasons:

1. The function $N^*(\Delta\phi)$, which represents the data from the mobility analyzer, can only be determined at a finite number of points, and

2. the data N^* as well as the input N are usually measured in terms of the number of particles which pass during a specified time interval. This number is not always large and is therefore subject to statistical fluctuation. Any quantity computed from N^* is similarly subject to fluctuations.

In this appendix, we attempt to indicate the magnitude of the errors resulting from these factors by employing simulation methods.

It is obvious that N, the number of particles which enter the mobility analyzer during one sampling cycle, is a Poisson random variable. Let its parameter be denoted by $\bar{N}$.. It follows that the time interval between the entrance of successive particles, expressed in fractions of the cycle time, is a negative exponential random variable with parameter $1/\bar{N}$. According to Abramowitz and Stegun(1964), this random variable can be generated by the expression

$$-\ln(U)/\bar{N} \qquad \text{D-1}$$

where U is a uniform random variable with range (0,1).

For each particle that enters the mobility analyzer, its mobility Z_p is a random variable with distribution $f(Z_p)$. In this

simulation, we use a normal distribution with mean $\bar{Z}_p$ and standard deviation σ_{Z_p} for $f(Z_p)$. According to the above reference, this random variable may be generated by the expression

$$\sigma_{Z_p}(-2\ln U_1)^{\frac{1}{2}}\cos(2\pi U_2) + \bar{Z}_p \qquad \text{D-2}$$

where U_1 and U_2 are a pair of uniform random variables, each with range (0,1).

According to section 5.4, the streamline ψ_{in} on which the particle enters the mobility analyzer is a uniform random variable with range (ψ_1,ψ_1'). This may be generated by the expression

$$(\psi_1' - \psi_1)U + \psi_1 \qquad \text{D-3}$$

where again U is a uniform random variable with range (0,1). Since the stream function involves an arbitrary additive constant, ψ_1 may be taken to be zero. The ψ's are defined in section 5.3.

The procedure for the simulation is as follows:

1. Assign values for the three independent flow rates q_o, q_a and q_s defined in section 5.3.
2. Assign values to the parameters $\bar{N}$, $\bar{Z}_p$ and σ_{Z_p}.
3. Assign a sequence of voltage settings to be investigated.
4. Compute the integrals I_0, I_1 and I_2 defined in section 5.4.
5. At each voltage setting, enter particles one at a time. For each particle, determine the time lapse since the entry of the previous particle by means of equation D-1. If the accumulated time for all the particles at the current voltage setting exceeds 1, jump to the next voltage setting. Otherwise, move to step 6 below.
6. Generate the mobility Z_p and the entering streamline ψ_{in} for the current particle, using equations D-2 and

D-3, respectively. If the expression

$$\psi_2' < \psi_{in} + Z_p\Delta\phi < \psi_2$$

is satisfied, increase the particle count $N^*(\Delta\phi)$ by one. Then move back to step 5 to start another particle. The ψ's and $\Delta\phi$ are defined in section 5.3.

7. When the complete set of data has been generated, compute the integrals I_0^*, I_1^* and I_2^* defined in section 5.4 and apply the formulae

$$N = I_0^*/I_0, \qquad \bar{Z}_p = (q_o/2\pi)I_1^*/NI_1$$

$$\overline{Z_p^2} = (q_o/2\pi)^2 I_2^*/(NI_2)$$

to estimate $\bar{N}$, $\bar{Z}_p$ and σ_{Z_p}.

The formulae in step 7 come from section 5.4.

Several simulations as outlined above have been carried out on the CDC 6600 digital computer. The required uniform random variables U were obtained by use of the library function RANF. The results of a few of these simulations are shown on the four pages following.

The first two pages following pertain to a very narrow mobility distribution with mean $1.4\text{x}10^{-5}\text{cm}^2$/volt-sec and standard deviation $2.0\text{x}10^{-7}$ cm^2/volt-sec. For each combination of flow rates and $\bar{N}$, five complete simulations were done. It appears that the fluctuations in the estimates of $\bar{N}$, $\bar{Z}_p$ and σ_{Z_p} decrease with increase of $\bar{N}$ and with decrease of the ratios q_s/q_o and q_a/q_o. For the condition q_o = 50 cc/sec, $q_s = q_a$ = 2.5 cc/sec and $\bar{N}$ = 400, the fluctuations are roughly

fluctuation in the estimate of $\bar{N}$ = 5%

fluctuation in the estimate of $\bar{Z}_p$ = 0.1%

fluctuation in the estimate of σ_{Z_p} = 10%

These values are very approximate because of the small number of

SIMULATION OF MOBILITY ANALYZER PERFORMANCE AND THE ENSUING DATA TREATMENT. THE NUMBER OF PARTICLES SENT INTO THE MOBILITY ANALYZER IN UNIT TIME IS PICKED FROM A POISSON DISTRIBUTION WITH PARAMETER NBAR (SHOWN BELOW). FOR EACH PARTICLE, THE MOBILITY IS PICKED FROM A NORMAL DISTRIBUTION WITH MEAN ZPBAR AND STANDARD DEVIATION SDZP. THE ESTIMATES FROM DATA OF THESE THREE PARAMETERS ARE NOBS, ZPOBS AND SDOBS, RESPECTIVELY. QO = THE MAIN OUTLET AIRFLOW, QA = THE AEROSOL FLOW AND QS = THE SAMPLING FLOW. THE MOBILITIES ARE IN CM/SEC PER MEGAVOLTS/CM. THE FLOW RATES ARE IN CC/SEC.

QO=	50.00000	QA=	2.50000	QS=	2.50000
NBAR=	100	ZPBAR=	14.000	SDZP=	.200
I0=	.0500209	I1=	.0500626	I2=	.0501253

VOLTS	COUNTS/UNIT TIME, FIVE SETS OF DATA				
7700.0000	0	0	0	0	0
7900.0000	0	0	0	0	0
8100.0000	1	0	0	1	3
8300.0000	12	11	13	15	20
8500.0000	60	54	55	49	49
8700.0000	76	77	78	70	79
8900.0000	52	54	51	40	61
9100.0000	16	18	12	22	22
9300.0000	3	0	2	1	2
9500.0000	0	0	0	0	0
9700.0000	0	0	0	0	0
NOBS =	101	98	97	91	108
ZPOBS =	14.002	13.988	14.009	14.004	13.996
SDOBS =	.198	.160	.165	.226	.248

QO=	50.00000	QA=	2.50000	QS=	2.50000
NBAR=	400	ZPBAR=	14.000	SDZP=	.200
I0=	.0500209	I1=	.0500626	I2=	.0501253

VOLTS	COUNTS/UNIT TIME, FIVE SETS OF DATA				
7700.0000	0	0	0	0	0
7900.0000	0	0	0	0	0
8100.0000	6	1	6	2	3
8300.0000	51	79	61	66	70
8500.0000	191	220	203	196	234
8700.0000	311	323	292	292	305
8900.0000	189	202	199	195	208
9100.0000	65	70	62	54	80
9300.0000	5	6	14	6	7
9500.0000	1	0	0	0	0
9700.0000	0	0	0	0	0
NOBS =	376	415	385	373	417
ZPOBS =	14.000	14.019	14.004	14.016	14.010
SDOBS =	.198	.205	.225	.197	.217

SIMULATION OF MOBILITY ANALYZER PERFORMANCE AND THE ENSUING DATA TREATMENT. THE NUMBER OF PARTICLES SENT INTO THE MOBILITY ANALYZER IN UNIT TIME IS PICKED FROM A POISSON DISTRIBUTION WITH PARAMETER NBAR (SHOWN BELOW). FOR EACH PARTICLE, THE MOBILITY IS PICKED FROM A NORMAL DISTRIBUTION WITH MEAN ZPBAR AND STANDARD DEVIATION SDZP. THE ESTIMATES FROM DATA OF THESE THREE PARAMETERS ARE NOBS, ZPOBS AND SDOBS, RESPECTIVELY. QO = THE MAIN OUTLET AIRFLOW, QA = THE AEROSOL FLOW AND QS = THE SAMPLING FLOW. THE MOBILITIES ARE IN CM/SEC PER MEGAVOLTS/CM. THE FLOW RATES ARE IN CC/SEC.

QO=	50.00000	QA=	5.00000	QS=	5.00000
NBAR=	100	ZPBAR=	14.000	SDZP=	.200
I0=	.1001673	I1=	.1005034	I2=	.1010101

VOLTS	COUNTS/UNIT TIME, FIVE SETS OF DATA				
7000.0000	0	0	0	0	0
7300.0000	0	0	0	0	0
7600.0000	0	0	0	0	0
7900.0000	11	15	14	4	7
8200.0000	41	39	42	41	49
8500.0000	74	84	67	77	62
8800.0000	104	80	72	80	77
9100.0000	60	57	58	59	56
9400.0000	14	10	26	24	23
9700.0000	1	5	0	1	0
10000.0000	0	0	0	0	0
NOBS =	105	100	96	98	94
ZPOBS =	14.000	14.043	14.001	13.950	13.991
SDOBS =	.094	.229	.308	.125	.229

QO=	50.00000	QA=	5.00000	QS=	5.00000
NBAR=	400	ZPBAR=	14.000	SDZP=	.200
I0=	.1001673	I1=	.1005034	I2=	.1010101

VOLTS	COUNTS/UNIT TIME, FIVE SETS OF DATA				
7000.0000	0	0	0	0	0
7300.0000	0	0	0	0	0
7600.0000	1	1	0	0	0
7900.0000	41	39	47	41	41
8200.0000	159	161	176	167	195
8500.0000	341	313	303	318	296
8800.0000	345	353	363	313	356
9100.0000	221	188	215	192	210
9400.0000	83	65	68	83	72
9700.0000	4	5	8	7	7
10000.0000	0	0	0	0	0
NOBS =	412	389	407	387	406
ZPOBS =	14.005	14.028	14.022	14.022	14.028
SDOBS =	.173	.134	.196	.212	.197

QO=	50.00000	QA=	2.50000	QS=	2.50000
NBAR=	400	ZPBAR=	100.000	SDZP=	30.000
I0=	.0500209	I1=	.0500626	I2=	.0501253

VOLTS	COUNTS/UNIT TIME, FIVE SETS OF DATA				
400.0000	0	0	0	0	0
503.5702	0	0	0	0	0
633.9573	1	0	1	0	1
798.1049	6	9	9	7	5
1004.7546	21	25	33	27	23
1264.9111	26	30	27	28	21
1592.4287	12	17	13	17	15
2004.7489	4	9	5	10	2
2523.8294	5	1	4	4	1
3177.3129	1	1	0	2	1
4000.0000	1	2	0	1	0
NOBS =	355	431	427	443	320
ZPOBS =	99.520	99.577	104.920	96.647	103.153
SDOBS =	29.520	27.475	27.866	28.155	26.851

QO=	50.00000	QA=	2.50000	QS=	2.50000
NBAR=	400	ZPBAR=	100.000	SDZP=	30.000
I0=	.0500209	I1=	.0500626	I2=	.0501253

VOLTS	COUNTS/UNIT TIME, FIVE SETS OF DATA				
400.0000	0	0	0	0	0
444.1345	0	0	0	0	0
493.1387	0	0	0	0	0
547.5498	0	0	0	0	0
607.9644	0	0	0	0	0
675.0450	0	0	1	2	4
749.5270	7	6	4	4	6
832.2270	15	11	17	13	11
924.0519	13	22	17	18	17
1026.0084	29	24	33	26	22
1139.2143	27	24	32	31	34
1264.9111	17	26	30	25	23
1404.4767	20	27	27	22	18
1559.4415	16	13	19	20	23
1731.5045	10	14	15	13	10
1922.5523	9	8	10	6	6
2134.6797	9	5	5	5	7
2370.2124	1	3	1	3	3
2631.7329	5	2	1	5	2
2922.1086	1	5	0	0	3
3244.5233	0	3	0	1	0
3602.5121	0	0	0	1	1
4000.0000	1	0	0	3	0
NOBS =	376	405	444	412	398
ZPOBS =	100.932	98.944	102.236	99.965	101.295
SDOBS =	29.333	29.051	25.887	28.848	29.897

QO=	50.00000	QA=	7.50000	QS=	7.50000
NBAR=	400	ZPBAR=	100.000	SDZP=	30.000
I0=	.1505676	I1=	.1517132	I2=	.1534527

VOLTS	COUNTS/UNIT TIME, FIVE SETS OF DATA				
400.0000	0	0	0	0	0
503.5702	0	0	0	0	0
633.9573	4	1	2	1	3
798.1049	28	33	38	33	36
1004.7546	87	76	81	68	65
1264.9111	77	63	78	82	62
1592.4287	49	48	47	35	35
2004.7489	15	29	27	17	23
2523.8294	8	13	7	12	11
3177.3129	5	4	2	5	3
4000.0000	3	0	1	1	0
NOBS =	423	412	436	391	367
ZPOBS =	102.348	99.363	102.559	101.309	102.787
SDOBS =	29.001	30.073	28.955	29.145	31.345

QO=	50.00000	QA=	7.50000	QS=	7.50000
NBAR=	400	ZPBAR=	100.000	SDZP=	30.000
I0=	.1505676	I1=	.1517132	I2=	.1534527

VOLTS	COUNTS/UNIT TIME, FIVE SETS OF DATA				
400.0000	0	0	0	0	0
444.1345	0	0	0	0	0
493.1387	0	0	0	0	0
547.5498	0	0	0	0	0
607.9644	0	1	2	5	2
675.0450	7	6	5	9	3
749.5270	19	21	19	20	14
832.2270	37	42	42	40	34
924.0519	62	60	57	60	47
1026.0084	70	85	59	84	72
1139.2143	66	88	73	79	64
1264.9111	67	81	74	75	61
1404.4767	61	64	57	54	53
1559.4415	47	48	39	48	61
1731.5045	34	38	38	30	39
1922.5523	16	25	23	32	24
2134.6797	16	11	18	22	22
2370.2124	12	12	16	12	11
2631.7329	5	6	9	11	4
2922.1086	4	4	2	5	6
3244.5233	4	2	6	5	3
3602.5121	1	4	2	3	3
4000.0000	0	1	5	2	2
NOBS =	368	417	378	414	365
ZPOBS =	101.978	102.056	100.162	101.386	98.108
SDOBS =	29.111	28.543	30.615	31.415	29.256

simulations.

The second two pages following pertain to a broad mobility spectrum with mean 1.0×10^{-4} cm^2/volt-sec and standard deviation 3.0×10^{-5} cm^2/volt-sec. The voltage settings in these cases form a geometric progression and cover a range of one decade. In two cases, 11 settings were used and in the other two 23 settings were used. Two combinations of flow rate settings were checked. The fluctuations appear to be about the same for each of the four cases considered:

fluctuation in the estimate of $\bar{N}$ = 8%

fluctuation in the estimate of $\bar{Z}_p$ = 2%

fluctuation in the estimate of σ_{Z_p} = 3%

It is interesting that doubling the number of data points does not appear to improve the results: 6 to 8 data points across the peak serve just as well as twice that number. It is somewhat disturbing that at the lower flow rates for q_a and q_s, the estimate of σ_{Z_p} appears to be systematically low.

APPENDIX E

THE EFFECT OF MISALIGNMENT IN THE MOBILITY ANALYZER

In the section 5.3 discussion of particle trajectories within the mobility analyzer, it was assumed that the analyzing region proper was bounded by two perfectly circular cylinders with a common axis. Standard machining practice is such, however, that it is difficult to insure alignment of parts to tolerances of less than a few thousandths of an inch. In this appendix, we explore the consequences of one particular type of misalignment.

Assume that the analyzing region proper is bounded by two perfectly circular cylinders whose axes are parallel but not coincident. This geometry is sometimes referred to as "eccentric cylinders". In this geometry, there is no single axis of symmetry. Therefore, it is not possible to define a stream function as was done for the coaxial cylinders in section 5.3. In order to make the analysis to follow manageable, it is necessary to restrict consideration to fluid flows for which the velocity vector is everywhere parallel to the cylinder axes: we shall assume fully developed flow between the cylinders. Thus the present model is more general in terms of geometry than that in section 5.3, but more restrictive as regards the flow fields considered.

The flow and electric fields in the space between the eccentric cylinders may be discussed in terms of the bipolar coordinates ξ,η. These are related to the ordinary Cartesian coordinates x,y by the mapping

$$x + iy = S\cdot\tan[\tfrac{1}{2}(\xi + i\eta)] \qquad \text{E-1}$$

where i is the unit imaginary number. The inverse mapping is

$$\xi + i\eta = -i \cdot \ln\left(\frac{x + i(y - S)}{x + i(y + S)}\right) \qquad \text{E-2}$$

The latter function has poles in the x,y plane at x,y = 0,±S. The curves η = constant consist of circles in the x,y plane with center at x,y = 0,S·coth(η) and radius S·csch(η).

Let β and α be the values of η which correspond to the inner and outer tubes, respectively, of the mobility analyzer. Let r_1 and r_2 be the radii of the inner and outer tubes, respectively. Let s be the spacing between their two axes. Then

$$r_1 = S \cdot \mathrm{csch}(\beta)$$

$$r_2 = S \cdot \mathrm{csch}(\alpha)$$

$$s = S \cdot \coth(\beta) - S \cdot \coth(\alpha)$$

By use of the identities for the hyperbolic functions, α and β may be eliminated from these equations to give

$$4S^2s^2 = [s^2 - (r_2 + r_1)^2][s^2 - (r_2 - r_1)^2]$$

which determines the mapping parameter S for given r_1, r_2 and s. The required values of α and β may then be found by use of the inverse hyperbolic functions.

The potential function for the electric field in the space between the two cylinders must satisfy Laplace's equation and take on the value V and 0 on the inner and outer cylinder, respectively. These conditions are met by the function

$$V(\eta - \alpha)/(\beta - \alpha)$$

where η is one of the bipolar coordinates, given in terms of x and

y by the imaginary part of equation E-2.

The x and y equations of motion for a particle with electric mobility Z_p are

$$dx/dt = \frac{-Z_p V}{\beta-\alpha}\,\partial\eta/\partial x, \qquad dy/dt = \frac{-Z_p V}{\beta-\alpha}\,\partial\eta/\partial y \qquad \text{E-3}$$

When these equations are re-expressed in terms of the variables ξ and η, the result is

$$d\xi/dt = 0, \qquad d\eta/dt = \frac{-Z_p V}{J(\beta-\alpha)} \qquad \text{E-4}$$

In these equations, J is the Jacobian of the coordinate transformation E-1:

$$J = \begin{vmatrix} \frac{\partial x}{\partial \xi} & \frac{\partial y}{\partial \xi} \\ \frac{\partial x}{\partial \eta} & \frac{\partial y}{\partial \eta} \end{vmatrix} = \frac{(1 + \cos\xi\cdot\cosh\eta)^2 + (\sin\xi\cdot\sinh\eta)^2}{(\cos\xi + \cosh\eta)^4} \qquad \text{E-5}$$

The motion of the particle in the direction parallel to the cylinder axes (the z-direction) is given by the local fluid velocity $w(\xi,\eta)$.

$$dz/dt = w(\xi,\eta)$$

The motion of the particle may therefore be described by the differential equation

$$dz/d\eta = \frac{-(\beta-\alpha)}{Z_p V}\,Jw$$

This may be integrated directly, since the bipolar coordinate ξ is a constant of the motion. Therefore the axial travel for a particle which starts at the outer cylinder $\eta = \alpha$ and stops at the inner cy-

linder $\eta = \beta$ is

$$L = \frac{-(\beta-\alpha)}{Z_p V} \int_{\alpha}^{\beta} J w d\eta \qquad \text{E-6}$$

The axial travel L therefore depends on the bipolar coordinate ξ, which varies along the circumference of the tubes. The value of L averaged with respect to ξ is related in a simple way to the volumetric flow in the space between the cylinders.

According to R. Berker(1963, p.74), the velocity w for fully developed flow between eccentric cylinders is

$$w = \frac{\Delta p S^2}{\mu L}\Bigg(\sum_{n=1}^{\infty} (-1)^n \frac{e^{-n\beta} \coth\beta \cdot \sinh\{n(\eta-\alpha)\}\cos(n\xi)}{\sinh\{n(\beta-\alpha)\}}$$

$$+ \sum_{n=1}^{\infty} (-1)^n \frac{e^{-n\alpha} \coth\alpha \cdot \sinh\{n(\eta-\alpha)\}\cos(n\xi)}{\sinh\{n(\beta-\alpha)\}} \qquad \text{E-7}$$

$$- \tfrac{1}{4} \frac{\cosh\eta - \cos\xi}{\cosh\eta + \cos\xi} - \tfrac{1}{4}(1 - 2\coth\beta)$$

$$- \tfrac{1}{2}(\coth\beta - \coth\alpha)(\beta-\eta)/(\beta-\alpha)\Bigg)$$

With this expression for w and equation E-5 for the Jacobian, the integral E-6 was evaluated for 11 equally spaced values of ξ. These 11 values were on the closed interval $[0,\pi]$, whose end points correspond to the smallest and the largest gap between the cylinders, respectively. This was done for several different values of the axis spacing s. The integral was evaluated by a numerical method and the resulting values are accurate to .0001 relative error.

The results of the calculations are given in table E-I. The quantities r_1, r_2 and s at the left of the table may be in any length units. The numbers in the body of the table are the axial travel L corresponding to the given value of ξ expressed in multiples of the mean axial travel. The first five lines of the table pertain to the apparatus used in this study, if the quantities r_1, r_2 and s are taken in inches. For this apparatus, it is believed that the tubes are within .002" of being concentric. The corresponding range of the axial travels is about 2%.

The last five lines in table E-I pertain to a different ratio of cylinder radii and are given purely for comparison. The effect of eccentric alignment of the mobility analyzer tubes is also indicated in figure E-1. In this figure, the ordinate is the ratio of the greatest axial travel to the least axial travel and the abscissa is the ratio of the maximum gap between the cylinders to the minimum gap.

Reference:

Berker, R. (1963)
"Integration des equations du mouvement d'un fluide visqueux incompressible"
Handbuch der Physik, Band VIII/2, Springer Verlag, Berlin.

Table E-1

Axial travel of a particle in a mobility analyzer
with an eccentrically located inner rod.

The three columns at the left are the tube radii and the spacing between axes, in arbitrary units. The remaining entries are the axial travel for different values of the angular coordinate ξ, each divided by the mean axial travel.

			angular.....coordinate.....ξ										
r_1	r_2	s	0	0.1π	0.2π	0.3π	0.4π	0.5π	0.6π	0.7π	0.8π	0.9π	1.0π
0.3750	0.7500	.0010	0.9894	0.9900	0.9914	0.9938	0.9967	1.0000	1.0032	1.0062	1.0086	1.0101	1.0106
0.3750	0.7500	.0020	0.9790	0.9800	0.9829	0.9875	0.9933	0.9999	1.0064	1.0124	1.0172	1.0202	1.0213
0.3750	0.7500	.0050	0.9479	0.9504	0.9575	0.9686	0.9830	0.9991	1.0156	1.0308	1.0431	1.0510	1.0538
0.3750	0.7500	.0100	0.8976	0.9022	0.9155	0.9368	0.9646	0.9965	1.0298	1.0610	1.0866	1.1035	1.1093
0.3750	0.7500	.0200	0.8022	0.8102	0.8338	0.8724	0.9242	0.9862	0.0534	1.1190	1.1747	1.2123	1.2256
0.3750	1.5000	.0010	0.9965	0.9967	0.9972	0.9980	0.9989	1.0000	1.0011	1.0020	1.0028	1.0033	1.0035
0.3750	1.5000	.0020	0.9931	0.9934	0.9944	0.9959	0.9978	1.0000	1.0021	1.0041	1.0056	1.0066	1.0069
0.3750	1.5000	.0050	0.9828	0.9836	0.9860	0.9898	0.9946	0.9999	1.0053	1.0101	1.0140	1.0165	1.0174
0.3750	1.5000	.0100	0.9657	0.9674	0.9721	0.9795	0.9890	0.9996	1.0104	1.0202	1.0281	1.0332	1.0350
0.3750	1.5000	.0200	0.9323	0.9354	0.9445	0.9589	0.9774	0.9985	1.0201	1.0402	1.0565	1.0671	1.0708

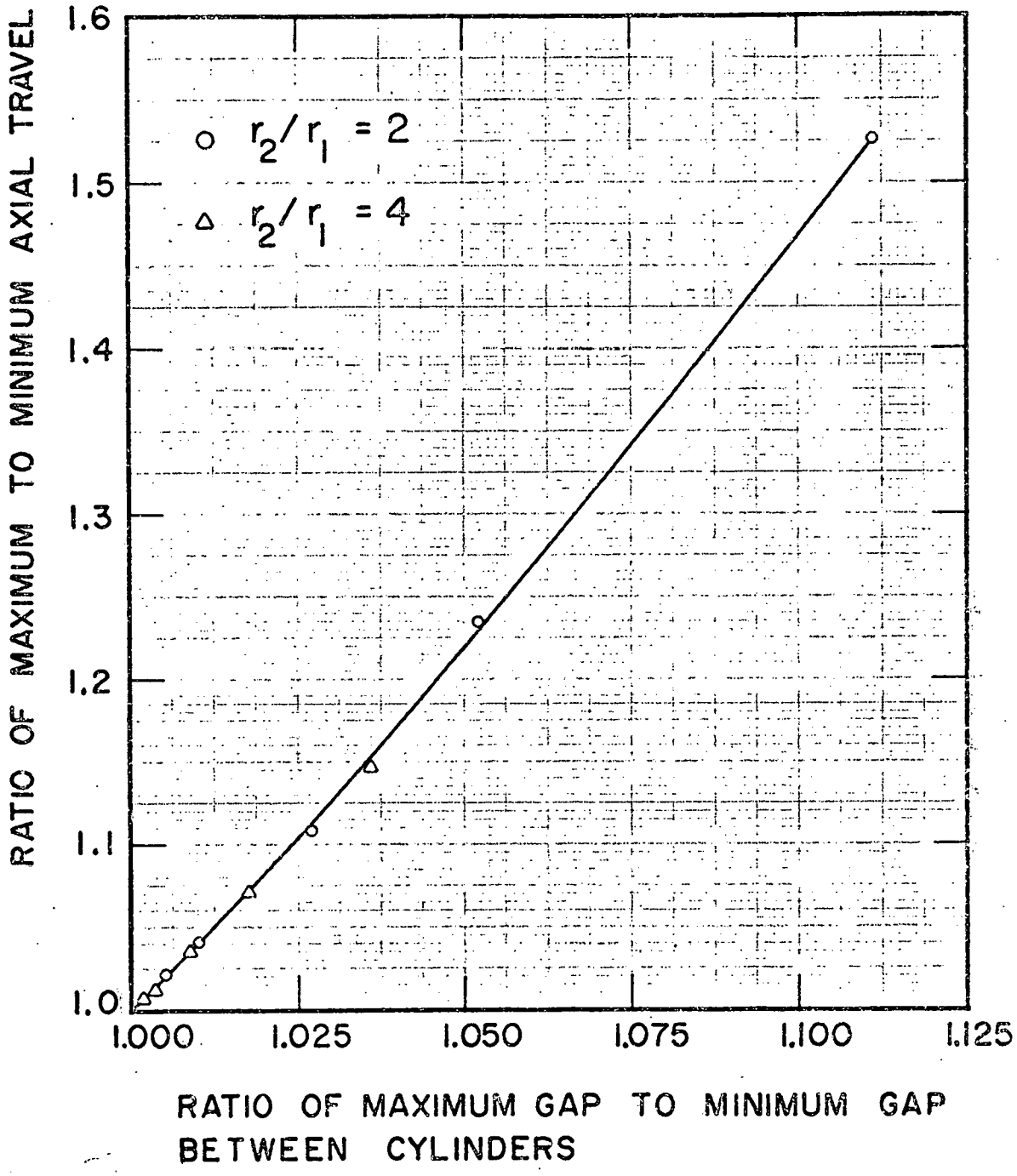

Figure E1. Effect of eccentricity in the mobility analyzer.